AFRL-RY-RS-TR-2007-221
Final Technical Report
October 2007

APPLICATION OF STATE-ESTIMATION TECHNIQUES FOR SPATIAL, TEMPORAL, AND POLARIZATION DIVERSE WAVEFORMS

Science Applications International Corp.

AIR FORCE RESEARCH LABORATORY
SENSORS DIRECTORATE
ROME RESEARCH SITE
ROME, NEW YORK

NOTICE AND SIGNATURE PAGE

Using Government drawings, specifications, or other data included in this document for any purpose other than Government procurement does not in any way obligate the U.S. Government. The fact that the Government formulated or supplied the drawings, specifications, or other data does not license the holder or any other person or corporation; or convey any rights or permission to manufacture, use, or sell any patented invention that may relate to them.

This report was cleared for public release by the Air Force Research Laboratory Public Affairs Office and is available to the general public, including foreign nationals. Copies may be obtained from the Defense Technical Information Center (DTIC) (http://www.dtic.mil).

AFRL-RY-RS-TR-2007-221 HAS BEEN REVIEWED AND IS APPROVED FOR PUBLICATION IN ACCORDANCE WITH ASSIGNED DISTRIBUTION STATEMENT.

FOR THE DIRECTOR:

/s/ /s/

HOWARD M. BEYER
Work Unit Manager

RICHARD G. SHAUGHNESSY
Chief, Rome Operations Site
Sensors Directorate

This report is published in the interest of scientific and technical information exchange, and its publication does not constitute the Government's approval or disapproval of its ideas or findings.

REPORT DOCUMENTATION PAGE

Form Approved
OMB No. 0704-0188

1. REPORT DATE *(DD-MM-YYYY)*	2. REPORT TYPE	3. DATES COVERED *(From - To)*
OCT 2007	Final	Aug 03 – Feb 07

4. TITLE AND SUBTITLE

APPLICATION OF STATE-ESTIMATION TECHNIQUES FOR SPATIAL, TEMPORAL, AND POLARIZATION DIVERSE WAVEFORMS

5a. CONTRACT NUMBER
F30602-03-C-0114

5b. GRANT NUMBER

5c. PROGRAM ELEMENT NUMBER
62204F

6. AUTHOR(S)

John W. Garnham, Jaime R. Roman, James M. Stiles and Wolfgang-Martin Boerner

5d. PROJECT NUMBER
517R

5e. TASK NUMBER
15

5f. WORK UNIT NUMBER
P1

7. PERFORMING ORGANIZATION NAME(S) AND ADDRESS(ES)

SAIC
10260 Campus Point Dr.
San Diego CA 92121-1522

8. PERFORMING ORGANIZATION REPORT NUMBER

9. SPONSORING/MONITORING AGENCY NAME(S) AND ADDRESS(ES)

AFRL/RYRT
25 Electronic Pky
Rome NY 13441-4515

10. SPONSOR/MONITOR'S ACRONYM(S)

11. SPONSORING/MONITORING AGENCY REPORT NUMBER
AFRL-RY-RS-TR-2007-221

12. DISTRIBUTION AVAILABILITY STATEMENT
APPROVED FOR PUBLIC RELEASE; DISTRIBUTION UNLIMITED. PA# AFRL/WS-07-2199

13. SUPPLEMENTARY NOTES

14. ABSTRACT

A novel radar system design philosophy is presented in which the radar adapts in time as the functional mode and environment evolve. In that context, the main subsystems change to meet performance and functional requirements. Two key aspects of the concept proposed herein are the consideration of the receiver function as a parameter estimation problem, and the selection of the waveform to be transmitted as an optimization problem with information-theoretic criteria. Two new information theoretic for waveform selection in radar and other sensing applications are introduced. One criterion is based on the concept of mutual information, and the other is based on changes in the Fisher information of the received signal. This second criterion is referred to herein as marginal information, to emphasize the fact that it is based on a change in information. Marginal information is itself a novel measure introduced in this work, and is shown to be inherently associated with minimum mean-squared error estimation criteria because Fisher information is related to the Cramer-Rao bound for the estimation error of any unbiased estimator.

15. SUBJECT TERMS
Space-Time Signals, Radar Transmit Signals, Optimal Signal Construction

16. SECURITY CLASSIFICATION OF:			17. LIMITATION OF ABSTRACT	18. NUMBER OF PAGES	19a. NAME OF RESPONSIBLE PERSON
a. REPORT	b. ABSTRACT	c. THIS PAGE			Howard Beyer
U	U	U	UL	203	19b. TELEPHONE NUMBER (*Include area code*) N/A

Table of Contents

ABSTRACT

A novel radar system design philosophy is presented in which the radar adapts in time as the functional mode and environment evolve. In that context, the main subsystems change to meet performance and functional requirements. Two key aspects of the concept proposed herein are the consideration of the receiver function as a parameter estimation problem, and the selection of the waveform to be transmitted as an optimization problem with information-theoretic criteria. Two new information theoretic criteria for waveform selection in radar and other sensing applications are introduced. One criterion is based on the concept of mutual information, and the other is based on changes in the Fisher information of the received signal. This second criterion is referred to herein as marginal information, to emphasize the fact that it is based on a change in information. Marginal information is itself a novel measure introduced in this work, and it is shown to be inherently associated with minimum mean-squared error estimation criteria because Fisher information is related to the Cramer-Rao bound for the estimation error of any unbiased estimator. This criterion is examined in the context of multiple targets in a clutter background, and results show that the utilization of multiple diversities does bring performance gains. Analogously, the application of the mutual information criteria to the area of waveform diversity for synthetic aperture radar (SAR) systems is examined. It is shown herein that such a framework provides the basis for a conceptually-simple and powerful criterion for context-dependent evaluation of candidate waveforms, as well as context-dependent design of waveforms. Furthermore, in the special case of zero-mean Gaussian-distributed clutter, interference, and noise, the mutual information criterion attains an analytically simple form – a scalar function of the singular values of a specific cross-covariance matrix. This criterion can be used in distinct optimization contexts (minimization or maximization) as a function of the problem to be addressed. In addition, the mutual information criterion inherently includes the statistical information of the sensed parameters. More specifically, in the context of a SAR system the criterion includes the covariance matrix of the set of illuminated ground scatterers. The formulation and simulation-based results are presented in the context of a first-order radar system model for simplicity, but the approach can be extended in a straightforward manner to cover more complex models. Results presented show that the mutual information criterion is an effective means for waveform selection (modulation type and/or polarization type) in an adaptive SAR system, and the marginal information criterion is also an effective means for waveform selection in SAR and moving target indication (MTI) radar systems.

1.0 INTRODUCTION

This research has its genesis in earlier work by the Principal Investigator (PI) in support of TechSat 21, an Air Force Research Laboratory (AFRL), Space Vehicles Directorate research program that started in the late 1990's. The TechSat 21 program envisioned an orbiting cluster of small radar satellites operating as a single large spacecraft. The idea of using waveform diversity (a term not in use at that point) to resolve the many grating lobes of the sparse array was central to the concept. In addition to work by the PI in this area, one of the research subcontractors to the program reported herein, J. M. Stiles of the University of Kansas (KU), was also a contributor to the TechSat 21 program. The early work on TechSat 21 focused on resolution of ambiguities by the transmission of different uncorrelated signals from each aperture (satellite) to ensure that the sparse array radar system forms a single large illuminated spot without grating lobes. Later in the TechSat 21 program, the effort focused on how to combine all the signals received by all the individual satellite receivers to form a SAR image or to operate in the GMTI mode. In both modes a major consideration was the avoidance of grating lobes on the receive function.

1.1 CONTRACT INFORMATION

This report is a summary of the work carried out by the SAIC-led team in the Adaptive Radar Program under contract number F30602-03-C-0114 for the AFRL, Sensors Directorate, Rome Research Site. As such, the report includes the contributions of the team members to the effort. Specifically, the efforts of Dr. James M. Stiles at KU and Dr. Wolfgang-Martin Boerner at the University of Illinois at Chicago (UIC), executed under subcontracts to SAIC, are gratefully acknowledged.

1.2 PROBLEM STATEMENT: ADAPTIVE RADAR SYSTEMS

Current operational radar systems have been designed to utilize one of multiple existing types of waveforms to accomplish the desired function (detection, tracking, etc.) as well as possible. Towards that end a large basis of waveform-related research has taken place, with emphasis on defining waveform sets with distinct properties, such as orthogonality and tolerance to Doppler changes (see, for example, [1-3], and the references therein). However, such an approach is inherently flawed because it splits the radar problem into a mathematical exercise in waveform design, and a radar design exercise focused on selecting a waveform among the existing sets.

The philosophy postulated herein is fundamentally distinct to that prevalent vision; namely, the waveform (and in general, the radar) design problem is postulated in the context of the radar system function and its operational conditions, and that problem is solved using powerful analytical and mathematical tools from information theory and parameter estimation. Specifically, implementation of the desired radar function is viewed as a parameter estimation problem, which allows application of well-developed estimation techniques such as the Kalman filter. This is in contrast to the standard matched filter (MF) receiver implementation. As a second key step, the information in the estimated parameters is utilized, together with knowledge of the previously-transmitted waveforms, to select the waveform to be transmitted during the next transmission interval. Two information-theoretic criteria (ITC) are utilized to accomplish the waveform selection process, and each is summarized below. It is important to note that both criteria operate as part of a general framework in which the radar system is adaptive, and the adaptation occurs in the transmitter and receiver, as well as in the array aperture. Furthermore, radar adaptation can be defined to cover various types of radar systems and functions, including synthetic aperture radar (SAR) and moving target indication (MTI). It is important to note that

the formulation established herein applies directly to multi-platform radar (sparse array) configurations as well as to other sensor systems, such as sonar.

As is well known [1-3], the MF maximizes receiver output signal-to-noise ratio (SNR) in additive (white or colored) noise, and is thus optimal for the single, isolated target detection problem. However, in many scenarios the receiver also encounters additive clutter and interference, and/or multiple targets are present in proximity. Under such conditions it is relevant to consider processing alternatives, as appropriate, to implement the radar function of interest. One attractive alternative is the parameter estimation approach as in [4], for example, and that is the direction pursued herein for the receiver processing step.

According to the first ITC, the selected waveform is the one that minimizes Shannon mutual information (MI) between the previously-received signal and the next received signal. This specific formulation is established here in the context of determination of the waveform type in an adaptive SAR system [5, 6]. The second ITC is based on the change in Fisher information due to a received measurement, and is referred to as marginal information for that reason. This alternative formulation is established in the context of SAR as well as MTI radar modes. Another key aspect of the second ITC is that it involves the representation of the transmit signal in terms of a set of orthonormal basis functions that span the bandwidth, time extent, and spatial extent of the radar [7, 8].

Previous related efforts in this area include the work of Bell [9], in which he studies the design of waveforms in the context of illumination of extended targets for a) target detection (with output SNR as criterion, as in the MF), and b) information extraction (with Shannon MI as criterion). This elegant work also includes the placement of realistic constraints on the waveform. However, the formulation is restricted to noise-only scenarios (no clutter or interference), and the single, isolated target case. For the information extraction problem, Bell determines the waveform that maximizes MI between the ensemble of responses from Gaussian-distributed targets and the received waveform, which is a different problem than the one addressed herein. Also recently, Venkata and Goodman [10] used the waveform design approach in [9] for target discrimination in a multi-target environment (one true target, many false ones).

1.3 Report Overview

The first-order radar system model adopted for a subset of the analyses carried out to date is summarized in Section 2, in Appendix A, and in Appendix G. This model is exercised to generate the results presented in Sections 3 and 4, as well as in Appendices B-D. Section 3 discusses receiver implementation using a parameter estimation approach, which is one of the key contributions of this work. Sections 4 and 5 present waveform selection via information-theoretic criteria, based on mutual information and on marginal information, respectively. A summary of the conclusions attained to date and a list of future work topics is presented in Section 6. The appendices provide further detail and simulation-based results for the areas considered in the main sections.

2.0 RADAR SYSTEM MODEL

Figure 2-1 presents a block diagram for a candidate Adaptive Radar configuration for SAR that includes the features mentioned in Section 1.2. Considering the receive path first, the receiver adapts to receive distinct waveforms, and the sensed signal is processed to generate estimates of the complex-valued scatterers in the region of interest. In turn, the estimated scatterer values are used, jointly with available external information, to generate an estimate of the covariance matrix of the scatterers. The scatterer covariance matrix and scenario and system information are used by the Waveform Selector to specify the waveform for transmission in the next interval of relevance. This is the key element in making the concept adaptive, and it is implemented via novel applications of information theory. In this report the waveform is selected among the members of a pre-specified (external information), finite set, $\{s_i(n) \mid i = 1, 2, \ldots, J\}$. However, a more general (and complex) procedure can be established to generate the waveform based on the information-theoretic criteria and subject to realistic constraints, as in [9]. The specified waveform is generated in a manner suitable for transmission, passed on to the transmitter, and finally to the antenna array (either contiguous or sparse). The highlighted blocks in Figure 2-1 are key novel elements of the radar concept postulated herein. Evaluation of these powerful concepts is carried out with the aid of a simple first-order model for the received signal.

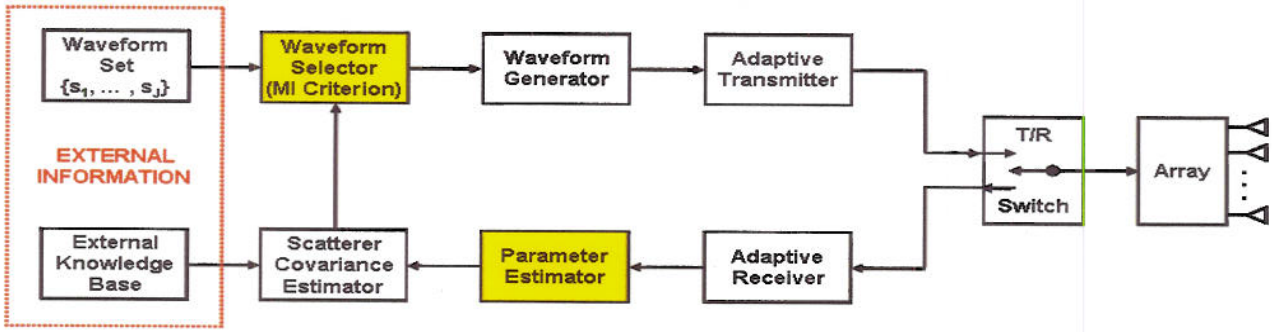

Figure 2-1. Candidate adaptive radar configuration for SAR, with key blocks highlighted (Parameter Estimator and Waveform Selector).

2.1 *MONOSTATIC SINGLE POLARIZATION MODEL*

Consider a monostatic airborne or spaceborne radar system operating in SAR mode. For such a system the received radar signal over an appropriately-selected time interval can be represented as vector **b** over (discrete) space and time. Specifically, the received signal admits a model of the form

$$\mathbf{b} = \mathbf{a} + \mathbf{w} = \mathbf{S}\boldsymbol{\alpha} + \mathbf{w}, \qquad (2.1\text{-}1)$$

where $\boldsymbol{\alpha}$ denotes the M-element vector of complex-valued scattering coefficients in the ground region of interest, $\mathbf{S}$ denotes the KxM sensing (measurement) complex-valued model matrix, and $\mathbf{w}$ denotes the K-element zero-mean, Gaussian-distributed complex-valued receiver noise vector that is uncorrelated over space and time and with (diagonal) covariance matrix $E[\mathbf{w}\mathbf{w}^H] = \mathbf{R}_{ww}$. Without loss of generality, $\boldsymbol{\alpha}$ is also a zero-mean, Gaussian-distributed random process with covariance matrix $E[\boldsymbol{\alpha}\boldsymbol{\alpha}^H] = \mathbf{R}_{\alpha\alpha}$, where the superscript H denotes Hermitian (conjugate transpose) operator. More detailed description of the radar signal model is in Appendix A. This model is exercised in obtaining the results presented in most of the work to date.

2.2 *MONOSTATIC FULLY POLARIMETRIC MODEL*

In order to accurately model polarimetric scattering, a vector model is required. Additionally, the concept of the polarization ellipse that describes the electric field vector rotations in space/time is a useful visualization and modeling aid. The concept of polarization basis vectors is useful mathematically, and has value in understanding and describing physical relationships. Different basis vector decompositions of the polarimetric electric field vector are possible for different applications, and each provides different physical and mathematical insight.

2.2.1 The Electromagnetic Vector Wave and Key Polarization Descriptors

The fundamental relations of radar polarimetry are obtained directly from Maxwell's equations [12, 13], where for the source-free isotropic, homogeneous, free space propagation space, and assuming IEEE standard [14] time-dependence $\exp(+j\omega t)$, the electric $\mathbf{E}$ and magnetic $\mathbf{H}$ fields satisfy with μ being the free space permeability and ε the free space permittivity

$$\nabla \mathrm{x}\mathbf{E}(\mathbf{r}) = -j\omega\mu\mathbf{H}(\mathbf{r}), \qquad \nabla \mathrm{x}\mathbf{H}(\mathbf{r}) = j\omega\varepsilon\,\mathbf{E}(\mathbf{r}) \tag{2.2-1}$$

which for the time-invariant case result in

$$(\nabla + k^2)\mathbf{E} = 0, \quad \mathbf{E}(\mathbf{r}) = E_0 \frac{\exp(-jkr)}{r}, \quad \mathbf{H}(\mathbf{r}) = H_0 \frac{\exp(-jkr)}{r} \tag{2.2-2}$$

for an outgoing spherical wave with propagation constant $k = \omega\,(\varepsilon\,\mu)^{1/2}$, and $c = (\varepsilon\,\mu)^{-1/2}$ being the free space velocity of electromagnetic waves. No further details are presented here, and we refer to Stratton [12] and Mott [15] for full presentations.

With the use of the standard spherical coordinate system $\left(r,\theta,\phi\,;\hat{\mathrm{u}}_r,\hat{\mathrm{u}}_\theta,\hat{\mathrm{u}}_\phi\right)$ with r,θ,ϕ denoting the radial, polar, azimuthal coordinates, and $\hat{\mathrm{u}}_r,\hat{\mathrm{u}}_\theta,\hat{\mathrm{u}}_\phi$ the corresponding unit vectors, respectively, the outward travelling wave is expressed as:

$$\mathbf{E} = \hat{\mathrm{u}}_\theta\, E_\theta + \hat{\mathrm{u}}_\phi E_\phi \quad \mathbf{H} = \hat{\mathrm{u}}_\theta\, H_\theta + \hat{\mathrm{u}}_\phi\, H_\phi \;,\; \mathbf{P} = \frac{\hat{\mathrm{u}}_r}{2}\left|\mathbf{E}\times\mathbf{H}^*\right| = \frac{\hat{\mathrm{u}}_r\,|\mathrm{E}|^2}{2Z_0} \;,\; Z_0 = \left(\frac{\mu_0}{\varepsilon_0}\right)^{1/2} = 120\pi\ [\Omega] \tag{2.2-3}$$

with $\mathbf{P}$ denoting the Poynting power density vector, and Z_0 being the intrinsic impedance of the medium (here vacuum). Far from the antenna in the far field region [12, 15], the radial waves of (2.2-3) take on plane wave characteristics, and assuming the wave to travel in the positive z-direction of a right-handed Cartesian coordinate system (x,y,z), the electric field $\mathbf{E}$, denoting the polarization vector, may be rewritten as

$$\mathbf{E} = \hat{\mathrm{u}}_x E_x + \hat{\mathrm{u}}_y E_y = \left|E_x\right| \exp(j\phi_x)\{\hat{\mathrm{u}}_x + \hat{\mathrm{u}}_y \left|\frac{E_y}{E_x}\right| \exp(j\phi)\}, \tag{2.2-4}$$

with $|E_x|, |E_y|$ being the amplitudes, ϕ_x, ϕ_y the phases, $\phi = \phi_y - \phi_x$ the relative phase, $|E_x / E_y| = \tan\alpha$ with ϕ_x, ϕ_y, α and ϕ defining the Deschamps parameters [16, 17]. Using these definitions, the 'normalized complex polarization vector **p**', and the 'complex polarization ratio ρ', can be defined as

$$\mathbf{p} = \frac{\mathbf{E}}{|\mathbf{E}|} = \frac{\hat{u}_x E_x + \hat{u}_y E_y}{|\mathbf{E}|} = \frac{E_x}{|\mathbf{E}|}\left(\hat{u}_x + \rho\, \hat{u}_y\right) \tag{2.2-5}$$

with $|\mathbf{E}|^2 = \mathbf{E}\cdot\mathbf{E}^* = E_x^{\,2} + E_y^{\,2}$ and $|\mathbf{E}| = E$ defines the wave amplitude, and ρ is given by

$$\rho = \frac{E_y}{E_x} = \left|\frac{E_y}{E_x}\right| \exp(j\phi), \qquad \phi = \phi_y - \phi_x. \tag{2.2-6}$$

2.2.2 The Polarization Ellipse and its Parameters

The tip of the real time-varying vector **E**, or **p**, traces an ellipse for general phase difference ϕ, where we distinguish between right-handed (clockwise) and left-handed (counter-clockwise) when viewed by the observer in direction of the travelling wave [15, 18], as shown in Figure 2-2 for the commonly used horizontal H (by replacing x) and vertical V (by replacing y) polarization states.

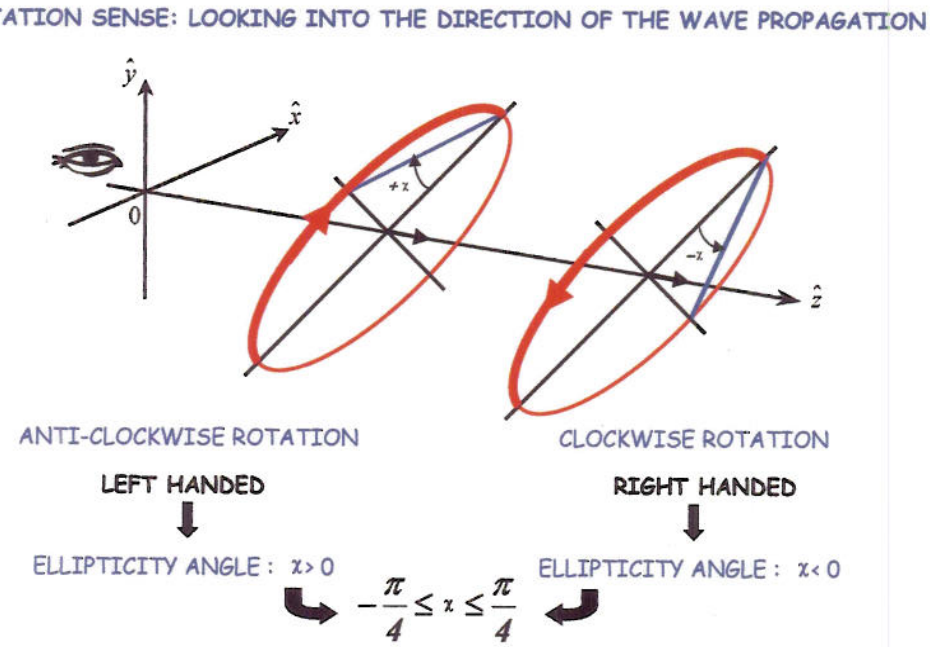

(a) Rotation sense (Courtesy of Prof. E. Pottier).

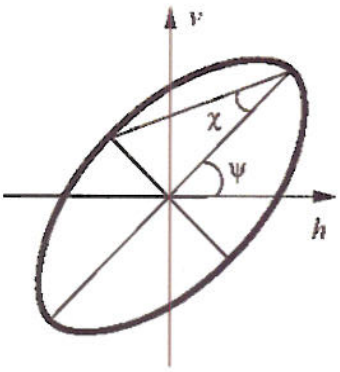

(b) Orientation ψ and ellipticity χ angles

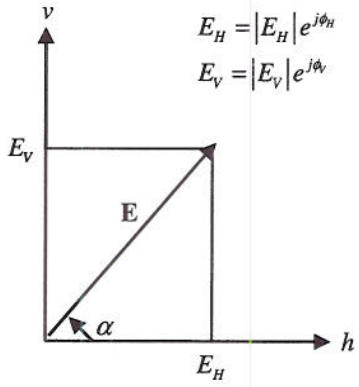

(c) Electric field vector definition.

Figure 2-2. Polarization ellipse adopted for standard definitions definitions.

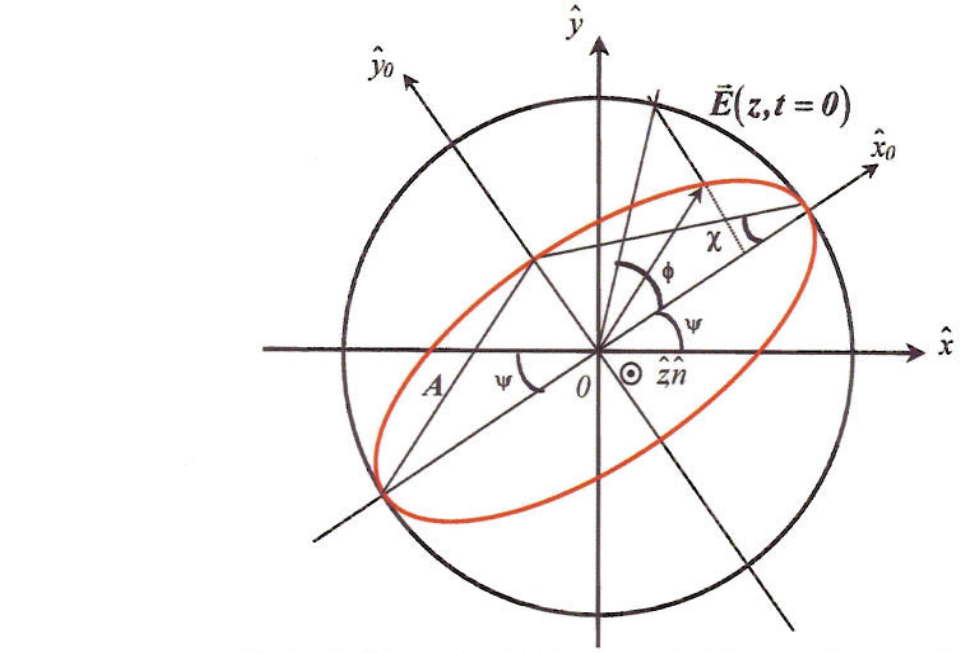

Figure 2-3. Polarization ellipse relations (Courtesy of Prof. E. Pottier).

There exist unique relations between the alternate representations, as defined in Figures 2-2 and 2-3 with the definition of the orientation ψ and ellipticity χ angles expressed, respectively, as

$$\alpha = |\rho| = \frac{|E_y|}{|E_x|},\ 0 \le \alpha \le \pi/2 \quad \text{and} \quad \tan 2\psi = \tan(2\alpha)\cos\phi \qquad -\pi/2 \le \psi \le +\pi/2 \qquad (2.2\text{-}7)$$

$$\tan\chi = \pm \textit{minor axis/major axis}, \qquad \sin 2\chi = \sin 2\alpha \sin\phi\ , \qquad -\pi/4 \le \chi \le \pi/4 \qquad (2.2\text{-}8)$$

where the + and – signs are for left- and right-handed polarizations, respectively.

For a pair of orthogonal polarizations $\mathbf{p}_1$ and $\mathbf{p}_2 = \mathbf{p}_{1_\perp}$,

$$\mathbf{p}_1 \cdot \mathbf{p}_2^{\,*} = 0 \qquad \rho_2 = \rho_{1_\perp} = -1/\rho_1^* \ , \qquad \psi_1 = \psi_2 + \frac{\pi}{2} \qquad \chi_1 = -\chi_2 \, . \qquad (2.2\text{-}9)$$

In addition, the following useful transformation relations exist:

$$\rho = \frac{\cos 2\chi \sin 2\psi + j \sin 2\chi}{1 + \cos 2\chi \cos 2\psi} = \tan\alpha \exp(j\phi)\,, \qquad (2.2\text{-}10)$$

where (α,ϕ) and (ψ,χ) are related by the following equations:

$$\cos 2\alpha = \cos 2\psi \cos 2\chi, \quad \tan\phi = \tan 2\chi / \sin 2\psi, \tag{2.2-11a}$$

and inversely,

$$\psi = \frac{1}{2}\arctan\left(\frac{2\mathrm{Re}\{\rho\}}{1-\rho\rho^*}\right) + \pi \quad \textbf{...mod}(\pi) \quad \chi = \frac{1}{2}\arcsin\left(\frac{2\mathrm{Im}\{\rho\}}{1-\rho\rho^*}\right). \tag{2.2-11b}$$

Another useful formulation of the polarization vector **p** was introduced by Huynen in terms of the parametric formulation [19, 20] derived from group-theoretic considerations based on the Pauli SU(2) matrix set $\psi_P\{[\sigma_i],\ i=0,1,2,3\}$ as further pursued by Pottier [21], where according to Equations (2.2-11a, b), for $\psi = 0$, and then rotating this ellipse by ψ:

$$\mathbf{p}(|\mathbf{E}|,\phi,\psi,\chi) = |\mathbf{E}|\exp(j\phi)\begin{bmatrix}\cos\psi & -\sin\psi\\ \sin\psi & \cos\psi\end{bmatrix}\begin{bmatrix}\cos\chi\\ -j\sin\chi\end{bmatrix}, \tag{2.2-12}$$

which will be utilized later on, and $\psi_P\{[\sigma_i],\ i=0,1,2,3\}$ is defined in terms of the classical unitary Pauli matrices $[\sigma_i]$ as

$$[\sigma_0]=\begin{bmatrix}1 & 0\\ 0 & 1\end{bmatrix}, \quad [\sigma_1]=\begin{bmatrix}1 & 0\\ 0 & -1\end{bmatrix}, \quad [\sigma_2]=\begin{bmatrix}0 & 1\\ 1 & 0\end{bmatrix}, \quad [\sigma_3]=\begin{bmatrix}0 & -j\\ j & 0\end{bmatrix}, \tag{2.2-13}$$

where the $[\sigma_i]$ matrices satisfy the unitarity condition and the commutation properties given by

$$[\sigma_i]^{-1}=[\sigma_i]^{T^*}, \quad \left|Det\{[\sigma_i]\}\right|=1, \quad [\sigma_i][\sigma_j]=-[\sigma_j][\sigma_i], \quad [\sigma_i][\sigma_i]=[\sigma_0], \tag{2.2-14}$$

and also satisfy the ordinary matrix product relations.

2.2.3 The Jones Vector and Changes of Polarization Bases

If instead of the basis {x y} or {H V}, we introduce an alternative presentation {m n} as a linear combination of two arbitrary orthonormal polarization states $\mathbf{E}_m$ and $\mathbf{E}_n$ for which

$$\mathbf{E} = \hat{\mathbf{u}}_m E_m + \hat{\mathbf{u}}_n E_n, \tag{2.2-15}$$

and the standard basis vectors are in general orthonormal, i.e.,

$$\hat{\mathrm{u}}_m \cdot \hat{\mathrm{u}}_n^{\dagger} = 0, \quad \hat{\mathrm{u}}_m \cdot \hat{\mathrm{u}}_m^{\dagger} = \hat{\mathrm{u}}_{\mathrm{n}} \cdot \hat{\mathrm{u}}_n^{\dagger} = 1, \tag{2.2-16}$$

with † denoting the Hermitian adjoint operator [22, 23, 24], and the Jones vector $\mathbf{E}_{mn}$ defined as

$$\mathbf{E}_{mn} = \begin{bmatrix} E_m \\ E_n \end{bmatrix} = \begin{bmatrix} |E_m| \exp j\phi_m \\ |E_n| \exp j\phi_n \end{bmatrix} = E_m \begin{bmatrix} 1 \\ \rho \end{bmatrix} = \frac{|\mathbf{E}| \exp(j\phi_m)}{\sqrt{1+\rho\rho^*}} \begin{bmatrix} 1 \\ \rho \end{bmatrix} = |\mathbf{E}| \exp(j\phi_m) \begin{bmatrix} \cos\alpha \\ \sin\alpha \exp(j\phi) \end{bmatrix} \tag{2.2-17}$$

with $\tan\alpha = |E_n / E_m|$ and $\phi = \phi_n - \phi_m$. This states that the Jones vector possesses, in general, four degrees of freedom. The Jones vector descriptions for characteristic polarization states are provided in Figure 2-4.

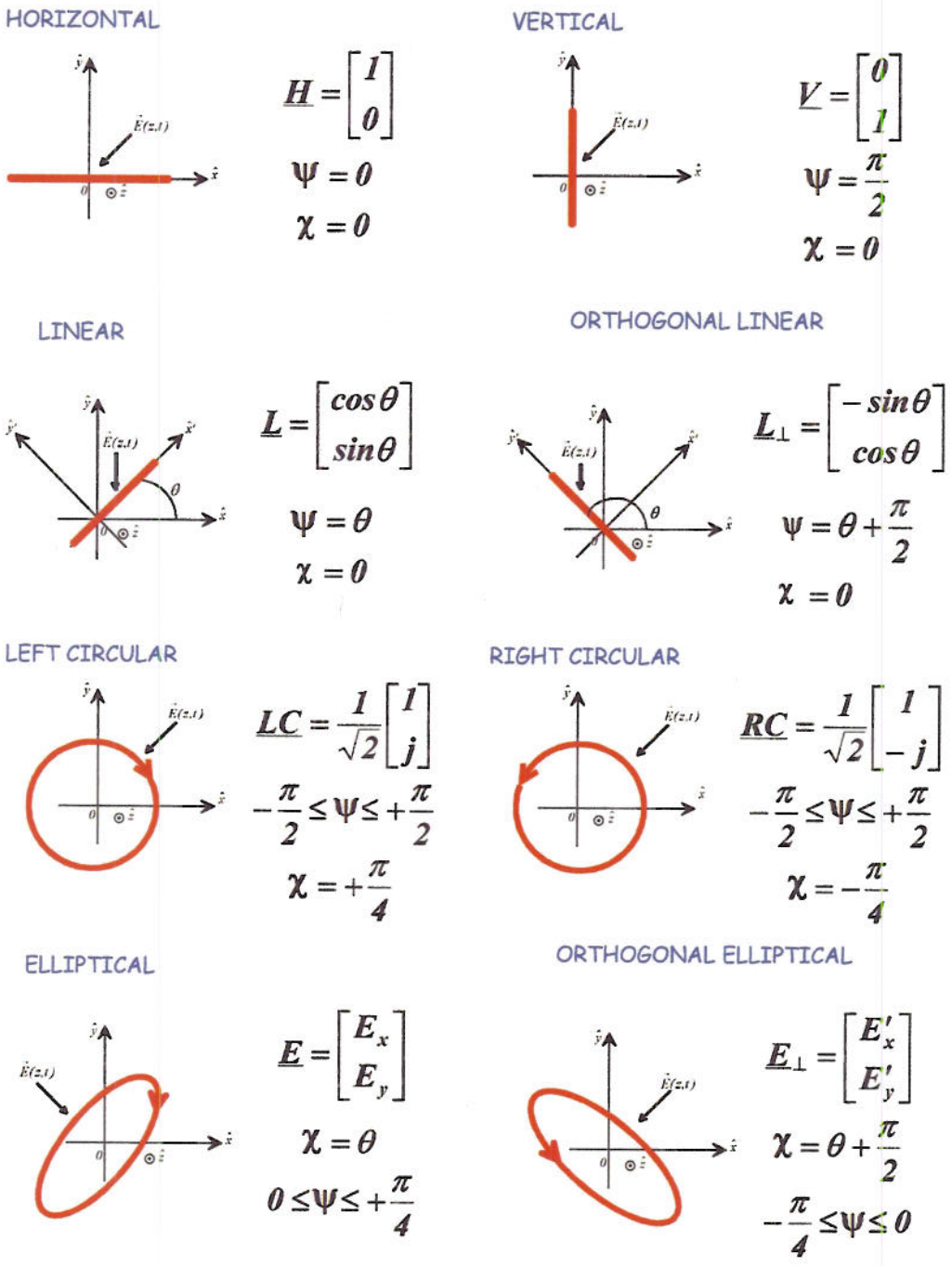

Figure 2-4. Jones vector descriptions for characteristic polarization states with direction of propagation out of the page (Courtesy of Prof. E. Pottier).

Since any monochromatic plane wave can be expressed as a linear combination of two orthonormal linear polarization states, defining the reference polarization basis, there exist an infinite number of such bases {i j} or {A B} for which

$$\mathbf{E} = \hat{\mathrm{u}}_m E_m + \hat{\mathrm{u}}_n E_n = \hat{\mathrm{u}}_i E_i + \hat{\mathrm{u}}_j E_j = \hat{\mathrm{u}}_A E_A + \hat{\mathrm{u}}_B E_B \qquad (2.2\text{-}18)$$

with corresponding Jones vectors presented in two alternate, most commonly used notations:

$$\mathbf{E}_{mn} = \mathbf{E}(m,n) = \begin{bmatrix} E_m \\ E_n \end{bmatrix}, \quad \mathbf{E}_{ij} = \mathbf{E}(i,j) = \begin{bmatrix} E_i \\ E_j \end{bmatrix}, \quad \text{and} \quad \mathbf{E}_{AB} = \mathbf{E}(A,B) = \begin{bmatrix} E_A \\ E_B \end{bmatrix}. \tag{2.2-19}$$

The unique transformation from the $\{\hat{\mathbf{u}}_m\ \hat{\mathbf{u}}_n\}$ to the arbitrary $\{\hat{\mathbf{u}}_i\ \hat{\mathbf{u}}_j\}$ or $\{\hat{\mathbf{u}}_A\ \hat{\mathbf{u}}_B\}$ basis is sought which is a linear transformation in the two-dimensional complex space,

$$\mathbf{E}_{ij} = [U_2]\mathbf{E}_{mn} \quad or \quad \mathbf{E}(i,j) = [U_2]\mathbf{E}(m,n) \quad \text{with} \quad [U_2]\,[U_2]^{\dagger} = [I_2]. \tag{2.2-20}$$

The transformation must satisfy the wave energy conservation with $[I_2]$ being the 2x2 identity matrix, and we may choose, as shown in [25],

$$\hat{\mathbf{u}}_i = \frac{\exp(j\phi_i)}{\sqrt{1+\rho\rho^*}}\begin{bmatrix} 1 \\ \rho \end{bmatrix} \quad \text{and} \quad \hat{\mathbf{u}}_j = \hat{\mathbf{u}}_{i_\perp} = \frac{\exp(j\phi_i)}{\sqrt{1+\rho\rho^*}}\begin{bmatrix} 1 \\ -\rho^{*-1} \end{bmatrix} = \frac{\exp(j\phi_i)}{\sqrt{1+\rho\rho^*}}\begin{bmatrix} -\rho^* \\ 1 \end{bmatrix}, \tag{2.2-21}$$

with $\phi_j' = \phi_j + \phi + \pi$ so that

$$[U_2] = \frac{1}{\sqrt{1+\rho\rho^*}}\begin{bmatrix} \exp(j\phi_i) & -\rho^*\exp(j\phi_j) \\ \rho\exp(j\phi_i) & \exp(j\phi_j) \end{bmatrix}, \tag{2.2-22}$$

yielding $Det\{[U_2]\} = \exp\{j(\phi_i + \phi_j')\}$ with $\phi_i + \phi_j' = 0$.

$[U_2]$ is a special unitary 2x2 complex matrix with unit determinant, implying that: (i) the amplitude of the wave remains independent of the change of the polarization basis, and (ii) the phase of the (absolute) wave may be defined consistently as the polarization basis is changed. These issues lead to

$$[U_2] = \frac{1}{\sqrt{1+\rho\rho^*}}\begin{bmatrix} 1 & -\rho^* \\ \rho & 1 \end{bmatrix}\begin{bmatrix} \exp(j\phi_i) & 0 \\ 0 & \exp(j\phi_i) \end{bmatrix}, \tag{2.2-23}$$

which possesses three degrees of freedom similar to the normalized Jones vector formulation, but in most cases the phase reference is taken as $\phi_i = 0$, which may not be the case in polarimetric interferometry [26]. For further details on the group-theoretic representations of the proper transformation relations see the formulations derived by Pottier in [21].

2.2.4 Radar Polarimetric Data Model

Consider a narrowband monostatic airborne or spaceborne radar system with full-polarization transmitter and receiver operating in synthetic aperture radar (SAR) mode. Further consider that the system transmits a short-duration pulse to provide inherent (without pulse compression) high range resolution. For such a system the received radar signal over an appropriately-selected time interval can be represented as vector $\mathbf{b}$ over space and time. Specifically, for a single transmitted and received pulse, the received (baseband) signal admits a model of the form

$$\mathbf{b} = \mathbf{a} + \mathbf{w} = \mathbf{H}\boldsymbol{\alpha} + \mathbf{w}\,, \tag{2.2-24}$$

where $\boldsymbol{\alpha}$ denotes the $(4M)$-element vector of M complex-valued scattering coefficients in the ground region of interest, and each ground scatterer is characterized by the four elements of its polarization scattering matrix in the conventional horizontal (H) and vertical (V) axes at the scatterer location. Matrix $\mathbf{H}$ denotes the Kx$(4M)$ sensing (measurement) model matrix, and $\mathbf{w}$ denotes the K-element zero-mean, Gaussian-distributed complex-valued receiver noise vector that is uncorrelated over space and time and with covariance matrix

$$\mathrm{E}\left[\mathbf{w}\,\mathbf{w}^{\mathrm{H}}\right] = \mathbf{R}_{\mathrm{ww}} = \sigma_w^2\,\mathbf{I}_K\,. \tag{2.2-25}$$

The random variates $\mathbf{w}$ are assumed to be analytic signals, which implies that they are circular random variates and admit the standard complex Gaussian probability density function (PDF) for such variates. For the case herein, $K = 2M$ since there are two measurements (H and V) for each ground scatterer.

The received signal vector ($\mathbf{b}$) and the scattering coefficient vector ($\boldsymbol{\alpha}$) are defined as partitioned vectors of the form

$$\mathbf{b} = \begin{bmatrix} \mathbf{b}_1 \\ \mathbf{b}_2 \\ \vdots \\ \mathbf{b}_M \end{bmatrix}, \tag{2.2-26}$$

$$\boldsymbol{\alpha} = \begin{bmatrix} \boldsymbol{\alpha}_1 \\ \boldsymbol{\alpha}_2 \\ \vdots \\ \boldsymbol{\alpha}_M \end{bmatrix}, \tag{2.2-27}$$

respectively. In turn, each of the M sub-vectors $\{\mathbf{b}_m \,|\, m = 1, 2, \ldots, M\}$ contains the two outputs of the full-polarization receiver in the H and V axes at the scatterer location,

$$\mathbf{b}_m = \begin{bmatrix} b_{m\mathrm{H}} \\ b_{m\mathrm{V}} \end{bmatrix}. \tag{2.2-28}$$

Likewise, each of the M sub-vectors $\{\boldsymbol{\alpha}_m \mid m = 1, 2, \ldots, M\}$ contains the four elements of the polarization scattering matrix for the mth scatterer in the H and V axes at the scatterer location,

$$\boldsymbol{\alpha}_m = \begin{bmatrix} \alpha_{m\mathrm{HH}} \\ \alpha_{m\mathrm{HV}} \\ \alpha_{m\mathrm{VH}} \\ \alpha_{m\mathrm{VV}} \end{bmatrix}. \tag{2.2-29}$$

With respect to the polarization scattering matrix elements in Equation (2.2-29), the first polarization-specific subscript represents the transmit component, and the second polarization-specific subscript represents the receive component [3]. The scattering coefficients satisfy various conditions, depending on the scatterer scenario. For example, $\alpha_{m\mathrm{HV}} = \alpha_{m\mathrm{VH}}$ is often satisfied. Identical partitioning and sub-partitioning is defined for vectors **a** and **w**.

The measurement involving the mth scatterer can be represented as two separate scalar measurements. Namely,

$$b_{m\mathrm{H}} = \alpha_{m\mathrm{HH}} h_{\mathrm{H}} + \alpha_{m\mathrm{VH}} h_{\mathrm{V}} + w_{m\mathrm{H}}, \tag{2.2-30a}$$

$$b_{m\mathrm{V}} = \alpha_{m\mathrm{HV}} h_{\mathrm{H}} + \alpha_{m\mathrm{VV}} h_{\mathrm{V}} + w_{m\mathrm{V}}, \tag{2.2-30b}$$

where variables h_{H} and h_{V} represent the complex-valued scalar modulation signal components for H and V, respectively. These scalars (h_{H} and h_{V}) are the elements of the phasor representing the electric field with full polarization in far-field conditions. This phasor is referred to as the Jones vector in the polarization literature (see, for example, [27]). In general form and in the H and V basis, the Jones vector for a full-polarization field is defined as

$$\mathrm{E} = \begin{bmatrix} E_{\mathrm{H0}}\, e^{j\delta_{\mathrm{H}}} \\ E_{\mathrm{V0}}\, e^{j\delta_{\mathrm{V}}} \end{bmatrix} = \begin{bmatrix} h_{\mathrm{H}} \\ h_{\mathrm{V}} \end{bmatrix}. \tag{2.2-31}$$

Here E_{H0} and E_{V0} denote the real-valued scalar amplitude of the H and V components of the electric field, respectively. Also, δ_{H} and δ_{V} denote the phase delay (radians) of the H and V components of the electric field, respectively. Equation (2.2-31) suggests that the four real-valued phasor parameters $\{E_{\mathrm{H0}}, E_{\mathrm{V0}}, \delta_{\mathrm{H}}, \delta_{\mathrm{V}}\}$ specify the electric field and its polarization state completely, and such is indeed the case. Alternative parameterizations are possible (such as the one involving the so-called geometrical parameters), but any single parameterization suffices to define the polarization state.

It follows from Equations (2.2-26) to (2.2-31) that the measurement matrix **H** in Equation (2.2-24) has a partitioned structure of the form

$$\mathbf{H} = \begin{bmatrix} \mathbf{H}_{00} & \mathbf{O} & \cdots & \mathbf{O} \\ \mathbf{O} & \mathbf{H}_{00} & \cdots & \mathbf{O} \\ \vdots & \vdots & \ddots & \vdots \\ \mathbf{O} & \mathbf{O} & \cdots & \mathbf{H}_{00} \end{bmatrix}, \tag{2.2-32}$$

where each $\mathbf{O}$ represents a 2x4 matrix of zeros, and the sub-matrix $\mathbf{H}_{00}$ that appears repeated M times along the block diagonal is of the form

$$\mathbf{H}_{00} = \begin{bmatrix} h_{\mathrm{H}} & 0 & h_{\mathrm{V}} & 0 \\ 0 & h_{\mathrm{H}} & 0 & h_{\mathrm{V}} \end{bmatrix}. \tag{2.2-33}$$

In summary, the received signal corresponding to the return of a single pulse illuminating the mth scatterer is given as

$$\mathbf{b}_m = \mathbf{H}_{00}\boldsymbol{\alpha}_m + \mathbf{w}_m, \tag{2.2-34}$$

for $m = 1, 2, \ldots, M$.

Finally, let the scattering coefficients be samples from a zero-mean multivariate complex-valued Gaussian distribution with $(4M)$x$(4M)$ covariance matrix

$$\mathrm{E}\left[\boldsymbol{\alpha}\boldsymbol{\alpha}^{\mathrm{H}}\right] = \mathbf{R}_{\alpha\alpha} \tag{2.2-35}$$

Random variates $\boldsymbol{\alpha}$ are assumed to be analytic signals, which implies that they are circular random variates and admit the standard complex Gaussian probability density function (PDF) for such variates.

The analytic model formulated above is of the form adopted in the formulation of the information theoretic criterion in [6]. Thus, the MI criterion applies directly to the polarization diversity problem as defined above, without any modification.

2.3 *Monostatic Temporal Diversity Model*

The signal model for temporal/modulation diversity is a straightforward extension to the single waveform case described in Section 2.1. The specific case considered next is a single aperture alternating between two different waveforms. The extension to more waveforms is straightforward. The receive signal model for the receiver at various times is shown below:

$$\mathbf{b}(\mathrm{n}) = \mathbf{H}(\mathrm{n})\boldsymbol{\alpha}_1(\mathrm{n}) + \mathbf{H}(\mathrm{n}\text{-}1)\boldsymbol{\alpha}_2(\mathrm{n}), \tag{2.3-1}$$

$$\mathbf{b}(\mathrm{n}+1) = \mathbf{H}(\mathrm{n}+1)\boldsymbol{\alpha}_1(\mathrm{n}+1) + \mathbf{H}(\mathrm{n})\boldsymbol{\alpha}_2(\mathrm{n}+1), \tag{2.3-2}$$

$$\mathbf{b}(n+2) = \mathbf{H}(n+2)\boldsymbol{\alpha}_1(n+2) + \mathbf{H}(n+1)\boldsymbol{\alpha}_2(n+2)\,, \tag{2.3-3}$$

where $\mathbf{b}(n)$ is the receive signal at PRI n, $\mathbf{H}(n)$ is the $\mathbf{H}$ matrix as defined previously for the waveform transmitted at PRI n, and $\boldsymbol{\alpha}_x(n)$ is the complex scattering coefficients at PRI n for ambiguous range bin section x. In this particular example $\boldsymbol{\alpha}_1$ is ambiguous with $\boldsymbol{\alpha}_2$. We can write an equation to simultaneously solve for two PRI's as follows:

$$\begin{bmatrix} \mathbf{b}(n) \\ \mathbf{b}(n+1) \end{bmatrix} = \begin{bmatrix} \mathbf{H}(n) & \mathbf{H}(n-1) \\ \mathbf{H}(n+1) & \mathbf{H}(n) \end{bmatrix} \begin{bmatrix} \underline{\boldsymbol{\alpha}}_1(n) \\ \underline{\boldsymbol{\alpha}}_2(n) \end{bmatrix} \tag{2.3-4}$$

where,

$$\underline{\boldsymbol{\alpha}}_1(n) = [\boldsymbol{\alpha}_1(n)+\boldsymbol{\alpha}_1(n+1)]/2\,, \tag{2.3-5}$$

$$\underline{\boldsymbol{\alpha}}_2(n) = [\boldsymbol{\alpha}_2(n)+\boldsymbol{\alpha}_2(n+1)]/2\,. \tag{2.3-6}$$

This equation is recalculated for each subsequent PRI as shown below

$$\begin{bmatrix} \mathbf{b}(n+1) \\ \mathbf{b}(n+2) \end{bmatrix} = \begin{bmatrix} \mathbf{H}(n+1) & \mathbf{H}(n) \\ \mathbf{H}(n+2) & \mathbf{H}(n+1) \end{bmatrix} \begin{bmatrix} \underline{\boldsymbol{\alpha}}_1(n+1) \\ \underline{\boldsymbol{\alpha}}_2(n+1) \end{bmatrix}. \tag{2.3-7}$$

All PRI's are solved in a like manner.

2.4 *Quasi-Monostatic Spatial Diversity Model*

The signal model for spatial/modulation diversity is a straightforward extension to the single waveform case described in Section 2.1. The specific example modeled is two independent transmitter/receiver pairs each transmitting a different waveform, and each receiving both signals. The generalization to more transmitters and receivers is obvious. The receive signal model for each receiver is shown below, which is an extension to the model in Equation (2.2-24) by a second waveform and different scattering coefficient due to the different transmitter/receiver geometry:

$$\mathbf{b}_1 = \mathbf{H}_1\boldsymbol{\alpha}_1 + \mathbf{H}_2\boldsymbol{\alpha}_{12}\,, \tag{2.4-1}$$

$$\mathbf{b}_2 = \mathbf{H}_1\boldsymbol{\alpha}_{12} + \mathbf{H}_2\boldsymbol{\alpha}_2\,, \tag{2.4-2}$$

where $\mathbf{b}_x$ is the received signal from receiver x, $\mathbf{H}_x$ is the $\mathbf{H}$ matrix as described previously for waveform x, and $\boldsymbol{\alpha}_x$ is the complex scattering coefficient vector for transmitter/receiver x, while $\boldsymbol{\alpha}_{xy}$ is the complex scattering coefficient vector for transmitter x and receiver y. It is assumed that $\boldsymbol{\alpha}_{xy} = \boldsymbol{\alpha}_{yx}$. We can rewrite these equations in matrix form as:

$$\begin{bmatrix} \mathbf{b}_1 \\ \mathbf{b}_2 \end{bmatrix} = \begin{bmatrix} \mathbf{H}_1 & \mathbf{H}_2 & \mathbf{0} \\ \mathbf{0} & \mathbf{H}_1 & \mathbf{H}_2 \end{bmatrix} \begin{bmatrix} \boldsymbol{\alpha}_1 \\ \boldsymbol{\alpha}_{12} \\ \boldsymbol{\alpha}_2 \end{bmatrix}. \tag{2.4-3}$$

Sample results from a simulation of a pulse compression processing function using this equation for two transmitter-receivers, one of which transmits an up-chirp LFM, and the second transmits an in-band, coherent down-chirp LFM, are presented in Figure 2-5.

Equation (2.4-3) is under-determined. The task is to determine an approximate relationship

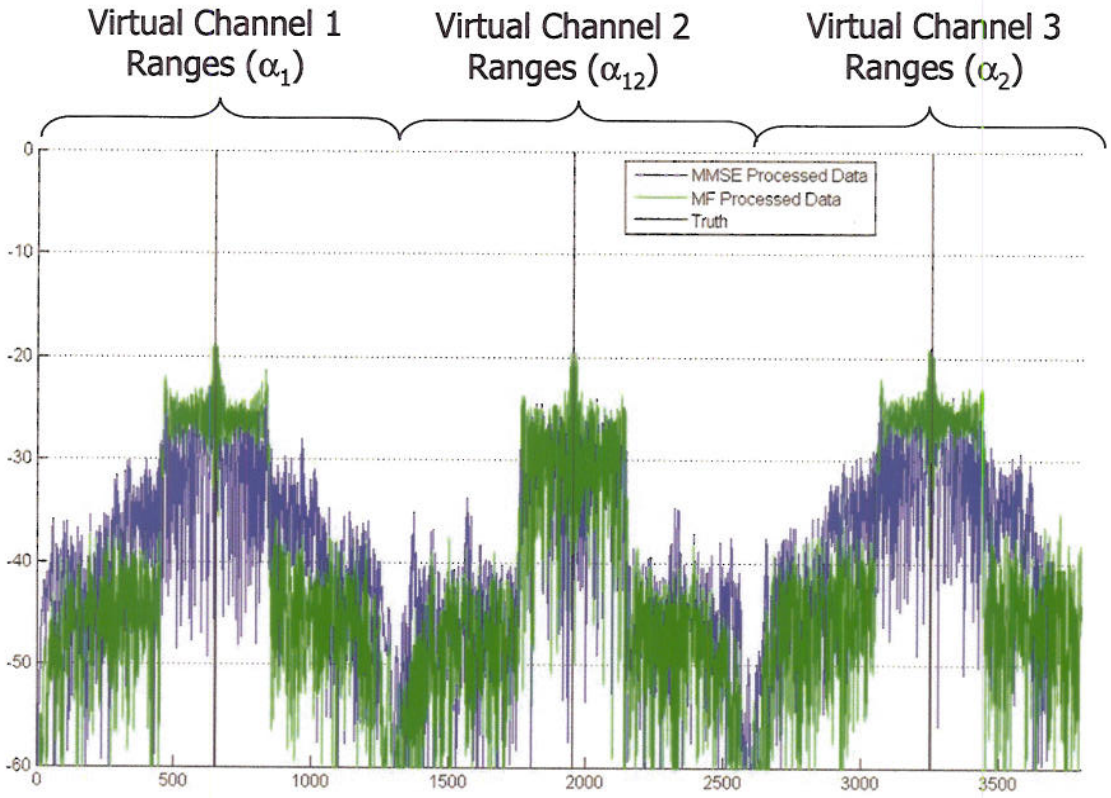

Figure 2-5. Simulation of Spatial Diversity Pulse Compression Eqn. (2.4-3) shows significant sidelobe improvement over MF bank approach

between the three alpha values to decrease the number of independent values to be estimated. We can imagine the case where the two apertures are contiguous with each other. In that case we could assume that the third virtual location formed by the two different transmitter receiver pairs at the midpoint between the two apertures would see scatterers that were the average of the other two values. In that case a linear fit from $\boldsymbol{\alpha}_1$ to $\boldsymbol{\alpha}_2$ would be an accurate model. As we begin to separate the apertures farther apart this approximation eventually becomes invalid. Future work is required to identify approximation error bounds as a function of separation. We can rewrite the three $\boldsymbol{\alpha}$'s in the following way:

$$\boldsymbol{\alpha}_1 = \boldsymbol{\alpha} - \Delta\boldsymbol{\alpha}\,, \tag{2.4-4}$$

$$\alpha_{12} = \alpha\,, \tag{2.4-5}$$

$$\alpha_2 = \alpha + \Delta\alpha\,. \tag{2.4-6}$$

Based on these definitions, Equation (2.4-3) is rewritten as

$$\begin{bmatrix} \mathbf{b}_1 \\ \mathbf{b}_1 \end{bmatrix} = \begin{bmatrix} (\mathbf{H}_1 + \mathbf{H}_2) & -\mathbf{H}_1 \\ (\mathbf{H}_1 + \mathbf{H}_2) & \mathbf{H}_2 \end{bmatrix} \begin{bmatrix} \alpha \\ \Delta\alpha \end{bmatrix}. \tag{2.4-7}$$

This equation, while slightly under-determined, is of the same proportion as the single waveform case, which admits adequate solutions in many cases [4]. Future work should evaluate both spatially diverse waveform approaches from Eqs. 2.4-7 and 2.4-3. Figure 2-6 shows a plot of the singular values of the singular value decomposition (svd) for both **H** matrix formulations, along with the time-diverse form of Eqn. 2.3-7, and a single up-chirp LFM waveform for comparison. Specifically, in this figure the time diverse case alternates between up/down LFM chirps, while the spatial case has $\mathbf{H}_1$ as an up-chirp LFM, and $\mathbf{H}_2$ as a down-chirp LFM. All matrices have singular values that are all greater than one, and hence have well-posed pseudo-inverses. It is interesting to note that the matrix with the lowest singular value is Eqn. 2.4-7 (red curve of Figure 2-6). This implies that despite being more under-determined, Eqn. (2.4-3) should have better noise suppression than Eqn. (2.4-7), combined with being a more accurate signal model. A comparison of the estimation biases and total errors requires further investigation, as does the effect of other waveform choices.

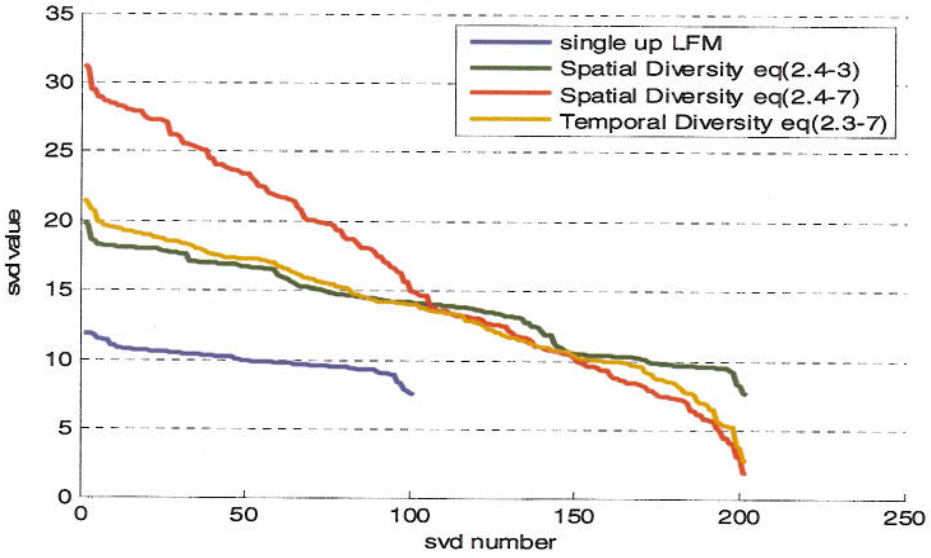

Figure 2-6. Comparison of singular values for single-, spatial-, and temporal-diversity measurement matrices (H) for waveform modulation cases.

2.5 *Alternative Space-Time Diversity Model*

A fundamental assumption in this research is that a radar is constructed wherein both the transmitter and receiver are described by true space-time functions. By true space-time, we mean that the functions that describe the transmit function and receiver weight function can be expressed as non-separable functions of space and time. For example, standard phased-array radar implements one transmitter, generating one temporal function. Likewise, one temporal receiver (i.e., one channel) is implemented. The spatial weighting for the transmitter and receiver array is a function of spatial position only, and thus the space-time function describing the system is simply a (separable) product of these spatial and temporal functions.

Conversely, for a true space-time radar the space-time functions describing the transmitter and receiver are non-separable. This result is accomplished in the transmitter by applying a coherent but independent temporal transmitter to each individual spatial element, and in the receiver by applying coherent but independent temporal receivers at each individual spatial element. The increase in both the dimensionality of the latter (non-separable) implementation over the former (separable) implementation is striking. In the separable case, the transmit/receive signal dimension is approximately the **sum** of the temporal time-bandwidth product and the number of spatial elements. For the non-separable implementation, the transmit/receive signal dimension is approximately the **product** of the temporal time-bandwidth product and the number of spatial elements.

Thus, a true-space time radar receiver implemented with an abundance of spatial antenna elements can provide a wealth of independent receiver measurements. This of course is an implementation that enables digital beamforming, a now relatively common technology. Far less common is the implementation of a non-separable space-time transmitter. Such a transmitter allows for coherent but dissimilar temporal functions to be transmitted at each spatial element. These dissimilar functions can be completely correlated (resulting again in a separable space-time function), completely uncorrelated (i.e., mutually orthogonal), or partially correlated. Determining how to construct an optimal set of these functions, given a specific set or radar task, was the goal of this research.

There are, of course, an unaccountably infinite number of non-separable space-time functions to consider when searching for an optimum solution, but this task is simplified in two ways. The first involves the design constraints associated with every radar system: limitations in bandwidth, time-width, aperture area, beamwidth, and transmit energy/power. A second simplification can occur if the space-time transmit function is expanded as a weighted superposition of space-time basis functions. The basis functions themselves are likewise constructed to fit completely the radar constraints of bandwidth, time-width, beamwidth, and aperture area.

To fully fill this signal space theoretically requires an infinite number of these basis functions. However, any space-time function can be represented approximately by a finite number of basis functions, provided that this finite value meets or exceeds the value of the signal time-bandwidth product times the aperture area-beamwidth product,

$$\vec{s}\,(\vec{r},t) \approx \sum_{n=1}^{N} s_n \, \hat{\phi}_n\,(\vec{r},t)\,. \tag{2.5-1}$$

Given this expansion, our optimization problem is reduced to finding an appropriate finite set of complex weight coefficients s_n. This expansion can be, but need not be, mathematically abstract.

Rather, the space-time basis functions can have a direct physical meaning. A spatial basis function can describe the impressed or equivalent currents of an antenna array element, while—for example—a temporal function can describe one of a set of pulse basis functions. In this manner, the coefficients s_n then describe physically the set of values driving the complex modulator at each array element.

In addition to simplifying the optimization problem, expanding the space-time transmit function as in Equation (2.5-1) allows modeling the propagation, scattering, and receiver phenomenology as a linear algebraic expression. This discrete linear model is more amenable to implementation as a software model/simulator; however, this model also allows the application of linear algebraic tools to search for optimal transmit vector solutions.

Specifically, start by defining a general space-time vector specifying a point in three dimensions of space and one of time as follows,

$$\bar{x} = [x, y, z, t] = [\bar{r}; t]\,. \tag{2.5-2}$$

Four position vectors are denoted to describe fields over each of 3 domains: the transmitted fields ($\bar{x}_t$), the scattered fields ($\bar{x}_s$), and the received fields ($\bar{x}_r$). The received space-time field is expressed in terms of a three-dimensional vector $\vec{r}$, which is required to define the polarization of this received signal across space and time; namely,

$$\vec{r}\,(\bar{x}_r) = \int \vec{\vec{H}}\,(\bar{x}_r; \bar{x}_s) \cdot \vec{\vec{\gamma}}\,(\bar{x}_s) \cdot \int \vec{\vec{G}}\,(\bar{x}_s; \bar{x}_t) \cdot \vec{s}\,(\bar{x}_t)\, d\bar{x}_t\, d\bar{x}_s\,. \tag{2.5-3}$$

The field $\vec{s}\,(\bar{x}_t)$ describes the transmit source over time and space. The matrix functions $\vec{\vec{G}}\,(\bar{x}_i; \bar{x}_t)$ and $\vec{\vec{H}}\,(\bar{x}_r; \bar{x}_s)$ are dyadic Green's functions that describe the propagation from the radar to the illuminated scatterers and back, while the dyadic $\vec{\vec{\gamma}}\,(\bar{x}_s)$ describes the polarimetric scattering response of all illuminated targets, for both distributed and point targets. The space-time transmit source is approximated by representing it in terms of a finite set of N vector space-time basis functions of the form

$$\vec{s}\,(\bar{x}_t) \approx \sum_{n=1}^{N} s_n\, \vec{\phi}_n\,(\bar{x}_t)\,. \tag{2.5-4}$$

Likewise, the scattering function $\vec{\vec{\gamma}}\,(\bar{x}_s)$ is approximated in terms of M basis functions $\vec{\vec{\psi}}_m\,(\bar{x}_s)$ as follows,

$$\vec{\vec{\gamma}}\,(\bar{x}_s) \approx \sum_{m=1}^{M} \gamma_m\, \vec{\vec{\psi}}_m\,(\bar{x}_s)\,. \tag{2.5-5}$$

Combining the three previous equations leads to

$$\vec{r}\,(\bar{x}_r) = \sum_m \gamma_m \sum_n s_n \int \vec{\vec{H}}\,(\bar{x}_r; \bar{x}_s) \cdot \vec{\vec{\psi}}_m\,(\bar{x}_s) \cdot \int \vec{\vec{G}}\,(\bar{x}_s; \bar{x}_t) \cdot \vec{\phi}_n\,(\bar{x}_t)\, d\bar{x}_t\, d\bar{x}_s\,. \tag{2.5-6}$$

Finally, the vector field $\vec{r}(\overline{x}_r)$ is expanded using a set of L vector basis functions $\vec{\varphi}_l(\overline{x}_r)$ as follows,

$$\vec{r}(\overline{x}_r) \approx \sum_{l=1}^{L} r_l \, \vec{\varphi}_l(\overline{x}_r). \tag{2.5-7}$$

If these vector basis functions are orthogonal, the scalar values r_l are determined as:

$$r_l = \int \vec{r}(\overline{x}_r) \cdot \vec{\varphi}_l(\overline{x}_r) \, d\overline{x}_r. \tag{2.5-8}$$

Then, combining Equations (2.5-6) to (2.5-8) leads to

$$r_l = \sum_m \gamma_m \sum_n s_n \int \vec{\varphi}_l(\overline{x}_r) \cdot \int \vec{\vec{H}}(\overline{x}_r;\overline{x}_s) \cdot \vec{\psi}_m(\overline{x}_s) \cdot \int \vec{\vec{G}}(\overline{x}_s;\overline{x}_t) \cdot \vec{\phi}_n(\overline{x}_t) \, d\overline{x}_t \, d\overline{x}_s \, d\overline{x}_r. \tag{2.5-9}$$

Evaluating the integrals, this expression simplifies to:

$$r_l = \sum_m \gamma_m \sum_n s_n \, \alpha_{lmn}, \tag{2.5-10}$$

where α_{lmn} is the following complex-valued scalar variable:

$$\alpha_{lmn} = \int \vec{\varphi}_l(\overline{x}_r) \cdot \int \vec{\vec{H}}(\overline{x}_r;\overline{x}_s) \cdot \vec{\psi}_m(\overline{x}_s) \cdot \int \vec{\vec{G}}(\overline{x}_s;\overline{x}_t) \cdot \vec{\phi}_n(\overline{x}_t) \, d\overline{x}_t \, d\overline{x}_s \, d\overline{x}_r. \tag{2.5-11}$$

Now select the sets of scalar values r_l, γ_m, and s_n to form the following column vectors:

$$\boldsymbol{\gamma} = \left[\gamma_1, \gamma_2, \gamma_3, \gamma_4, \cdots, \gamma_M\right]^T, \tag{2.5-12a}$$

$$\mathbf{s} = \left[s_1, s_2, s_3, s_4, \cdots, s_N\right]^T, \tag{2.5-12b}$$

$$\mathbf{r} = \left[r_1, r_2, r_3, r_4, \cdots, r_L\right]^T. \tag{2.5-12c}$$

The set of scalar values α_{lmn} can be organized into a "data cube" in each of the three dimensions with indices l, m, and n. This data cube can be described as the following set of MN column vectors with dimension L,

$$\mathbf{a}_{mn} = \left[\alpha_{1mn}, \alpha_{2mn}, \alpha_{3mn}, \cdots, \alpha_{Lmn}\right]^T. \tag{2.5-13}$$

The data cube can be described also as a set of M matrices, each of dimension LxN:

$$\mathbf{H}_m = \left[\mathbf{a}_{m1}; \mathbf{a}_{m2}; \mathbf{a}_{m3}; \cdots; \mathbf{a}_{mN}\right], \tag{2.5-14}$$

for $m = 1, 2, \ldots, M$. Alternatively, the data cube can be described as set of N matrices, each of dimension LxM:

$$\mathbf{B}_n = \left[\mathbf{a}_{1n}; \mathbf{a}_{2n}; \mathbf{a}_{3n}; \cdots; \mathbf{a}_{Mn}\right], \tag{2.5-15}$$

for $n = 1, 2, \ldots, N$. Using these definitions, we can write the measurement vector $\mathbf{r}$ as:

$$\begin{aligned} \mathbf{r} &= \sum_n s_n \, \mathbf{B}_n \gamma \\ &= \sum_n s_n \, \upsilon_n \quad , \\ &= \Upsilon \mathbf{s} \end{aligned} \tag{2.5-16}$$

where we have defined vector υ_n as:

$$\upsilon_n = \mathbf{B}_n \boldsymbol{\gamma}, \tag{2.5-17}$$

and matrix Υ as:

$$\Upsilon = \left[\upsilon_1; \upsilon_2; \upsilon_3; \cdots; \upsilon_N\right]. \tag{2.5-18}$$

It is apparent that matrix Υ relates the transmit signal vector $\mathbf{s}$ to the measurement vector $\mathbf{r}$. Matrix Υ is, therefore, a linear operator that describes the linear system that the transmit signal passes through as it moves from transmitter to receiver. As such, it includes the description of the scatterers it encounters (i.e., $\boldsymbol{\gamma}$). Vector υ_n can be viewed as the normalized response at the receiver due to transmit symbol s_n. In other words, $\mathbf{r} = \upsilon_n$ if the transmit signal consists only of the single symbol $s_n = 1$. Therefore, the measurement vector $\mathbf{r}$ is a weighted superposition of the response due to each transmit symbol.

Alternatively, the measurement vector $\mathbf{r}$ can be represented as:

$$\begin{aligned} \mathbf{r} &= \sum_m \gamma_m \, \mathbf{H}_m \mathbf{s} \\ &= \sum_m \gamma_m \, \rho_m \quad , \\ &= \mathbf{P} \gamma \end{aligned} \tag{2.5-19}$$

where we have defined vector ρ_m as:

$$\rho_m = \mathbf{A}_m \mathbf{s}, \tag{2.5-20}$$

and matrix $\mathbf{P}$ as:

$$\mathbf{P} = \left[\rho_1; \rho_2; \rho_3; \cdots; \rho_M\right]. \tag{2.5-21}$$

In this case, it is apparent that matrix **P** relates the scattering parameters $\boldsymbol{\gamma}$ to the measurements **r.** In this case, we can view the "signal" as $\boldsymbol{\gamma}$, which passes through a linear system described by matrix **P**. This system is, of course, dependent on the transmitter signal, and thus matrix **P** is a function of vector **s**. Each vector $\boldsymbol{\rho}_m$ can be viewed as the normalized response of scatterer γ_m. In other words, $\mathbf{r} = \boldsymbol{\rho}_m$ if the only scatterer illuminated is $\gamma_m = 1$. Therefore, the measurement vector **r** can be viewed as a weighted superposition of the response from each illuminated target.

Other useful relations can be identified. In particular, notice that

$$\mathbf{P} = \sum_{n=1}^{N} s_n \mathbf{B}_n = \sum_{m=1}^{M} \mathbf{H}_m \mathbf{s} \mathbf{e}_m' , \tag{2.5-22}$$

and also that

$$\Upsilon = \sum_{m=0}^{M} \gamma_m \mathbf{H}_m = \sum_{n=1}^{N} \mathbf{B}_n \boldsymbol{\gamma} \mathbf{e}_n' , \tag{2.5-23}$$

where $\mathbf{e}_n$ is a vector whose elements are all zeros, with the exception of element n, whose value is unity (one). For example,

$$\mathbf{e}_3 = [0, 0, 1, 0, \ldots]^T . \tag{2.5-24}$$

The usefulness of these representations is dependent on the desired task. For example, the most prevalent radar problem is to estimate the parameters of the illuminated targets. For that task, the representation $\mathbf{r} = \mathbf{P}\boldsymbol{\gamma}$ is the obvious choice. Adding a random noise vector to represent measurement noise, the appropriate resulting model is

$$\mathbf{r} = \mathbf{P}\boldsymbol{\gamma} + \mathbf{n} . \tag{2.5-25}$$

If, however, the task is to determine the optimal transmit vector **s,** a model representation of the form

$$\mathbf{r} = \sum_{m} \gamma_m \, \mathbf{H}_m \mathbf{s} + \mathbf{n} \tag{2.5-26}$$

is more useful.

This model was adopted to generate a software simulator (in MATLAB) to model space-time radar scenarios. The model allows us to generate accurate receiver sample data (i.e., measurement vector **r**) for specific target scenarios and transmit vectors **s.** Moreover, almost every optimization criterion used to determine an optimal vector **s** was dependent on the set of matrices $\mathbf{H}_m$. The model provided an accurate calculation of this set. Although the model adopts various key assumptions for the sake of simplicity (e.g., flat-earth, free-space propagation, uncoupled scatterers), it allows for the simulation of distributed and point scatterers, moving and stationary scatterers, and airborne and surface scatterers. Thus, complex-valued sampled data can be generated for SAR, GMTI, and AMTI scenarios, as well as hybrid modes that include a disparate set of target types. Further details of the analytic and software model, including the

input/output requirements, propagation and scattering models, and basis function selection, are included in Appendix G.

3.0 Receiver Processing (Pulse Compression) Via Parameter Estimation

In the context of the SAR system in Figure 1, the adaptive receiver generates the complex-valued (quadrature) baseband received signal, which must be processed to extract the complex-valued scatterer information. This is accomplished typically via application of a matched filter (MF) to implement the pulse compression and azimuth compression operations. However, as stated previously, the approach pursued herein is to apply modern and powerful estimation theory techniques in place of the MF processor. For simplicity, only the pulse compression operation is considered at this time. This restriction allows for a considerable reduction of the level of analyses and simulations required to establish the approach, while minimizing the loss of generality.

With the signal model formulated as in Equation (2.1-1), the solution for determining the complex scattering coefficients for each range bin can be solved as an inverse problem. Instead of solving the problem using the conventional MF, it is treated as a parameter estimation problem for which there are a number of different approaches that solve this inverse problem. To date we have investigated a few of them. Consider first the least-squares (LS) class of methods, which is related to the maximum likelihood (ML) class of methods for the model form considered herein. If $\mathbf{S}$ is a square and full-rank matrix (corresponding to the case where the number of measurements is the same as the number of unknowns), the standard matrix inverse is applied to Equation (2.1-1) to obtain

$$\boldsymbol{\alpha} = \mathbf{S}^{-1}\,\mathbf{b} - \mathbf{S}^{-1}\,\mathbf{w}. \tag{3.0-1}$$

Two different sets of conditions lead to a rectangular measurement matrix $\mathbf{S}$. The first condition arises when the number of measurements is larger than the number of unknowns. This is an over-determined linear system of equations, and the associated measurement matrix is full-rank in most practical situations. The pseudo-inverse is the technique that leads to the best solution in this case, and that solution is obtained as

$$\boldsymbol{\alpha} = \mathbf{S}^{\#}\,\mathbf{b} - \mathbf{S}^{\#}\,\mathbf{w}, \tag{3.0-2}$$

where the pseudo-inverse operation is denoted by the superscript #. For a full-rank matrix the pseudo-inverse can be expressed as $\mathbf{S}^{\#} = (\mathbf{S}^{H}\mathbf{S})^{-1}\mathbf{S}^{H}$. The second condition leading to a rectangular measurement matrix arises when the number of measurements is less than the number of unknowns. This leads to an under-determined linear system of equations, and the associated measurement matrix is also full-rank in most practical situations, but the space spanned by the measurement matrix operator is a subspace of the space spanned by the measurements. For this case the pseudo-inverse as in Equation (3.0-2) is also the technique that leads to the best solution, but such solution may be inadequate. In addition, the pseudo-inverse must be calculated with an appropriate numerically-robust technique, such as the singular value decomposition. In the rare cases where the measurement matrix is rank-deficient or numerically ill-conditioned, an appropriate LS formulation has to be adopted. In most cases, a LS solution involving diagonal loading (also known as regularization) suffices to provide adequate performance.

Another alternative parameter estimation approach is the minimum mean-squared error (MMSE) estimator, which allows the inclusion of known measurement noise covariance matrix ($\mathbf{R}_{ww}$) and scattering coefficients covariance matrix ($\mathbf{R}_{\alpha\alpha}$) information into the parameter estimation formulation. Specifically, the MMSE estimator is of the form

$$\boldsymbol{\alpha} = [\mathbf{S}\mathbf{R}_{\alpha\alpha}\mathbf{S}^{H} + \mathbf{R}_{ww}]^{-1}\mathbf{R}_{\alpha\alpha}\mathbf{S}^{H}\,\mathbf{b} - [\mathbf{S}\mathbf{R}_{\alpha\alpha}\mathbf{S}^{H} + \mathbf{R}_{ww}]^{-1}\mathbf{R}_{\alpha\alpha}\mathbf{S}^{H}\,\mathbf{w}. \tag{3.0-3}$$

In Equations (3.0-1)-(3.0-3), the estimation (or residual) error is the second term, which includes the measurement noise **w**. These approaches are described in more detail in Appendices B and C.

3.1 *Spatial Diversity Waveform Receiver Processing*

There are a number of different ways to compress the signals of the spatial diverse signal model case. Consider the two cases described in Equations (2.4-3) and (2.4-7); these two can be rewritten in the simplified form of Equation (2.1-1) in a straightforward manner. That equation form is

$$\mathbf{b} = \mathbf{S}\alpha + \mathbf{w}, \tag{3.1–1}$$

and repeating the expression herein simplifies the discussion below. As discussed above in Section 3.0, Equation (3.1-1) can be solved using the LS (or ML) approach (Equation (3.0-2)), or using the MMSE approach (Equation (3.0-3)). It is important to note that a matrix inverse is required for both estimates. For mathematical robustness, and to support non-square matrix inversion when the need arises, the pseudo-inverse is required in Equation (3.0-2), and desirable in Equation (3.0-3). The singular values of matrix **S** or $[\mathbf{S}\mathbf{R}_{\alpha\alpha}\mathbf{S}^{H} + \mathbf{R}_{ww}]$, the matrices for which the inverse is required, play an important role in determining the effect on the noise **w** of each signal processing method. The smaller the values of particular singular values, the larger the inverse of these singular values; specifically, actual amplification of the noise does occur along the subspace dimensions corresponding to singular values less than unity in value (all singular values are non-negative). Under typical conditions, the best noise suppression is attained with a set of singular values in which all are as large are possible and have the same value. With respect to the two systems under consideration, it is instructive to note that while the some of the singular values for the system matrix in Equation (2.4-7) are significantly larger than the singular values for the system matrix in Equation (2.4.3), those for Equation (2.4-7) are very distinct from each other, and some are significantly smaller also. This implies that parameter estimation solutions for the system in Equation (2.4.3) will have better noise suppression than those the system in Equation (2.4-7). However, the system in Equation (2.4-3) is more underdetermined than the system in Equation (2.4-7), and that may lead to an increase in the bias component of the residual error.

3.2 *Temporal Diversity Waveform Receiver Processing*

The model issues involving temporal diversity are different than those for spatial diversity. In particular, Equation (2.3-7) is the relevant system model representation, and notice that this system involves more than one instant of time. In the simple case where two waveforms are alternated every other PRI there are only two forms of the system matrix: **S**(n) and **S**(n+1), because **S**(n+2) = **S**(n) and **S**(n+3) = **S**(n+1). The equations for **S**(n) and **S**(n+1) are repeated next, for convenience, as

$$\mathbf{S}(n) = \begin{bmatrix} \mathbf{H}(n+1) & \mathbf{H}(n) \\ \mathbf{H}(n+2) & \mathbf{H}(n+1) \end{bmatrix}, \tag{3.2-1}$$

$$\mathbf{S}(n+1) = \begin{bmatrix} \mathbf{H}(n+2) & \mathbf{H}(n+1) \\ \mathbf{H}(n+3) & \mathbf{H}(n+2) \end{bmatrix}. \tag{3.2-2}$$

Since only two waveforms are transmitted every other PRI, it is convenient to introduce the following definitions,

$$\mathbf{H}_1 = \mathbf{H}(n) = \mathbf{H}(n+2), \tag{3.2-3a}$$

$$\mathbf{H}_2 = \mathbf{H}(n+1) = \mathbf{H}(n+3). \tag{3.2-3b}$$

Then Equations (3.2-1) and (3.2-2) become,

$$\mathbf{S}(n) = \begin{bmatrix} \mathbf{H}_2 & \mathbf{H}_1 \\ \mathbf{H}_1 & \mathbf{H}_2 \end{bmatrix}, \tag{3.2-4}$$

$$\mathbf{S}(n+1) = \begin{bmatrix} \mathbf{H}_1 & \mathbf{H}_2 \\ \mathbf{H}_2 & \mathbf{H}_1 \end{bmatrix}, \tag{3.2-5}$$

respectively. Notice that the parameter estimation methods mentioned in Section 3.0 apply directly to obtain a solution for the adopted model. Other forms for the system matrix, **S**, need to be derived to represent the more general case (involving multiple transmitted waveforms).

3.3 Space-time Diversity Waveform receiver Processing

Inherent in an information theoretic approach for sensing is the notion that information is contained within the measured data, and thus independent of the estimator chosen to operate on this data. A poor estimate (with a large error) is therefore due to either a lack of inherent information, or an estimator that poorly extracts the information available. Fisher's Information measure and the associated Cramer-Rao bound (CRB) constitute a set of measures that are applied in a large number of cases. Specifically, the CRB provides a lower bound on the estimation error for any unbiased estimator, thus providing a method to measure the inherent information in sensed data — a method independent of the chosen estimator.

Based on the above-listed issues, a transmit function can be optimized such that it maximizes the information content of the received data, but this information may be lost if an efficient estimator is not used. The problem with this, from the standpoint of radar signal processing, is that the most prevalent processor is the correlation processor, otherwise known as the matched filter (MF). From Fisher's information viewpoint, it is desired to minimize the estimation error in the mean-squared sense. The MF, however, does not provide, in general, the Minimum Mean-Squared Error (MMSE) estimate.

This is a significant issue with regard to highly diverse transmit waveforms (e.g., non-separable space-time functions) and receiver measurements. The increased diversity opens the radar design space such that radar performance can be substantially improved without changing the fundamental constraints of time-width, bandwidth, beamwidth, aperture area, and energy. However, the conventional MF is unequipped to take advantage of the increase in information that diverse systems can provide. If information can lead to decreased estimation error in the mean-squared sense, then MMSE estimators (e.g., Wiener filters) must be employed. In that manner the processor optimization criteria matches the waveform design criteria.

One key issue with MMSE estimators is their computational cost. For a linear MMSE estimator, this cost is not associated with the application of the estimator — its application requires no more operations than a MF — but instead is associated with the construction of this estimator. The construction of a linear MMSE estimator requires (for discrete measurements) a large matrix inverse, an operation not required by the MF. As the dimensionality of both the target set and the received measurements increase, this inverse becomes increasingly problematic.

As a result, to take full and efficient advantage of the increase in information provided by a diverse radar system, methods for simplifying and/or approximating the MMSE estimator are required. These methods include iterative solutions such as the iterative MMSE (i.e., Kalman filter), and reduced rank methods such as the Multi-Stage Wiener Filter (MSWF). Further details on this significant issue are provided in [28]. For example, in [28] it is shown that the Kalman filter and the MSWF can be combined into a single estimation algorithm. A Kalman filter provides a linear MMSE estimate of all target parameters using an iterative subset of the measurements, and is an algorithm that works well as long as the target parameter set is of reasonable length. Conversely, the MSWF uses all of the measurements to estimate subsets of the target parameters, and is an algorithm that works well as long as the number of measurements is of reasonably length. The work presented in [28] provides a solution that combines these estimators, such that subsets of the target parameters are estimated using an iterative subset of the radar measurements. In this manner, each iteration of the combined estimation algorithm is kept reasonably small (neither the number of target parameters nor number of measurements is unreasonably large).

4.0 WAVEFORM SELECTION VIA MUTUAL INFORMATION

A novel criterion for waveform selection in radar and other sensing applications is presented that is based on the information theoretic concept of mutual information (MI). In addition, its application to the area of waveform diversity for SAR systems is examined. MI is a measure of the information (in the sense of Shannon) in a random variable (or vector) about another random variable (or vector). It is shown herein that such a framework provides the basis for a conceptually-simple and powerful criterion for context-dependent evaluation of candidate waveforms, as well as context-dependent design of waveforms. Furthermore, in the special case of zero-mean Gaussian-distributed clutter, interference, and noise, the criterion attains an analytically simple form — a scalar function of the singular values of a specific cross-covariance matrix. The criterion can be used in distinct optimization contexts (minimization or maximization) as a function of the problem to be addressed. In addition, the criterion inherently includes the statistical information of the sensed parameters. More specifically in the context of a SAR system, the criterion includes the covariance matrix of the set of illuminated ground scatterers. The formulation and simulation-based results are presented in the context of the first-order radar system model of Section 2, but the approach can be extended in a straightforward manner to cover more complex models. Results presented show that the criterion is an effective means for waveform selection in an adaptive SAR system.

4.1 WAVEFORM SELECTION VIA MUTUAL INFORMATION

In Equation (2.1-1) (also Equation (3.1-1)), let the scattering coefficients, $\boldsymbol{\alpha}$, be samples from a zero-mean multivariate complex-valued Gaussian distribution with covariance matrix $E[\boldsymbol{\alpha}\boldsymbol{\alpha}^H] = \mathbf{R}_{\boldsymbol{\alpha}\boldsymbol{\alpha}}$. Random variates $\boldsymbol{\alpha}$ and $\mathbf{w}$ are independent of each other; further, each is assumed to be an analytic signal. Thus, each is a proper (sometimes referred to as circular) random variate [29] and each admits a complex Gaussian probability density function (PDF), denoted as $p(\cdot)$, of the form (shown here for an Mx1 random vector $\boldsymbol{\alpha}$),

$$p(\boldsymbol{\alpha}) = \pi^{-M} \left|\mathbf{R}_{\boldsymbol{\alpha}\boldsymbol{\alpha}}\right|^{-1} \exp\left[-\boldsymbol{\alpha}^H \mathbf{R}_{\boldsymbol{\alpha}\boldsymbol{\alpha}}^{-1} \boldsymbol{\alpha}\right]. \tag{4.1-1}$$

It follows from the model form that the random vector $\mathbf{b}$ also admits a complex Gaussian PDF. When the above conditions (analytic signals, circularity) fail to be met, the random variates admit only a real Gaussian PDF for the concatenated vector of the real and imaginary parts, but the concepts and issues discussed herein apply with appropriate modifications.

Measurement matrix $\mathbf{S}$ inherently includes the waveform function parameters. The manner of inclusion depends on the sophistication and detail of the adopted model and the intended purpose. For example, in the context of the typical first-order model for pulse compression using a linear frequency modulation (LFM) waveform $\{s_1(n) \mid n = 0, 1, \ldots, N\text{-}1\}$ over a single range strip [4], matrix $\mathbf{S}$ is the so-called (partial) convolution matrix of the waveform, and its entries in each column are the elements of the waveform and zeros. Equation (2.1-1) (also (3.1-1)) thus contains the system model on which a waveform design criterion can be formulated.

4.2 SHANNON MUTUAL INFORMATION

MI between two random vectors $\mathbf{b}_1$ and $\mathbf{b}_2$, denoted as $\boldsymbol{MI}(\mathbf{b}_1,\mathbf{b}_2)$, is a measure of the information in $\mathbf{b}_1$ about $\mathbf{b}_2$, or equivalently, the information in $\mathbf{b}_2$ about $\mathbf{b}_1$ [30]. Specifically,

$$\boldsymbol{MI}(\mathbf{b}_1,\mathbf{b}_2) = \boldsymbol{H}(\mathbf{b}_1) - \boldsymbol{H}(\mathbf{b}_1|\mathbf{b}_2) = \boldsymbol{H}(\mathbf{b}_2) - \boldsymbol{H}(\mathbf{b}_2|\mathbf{b}_1), \tag{4.2-1}$$

$$\boldsymbol{MI}(\mathbf{b}_1,\mathbf{b}_2) = \boldsymbol{H}(\mathbf{b}_1) + \boldsymbol{H}(\mathbf{b}_2) - \boldsymbol{H}(\mathbf{b}_1,\mathbf{b}_2), \tag{4.2-2}$$

where $\boldsymbol{H}(\mathbf{b}_i)$ denotes the entropy of the random vector $\mathbf{b}_i$, $\boldsymbol{H}(\mathbf{b}_i|\mathbf{b}_j)$ denotes the conditional entropy of $\mathbf{b}_i$ conditioned on $\mathbf{b}_j$, and $\boldsymbol{H}(\mathbf{b}_1,\mathbf{b}_2)$ denotes the joint entropy of random vectors $\mathbf{b}_1$ and $\mathbf{b}_2$. For a continuous (as opposed to discrete) distribution such as the Gaussian, these measures are defined respectively as

$$\boldsymbol{H}(\mathbf{b}_i) = -\int_{-\infty}^{\infty} \cdots \int \ln[p(\mathbf{b}_i)]\, p(\mathbf{b}_i)\, d\mathbf{b}_i\,, \tag{4.2-3}$$

$$\boldsymbol{H}(\mathbf{b}_i|\mathbf{b}_j) = -\int_{-\infty}^{\infty} \cdots \int \ln[p(\mathbf{b}_i|\mathbf{b}_j)]\, p(\mathbf{b}_i,\mathbf{b}_j)\, d\mathbf{b}_i d\mathbf{b}_j\,, \tag{4.2-4}$$

$$\boldsymbol{H}(\mathbf{b}_1,\mathbf{b}_2) = -\int_{-\infty}^{\infty} \cdots \int \ln[p(\mathbf{b}_1,\mathbf{b}_2)]\, p(\mathbf{b}_1,\mathbf{b}_2)\, d\mathbf{b}_1 d\mathbf{b}_2. \tag{4.2-5}$$

In these definitions natural (base e) logarithms are utilized, which is convenient when the Gaussian distribution is involved; however, any other base can be applied. Also, these definitions apply to any multivariate continuous distribution, so the concepts that follow are generic.

4.3 *Waveform Selection Process and MI Criterion (MIC)*

Based on Equation (2.1-1) (also Equation (3.1-1)), let $\mathbf{b}_1$ denote the received signal vector for the last-transmitted waveform $\{s_1(n)\}$, and let $\mathbf{b}_i$ denote the received signal vector for the waveform to be transmitted in the next interval (the procedure is applied to all waveforms $\{s_i(n)\}$ in the candidate set). The scatterers to be illuminated with the waveform to be selected are assumed to be represented by the same known PDF (same form and parameters) as those illuminated with the last-transmitted waveform. The scenario, system, and waveform parameters specify the sensor model matrices, $\mathbf{S}_1$ and $\mathbf{S}_i$. Since waveform $\{s_1(n)\}$ has been transmitted already, it is postulated herein that the next waveform to be transmitted should maximize the amount of new information collected by the sensor in the next illumination time window. This can be attained if the MI between the last-received received signal ($\mathbf{b}_1$) and the to-be-received signal ($\mathbf{b}_i$) is minimal. Thus, the MI Criterion (MIC) is postulated herein as:

$$\text{MIC} = \min_{s_i(n)} \{\boldsymbol{MI}(\mathbf{b}_1,\mathbf{b}_i)\}. \tag{4.3-1}$$

MIC selects the waveform $\{s_i(n)\}$ that minimizes $\boldsymbol{MI}(\mathbf{b}_1,\mathbf{b}_i)$ jointly with waveform $\{s_1(n)\}$, and is valid for any multivariate PDFs that describe the scatterer and noise processes. Further, the criterion can be utilized to design a waveform (possibly subject to a set of constraints) that minimizes Equation (4.3-1) using advanced optimization techniques.

4.4 *Gaussian-Distributed Processes*

Robustly, the MI expression attains a very simple form for the case where all random processes are described by the complex Gaussian PDF, as in Equation (4.1-1). That is, the MI between $\mathbf{b}_1$ and $\mathbf{b}_i$, both Kx1 vectors defined as in Equation (2.1-1) (also Equation (3.1-1)), is of the form

$$MI(\mathbf{b}_1, \mathbf{b}_i) = -\sum_{k=1}^{K} \ln\left[1 - d_k^2\right], \tag{4.4-1}$$

where $\{d_k \mid k = 1, 2, \ldots, K\}$ are the real-valued singular values (sv) of an auxiliary KxK (cross) covariance matrix $\mathbf{R}_{zx}$ defined as

$$\mathrm{E}\left[\mathbf{z}\mathbf{x}^{\mathrm{H}}\right] = \mathbf{R}_{zx} = \mathbf{R}_{ii}^{-1/2}\mathbf{R}_{i1}\mathbf{R}_{11}^{-1/2}. \tag{4.4-2}$$

The singular values satisfy the conditions $1 \geq d_1 \geq d_2 \ldots \geq d_K \geq 0$, and $\mathbf{R}_{11}$, $\mathbf{R}_{i1}$, and $\mathbf{R}_{ii}$, are the following covariance matrices,

$$\mathrm{E}\left[\mathbf{b}_1\mathbf{b}_1^{\mathrm{H}}\right] = \mathbf{R}_{11} = \mathbf{S}_1\mathbf{R}_{\alpha\alpha}\mathbf{S}_1^{\mathrm{H}} + \mathbf{R}_{ww}. \tag{4.4-3}$$

$$\mathrm{E}\left[\mathbf{b}_i\mathbf{b}_1^{\mathrm{H}}\right] = \mathbf{R}_{i1} = \mathbf{S}_i\mathbf{R}_{\alpha\alpha}\mathbf{S}_1^{\mathrm{H}}, \tag{4.4-4}$$

$$\mathrm{E}\left[\mathbf{b}_i\mathbf{b}_i^{\mathrm{H}}\right] = \mathbf{R}_{ii} = \mathbf{S}_i\mathbf{R}_{\alpha\alpha}\mathbf{S}_i^{\mathrm{H}} + \mathbf{R}_{ww}. \tag{4.4-5}$$

The noise covariance matrix is missing in (4.4-4) because the expectation is over variables at two distinct time instants, and the noise is uncorrelated in space and time. Also, random vectors **x** and **z** that appear in (4.4-2) are defined as

$$\mathbf{x} = \mathbf{R}_{11}^{-1/2}\mathbf{b}_1, \tag{4.4-6}$$

$$\mathbf{z} = \mathbf{R}_{ii}^{-1/2}\mathbf{b}_i. \tag{4.4-7}$$

Equations (4.4-6) and (4.4-7) correspond to the definition of whitened versions of $\mathbf{b}_1$ and $\mathbf{b}_i$, respectively, and thus imply that the covariance matrices of **x** and **z** are both identity matrices.

From Equation (4.3-1), the MIC for the Gaussian case is simple to calculate, although non-trivial computations are involved. Of significance is the fact that the sv in the proper Gaussian version of the criterion are the correlation coefficients of the complex-valued random variable vector pair **x** and **z**. Furthermore, these sv are the canonical correlations for the complex-valued random variable vector pair $\mathbf{b}_1$ and $\mathbf{b}_i$ [31, 32].

Appendix D describes the application of this approach to select waveform polarization from pulse to pulse to improve the performance of a full-polarization radar.

5.0 Waveform Selection Via Marginal Information

Professor J. M. Stiles and several of his graduate students at the University of Kansas [7, 8] have developed alternative approaches to the implementation of the adaptive radar system philosophy outlined in Sections 1 and 2 (see also Appendices F and G). In particular, during the first part of their subcontract work they formulated an approach for optimal space-time waveform design in the context of multi-aperture radar, but their approach is applicable to other radar configurations. A key aspect of this work is that the transmit signal is expanded in terms of a set of orthonormal basis functions that span the bandwidth, time extent, and spatial extent of the radar (Section 2.5). Stiles et al. have applied several criteria to obtain the basis coefficients that optimize the joint detection of multiple targets, and have shown that maxi-min or mini-max criteria are preferred in most cases. More recently, in the second part of their effort they continue with the orthonormal basis expansion approach as in their early work, but focus on minimization of the error in the estimate of the complex scattering coefficient of each target in a multiple target environment. This emphasis results in involvement of the Fisher information matrix in the formulation, and they establish an information-theoretic criterion for the optimal selection of the transmit space-time waveform (Section 3.3). The criterion involves the change in Fisher information due to a received measurement (Appendix F), which is a different application of information theory concepts than the one presented in Section 4. However, the same novel adaptive radar philosophy is pursued in their work as well.

The first step in any optimization process is to determine the specific criterion that is to be optimized. Inherent in this choice is the fact that a perfect solution is not achievable typically — not that a perfect solution is indefinable, but rather either this perfect solution does not exist mathematically, or it cannot be determined mathematically. Thus, the optimization problem becomes one of finding the best among the set of all imperfect solutions. As a result, there are many criteria that present logical and justifiable reasons for choosing that criterion; in other words, the "best" criterion is typically a subjective and arguable choice. Certainly this is true with the problem of finding an optimal space-time transmit function for a specific radar task or mode. Although the perfect transmit function does not exist in general, it is nevertheless instructive to define the characteristics of such a function. These characteristics will lead to a logical set of optimization criteria.

Towards that objective, first make a simple delineation involving the collection of scatterers occupying a surface or volume of interest. Some of those scatterers have characteristics that make them of interest to our sensing problem — it is desired to detect their presence, and/or estimate one or more of their physical characteristics (e.g., RCS, velocity, altitude). Scatterers of this type are denoted as targets. Undoubtedly, there will be other scatterers within the sensed region in which there is no interest at all. Scatterers of this type are denoted as clutter.

Given that our received observations are corrupted with thermal noise, and that the space-time transmit function has finite energy, then a perfect (ideal) space-time transmit function would distribute its available energy equally (presumably) across all targets, while wasting none of its energy exciting any of the clutter objects. This alone, however, would not constitute a perfect transmit function. With regard to the detection and estimation of one specific target, all other targets essentially become clutter objects. Since the response from each target is energetic, the response from one or more targets can interfere significantly in the detection/estimation of

another. To eliminate this interference, the transmit function would be constructed ideally such that the responses from all illuminated targets form an orthogonal set — the responses from all targets would be uncorrelated. For example, in SAR applications, this result would provide a perfect (i.e., "thumbtack") ambiguity function, meaning the responses from dissimilar resolution cells are perfectly uncorrelated.

Thus, a necessary set of conditions for a perfect space-time transmit function is that it distributes no energy on clutter objects, it distributes available energy equally across all target objects, and the measured responses from all targets form an orthogonal set (the transmit function "whitens" target responses). However, these conditions are generally insufficient to specify a perfect transmit function, since the final objective is to detect and/or estimate targets and target properties with zero error. Thus, the perfect space-time transmit function results in a measurement containing perfect information about the desired properties of an illuminated target set.

Based on these specifications, it is evident that a perfect transmit function exists only for the most trivial of radar problems. But the discussion above leads us to several potential optimization criteria, some of which are traditional radar criteria, but others are not. For example, such candidates include a transmit function that maximizes the energy placed on the target set, or one that minimizes the energy placed on the clutter objects, or one that maximizes the ratio of the two. Given the transmit signal expansion (i.e., the space-time transmit function defined completely by complex-valued vector **s** in Section 2.5), eigen-analysis methods can be used to determine the transmit vector **s** that optimizes the average target energy, or the average clutter energy, or the average target-to-clutter ratio. The key term for these criteria is "average." At first glance, maximizing the average target energy or the average target-to-clutter ratio is a logical goal that results in desirable sensing results. A key issue with these average criteria is that often the solution ignores one or more targets — little or no energy is placed on them — in order to maximize the overall average measure. From a radar perspective, this is a poor solution, since the ignored targets could be the most important (e.g., most dangerous or lethal) in the illuminated scene. Again, recall that a perfect transmit function would both maximize and uniformly distribute the available energy.

In the search for criteria that avoid the "average" aspect, an attractive candidate is the maxi-min criterion, wherein the objective is to find a vector **s** that maximizes the individual target energy or individual target-to-clutter ratio of the single target whose energy or SCR is the smallest. The largest possible maxi-min solution (if it exists) is one where the available energy is both maximally applied and uniformly distributed — precisely the condition achieved by the ideal transmit function. A key problem with the maxi-min criterion is that, unlike the average criterion, there is no method for determining the optimal transmit vector **s**. In particular, it is unknown beforehand which target will in fact be the minimum. Our solution to this problem was to determine instead a lower bound on the target energy or SCR of any and all illuminated targets. Then an iterative solution is imposed that sequentially increases this lower bound. Provided that this bound is tight, the attained solution is likely to be qualitatively equivalent to the unknown optimum maxi-min solution. Further details of this approach and the associated procedures are in Appendices F and G, and [34].

An interesting result of the work summarized herein is that the solutions found for non-separable space-time functions were significantly better than those constrained to separable functions only (e.g., traditional phased array). Additionally, it was shown that the solutions improved (i.e., the maxi-min value increased) as the dimension of space-time transmit vector **s** was increased (i.e.,

the number of available basis functions increased). Each of these results demonstrate that space-time transmit signal diversity allows for the construction of better transmit functions which in turn leads to increased radar performance.

As stated earlier, maximizing target energy or target-to-clutter ratio alone is insufficient towards the minimization of estimation or detection error. For a multiple target case (e.g., the independent resolution cells of a SAR image), the measured responses from dissimilar targets must also be uncorrelated. This problem is most severe for the SAR/ISAR imaging case, where decorrelated target (resolution cell) responses are essential for achieving an acceptable ambiguity function. Unfortunately, an optimization criterion that maximizes a target-to-clutter ratio provides no optimization with regard to target decorrelation. As a result, a radar implementing an SCR-optimized transmit function may still exhibit substandard detection and estimation accuracy.

Thus, decorrelating (i.e., whitening) all target responses is likewise a logical goal for a new optimization criterion. Determining a solution for a criterion of this type, however, is problematic. Target energy and SCR criteria are expressed in terms of real, non-negative values. As a result, eigen-analysis solutions are available, and in fact were used exclusively in our research. In contrast, the correlation of two responses from dissimilar targets is expressed as a complex value, and so eigenvector solutions are not applicable directly. Instead, a real-valued non-negative bound was constructed; namely, an upper bound on the largest possible correlation between any two illuminated targets (e.g., a bound on the largest sidelobe of the ambiguity function). Similar to the iterative procedure for optimizing the maxi-min SCR criterion, a solution that sequentially lowered this upper bound on maximum target correlation was implemented. In this way, an approach to determine a solution that optimized a mini-max criterion for target correlation was formulated. Details of this research are provided in [35].

This optimization algorithm and criterion (see [35]) appeared to be moderately effective in decorrelating target responses, although there was evidence that this upper bound, in at least some instances, was more loose than desired. In other words, this is indicative that there is a high likelihood of the existence of significantly better solutions than the one produced by our algorithm. Nevertheless, the research again showed that non-separable space-time transmit functions generated superior solutions than those provided by the separable variety, and also that transmit vectors with higher dimensionality (i.e., diversity) also resulted in lower target correlation.

As stated before, all of the optimization criteria discussed thus far are both logical and defensible with regard to optimizing radar efficacy. However, by itself no criterion is sufficient to achieve this goal. One criterion might be more effective than another for a particular application, but none can be considered to be universally the best. One approach to a robust solution is to combine disparate criteria into a single cost function. For example, a metric that effectively combines the maxi-min SCR criterion with the mini-max target correlation criterion can be defined. The application of this type of hybrid criterion presents three distinct issues. First, the method of combining two or more criteria is subjective — the amount to which each should be weighted in the cost function is at best uncertain. Second, determining the solution that optimizes this cost function is likely to be extremely difficult; almost certainly intelligent search methods such as Genetic Algorithms (GA) would be required. Finally, as stated before, the optimization criteria discussed here are insufficient for maximizing radar performance even when taken in aggregate. This is true because in addition to maximizing SCR and minimizing target correlation, the responses from each individual target must contain information about the parameter(s) of interest

to be estimated about that target. Specifically, the response from a given target must be sensitive to the parameter of interest. The response must not remain invariant with respect to changes in the desired parameter value, or else the measurement will provide no useful information — regardless of SCR or target correlation. A measurement contains information only if the measurement changes in a distinct and significant manner as the target parameter itself is modified. For example, the scattering coefficient or RCS of a target is proportional to the energy of its response. The measured target response thus carries information about target RCS, but noise, clutter, and correlated target responses combine to obfuscate this information.

Thus, it is possible to conclude that a transmit function should be optimized using the criterion that maximizes the desired information collected in the receiver measurements. This might seem to be a rather esoteric criterion that leads us back to the starting point —maximize information by optimizing each characteristic of an ideal transmit function (e.g., maximize target energy, minimize clutter energy, minimize target correlation). However, information theory provides mathematical specificity to the definition of information, and thus offers an attractive direction in which to proceed.

Information is defined as the inverse of uncertainty, and in the context of a radar system, uncertainty is defined in terms of mean-squared error. For multiple parameter estimates involving many targets, the mean-squared error is expressed as an error covariance matrix. Therefore, a transmit function that provides optimum information can be defined as one that results in the best possible estimation error covariance matrix. Although this error is dependent on the estimator implemented to provide the estimate, it is possible to include the concept of information by the use of the Fisher's Information Matrix (FIM). This matrix is evaluated independently of the implemented estimator, and its inverse (the Cramer-Rao bound) provides a lower bound on the error covariance matrix provided by any unbiased estimator. Thus, it follows that an optimum transmit function is one that results in the smallest possible Cramer-Rao Bound (CRB).

It can be shown that for the radar problem the CRB improves as target energy is increased, as clutter energy is decreased, and as target correlation is decreased. Thus, the Fisher's information is effectively a hybrid cost function involving each of the optimization criteria previously discussed. However, this hybrid cost function also evaluates the sensitivity of the measurements to changes in the desired target parameters, and also applies an objective weighting to each of the ideal characteristics of the transmit function — a weighting that results in the best possible error covariance. Therefore, the FIM resolves two of the three problems associated with the hybrid cost function discussed earlier. The remaining task is to find the solution to this optimization problem; that is, to find the specific space-time transmit vector **s** that provides the best possible CRB.

As discussed earlier, intelligent search methods (e.g., genetic algorithms) can be applied to this problem, but given the large dimension of vector **s**, such solutions are likely to be very slow and cumbersome to implement. Instead, an iterative approach was developed to the construction of informationally-optimum transmit vectors. Recall that each element of transmit vector **s** is the complex-valued coefficient associated with one space-time transmit basis function. Our algorithm attempts to optimize sequentially the information associated with each element (or small groups of elements) of transmit vector **s**. However, instead of attempting to maximize the information provided by each transmit element, the approach adopted is to maximize the increase in information provided by each element. In other words, maximize the new information provided by each successive element — information not provided previously by other elements.

The increase in information described above is labeled herein as the Marginal Information, a quantity that is analogous to mutual information in Shannon's information theory. Like Fisher's Information, marginal information is expressed in matrix form; thus, one of the questions in this research is to identify or establish candidate metrics for evaluating these matrix quantities. Essentially, the questions to be answered include the following ones. What makes one matrix better than another? How can a set of matrices be ordered in terms of "goodness"? The linear algebra literature provides several candidate metrics, including the matrix trace (A-optimality) and the matrix determinant (D-optimality).

Perhaps the most intriguing aspect of using marginal information to construct sequentially a transmit vector is that this criterion for ordering a set of matrices can be altered adaptively. This provides a convenient and powerful method for implementing so-called cognitive radar, where the transmit function is modified adaptively as the radar collects and processes the received data. As measurement data is evaluated, certain targets and/or target parameters are identified as particularly important, suspicious, or ambiguous. Conversely, other targets may be discarded as unimportant or completely identified. Either way, the desired information about the set of illuminated targets will change as the nature of these targets is revealed.

The change in desired information can be directly and quantitatively used when evaluating and ordering the marginal information of a transmit vector element. In other words, the marginal information criterion used to determine sequentially the elements of a transmit vector **s**, can be changed adaptively in a manner that reflects the target information inferred by the measured data. To demonstrate the potential of this methodology, this adaptivity was exercised in a sequential detection simulation, wherein objects are removed from the marginal information criterion once they are identified with a requisite certainty. The results showed that adding adaptivity to the transmit function construction resulted in a significant increase in both detection accuracy and speed to reach the solution. Details of this marginal information research are provided in Appendix F and [28, 36].

The results summarized herein and detailed in the various relevant appendices are very interesting and encouraging. Despite the sequential nature of the transmit vector construction (which introduces issues such as the lack of global optimality), the results show that a transmit vector can be constructed based solely on the criterion that measurement information is maximized (uncertainty is reduced). Moreover, the results appear to be superior to those obtained by other known methods. In particular, the results are superior for non-separable space-time functions (in relation to the conventional separable functions), and performance improvements (estimation error is reduced) are achieved as the dimensionality (i.e., diversity) of the transmit vector is increased. Especially interesting are the results of adaptive detection research, which demonstrate the great potential for using information theoretic methods in the construction of "cognitive" radar, as stated in Section 1.

6.0 Conclusions and Future Work

A novel formulation was introduced for radar pulse compression using parameter estimation techniques for both single-waveform and two frequency-separated waveforms. This approach enables the ability to achieve the resolution of the combined bandwidth of the two separate waveforms.

The team demonstrated also two similar but different information theoretic criteria for adaptive diverse waveform (modulation type and/or polarization type) selection and for adaptive (cognitive) radar system in general. One criterion is based on Shannon mutual information and the other is based on marginal information. In fact, the concept of marginal information itself is a novel contribution. These approaches have been applied to waveform modulation diversity, waveform polarization diversity, and space-time waveform diversity.

Future activities include extension of the signal model and the pulse compression parameter estimation approach to cover spatially diverse waveforms with modulation diversity, in addition to frequency diversity. Other significant activities include application of the two information theoretic waveform selection approaches to cover joint multiple waveform and system diversities (for example, modulation diversity for space and time), and multiple radar system modes.

REFERENCES

[1] A. W. Rihaczek, *Principles of High-Resolution Radar*. Marina del Rey, CA: MARK Resources, Inc., 1977.

[2] M. I. Skolnik, *Introduction to Radar Systems* (2nd ed.). New York, NY: McGraw-Hill Book Co., 1980.

[3] F. E. Nathanson, *Radar Design Principles* (2nd ed.). New York, NY: McGraw-Hill Book Co., 1991.

[4] J. W. Garnham, J. R. Roman, and P. Antonik, "Waveform diversity pulse compression using Kalman filter based estimation approach," *Procs. IEEE 2006 Int'l. Waveform Diversity & Design Conf.*, Lihue, HI, USA, 22-27 January 2006.

[5] J. R. Roman, J. W. Garnham, and P. Antonik, "Information theoretic criterion for waveform diversity," *Procs. Fourth IEEE Workshop on Sensor Array and Multi-channel Processing (SAM 2006)*, Waltham, MA, USA, 12-14 July 2006, pp. 444-448.

[6] J. R. Roman, J. W. Garnham, and P. Antonik, "Polarization diversity using mutual information," *Procs. 2007 IEEE Radar Conf.*, Waltham, MA, USA, 17-20 April 2007, pp. 828-833.

[7] J. Stiles, V. Sinha, and A. Deekonda, "Optimal space-time transmit signals for multi-mode radar," *Procs. IEEE 2006 Int'l. Waveform Diversity & Design Conf.*, Lihue, HI, USA, 22-27 January 2006.

[8] J. Stiles, V. Sinha, and A. P. Nanda, "Space-time transmit signal construction for multi-mode radar," *Procs. IEEE 2006 Radar Conf.*, Verona, NY, USA, 24-27 April 2006, pp. 573-579.

[9] M. R. Bell, "Information theory and radar waveform design," *IEEE Trans. Inform. Theory*, vol. 39, pp. 1578-1597, Sept. 1993.

[10] P. R. Venkata and N. A. Goodman, "Novel iterative techniques for radar target discrimination," *Procs. IEEE 2006 Int'l. Waveform Diversity & Design Conf.*, Lihue, HI, USA, 22-27 January 2006.

[11] J. M. Stiles, *Space-Time Radar Transmission, Target and Measurement Model*. Radar Systems Lab (RSL) internal memo, University of Kansas, Lawrence, Kansas, June 2006.

[12] J. A. Stratton, *Electromagnetic Theory*. New York, NY: McGraw-Hill Book Co., 1941.

[13] M. Born and E. Wolf, *Principles of Optics* (3rd ed.). New York, NY: Pergamon Press, 1965.

[14] IEEE, *1983 Standard Test Procedures for Antennas* (ANSI/IEEE-Std. 149-1979). Piscataway, NJ: IEEE-Publishing, ISBN 0-471-08032-2, 1983 (also see: No. 145-1983: Definitions of Terms for Antennas, *IEEE Transactions on Antennas and Propagation*, Vol. AP-31, No. 6, Nov. 1983, pp. II – 26).

[15] H. Mott, *Antennas for Radar and Communications, A Polarimetric Approach*. New York, NY: John Wiley & Sons, 1992.

[16] G. A. Deschamps, "Geometrical representation of the polarization of a plane electromagnetic wave," *Proceedings of the IRE*, vol.39, no.5, pp. 540-544, 1951.

[17] G. A. Deschamps and P. E. Mast, "Poincaré sphere representation of partially polarized fields," *IEEE Transactions on Antennas and Propagation*, Vol. 21, No. 4, pp. 474-478, 1973.

[18] W.-M. Boerner, H. Mott, E. Lüneburg, C. Livingston, B. Brisco, R. J. Brown and J. S. Paterson (with contributions by S. R. Cloude, E. Krogager, J. S. Lee, D. L. Schuler, J. J.

van Zyl, D. Randall, P. Budkewitsch and E. Pottier), "Polarimetry in Radar Remote Sensing: Basic and Applied Concepts," Chapter 5 in F. M. Henderson and A. J. Lewis, (eds.), *Principles and Applications of Imaging Radar, Vol. 2* of R. A. Reyerson (ed.), *Manual of Remote Sensing* (3rd ed).

[19] J. R. Huynen, *Phenomenological Theory of Radar Targets*, Ph. D. Thesis, University of Technology, Delft, The Netherlands, December 1970.

[20] J. L. Eaves and E. K. Reedy (eds.), *Principles of Modern Radar*. New York, NY: Van Nostrand Reinhold Co., 1987.

[21] E. Pottier, "La polarimétrie radar appliquée à la télédétection," Ecole Supérieure des Télécommunications de Tunis, Tunis, Tunisie, 17 December 1999.

[22] R. M. A. Azzam and N. M. Bashara, *Ellipsometry and Polarized Light*. Amsterdam, The Netherlands: North Holland Pub. Co., 1977.

[23] E. Lüneburg, "Radar polarimetry: A revision of basic concepts," in H. Serbest and S. Cloude (eds.), *Direct and Inverse Electromagnetic Scattering*, Pittman Research Notes in Mathematics Series 361. Harlow, U. K.: Addison Wesley Longman, 1996.

[24] E. Lüneburg, "Principles of radar polarimetry," *Procs. of the IEICE Trans. on Electronic Theory*, Vol. E78-C, No. 10, pp. 1339-1345, 1995 (see also: E. Lüneburg, "Polarimetric target matrix decompositions and the 'Karhunen-Loeve expansion'", *Procs. IGARSS '99*, Hamburg, Germany, 28 June-2 July 1999).

[25] W.-M. Boerner, W.-L. Yan, A.-Q. Xi and Y. Yamaguchi, "On the Principles of Radar Polarimetry: The Target Characteristic Polarization State theory of Kennaugh, Huynen's Polarization Fork Concept, and Its Extension to the Partially Polarized Case", Invited Review, *IEEE Proceedings, Special Issue on Electromagnetic Theory*, Vol. 79, No. 10, pp. 1538-1550, Oct. 1991.

[26] S. R. Cloude and K. P. Papathanassiou, "Coherence optimization in polarimetric SAR interferometry," *Procs. IGARSS '97*, Vol. IV, Singapore, 3-9 Aug. 1997, pp. 1932-1934.

[27] J. J. Morisaki, *Basic Formulations for Radar Polarimetry*. M. S. Thesis, Electrical Engineering Dept., University of Illinois at Chicago, Chicago, Illinois, 2004.

[28] P. S. Tan, *Reduced Rank Filtering Techniques for Processing Multi-Aperture Radar*. M. S. Thesis, Electrical Engineering Dept., University of Kansas, Lawrence, Kansas, 2006 (available at www.ittc.ku.edu/research/thesis).

[29] P. J. Schreier and L. L. Scharf, "Second-order analysis of improper complex random vectors and processes," *IEEE Trans. Sig. Proc.*, vol. 51, pp. 714-725, March 2003.

[30] P. Beckmann, *Probability in Communication Engineering*. New York, NY: Harcourt, Brace & World, Inc., 1967.

[31] H. Hotelling, "Relations between two sets of variables," *Biometrika*, vol. 28, pp. 321-377, 1936.

[32] J. R. Roman, *Adaptive Sidelobe Canceling Using Complex-Valued Canonical Variables*. Tech. Report AFRL-SN-RS-TR-1998-46, Rome, NY: AFRL, Sensors Directorate, Rome Site, 1998.

[33] J.M. Stiles, *A Fisher's Information Criterion for Space-Time Transmit Signal Selection*. Radar Systems Lab (RSL) internal memo, University of Kansas, Lawrence, Kansas, Sept. 2005.

[34] V. Sinha, *Illumination Optimized Transmit Signals for Space-Time Multi-Aperture Radar*. M. S. Thesis, Electrical Engineering Dept., University of Kansas, Lawrence, Kansas, 2006 (available at: www.ittc.ku.edu/research/thesis).

[35] A. T. Deekonda, *Optimal Space-Time Transmit Signal Design for Multi-Static Radar*. M. S. Thesis, Electrical Engineering Dept., University of Kansas, Lawrence, Kansas, 2005 (available at: www.ittc.ku.edu/research/thesis).

[36] A. P. Nanda, *An Information Theoretic Approach of Transmit Signal Design for MIMO Radar*. M. S. Thesis, Electrical Engineering Dept., University of Kansas, Lawrence, Kansas, 2006 (available at www.ittc.ku.edu/research/thesis).

[37] J. W. Garnham, "Application of digital beamforming for look-down, clutter-limited, MTI radar – with specific application to space based radar", *Procs. IEEE Aerospace Conf.*, Snowmass at Aspen, CO, USA, 1-8 Feb. 1998, pp. 349-357.

[38] J. M. Anderson, *Nonlinear Suppression of Range Ambiguity in Pulse Doppler Radar*. Ph. D. Dissertation, Air Force Institute of Technology, WPAFB, OH, USA, Dec. 2001.

[39] A. Nelander, "Processing for continuous radar waveforms", *Procs. IEE Waveform Diversity and Design Conf.*, Edinburgh, Scotland, UK, 8-11 Nov. 2004.

[40] S. D. Blunt and K. Gerlach, "Joint adaptive pulse compression to enable multistatic radar", *Procs. IEE Waveform Diversity and Design Conf.*, Edinburgh, Scotland, UK, 8-11 Nov. 2004.

APPENDIX A: PARAMETER ESTIMATION PHYSICAL MODEL FOR RADAR PULSE COMPRESSION

John W. Garnham
Jaime R. Roman

Abstract: Parameter estimation is enabling for radar pulse compression using waveform diversity. This approach improves overall radar system accuracy for many scenarios in relation to the typical matched filter (MF), as well as minimizes the accuracy degradation due to multiple waveforms simultaneous returns at the receiver. In a typical situation with MF detection involving multiple simultaneous waveforms, the undesired cross-correlation between two distinct waveforms increases the undesired background level. The application of parameter estimation to estimate all the unknown parameters utilizing the sensed data involving all waveforms mitigates the error induced due to multiple signals. The model described is for a single transmitter, but future work will address the case of multiple transmitters and receivers, with each transmitter transmitting a different waveform.

The scenarios adopted for the distinct radar system configurations are sufficiently generic to indicate the broad scope of applicability of the approach, while being sufficiently specific to allow the generation of representative models with adequate analytic detail for each scenario. An appropriate first-order physical model of the radar from the transmitted waveform to the received signal is developed herein by adopting several assumptions and simplifications. The resulting model is an analytical representation of the relevant physical fundamentals for a generic airborne or space-borne surveillance radar scenario involving ground-based targets, and the associated geometry. Within such context, the model is restricted to include only range and elevation angle (at a fixed azimuth angle), effectively considering only the monostatic slant plane. Extension of the model to include azimuth angle is a future effort; such generalization is necessary for the bistatic and the more general multi-static cases.

Physical Model for Monostatic (Single-Platform) Scenarios

Consider an airborne or space-borne platform carrying a radar system with a rectangular electronically-scanned array (ESA) pointed towards the surface of the Earth, and the radar system is operating in synthetic aperture radar (SAR) mode using a single-polarization waveform. Thus, the radar generates a high-resolution range-azimuth map of a specified region-of-interest (ROI) in the illuminated ground, which is at the far-field of the ESA. High range resolution is attained via long-duration, high-bandwidth transmit waveform, and pulse compression at the receiver. In such context, the received radar signal after conversion to baseband at the output of the ESA can be expressed in the form

$$b(\overline{\mathbf{u}}) = b(\mathbf{u},t) = C_{\mathrm{R}} C_{\mathrm{T}} \int_{t \subset \mathcal{T}} \iiint_{\mathbf{u} \subset \mathcal{R}} \alpha(\overline{\mathbf{u}}) E_{\mathrm{R}}(\overline{\mathbf{u}}) E_{\mathrm{T}}(\overline{\mathbf{u}}) s(\overline{\mathbf{u}})\, d\mathbf{u}\, dt + w(\overline{\mathbf{u}}) \tag{A-1}$$

where the following definitions apply:

$b(\mathbf{u},t)$	received radar signal at platform location $\mathbf{u}$ and time t;
$\overline{\mathbf{u}}$	four-dimensional vector of position, $\mathbf{u}$, and time, t;
$\alpha(\mathbf{u},t)$	scattering coefficient process at location $\mathbf{u}$ and time t;
$E_{\mathrm{T}}(\mathbf{u},t)$	transmit ESA electric field strength at location $\mathbf{u}$ and time t;
$E_{\mathrm{R}}(\mathbf{u},t)$	receive ESA electric field strength at location $\mathbf{u}$ and time t;
$s(\mathbf{u},t)$	transmit waveform at location $\mathbf{u}$ and time t;
$w(\mathbf{u},t)$	receiver white Gaussian noise process at platform location $\mathbf{u}$ and time t;

C_T, C_R transmit (T) and receive (R) radar system parameters (power; wavelength; etc.);

$\mathcal{T}$ coherent processing interval (CPI) time duration; and

$\mathcal{R}$ illuminated ground region.

The above expression includes effects such as range and Doppler ambiguities, internal clutter motion, and spatial clutter variability. However, a computer implementation of this expression in its most general form is difficult to attain, and includes factors that are of second-level importance for the type of analysis intended herein. Thus, a set of assumptions is introduced next in order to generate an amenable expression.

Assumption 1: Let the time duration $\mathcal{T}$ be the round-trip time for one pulse of (uncompressed) duration τ_u to illuminate a ground segment corresponding to an integer number N_τ of uncompressed range resolution intervals Δr_u. This corresponds to setting the time duration as the set of time values $t \subset [t_0, t_e]$, for appropriately-selected t_0 and t_e.

Assumption 2: Let the transmit and receive electric field strength functions $E_T(\mathbf{u},t)$ and $E_R(\mathbf{u},t)$ be replaced by an ideal two-dimensional, unity-strength, flat-top model of length in the azimuth direction equal to one compressed azimuth resolution interval Δa, and length in the elevation direction equal to the projection of N_τ uncompressed range resolution intervals on the ground. This assumption results in the radar return including only the effects of the scatterers in a strip of ground (the region $\mathcal{R}$) of width Δa and length $N_\tau \Delta r_u$. Thus, range and Doppler ambiguities are eliminated because they fall outside the illuminated region; furthermore, range-dependent terms such as the Green's function factor are eliminated also.

Assumption 3: Let the transmit and receive radar system parameters, C_T and C_R, be unity-valued, which corresponds to a normalization of the return signal.

Under these assumptions and via various algebraic manipulations, Equation (A-1) becomes

$$b(t) = \int_{t_0}^{t_e} \alpha(t-\bar{t})\, s(\bar{t})\, d\bar{t} + w(t) = \int_{t_0}^{t_e} \alpha(\bar{t})\, s(t-\bar{t})\, d\bar{t} + w(t) = s(t) * \alpha(t) + w(t) \tag{A-2}$$

which is the continuous-time convolution (denoted as $*$) of the transmit waveform with the scattering process on the single down-range strip of ground. Another assumption is required to attain the desired expression.

Assumption 4: Let the area of each range cell ($\Delta a \times \Delta r$) be sufficiently large with respect to the radiation wavelength so that it encompasses a large number of individual scatterers. Under such conditions, each range cell is represented as a single, fixed (no motion), complex-valued, Gaussian-distributed scatterer at its center. Furthermore, the transmit waveform $s(t \mid t \subset [0, \tau_u])$ can be replaced by its discrete-time version $s(k\Delta t \mid k = 0, 1, \ldots, K-1)$, where Δt corresponds to the sampling time dictated by the instantaneous bandwidth f_{BW}. Similarly, the white noise process can be replaced by its discrete-time equivalent.

Based on Assumption 4, the integral in Equation (A-2) is replaced by a discrete sum with lower limit corresponding to the start of the transmit waveform at t_0, which can be set equal to 0 (time axis shift). Analogously, the sum upper limit is set corresponding to the end of the transmit waveform, which is $t_e = (K-1)\Delta t$. The start of the desired radar return signal collection can be set equal to zero also, $t_s = 0$; and the completion of the desired radar return signal collection is $t_f = N_\tau \tau_u$. From the discrete-time representation of the waveform, $\tau_u = K\Delta t$; so, $t_f = N_\tau K \Delta t$. For simplicity, let $N = N_\tau K$, which implies that the set of N measurements is an integer multiple of the waveform duration. Then, Equation (A-2) is replaced by

(A-3) $$b(n\Delta t) = \sum_{k=0}^{K-1} s(k\Delta t)\,\alpha(n\Delta t - k\Delta t)\Delta t + w(n\Delta t) \qquad n = 0, 1, \ldots, N-1$$

For simplicity, let $\Delta t = 1$; then

(A-4) $$b(n) = \sum_{k=0}^{K-1} s(k)\,\alpha(n-k) + w(n) = a(n) + w(n) \qquad n = 0, 1, \ldots, N-1$$

which is the desired expression – the discrete-time convolution of the transmit waveform with the scattering process on the single down-range strip of ground. In essence, the generation of a SAR map is attained by solving the linear set of equations (A-4) for the unknown scattering coefficients. Notice that the discrete-time sequence $\{a(n \mid n = 0, 1, \ldots, N-1\}$ is introduced to denote the noise-free observations.

Equation (A-4) represents the radar return signal of interest because it includes the desired scatter information that provides the SAR map, $\{\alpha(n \mid n = 0, 1, \ldots, N-1\}$. However, upon close examination of Equation (A-4) for the index values at the leading edge of the region, it is clear that the sensed signal includes the effects of the $K-1$ scatterers immediately preceding the start of the desired region, $\{\alpha(n \mid n = -K+1, -K+2, \ldots, -1\}$. Even though the desired SAR map starts at $n = 0$, the effects of the scatterers in locations corresponding to negative values of the index must be taken into account in the model if they are illuminated by the radiated pulse.

The set of linear equations (A-4) can be written in matrix form, and the resulting matrix exhibits a block-diagonal structure, but its dimensions are large. However, the dimensionality of the transmit waveform, K, is often much smaller than the total number of baseband observations, N. Of course, the number of scatterers to be estimated specifies the number of baseband observations. Figure A-1 illustrates the time line associated with the collection of N measurements, represented as N time intervals. Also illustrated is the duration of the transmitted waveform, represented as K time intervals. In addition, this figure indicates that the total number of measurements is assumed to be an integer multiple of the waveform duration. In this figure each time interval of duration K is represented with a unique color to emphasize the block nature of the measurements that is dictated by the convolution operator.

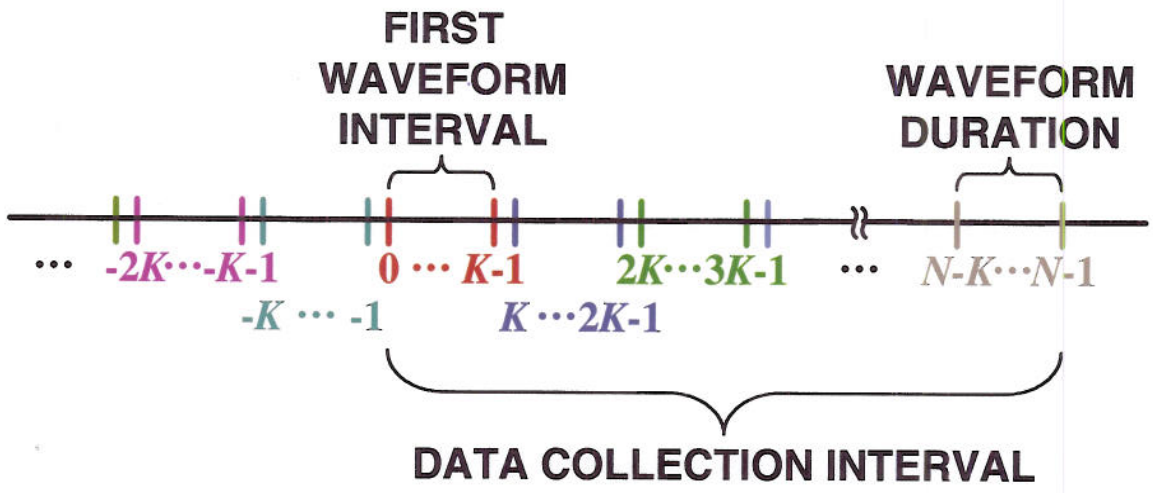

Figure A-1. Measurement timeline with normalized (unity-value) intervals.

Consider the first set of K measurements, corresponding to the first waveform interval indicated in Figure A-1. In particular, consider the noise-free measurement set, $\{a(n \mid n = 0, 1, \ldots, K-1\}$, because it exhibits the specific structure of the convolution operator. For these measurements it follows from Equation (A-4) that

$$\text{(A-5)} \qquad \begin{bmatrix} a(0) \\ a(1) \\ a(2) \\ \vdots \\ a(K-2) \\ a(K-1) \end{bmatrix} = \left[\begin{array}{ccccc|ccccc} 0 & s(K-1) & s(K-2) & \cdots & s(1) & s(0) & 0 & 0 & \cdots & 0 \\ 0 & 0 & s(K-1) & \cdots & s(2) & s(1) & s(0) & 0 & \cdots & 0 \\ 0 & 0 & 0 & \cdots & s(3) & s(2) & s(1) & s(0) & \cdots & 0 \\ \vdots & \vdots & \vdots & \ddots & \vdots & \vdots & \vdots & \vdots & \cdots & \vdots \\ 0 & 0 & 0 & \cdots & s(K-1) & s(K-2) & s(K-3) & s(K-4) & \ddots & 0 \\ 0 & 0 & 0 & \vdots & 0 & s(K-1) & s(K-2) & s(K-3) & \cdots & s(0) \end{array}\right] \left[\begin{array}{c} \alpha(-K) \\ \alpha(-K+1) \\ \alpha(-K+2) \\ \vdots \\ \alpha(-1) \\ \hline \alpha(0) \\ \alpha(1) \\ \alpha(2) \\ \vdots \\ \alpha(K-1) \end{array}\right]$$

Notice that this is a set of K linear equations in $2K$ unknowns, even though the K scatterers in the time instants prior to data collection initiation, $\{\alpha(n \mid n = -K, -K+1, \ldots, -1\}$, are outside the ROI. However, this matrix equation does highlight the effect of those scatterers in the first $K-1$ measurements of interest. Notice also that the first column on the matrix in this equation is a zero column, and as such it could be eliminated from the expression (along with the first element $\alpha(-K)$). But this form of the expression is introduced for notational convenience associated with the introduction of block elements, as shown next.

The structure exhibited in Equation (A-5) is repeated for each one of the K-element measurement sets in the total data set. Also, the partitions indicated in the right-hand-side of Equation (A-5) suggest a compact notation, as follows. Let $\mathbf{a}(n)$ denote a time-indexed K-element column vector with its elements given by the elements in the set $\{a(n+k \mid k = 0, 1, \ldots, K-1\}$ arranged in sequential order; that is,

$$\text{(A-6)} \qquad \mathbf{a}(n) = \begin{bmatrix} a(n) \\ a(n+1) \\ \vdots \\ a(n+K-1) \end{bmatrix} \qquad n = 0, K, 2K, \ldots, N-K$$

Further, define such vectors for each of the sequences $\{b(n)\}$, $\{\alpha(n)\}$, and $\{w(n)\}$. Also define the following two KxK matrices as suggested by the partition in Equation (A-5),

$$\text{(A-7)} \qquad \mathbf{S}_U = \begin{bmatrix} 0 & s(K-1) & s(K-2) & \cdots & s(1) \\ 0 & 0 & s(K-1) & \cdots & s(2) \\ 0 & 0 & 0 & \cdots & s(3) \\ \vdots & \vdots & \vdots & \ddots & \vdots \\ 0 & 0 & 0 & \cdots & s(K-1) \\ 0 & 0 & 0 & \vdots & 0 \end{bmatrix}$$

$$\text{(A-8)} \qquad \mathbf{S}_L = \begin{bmatrix} s(0) & 0 & 0 & \cdots & 0 \\ s(1) & s(0) & 0 & \cdots & 0 \\ s(2) & s(1) & s(0) & \cdots & 0 \\ \vdots & \vdots & \vdots & \cdots & \vdots \\ s(K-2) & s(K-3) & s(K-4) & \ddots & 0 \\ s(K-1) & s(K-2) & s(K-3) & \vdots & s(0) \end{bmatrix}$$

Now it is possible to represent the set of noise-free Equations (A-4) in compact notation as

$$\text{(A-9a)}\qquad \begin{bmatrix} \mathbf{a}(0) \\ \mathbf{a}(K) \\ \vdots \\ \mathbf{a}(N-2K) \\ \mathbf{a}(N-K) \end{bmatrix} = \begin{bmatrix} \mathbf{S}_U & \mathbf{S}_L & \mathbf{O} & \cdots & \mathbf{O} & \mathbf{O} & \mathbf{O} \\ \mathbf{O} & \mathbf{S}_U & \mathbf{S}_L & \cdots & \mathbf{O} & \mathbf{O} & \mathbf{O} \\ \vdots & \vdots & \vdots & \ddots & \vdots & \vdots & \vdots \\ \mathbf{O} & \mathbf{O} & \mathbf{O} & \cdots & \mathbf{S}_U & \mathbf{S}_L & \mathbf{O} \\ \mathbf{O} & \mathbf{O} & \mathbf{O} & \cdots & \mathbf{O} & \mathbf{S}_U & \mathbf{S}_L \end{bmatrix} \begin{bmatrix} \boldsymbol{\alpha}(-K) \\ \boldsymbol{\alpha}(0) \\ \boldsymbol{\alpha}(K) \\ \vdots \\ \boldsymbol{\alpha}(N-3K) \\ \boldsymbol{\alpha}(N-2K) \\ \boldsymbol{\alpha}(N-K) \end{bmatrix}$$

$$\text{(A-9b)}\qquad \mathbf{a} = \mathbf{S}\boldsymbol{\alpha}$$

where **O** represents a KxK matrix of zeros, and **S** denotes the waveform convolution matrix,

$$\text{(A-10)}\qquad \mathbf{S} = \begin{bmatrix} \mathbf{S}_U & \mathbf{S}_L & \mathbf{O} & \cdots & \mathbf{O} & \mathbf{O} & \mathbf{O} \\ \mathbf{O} & \mathbf{S}_U & \mathbf{S}_L & \cdots & \mathbf{O} & \mathbf{O} & \mathbf{O} \\ \vdots & \vdots & \vdots & \ddots & \vdots & \vdots & \vdots \\ \mathbf{O} & \mathbf{O} & \mathbf{O} & \cdots & \mathbf{S}_U & \mathbf{S}_L & \mathbf{O} \\ \mathbf{O} & \mathbf{O} & \mathbf{O} & \cdots & \mathbf{O} & \mathbf{S}_U & \mathbf{S}_L \end{bmatrix}$$

Analogously, the set of Equations (A-4) admits a compact notation as

$$\text{(A-11)}\qquad \mathbf{b} = \mathbf{a} + \mathbf{w} = \mathbf{S}\boldsymbol{\alpha} + \mathbf{w}$$

Another useful set of relations is obtained by the partitioning inherent in Equation (A-9a) and the corresponding expression for Equation (A-11). Specifically,

$$\text{(A-12)}\qquad \mathbf{b}(n) = \mathbf{a}(n) + \mathbf{w}(n) = \mathbf{S}_U\boldsymbol{\alpha}(n-K) + \mathbf{S}_L\boldsymbol{\alpha}(n) + \mathbf{w}(n) \qquad n = 0, K, 2K, \ldots, N\text{–}K$$

There are N_τ individual equations in (A-12) over the specified range of n (recall that $N = N_\tau K$). These relations are useful for the development of sub-optimal processing methods, as discussed later.

Equations (A-11) (or, equivalently, Equations (A-12)) represent a set of N linear equations in $N + K$ unknowns and in additive white noise. The unknowns include the set of N scatterers in the ROI, $\{\alpha(n \mid n = 0, 1, \ldots, N\text{–}1\}$, as well as the set of K scatterers prior to the start of the ROI, $\{\alpha(n \mid n = -K, -K+1, \ldots, -1\}$. Strictly speaking, the scatterer $\alpha(-K)$ has no effect on any of the N measurements since the first column of matrix **S** is all zeros (Equations (A-5), (A-7), and (A-9a)), so it is unnecessary to count it as an unknown. However, its inclusion allows the preservation of the block structure in matrix **S** and in Equations (A-12). Sometimes it is assumed that the K scatterers prior to the start of the ROI are zero in order to have N equations in N unknowns (which is a better-posed numerical problem than N equations in $N + K$ unknowns), but this is an incorrect model assumption in most cases. Failure to estimate those scatterers leads to worse estimates of the ROI scatterers even in the noise-free case, as shown later.

APPENDIX B: WAVEFORM DIVERSTITY PULSE COMPRESSION

Abstract

In the context of waveform diversity for radar system design, one of the diversity domains is the spatial domain, wherein different waveforms are transmitted from different spatial locations. Such an approach requires at least one more diversity domain to ensure that the different signals can be separated at each individual receiver; otherwise it reduces to transmit beamforming. This appendix investigates the specific case where two separated transmitters transmit two signals with the same frequency band and bandwidth, but with different modulation (up-chirp and down-chirp LFM). An approach based on a Kalman filter (KF) is described herein, and results obtained by processing simulated data are compared to results obtained using a conventional matched filter (MF). The results indicate that the KF provides improved pulse compression accuracy over the MF in the range of cases considered herein. Additionally, the KF estimates the complex phase and the magnitude better than the MF. For applications where phase history is important, the KF seems to have an advantage.

B 1.0 Introduction

Spatially diverse waveforms offer potential for improved radar performance in various contexts, provided the individual waveforms can be separated at the receiver. One application is lossless beamspoiling in situations where a system has more SNR than needed, but with a small beam spot, and other system performance constraints that require a minimum dwell time. A specific example is SAR imaging, wherein the desired resolution sets the minimum dwell time, regardless of actual SNR achieved by the system. Consider a case where the system is designed to operate at long ranges and low grazing angles. Then, when the need to operate at closer ranges and lower grazing angle arises, the SNR for those conditions is likely very high, and the illumination beam footprint is small. If maximum area coverage rate is desired, then the ability to spoil the beam losslessly on transmit to illuminate a larger footprint to the limit of the available SNR is beneficial. This can be achieved by having multiple sub-apertures of the antenna transmit different waveforms resulting in a larger spot size, while still having the full antenna receive both signals. A variation on this theme involves the case where the individual transmitters are separated along an axis perpendicular to the SAR velocity vector, and single-pass 3D IFSAR is possible, due to the transmitter separation, with only a single receive channel.

Another potential application is Moving Target Indication (MTI) radar [37], where clutter power is the major performance limiter in most cases (as opposed to SNR). In these cases a high SNR also results in a high SCR. The ability to transmit separate waveforms on two half-size apertures doubles the transmit footprint size, and the system can dwell twice as long for the same area coverage rate. Also, clutter cell size is reduced by half, so that only half the clutter power must be suppressed, on average, assuming typical post-Doppler STAP. Such reduction in clutter power improves system detection performance.

The up- and down-chirp LFM waveforms have significant cross-correlation values at all lags. Thus, the applicability of MF processing is limited in the case of two simultaneously transmitted waveforms (particularly in the case of extended ground clutter). Anderson [38] has considered these two waveforms to suppress range ambiguity by the use of time diversity in the context of a MF receiver. Specifically, the two different LFM waveforms were transmitted every other PRI, and non-linear processing techniques applied to suppress the cross-correlation inherent with the MF approach. See also the recent work of Nelander [39] and Blunt and Gerlach [40] (as well as the references therein).

B 2.0 Problem formulation and solution approach

Fig. B-1 illustrates the three configurations considered herein. Specifically, configuration 1 (C1) consists of two separate (but close) transmitter/receiver (T/R) systems, each transmitting an LFM waveform, and each receiving both returns (for simplicity, only one T/R system is analyzed, as shown). The LFM waveforms consist of an up-chirp and a down-chirp, with the same frequency range, bandwidth, and time duration. Configuration 2 (C2) is a single T/R with a single LFM waveform (up-chirp), and Configuration 3 (C3) is a single transmitter transmitting the sum of the two LFM waveforms.

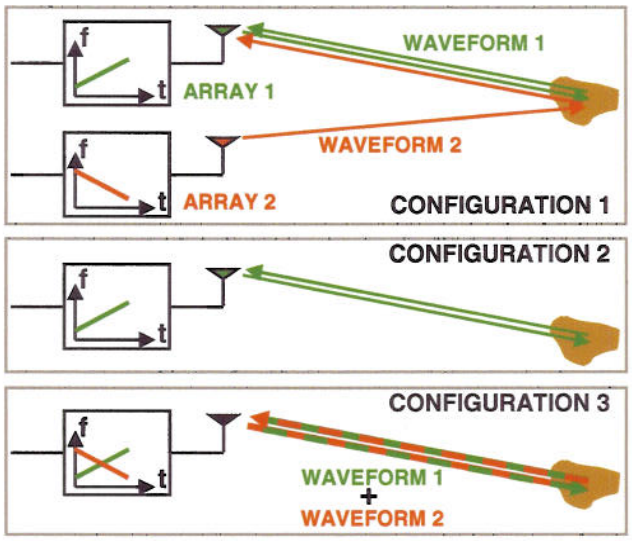

Figure B-1. Three distinct configurations for analysis.

Two processing approaches are considered for each of the configurations: the MF, and the KF. The KF admits various alternative implementations (optimal as well as sub-optimal), but the results presented are for the optimal block filter formulation, which is analogous to the MF structure and thus allows emphasizing various relevant issues. The processing approaches depend on the model adopted for each of the three configurations. C2 and C3 assume the typical model for a single platform scenario; namely,

$$\mathbf{b} = \mathbf{S}\mathbf{a} + \mathbf{w} \qquad \text{(B-1)}$$

where **b** denotes the $(M-N)$-element received (baseband) signal vector, **a** denotes the M-element vector of scattering coefficients in the selected range trace, **w** denotes the $(M-N)$-element sensor noise vector, and **S** denotes the $(M-N)\times M$ convolution matrix. The columns of **S** consist of zeros and the elements of the N-element wavelength vector **s**. In turn, C1 assumes a model of the form

$$\mathbf{b} = \mathbf{S}_1\mathbf{a} + \mathbf{S}_2\mathbf{a}e^{i\delta\phi} + \mathbf{w} \qquad \text{(B-2)}$$

where $e^{i\delta\phi}$ represents the delay due to the additional travel for the waveform emitted from T/R 2. Both of these models are defined to include the effects of the N scatterers located prior to the first scatterer of interest. These scatterers are included since it is inappropriate to assume they are zero-valued. In addition, they are estimated even though they are out of the region of interest.

B 2.1 Matched filter approach

The MF approach for C1 is presented in Fig. B-2. C2 and C3 admit the conventional approach. The auto- and cross-correlation for each of the two LFM waveforms are shown in Fig. B-3 for a time-bandwidth (TB) product of 100. Notice that the cross-correlation function (black curve) is quite a bit higher than most of the auto-correlation sidelobes (blue curve). It is this effect that limits the use of LFM waveforms with a MF for applications of spatial diversity where the separate detection of the two waveforms is important. Fig. B-4 shows the (magnitude) output of a MF for an input as in C2 (black curve), and for an input as in C3 (red curve); also shown is the cross-correlation between the two LFM waveforms (blue curve), all for TB = 100. Notice that the cross-correlation eclipses the auto-correlation sidelobes, as expected based on Fig. B-3. Results obtained using a temporal weighting (taper) lead to the well-known effect (wider main beam and lower sidelobes) on each curve, so the conclusion is the same if a taper is used.

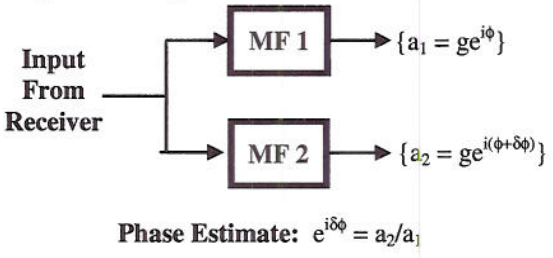

Figure B-2. Matched filter processing for Configuration 1

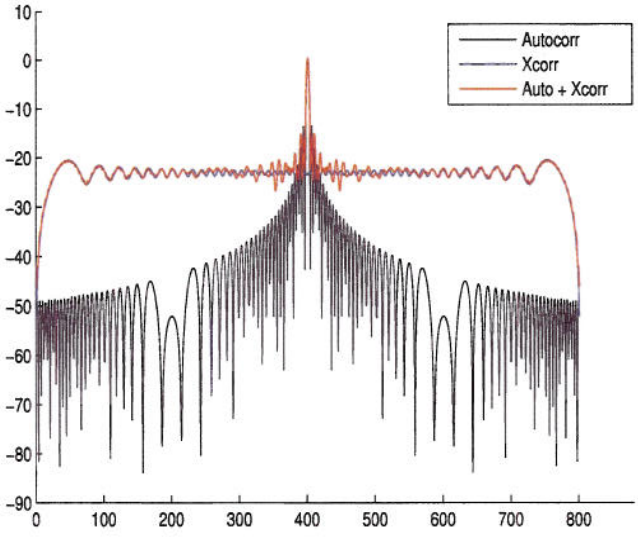

Figure B-3. LFM up- and down-chirp auto- and cross-correlation.

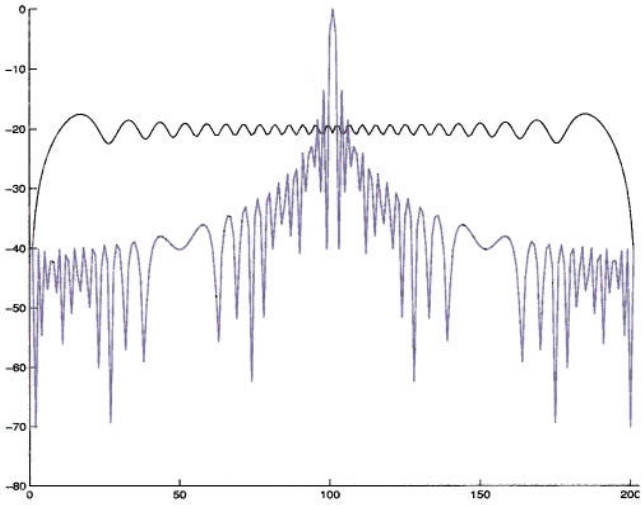

Figure B-4. Single- and dual-waveform MF response.

B 2.2 Kalman filter approach

The block KF form (with known noise covariance) is adopted, since this leads to alternative sub-optimal formulations. The formulation considered can be generated a priori, and applied subsequently. It is possible to demonstrate that the KF performance is dictated mostly by the structure of the model measurement matrix, **S**. In fact, it can be shown that the "sidelobe" structure and noise performance are related to the singular values of matrix **S**, and to the singular values of a circulant matrix formed using the waveform elements as its first row. This feature implies that alternative implementations of a given type of waveform can lead to distinct KF performance. In contrast, the MF is almost insensitive to such changes; thus, selecting a waveform based on such considerations improves KF performance, but has minimal impact on MF performance. Fig. B-5 presents the singular values of an up-chirp LFM for two distinct frequency ranges in C2. The case with symmetry about the frequency-domain origin (blue curve) exhibits little variation over its extent, and none of the values go below unity. It turns out that this implies a significant performance improvement for the KF in relation to the (frequency-domain) asymmetric case (red curve). This provides a valuable design approach. Fig. B-6 shows that the singular values of matrix **S** for up- and down-chirp LFM for C1 and C3 are identical. Finally, Fig. B-7 shows that the singular values of several matrices formed using a frequency-asymmetric up-chirp LFM in the context of C2 are very similar. The nominal **S**

matrix (blue curve), the full **S** matrix (thick red curve), and the related circulant matrix (black curve) cases are based on standard definitions. The extrapolated nominal case (yellow curve), however, is a plot of the (M–N = 360) nominal singular values (blue) plotted every 4/3 units.

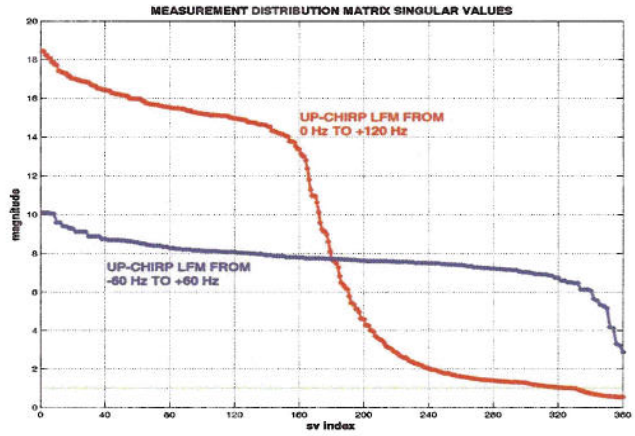

Figure B-5. **S** matrix singular values with two up-chirps in C2.

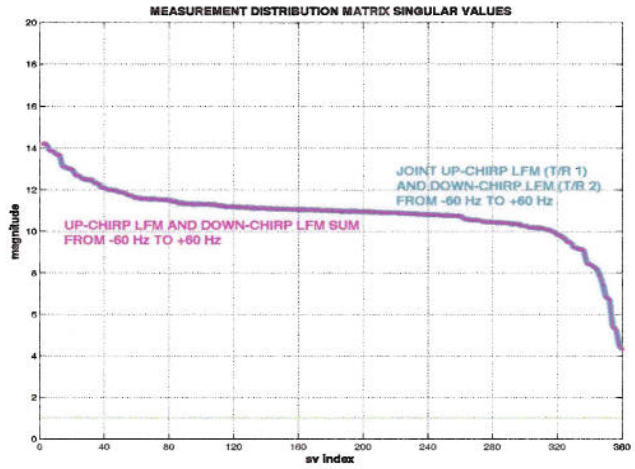

Figure B-6. **S** matrix singular values for up- and down-chirp LFM for C1 (cyan) and C3 (magenta).

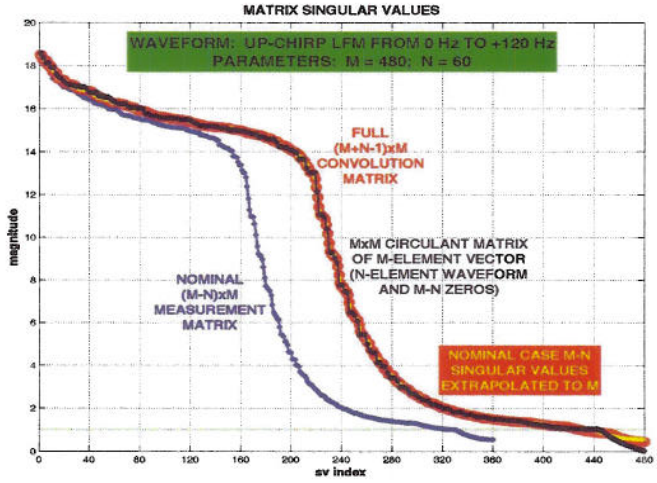

Figure B-7. Singular values of several matrices formed using a frequency-asymmetric up-chirp LFM.

B 3.0 Simulation-based analyses

The results presented herein were obtained using a MATLAB-based simulation. An LFM waveform is generated and convolved with a data set consisting of a point target in random background (point scatterers) at a fixed SBR of 15 dB. All RMS results are based on 1,000 independent runs. The LFM is designed with a symmetric frequency response, as discussed above. The runs made are the most stressing for the KF to show improvement since the modeled background is approximately 5 dB higher than the MF sidelobe levels. For background that has scattering magnitude lower than the MF sidelobe level, the KF should show further performance gains.

Fig. B-8 shows RMS scatterer magnitude estimation error for the point target with C2. The KF exhibits a slight advantage for all the SNR values shown. A similar plot is obtained for the RMS over all scatterers. Fig. B-9 presents analogous results for C2, and similar observations apply. Also, the RMS over all scatterers exhibits similar characteristics (but on a lower RMS scale). Examination of Fig. B-9 in relation to Fig. B-8, leads to the conclusion that neither filter does as well in the dual-waveform, dual-array system as in the single-waveform case. The high sidelobe levels from the MF cross-correlation degrade the MF results. The sidelobe levels are mitigated in the KF case, but it appears that the under-determined nature of the measurement equation has degraded the KF's ability to suppress noise as well. In C1 the processor has to estimate roughly twice as many scatterer values (one for each waveform/transmitter) from the same amount of data. A direct manifestation of this is observed in the single-run power estimates in Figs. B-10 and B-11. These two figures show that the RMS performance of the KF and MF for C1 and C2 at 0 dB SNR is similar, although there is a higher bias-like error for C1. The higher bias-like error with MF as well as KF processing is the source of the higher total RMS error in Fig. B-9 (recall that RMS error includes both bias and standard deviation terms). These visual observations from Figs. B-10 and B-11 are consistent with the statistical results in Figs. B-8 and B-9. The increased bias level of C1 in relation to C2 for the scatterer estimation error is likely due to the increased sidelobe level from the two waveforms.

Results were obtained for C3 also, but are not shown. There is little reason to transmit both up- and down-chirps from a single antenna simultaneously. For C3, however, the KF has slightly better performance at low SNR, whereas at higher SNR they have similar performance.

A single case was run for C1 using a larger number of scatterers and with lower SBR as well as lower SNR in order to demonstrate the reason for the enhanced performance of the KF approach to pulse compression for multiple waveforms over the MF approach (Figure B-12). The sidelobe levels are indeed noticeably higher for the MF.

Preliminary results (not shown) indicate that the KF consistently provides slightly better estimates of magnitude and phase than the MF. This difference in estimation performance is obscured in complex phase error plots, but can be measured in RMS values.

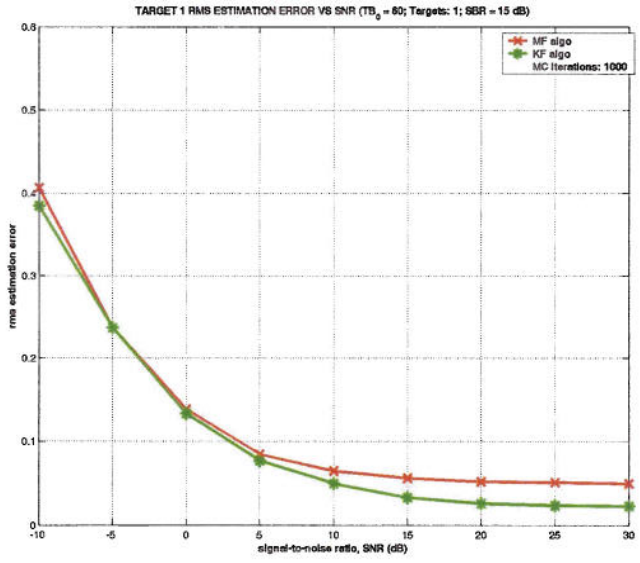

Figure B-8. RMS error for single point target in random background for KF (green) and MF (red) in C2.

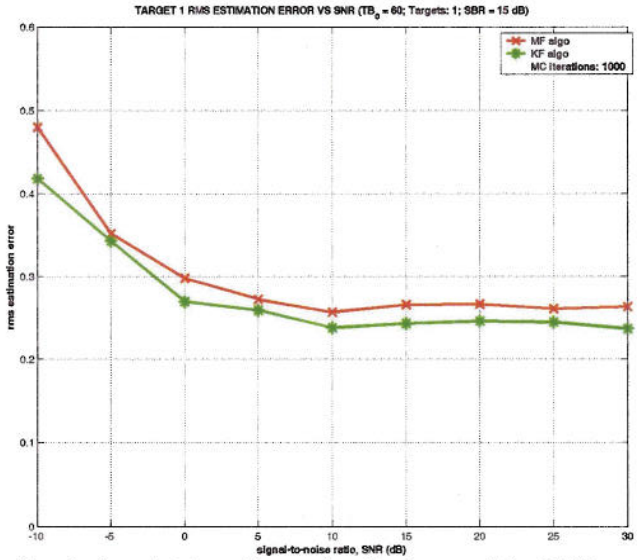

Figure B-9. RMS error for single point target in random background for KF (green) and MF (red) in C1.

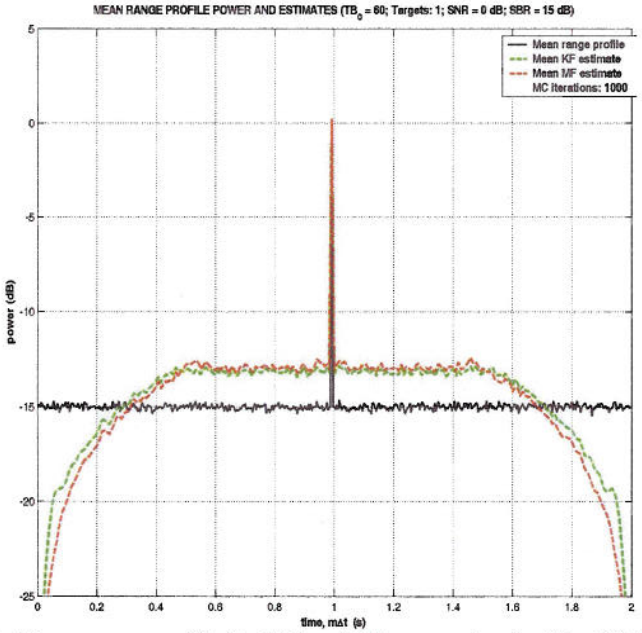

Figure B-10. Mean range profile for MF and KF processing in C2 at 0 dB pre-compression SNR.

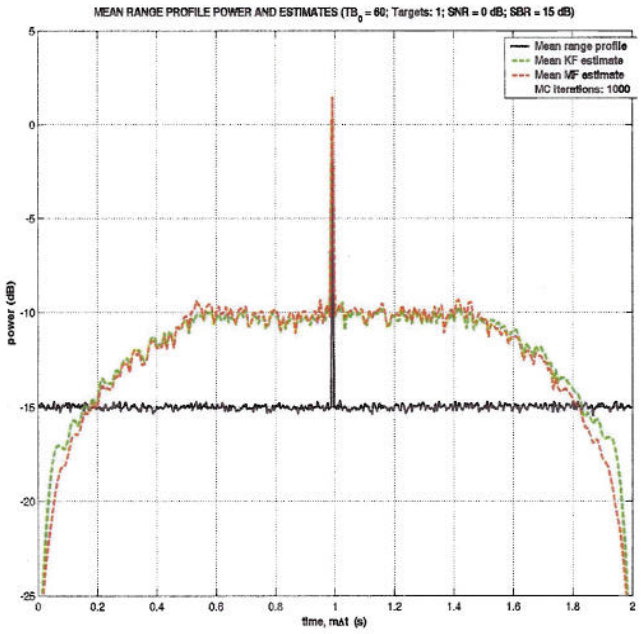

Figure B-11. Mean range profile for MF and KF processing in C1 at 0 dB pre-compression SNR.

B 4.0 Conclusions

Performance results to date show that for C1 (spatially diverse transmitters each transmitting an up-chirp or down-chirp), the KF has better pulse compression performance than the MF. Somewhat surprisingly, the KF performs better than the MF over a wide set of SNR values for C2 (single waveform case) also. In scenarios where sidelobe suppression is more important than SNR maximization, the KF is the better choice. From a computational viewpoint, the KF imposes a significantly larger burden than the MF. However, the KF formulation adopted herein allows pre-calculation of the Kalman gain, and furthermore, allows the definition of various sub-optimal approaches with large reductions in processing load and minimal loss in performance.

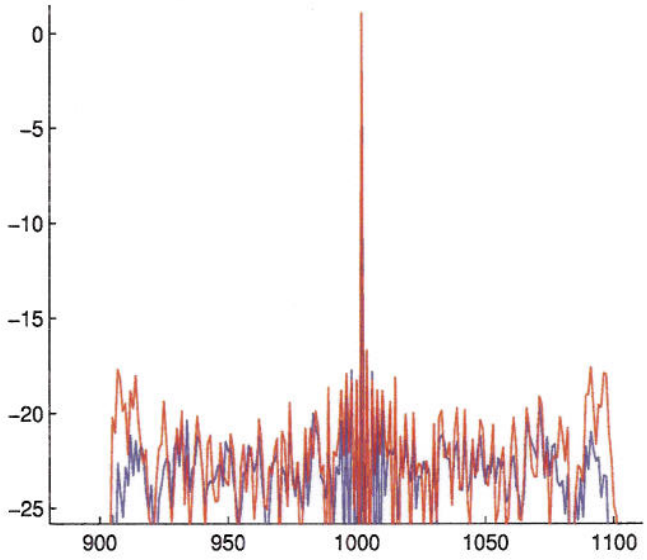

Figure B-12. MF (red) and KF (blue) pulse compression for C1 with low SCR and high SNR (single realization).

APPENDIX C: RANGE-COHERENT SPATIALLY-DIVERSE SUB-BAND COMBINATION

This appendix presents an approach for estimation of the complex-valued ground scattering coefficients in the range direction using frequency-diverse waveforms as well as spatial diversity. The approach can be applied in the context of airborne and/or space-borne radar scenarios. Specifically, the proposed approach involves the coherent combination of two contiguous, non-overlapping bandwidth radar waveforms transmitted simultaneously from two separate cross-track transmitters (with respect to the platform motion track). This increases the effective length of the interferometric baseline as well as the number of unique baselines being measured (2 vs 1), and adds one redundant baseline measurement, which is used for error detection and correction between the individual transmitters/receivers. The configuration formulated herein could be used on an airborne platform to increase the effective transmitted power (due to the second transmitting antenna), and to increase the height resolution (due to the longer effective baseline being sampled), in relation to the single-transmitter, dual-receiver case. Another possibility is the case of two individual free-flying UAV aircraft with a SAR payload, combining their capability to provide single pass IFSAR and the resulting HRTI product.

The configuration considered herein is based on two complete radar systems (full transmit and receive capability), co-located in the plane defined by the down-range direction axis and its projection on the ground, as shown in Figure C-1. Each radar transmits a modulated waveform (possibly phase modulated) on its assigned frequency band, and receives and processes both returns. Further, the frequency band assigned to each transmitter is one-half of the desired total contiguous bandwidth, so that the combined waveform of the two transmissions covers the desired total bandwidth. Such a dual-radar, jointly-operating configuration is an example of a Multi-Input Multi-Output (MIMO) system. The ground is modeled as a set of point scatterers $\{g_i\}$, with one point scatterer at the center of each range bin of width Δr, the range resolution. In turn, Δr is defined by the bandwidth of the transmitted waveform. Another important assumption is that the frequency difference between the two transmitted signals is small enough such that the value of the complex scattering coefficient is the same for each sub-band signal when sensed from each of the two receiver/transmitter combinations. At reception, each receiver separates via frequency-domain filtering the return due to each of the two transmitted signals (with negligible out-of-band residuals), and compresses each return signal separately. A key assumption is that the separation between the two radars is small enough to be within the monostatic limit. This ensures that the radar-to-range bin geometry is sufficiently similar so that the dimensions and orientations of the two set of range bins are compatible and overlap (see Figure C-2). In the example on the left in Figure C-2, the red and blue sets of range bins have good compatibility and overlap, whereas the green set of range bins has poor compatibility and overlap with both of the other two (likely due to the radar being out-of-plane with the other two radars). In the example on the right, the red and blue sets of range bins exhibit good alignment at the bottom but have a consistently-increasing misalignment along the range dimension leading to almost complete misalignment at the top. This condition is likely due to a large in-plane separation between the two radar systems. Again, the geometry is assumed to be such that these deleterious effects can be ignored.

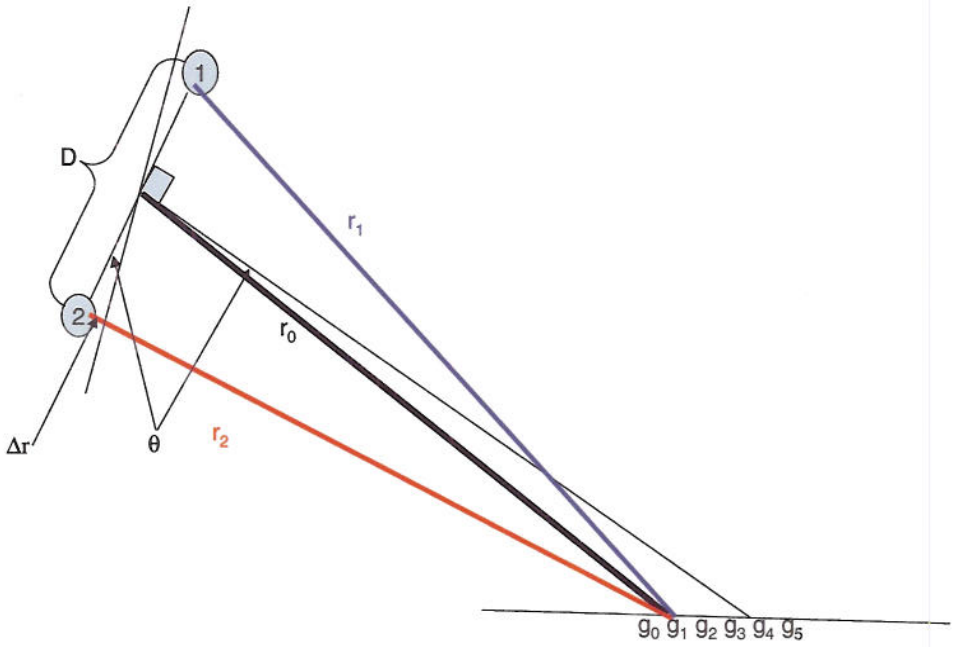

Figure C-1. Scenario definition and geometry.

The two bistatic transmit/receive pairs share a common virtual phase center (via the bistatic equivalence theorem) and resulting slant plane. Such common geometry (redundant spatial information) can be used to align the data in

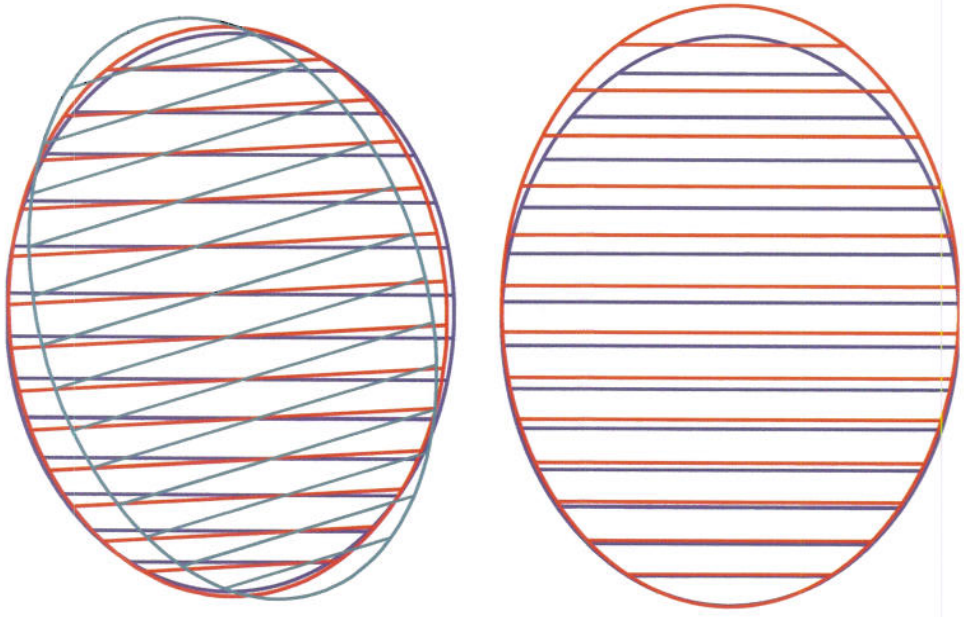

Figure C-2. Range bin overlap for different geometries.

the range dimension, thus correcting for system timing synchronization errors that result in relative phase errors between the two different transmitters/receivers. This is accomplished by determining the discrepancy between the two cross-radar (transmitter k and receiver ℓ, with $k \neq \ell$) signals. The calculated phase discrepancy is then applied to the monostatic (transmitter k and receiver k) signals to align them also. A key assumption is that a separate relative position and timing metrology subsystem corrects the relative timing between the two radars to less than a cycle of the center frequency to resolve the 2π phase ambiguity.

The approach used to align the data utilizes the fact that the path from transmitter 1 to scatterer i to receiver 2 is the same as the path from transmitter 2 to scatterer i to receiver 1. Let $\{s_{k\ell}(n)\}$ denote the baseband signal (after pulse compression) at discrete time instant n received at receiver ℓ from transmitter k. Then $\{s_{12}(n)\}$ and $\{s_{21}(n)\}$ correspond to cross-radar signals. Any difference in the cross-radar signals is due to amplitude and/or phase errors between the two radars receivers and to noise-like effects. Thus, let $\{\varepsilon_n\}$ denote the unknown complex-valued scalar factor representing the discrepancy between $\{s_{12}(n)\}$ and $\{s_{21}(n)\}$; specifically,

(C-1) $$s_{12}(n) = \varepsilon_n \, s_{21}(n) \qquad n = 0, 1, \ldots, N\text{-}1$$

Now the N unknown scalars are obtained as

(C-2) $$\varepsilon_n = \frac{s_{12}(n)}{s_{21}(n)} \qquad n = 0, 1, \ldots, N\text{-}1$$

It is important to recognize that both numerator and denominator in the right-hand-side of the above relation include an appropriate receiver noise term (temporally and spatially uncorrelated), which places a limit on the accuracy of the resulting estimate of the unknown discrepancy.

Each scalar value in Equation (C-2) has a magnitude and phase. It is assumed herein that over a single PRI ($n = 0, 1, \ldots, N\text{-}1$) the magnitude of ε_n is a constant denoted as A_ε, and its phase, denoted as ϕ_n, admits a linear variation. Specifically, each scalar satisfies the relation

(C-3) $$\varepsilon_n = A_\varepsilon \, \mathrm{e}^{i\phi_n} = A_\varepsilon \, \mathrm{e}^{i(\phi_0 + (n-1)\phi_\Delta)} \qquad n = 0, 1, \ldots, N\text{-}1$$

Given Equation (C-3), a set of relations can be defined to obtain the model parameters A_ε, ϕ_0, and ϕ_Δ. First, the magnitude A_ε is obtained simply as

(C-4) $$A_\varepsilon = \frac{1}{N} \sum_{n=0}^{N-1} |\varepsilon_n|$$

Next, Equation (C-3) implies that

(C-5) $$\phi_n = \phi_0 + (n-1)\,\phi_\Delta \qquad n = 0, 1, \ldots, N\text{-}1$$

The equation for $n = 0$ is a special case since it provides the initial condition in a recursive approach to the solution; thus, for that case the term $-\phi_\Delta$ is dropped, and it follows trivially that

(C-6) $$\phi_0 = \phi_0$$

The remaining N-1 equations are re-arranged and combined linearly to yield an estimate of ϕ_Δ as

(C-7) $$\phi_{\Delta} = \frac{1}{N-1}\sum_{n=1}^{N-1}\frac{1}{n}(\phi_n - \phi_0)$$

This completes the model for the discrepancy.

Angle θ in Figure C-1 is the angle between the two range directions; namely, the range direction from virtual phase center to the reference ground location (reference range bin), and the range direction from virtual phase center to the *i*th range bin. Thus, there are multiple such angles (one for each range bin), and $\theta(i)$ is the appropriate representation. Likewise, the range variables in Figure C-1 (r_1, r_2, and Δr) are also functions of the discrete index i. However, the functional dependence on the index i (on these and other variables) is dropped hereafter for simplicity. Solving for θ allows us to calculate the height of the range bin, but the derivation of the relations to generate θ remains as a task for the next period.

Consider the block diagram in Figure C-3, wherein the outputs are a set of time sequences consisting of the output of the pulse compression operations. Specifically, $P_{k\ell}$ represents the compressed signal in receiver ℓ of the waveform transmitted by transmitter k (actually, the extended-notation representation is $p_{k\ell}(n)$, since it is a time sequence, but the functional dependence is dropped). Analogously, the primed variable $P'_{k\ell}$ represents the time-shifted compressed signal in receiver ℓ of the waveform transmitted by transmitter k. Time-shifted pulse compression is defined in Figure C-4, where it is indicated that only a single time shift is applied. Now let $\Delta\phi_1$ denote the phase offset between P_{11} and P_{12} ($\Delta\phi_1$ is a function of time).. Similarly, let $\Delta\phi_2$ denote the phase offset between P_{22} and P_{21} ($\Delta\phi_2$ is a function of time). These variables are related to the range differences $\Delta r_1 1$ and Δr_2 in Figure C-1 according to

(C-8) $$\Delta\phi_1 = 2\pi\Delta r_1/\lambda_1$$

(C-9) $$\Delta\phi_2 = 2\pi\Delta r_2/\lambda_2$$

However, the phase offsets can be obtained via appropriate processing of the compressed signal sequences, as indicated next.

The receiver processing approach in Figure C-3 is based on the signal model established next with the aid of Figure

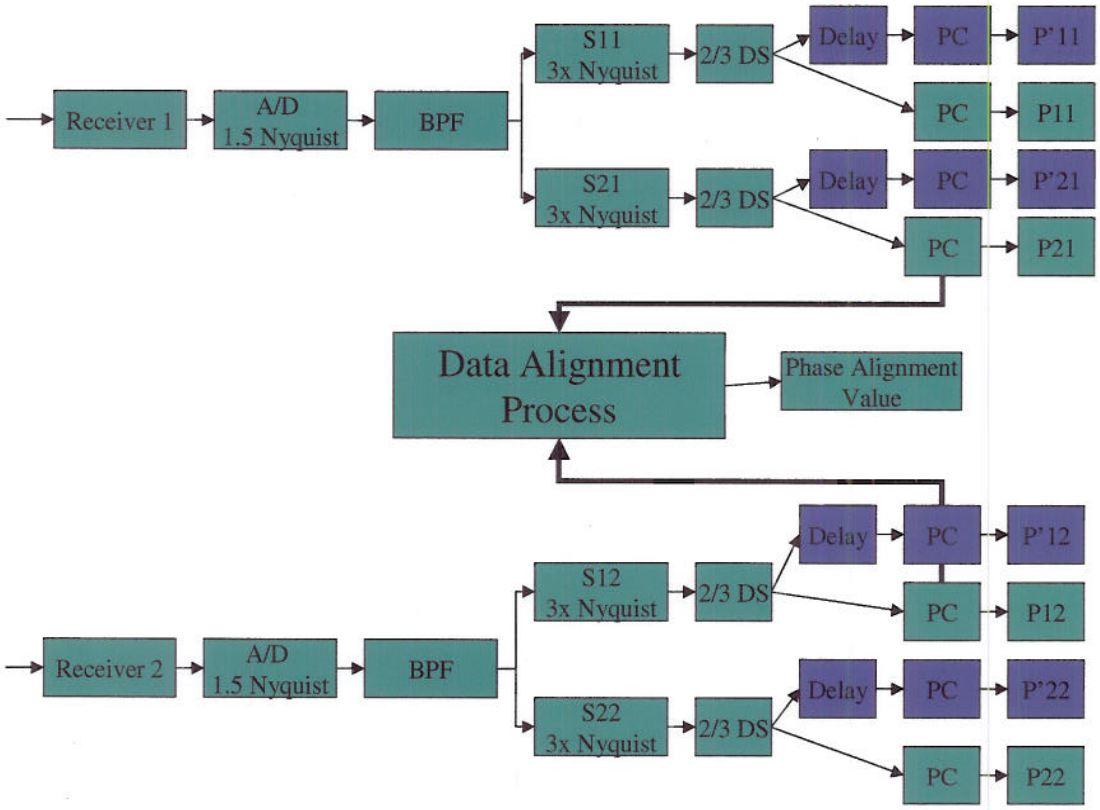

Figure C-3. Dual receiver processing block diagram.

C-5. Three adjacent ground resolution cells (range bins) are shown at the top of Figure C-5. The width of each

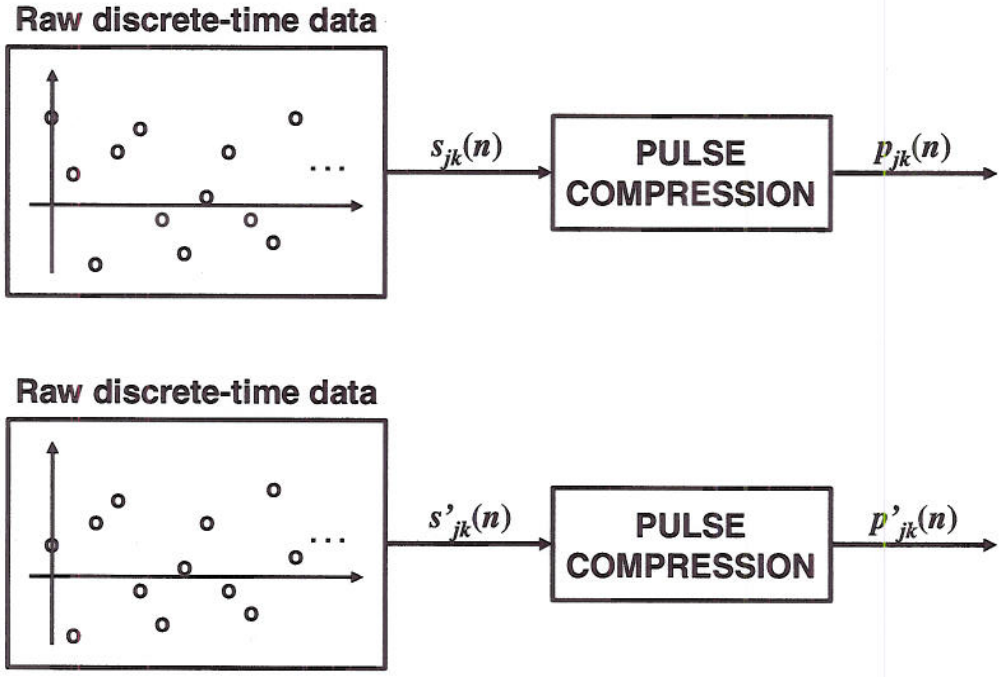

Figure C-4. Time-shifted pulse compression operation.

resolution cell corresponds to the total system bandwidth resolution, while the resolution of each half-bandwidth transmitted signal is one-half the range resolution. This is illustrated in the figure by the colored broad lines, which are twice as long as the length of one resolution cell. Thus, each pulse-compressed return (monostatic as well as cross-radar) from a single transmitter/receiver pair encompasses two separate but adjacent scatterers; that is, each time sample in the pulse compressed signal represents the joint return from the two complex scatterers, and is modeled as a single (combined) scatterer centered at the mid-point of the two full-bandwidth range bins. The separation of each pair of scatterers from the center of the half-bandwidth range bin is represented as a phase shift of the reflected signal of either $+\pi/4$ or $-\pi/4$, in relation to a scatterer located at the center of the half-bandwidth range bin. Thus, the first time sample of the pulse compressed signal for transmitter 1 and receiver 1 (P_{11}) is the sum of the scattered return from g_0 and g_1; likewise for P_{12}, P_{21}, and P_{22} (as indicated in Figure C-5). The "prime" signals (P'_{jk}) represent the output of the pulse compression operator to an input that consists of the raw return data with a starting time of one full-bandwidth time sample after the start time of the un-primed data (see Figure C-4). Thus, the first time sample of the pulse compressed "prime" signal for transmitter 1 and receiver 1 (P'_{11}) is the sum of the scattered return from g_1 and g_2; likewise for P'_{12}, P'_{21}, and P'_{22} (as indicated in Figure C-5).

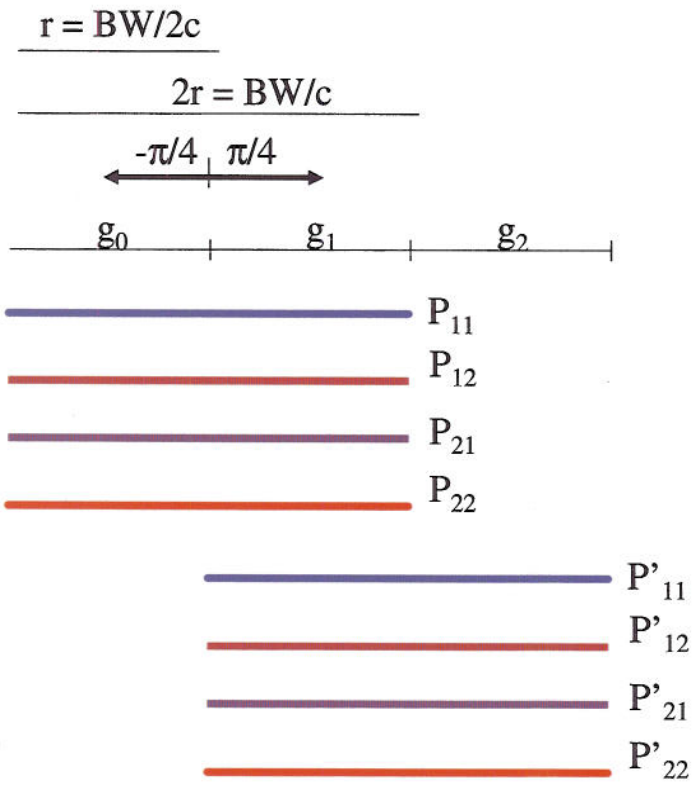

Figure C-5. Pulse-compressed signals information content.

Based on the above discussion, the following relations represent the various return signals at the first time sample (and analogous expressions are valid for subsequent time samples),

(C-10) $P_{11} = (K^* g_0 + K g_1) L_1$

(C-11) $P_{12} = (K^* g_0 + K g_1)$

(C-12) $P_{21} = (K^* g_0 + K g_1)$

(C-13) $P_{22} = (K^* g_0 + K g_1) L_2$

(C-14) $P'_{11} = (K^* g_1 + K g_2) L_1$

(C-15) $P'_{12} = (K^* g_1 + K g_2)$

(C-16) $P'_{21} = (K^* g_1 + K g_2)$

(C-17) $P'_{22} = (K^* g_1 + K g_2) L_2$

where the following definitions have been introduced for notational simplicity,

(C-18a) $K = e^{i(\pi/4)}$

(C-18b) $K^* = e^{i(-\pi/4)}$

(C-19) $L_1 = e^{i(\Delta\phi_1)}$

(C-20) $L_2 = e^{i(\Delta\phi_2)}$

(C-21) $g_k = A_k e^{i(\gamma_k)}$

Equations (C-10)-(C-17) can be combined and expressed in matrix form as (using Equations (C-18)-(C-21) also)

(C-22)
$$\begin{bmatrix} P_{11} \\ P_{12} \\ P_{21} \\ P_{22} \\ P'_{11} \\ P'_{12} \\ P'_{21} \\ P'_{22} \end{bmatrix} = \begin{bmatrix} L_1K^* & L_1K & 0 \\ K^* & K & 0 \\ K^* & K & 0 \\ L_2K^* & L_2K & 0 \\ 0 & L_1K^* & L_1K \\ 0 & K^* & K \\ 0 & K^* & K \\ 0 & L_2K^* & L_2K \end{bmatrix} \begin{bmatrix} g_0 \\ g_1 \\ g_2 \end{bmatrix}$$

Unfortunately, this is a system of nonlinear equations since it includes products between the unknown variables: g_0, g_1, g_2, L_1, and L_2. The system of equations (C-22) can be solved using nonlinear techniques; however, such methods present convergence and other computational issues, so alternative approaches are desired. Notice that the nonlinearities involved are simple products of the unknowns. Thus, one alternative approach consists of transforming the above system of equations into a linear system of equations by applying the natural logarithm (ln) operator to each one of the scalar equations. Following this procedure leads to,

(C-23) $\ln(P_{11}) = i(\Delta\phi_1) + \ln(K^* g_0 + K g_1)$

(C-24) $\ln(P_{12}) = \ln(K^* g_0 + K g_1)$

(C-25) $\ln(P_{21}) = \ln(K^* g_0 + K g_1)$

(C-26) $\ln(P_{22}) = i(\Delta\phi_2) + \ln(K^* g_0 + K g_1)$

(C-27) $\ln(P'_{11}) = i(\Delta\phi_1) + \ln(K^* g_1 + K g_2)$

(C-28) $\ln(P'_{12}) = \ln(K^* g_1 + K g_2)$

(C-29) $\ln(P'_{21}) = \ln(K^* g_1 + K g_2)$

(C-30) $\ln(P'_{22}) = i(\Delta\phi_2) + \ln(K^* g_1 + K g_2)$

To simplify notation further (and thus bring out the fundamental structure in the system of equations), let

(C-31) $a = K^{*}g_0 + Kg_1$

(C-32) $b = K^{*}g_1 + Kg_2$

As before, it is convenient to express Equations (C-23)-(C-30) in matrix form as

(C-33)
$$\begin{bmatrix} \ln(P_{11}) \\ \ln(P_{12}) \\ \ln(P_{21}) \\ \ln(P_{22}) \\ \ln(P'_{11}) \\ \ln(P'_{12}) \\ \ln(P'_{21}) \\ \ln(P'_{22}) \end{bmatrix} = \begin{bmatrix} 1 & 0 & 1 & 0 \\ 1 & 0 & 0 & 0 \\ 1 & 0 & 0 & 0 \\ 1 & 0 & 0 & 1 \\ 0 & 1 & 1 & 0 \\ 0 & 1 & 0 & 0 \\ 0 & 1 & 0 & 0 \\ 0 & 1 & 0 & 1 \end{bmatrix} \begin{bmatrix} \ln(a) \\ \ln(b) \\ i\Delta\phi_1 \\ i\Delta\phi_2 \end{bmatrix}$$

where Equations (C-31) and (C-32) have been applied. Using compact vector-matrix notation, and introducing temporally-uncorrelated zero-mean Gaussian-distributed additive noise with diagonal covariance matrix (denoted as **v**) in the model leads to

(C-34) $\mathbf{m} = \mathbf{T}\mathbf{s} + \mathbf{v}$

where **s** is the vector of the unknown variables. Figure 6 links the data flow in the dual receiver block diagram to the above equations.

Matrix **T** is rectangular (with more rows than columns) and is full rank. Equation (C-34) can be solved via the pseudo-inverse of **T**, denoted as $\mathbf{T}^{\#}$. Specifically,

(C-35) $\mathbf{s} = \mathbf{T}^{\#}\mathbf{m} - \mathbf{T}^{\#}\mathbf{v}$

The preferred technique for computing the pseudo-inverse of a rectangular matrix is via the singular value decomposition (svd) of the matrix. Besides providing robust numerical features, the svd of **T** provides insight into the subspaces (range and nullity) of the matrix **T**, and also provides the singular values of **T**, which indicate the

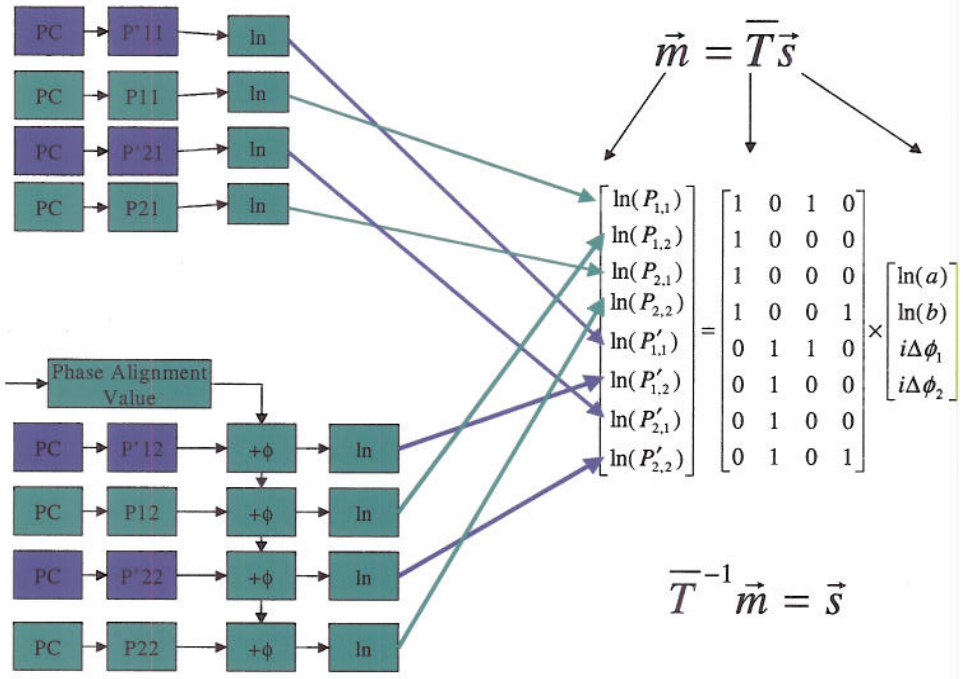

Figure C-6. Mapping from block diagram to equation.

relative importance of the ordered basis vectors that span the range of **T**.

Since the model in Equation (C-35) contains an additive noise term, then the approach described above also provides a mechanism to analyze the first- and second-order statistics of the residual noise term (the noise remaining after solving for **s**). Given the characteristics of the noise (zero mean and diagonal covariance matrix $\mathbf{R}_{vv} = \sigma_v^2 \mathrm{I}$,), the covariance matrix of the residual noise term, $\mathbf{R}_{uu}$, is given as

(C-36) $$\mathbf{R}_{uu} = \begin{bmatrix} 0.375 & 0.125 & -0.25 & -0.25 \\ 0.125 & 0.375 & -0.25 & -0.25 \\ -0.25 & -0.25 & 0.75 & 0.25 \\ -0.25 & -0.25 & 0.25 & 0.75 \end{bmatrix}$$

After normalization this matrix becomes,

(C-37) $$\mathbf{R_{uu}} = \begin{bmatrix} 1 & 1/3 & -1/3 & -1/3 \\ 1/3 & 1 & -1/3 & -1/3 \\ -2/3 & -2/3 & 1 & 1/3 \\ -2/3 & -2/3 & 1/3 & 1 \end{bmatrix}$$

The solution provided above by equation (C-35) generates an estimate of the two unknown phases, $\Delta\phi_1$ and $\Delta\phi_2$. However, the ln(a) and ln(b) terms need to be transformed into the desired g_k values.

The first step to determine the g_k values is to take the exponential of ln(a) and ln(b) to calculate a and b. Using Equations (C-27) and (C-28), the following two equations can be stated,

(C-38) $$\Delta a = a - \hat{a} = (K^* g_0 + K g_1) - (K^* \hat{g}_0 + K \hat{g}_1)$$

(C-39) $$\Delta b = b - \hat{b} = (K^* g_1 + K g_2) - (K^* \hat{g}_1 + K \hat{g}_2)$$

Where $\hat{a}$ is the estimate of a, $\hat{b}$ is the estimate of b, and $\hat{g}$ is the estimate of g. Further, let

$\Delta g_0 = g_0 - \hat{g}_0 = 0$ (assuming that the estimate for g_0 is "very close")

$\Delta g_1 = g_1 - \hat{g}_1$

$\Delta g_2 = g_2 - \hat{g}_2$

$KK^* = 1$

Then Equations (C-38) and (C-39) can be re-written as

(C-40) $$K\Delta a = K^2 \Delta g_1$$

(C-41) $$K\Delta b = \Delta g_1 + K^2 g_2$$

and expressed in compact matrix form,

(C-42) $$\begin{bmatrix} K\Delta a \\ K\Delta b \end{bmatrix} = \begin{bmatrix} K^2 & 0 \\ 1 & K^2 \end{bmatrix} \begin{bmatrix} \Delta g_1 \\ \Delta g_2 \end{bmatrix}$$

The above system is upper-triangular and admits a trivial solution, which is

(C-43) $\Delta g_1 = K^{-1} \Delta a$

(C-44) $\Delta g_2 = K^{-1} \Delta b - K^{-3} \Delta a$

This procedure presented to this point provides a solution for the first time interval. After updating the estimates for g_1 and g_2 the process continues to the next step. Specifically, to update the g_2 estimate and the g_3 estimate as indicated in Figure C-7 (which is analogous to Figure C-5 for the first time interval).

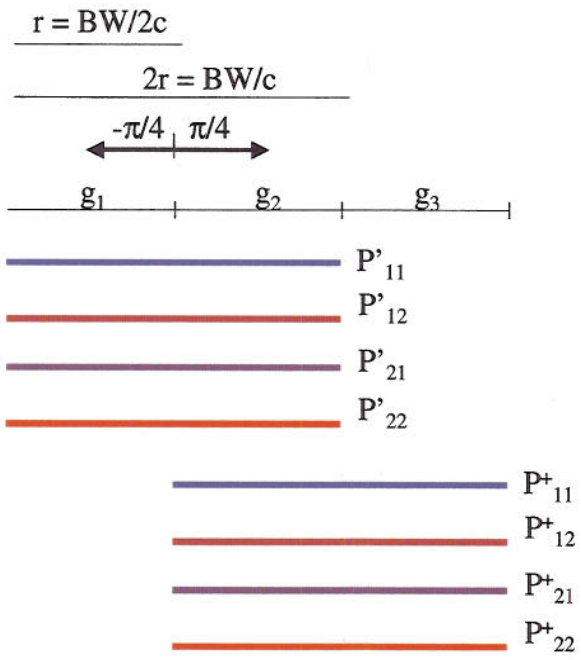

Figure C-7. Data relationship for time-shift in next interval.

APPENDIX D: AN INFORMATION THEORETIC CRITERION APPLIED TO POLARIZATION DIVERSITY

D 1.0 Introduction

This technical memo presents an analytic model and the associated formulation for the application of the SAIC information theoretic criterion to polarization diversity. Specifically, the mutual information (MI) criterion developed by Roman et al. [5] in the context of generic radar sensing is applied to the automatic determination of the polarization modulation to be applied from pulse-to-pulse. Mutual information (MI) is a measure of the information (in the sense of Shannon) in a random variable (or vector) about another random variable (or vector). Roman et al. [5] show that such a framework provides the basis for a simple yet powerful criterion for context-dependent evaluation of candidate waveforms, as well as the context-dependent design of waveforms. Herein, the context-dependent descriptor means that the criterion inherently includes the statistical information of the sensed parameters (the covariance matrix of the set of illuminated ground scatterers). Furthermore, the criterion can be used in distinct optimization contexts (minimization or maximization) as a function of the problem to be addressed. However, the minimization context is the relevant approach for polarization diversity as considered herein. It should be apparent that the methodology applies with obvious modifications to modulation changes from one coherent processing interval (CPI) to another.

D 2.0 Analytic Model For Full-Polarization Radar System

Consider a narrowband monostatic airborne or spaceborne radar system with full-polarization transmitter and receiver operating in synthetic aperture radar (SAR) mode. Further consider that the system transmits a short-duration pulse to provide inherent (without pulse compression) high range resolution. For such a system the received radar signal over an appropriately-selected time interval can be represented as vector $\mathbf{b}$ over space and time. Specifically, for a single transmitted and received pulse, the received (baseband) signal admits a model of the form

$$\mathbf{b} = \mathbf{a} + \mathbf{w} = \mathbf{H}\boldsymbol{\alpha} + \mathbf{w} \tag{D-1}$$

where $\boldsymbol{\alpha}$ denotes the $(4M)$-element vector of M complex-valued scattering coefficients in the ground region of interest, and each ground scatterer is characterized by the four elements of its polarization scattering matrix in the conventional horizontal (H) and vertical (V) axes at the scatterer location. Matrix $\mathbf{H}$ denotes the Kx$(4M)$ sensing (measurement) model matrix, and $\mathbf{w}$ denotes the K-element zero-mean, Gaussian-distributed complex-valued receiver noise vector that is uncorrelated over space and time and with covariance matrix

$$\mathrm{E}\left[\mathbf{w}\mathbf{w}^{\mathrm{H}}\right] = \mathbf{R}_{\mathbf{ww}} = \sigma_w^2 \mathbf{I}_K \tag{D-2}$$

The random variates $\mathbf{w}$ are assumed to be analytic signals, which implies that they are circular random variates and admit the standard complex Gaussian probability density function (PDF) for such variates. For the case herein, $K = 2M$ since there are two measurements (H and V) for each ground scatterer

The received signal vector ($\mathbf{b}$) and the scattering coefficient vector ($\boldsymbol{\alpha}$) are defined as partitioned vectors of the form

$$\mathbf{b} = \begin{bmatrix} \mathbf{b}_1 \\ \mathbf{b}_2 \\ \vdots \\ \mathbf{b}_M \end{bmatrix} \tag{D-3}$$

(D-4) $$\boldsymbol{\alpha} = \begin{bmatrix} \boldsymbol{\alpha}_1 \\ \boldsymbol{\alpha}_2 \\ \vdots \\ \boldsymbol{\alpha}_M \end{bmatrix}$$

respectively. In turn, each of the M sub-vectors $\{\mathbf{b}_m \mid m = 1, 2, \ldots, M\}$ contains the two outputs of the full-polarization receiver in the H and V axes at the scatterer location,

(D-5) $$\mathbf{b}_m = \begin{bmatrix} b_{m\mathrm{H}} \\ b_{m\mathrm{V}} \end{bmatrix}$$

Likewise, each of the M sub-vectors $\{\boldsymbol{\alpha}_m \mid m = 1, 2, \ldots, M\}$ contains the four elements of the polarization scattering matrix for the mth scatterer in the H and V axes at the scatterer location,

(D-6) $$\boldsymbol{\alpha}_m = \begin{bmatrix} \alpha_{m\mathrm{HH}} \\ \alpha_{m\mathrm{HV}} \\ \alpha_{m\mathrm{VH}} \\ \alpha_{m\mathrm{VV}} \end{bmatrix}$$

With respect to the polarization scattering matrix elements in Equation (D-6), the first polarization-specific subscript represents the transmit component, and the second polarization-specific subscript represents the receive component [3]. The scattering coefficients satisfy various conditions, depending on the scatterer scenario. For example, $\alpha_{m\mathrm{HV}} = \alpha_{m\mathrm{VH}}$ is often satisfied. Identical partitioning and sub-partitioning is defined for vectors **a** and **w**.

The measurement involving the mth scatterer can be represented as two separate scalar measurements; namely,

(D-7a) $$b_{m\mathrm{H}} = \alpha_{m\mathrm{HH}} h_{\mathrm{H}} + \alpha_{m\mathrm{VH}} h_{\mathrm{V}} + w_{m\mathrm{H}}$$

(D-7b) $$b_{m\mathrm{V}} = \alpha_{m\mathrm{HV}} h_{\mathrm{H}} + \alpha_{m\mathrm{VV}} h_{\mathrm{V}} + w_{m\mathrm{V}}$$

where variables h_{H} and h_{V} represent the complex-valued scalar modulation signal components for H and V, respectively. These scalars (h_{H} and h_{V}) are the elements of the phasor representing the electric field with full polarization in far-field conditions. This phasor is referred to as the Jones vector in the polarization literature (see, for example, [27]). In general form and in the H and V basis, the Jones vector for a full-polarization field is defined as

(D-8) $$\mathrm{E} = \begin{bmatrix} E_{\mathrm{H0}}\, e^{j\delta_{\mathrm{H}}} \\ E_{\mathrm{V0}}\, e^{j\delta_{\mathrm{V}}} \end{bmatrix} = \begin{bmatrix} h_{\mathrm{H}} \\ h_{\mathrm{V}} \end{bmatrix}$$

Here E_{H0} and E_{V0} denote the real-valued scalar amplitude of the H and V components of the electric field, respectively; also, δ_{H} and δ_{V} denote the phase delay (radians) of the H and V components of the electric field, respectively. Equation (D-8) suggests that the four real-valued phasor parameters $\{E_{\mathrm{H0}}, E_{\mathrm{V0}}, \delta_{\mathrm{H}}, \delta_{\mathrm{V}}\}$ specify the electric field and its polarization state completely, and such is indeed the case. Alternative parameterizations are possible (such as the one involving the so-called geometrical parameters), but any single parameterization suffices to define the polarization state.

It follows from Equations (D-1) and (D-3) to (D-7) that the measurement matrix $\mathbf{H}$ has a partitioned structure of the form

$$\mathbf{H} = \begin{bmatrix} \mathbf{H}_{00} & \mathbf{O} & \cdots & \mathbf{O} \\ \mathbf{O} & \mathbf{H}_{00} & \cdots & \mathbf{O} \\ \vdots & \vdots & \ddots & \vdots \\ \mathbf{O} & \mathbf{O} & \cdots & \mathbf{H}_{00} \end{bmatrix} \tag{D-9}$$

where each $\mathbf{O}$ represents a 2x4 matrix of zeros, and the sub-matrix $\mathbf{H}_{00}$ that appears repeated M times along the block diagonal is of the form

$$\mathbf{H}_{00} = \begin{bmatrix} h_{\mathrm{H}} & 0 & h_{\mathrm{V}} & 0 \\ 0 & h_{\mathrm{H}} & 0 & h_{\mathrm{V}} \end{bmatrix} \tag{D-10}$$

In summary, the received signal corresponding to the return of a single pulse illuminating the mth scatterer is given as

$$\mathbf{b}_m = \mathbf{H}_{00}\boldsymbol{\alpha}_m + \mathbf{w}_m \tag{D-11}$$

for $m = 1, 2, \ldots, M$.

Finally, let the scattering coefficients be samples from a zero-mean multivariate complex-valued Gaussian distribution with $(4M)$x$(4M)$ covariance matrix

$$\mathrm{E}\left[\boldsymbol{\alpha}\boldsymbol{\alpha}^{\mathrm{H}}\right] = \mathbf{R}_{\alpha\alpha} \tag{D-12}$$

Random variates $\boldsymbol{\alpha}$ are assumed to be analytic signals, which implies that they are circular random variates and admit the standard complex Gaussian probability density function (PDF) for such variates.

The analytic model formulated above is of the form adopted in the formulation of the information theoretic criterion in [5]. Thus, the MI criterion applies directly to the polarization diversity problem as defined above, without any modification.

D 3.0 Simulation-Based Analysis

The specific context in which the MI criterion is applied herein is to determine which polarization waveform (state) to transmit at time $(n+1)\Delta t$ given that a specific polarization waveform has been transmitted at time $n\Delta t$. Specifically, mutual information is determined between pairs of received signals, where one of the signals is the return from the waveform transmitted at time $n\Delta t$, and the other signal is the expected return from each of the alternative waveform candidates. Then the candidate waveform that minimizes the mutual information is the one selected. Such procedure results in a pulse sequence that collects maximally-independent information from pulse-to-pulse.

For computational and notational simplicity, it is assumed that all scatterers are independent and identically-distributed; thus, the covariance matrix $\mathbf{R}_{\alpha\alpha}$ is block diagonal. That is,

(D-13)
$$\mathbf{R}_{\alpha\alpha} = \begin{bmatrix} \mathbf{R}_{00} & \mathbf{O} & \cdots & \mathbf{O} & \mathbf{O} \\ \mathbf{O} & \mathbf{R}_{00} & \cdots & \mathbf{O} & \mathbf{O} \\ \vdots & \vdots & \ddots & \vdots & \vdots \\ \mathbf{O} & \mathbf{O} & \cdots & \mathbf{R}_{00} & \mathbf{O} \\ \mathbf{O} & \mathbf{O} & \cdots & \mathbf{O} & \mathbf{R}_{00} \end{bmatrix}$$

Matrix $\mathbf{R}_{00}$ is repeated in the diagonal because the M scatterers are statistically-independent. In other words, the 4x4 matrix $\mathbf{R}_{00}$ is the covariance matrix of each 4-element scatterer sub-vector:

(D-14)
$$\mathbf{R}_{00} = \mathrm{E}\left[\boldsymbol{\alpha}_m \boldsymbol{\alpha}_m^{\mathrm{H}}\right]$$

The form and values of this matrix is varied in the cases considered next. It is important to note that, besides simplifying various aspects of the analysis, the form adopted for the covariance matrix $\mathbf{R}_{\alpha\alpha}$ allows the gaining of insight as to the operation of the MI criterion in the context of polarization diversity.

There are eight characteristic polarization states, and Table D-1 presents the phasor parameter values for each polarization state as a function of a set of three arbitrary angle parameters. The nominal range of values for each of the arbitrary parameters in the table, the set $\{\theta, \phi, \delta\}$, is presented below the table. This table is used to generate the **H** matrix corresponding to each polarization state.

Table D-1. Phasor parameter values for the characteristic polarization states.

POLARIZATION STATE	E_{H}	E_{V}	δ_{H}	δ_{V}
Horizontal	1	0	ϕ	ϕ
Vertical	0	1	ϕ	ϕ
Linear	$\cos(\theta)$	$\sin(\theta)$	ϕ	ϕ
Orthogonal Linear	$-\sin(\theta)$	$\cos(\theta)$	ϕ	ϕ
Left Circular	$1/\sqrt{2}$	$1/\sqrt{2}$	0	$\pi/2$
Right Circular	$1/\sqrt{2}$	**Error! Objects cannot be created from editing field codes.**	0	$-\pi/2$
Elliptical	$\cos(\theta)$	$\sin(\theta)$	ϕ	$\delta+\phi$
Orthogonal Elliptical	$-\sin(\theta)$	$\cos(\theta)$	ϕ	$\delta+\phi$

Nominal values: $0 \le \theta \le \pi/2$; $0 \le \phi \le \pi/2$; $0 \le \delta \le \pi/2$

In all of the cases considered herein, the nth pulse is adopted to be linear polarization with $\theta = \pi/4$ and $\phi = \pi/6$. The $(n+1)$th pulse is considered to be each one of the eight alternative polarizations, with comparable values for the arbitrary parameters, $\{\theta, \phi, \delta\}$.

D 3.1 Case 1: Identity Scatterer Covariance

For this case,

(D-15) $$\mathbf{R}_{00} = \mathbf{I}$$

which is a special covariance matrix structure, and serves as "reference" for the cases with non-trivial covariance matrix. Figure D-1 presents the MI criterion evaluated using the eight alternative polarization states, as summarized above. Notice that, as expected, the linear polarization (which is the one that matches the one utilized for the first pulse) has infinite mutual information. Also as expected, the orthogonal linear polarization has zero mutual information, and thus minimizes the criterion.

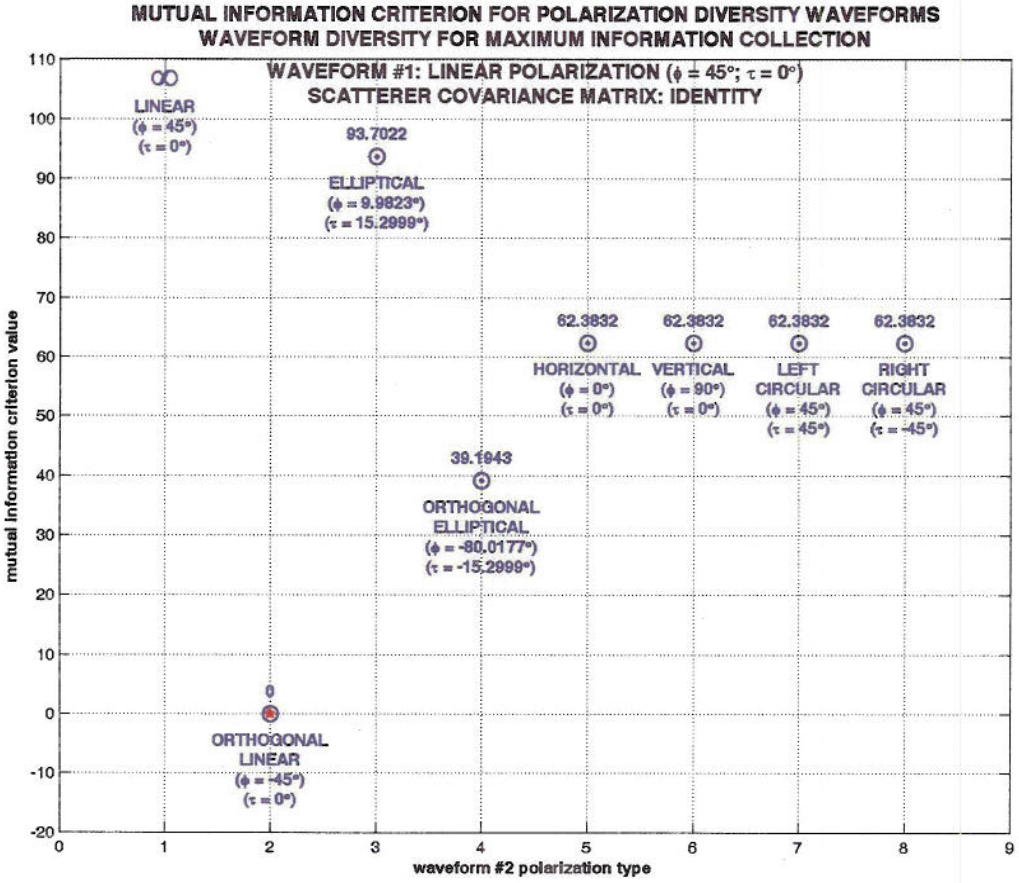

Figure D-1. MI criterion for identity scatterer covariance matrix.

D 3.2 Case 2: Diagonal Scatterer Covariance

For this case,

(D-16) $$\mathbf{R}_{00} = diag[1.0 \quad 0.05 \quad 0.05 \quad 0.3]$$

which has a simple yet non-trivial structure because the expected result is less intuitive. Figure D-2 presents the MI criterion evaluated using the eight alternative polarization states, as summarized above. As before, the linear polarization (which is the one that matches the one utilized for the first pulse) has infinite mutual information. For this case the vertical polarization minimizes the criterion. This can be inferred (though based significantly on hindsight) from the fact that the covariance matrix component corresponding to the VV scatterer variance is significantly less than the component corresponding to the HH scatterer variance.

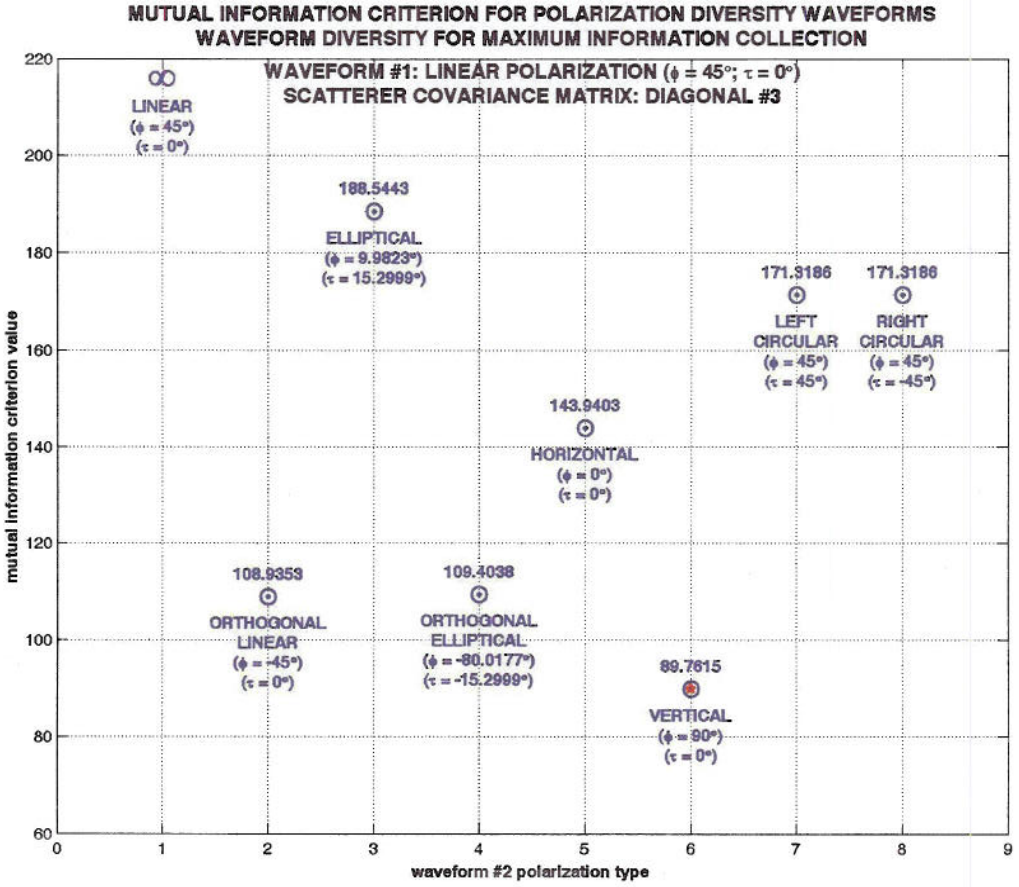

Figure D-2. MI criterion for diagonal (Equation (16)) scatterer covariance matrix.

D 3.3 Case 3: Full Scatterer Covariance

For this case,

$$\mathbf{R}_{00} = \begin{bmatrix} 0.985 & -0.636 - j0.376 & 0.014 + j0.173 & 0.072 - j0.041 \\ -0.636 + j0.376 & 0.924 & -0.166 - j0.245 & 0.426 + j0.173 \\ 0.014 - j0.173 & -0.166 + j0.245 & 0.908 & -0.536 + j0.121 \\ 0.072 + j0.041 & 0.426 - j0.173 & -0.536 - j0.121 & 1.000 \end{bmatrix} \tag{D-17}$$

which a fully non-trivial structure. This covariance matrix was generated randomly but subject to the constraints required to assure a valid covariance matrix as the result. Figure D-3 presents the MI criterion evaluated using the eight alternative polarization states, as summarized above. As before, the linear polarization (which is the one that matches the one utilized for the first pulse) has infinite mutual information. For this case the left circular polarization minimizes the criterion, and it is non-trivial to assess that result due to the structure of the covariance matrix. This example illustrates the value of the technique to provide a result that is otherwise unattainable. Of

course, the situation wherein the scatterers are correlated is even more difficult to assess without utilization of the criterion because the covariance matrix structure is no longer block diagonal.

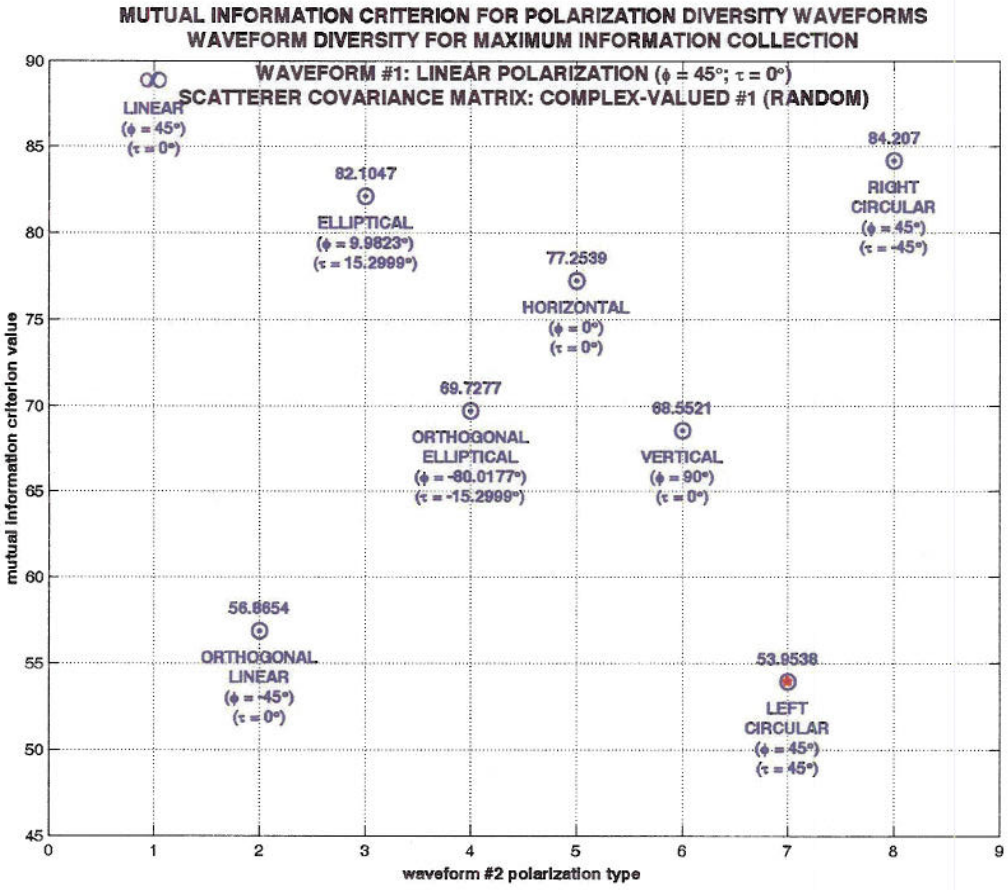

Figure D-3. MI criterion for full (Equation (D-17)) scatterer covariance matrix.

APPENDIX E: SUMMARY OF BASIC POLARIMETRIC RADAR THEORY

by

Jorge J. Morisaki
Wolfgang-Martin Boerner
Communications, Sensing and Navigation Laboratory
Department of Electrical and Computer Engineering
University of Illinois at Chicago
900 W Taylor Street, SEL-W4210
Chicago, IL/USA-60607-7018

LIST OF CONTENTS

E 1.0 INTRODUCTION

The objective of this effort was to investigate the mathematical theory and determine algorithms necessary to model full polarization scattering physics in a state-estimation signal processing algorithm applied to fully polarimetric radar.

In a first step, the existing fundamental radar theory was exhaustively reviewed, upon which the concise formulation of polarimetric radar theory was derived, as summarized in the M. Sc. Thesis of J. J. Morisaki. Pertinent sections of the thesis document were extracted and are presented in this appendix.

The relevant fundamental field equations are first provided. The importance of the propagation and scattering behavior in various frequency bands, the electrodynamic foundations such as Maxwell's equations, the Helmholtz vector wave equation, and especially the fundamental laws of polarization are first introduced. The fundamental terms which represent the polarization state are introduced, defined and explained. Main points of view are the polarization ellipse, the polarization ratio, the Stokes Parameter and the Stokes and Jones vector formalisms, as well as their presentation on the Poincaré sphere and on relevant map projections. The Polarization Fork descriptors with the associated van Zyl polarimetric power density and Agrawal polarimetric phase correlation signatures are also introduced in order to make understandable the polarization state formulations of electromagnetic waves in the frequency domain. The polarization state of electromagnetic waves under scattering conditions (e.g. in the radar case) will be described by matrix formalisms. Each scatterer is a polarization transformer. Under normal conditions the transformation from the transmitted wave vector to the received wave vector is linear, and this behavior is principally described by the scattering matrix. This matrix contains all the information about the scattering process and the scatterer itself. The different relevant matrices, the respective terms like Jones Matrix, S-matrix, Müller M-matrix, Kennaugh K-matrix, etc. and their interconnections are defined and described together with change of polarization bases transformation operators, whereupon the optimal (characteristic) polarization states are determined for the coherent and partially coherent cases.

Radar Polarimetry (*Polar*: polarization, *Metry*: measure) is the science of acquiring, processing and analyzing the polarization state of an electromagnetic field. Radar polarimetry is concerned with the utilization of polarimetry in radar applications as reviewed most recently in Boerner [E1] where a host of pertinent references are provided. Although polarimetry has a long history which reaches back to the 18th century, the earliest work that is related to radar dates back to the 1940s. In 1945 G.W. Sinclair introduced the concept of the scattering matrix as a descriptor of the radar cross section of a coherent scatterer [E2], [E3]. In the late 1940s and the early 1950s major pioneering work was carried out by E.M. Kennaugh [E4, E5]. He formulated a backscatter theory based on the eigenpolarizations of the scattering matrix introducing the concept of optimal polarizations by implementing the concurrent work of G.A. Deschamps, H. Mueller, and C. Jones. Work continued after Kennaugh, but only a few notable contributions, such as those of G.A. Deschamps 1951 [E6], C.D. Graves 1956 [E7], and J.R. Copeland 1960 [E8], were made until Huynen's studies in 1970s. The beginning of a new age was the treatment presented by J.R. Huynen in his doctoral thesis of 1970 [E9], where he exploited Kennaugh's optimal polarization concept [E5] and formulated his approach to target radar phenomenology. With this thesis, a renewed interest for radar polarimetry was raised. However, the full potential of radar polarimetry was never fully realized until the early 1980s, due in no small parts to the advanced radar device technology [E10, E11]. Technological problems led to a series of questions in the 1960s and 1970s about the practical use of radar systems with polarimetric capability [E12] which is still lagging on until today. Among the major contributions of the 1970s and 1980s are those of W-M Boerner [E13, E14, E15], who pointed out the importance of polarization first in addressing vector electromagnetic inverse scattering [E13] problems which cannot be solved without full comprehension multi-static radar polarimetry. He initiated a critical analysis of Kennaugh's and Huynen's work and extended Kennaugh's optimal polarization theory [E16]. He has been influential in causing the radar community to recognize the need of polarimetry in remote sensing applications, and especially in SAR polarimetry. A detailed overview on the history of polarimetry can be found in [E13, E14, E15] while a historical review of polarimetric radar technology is also given in [E13, E17, E18].

Polarimetry deals with the full vector nature of polarized (vector) electromagnetic waves throughout the frequency spectrum from Ultra-Low-Frequencies (ULF) via the infrared and optical spectral domain to above the Far-Ultra-Violet (FUV) [E19, E20]. Whenever there are abrupt or gradual changes in the index of refraction (or permittivity,

magnetic permeability, and conductivity), the polarization state of a narrow band (single-frequency) wave is transformed, and the electromagnetic "vector wave" is re-polarized. When the wave passes through a medium of changing index of refraction, or when it strikes an object such as a radar target and/or a scattering surface and it is reflected, then characteristic information about the reflectivity, shape and orientation of the reflecting body can be obtained by implementing polarization control and utilaztion [E10, E11]. The complex direction of the electric field vector, in general describing an ellipse in a plane transverse to propagation, plays an essential role in the interaction of electromagnetic vector waves with material bodies and the propagation medium [E21, E22, E13, E14, E16]. Whereas this polarization transformation behavior, expressed in terms of the polarization ellipse is named ellipsometry in optical sensing and imaging [E21, E23], it is denoted as polarimetry in radar, lidar/ladar and SAR sensing and imaging [E12, E14, E15, E19] - using the ancient Greek meaning of measuring orientation and object shape. Thus, ellipsometry and polarimetry are concerned with the control of the coherent polarization properties of optical and radio waves, respectively [E21, E19]. With the advent of optical and radar polarization phase control devices, ellipsometry advanced rapidly during the Forties (Mueller and Land [E24, E21]) with the associated development of mathematical ellipsometry, (the introduction of the 2 x 2 coherent Jones forward scattering (propagation) and the associated 4 x 4 average power density Mueller (Stokes) propagation matrices [E21];) Polarimetry developed independently in the late Forties with the introduction of dual polarized antenna technology (Sinclair, Kennaugh, et al. [E2, E3, E4, E5]), and the subsequent formulation of the 2 x 2 coherent Sinclair radar back-scattering matrix and the associated 4 x 4 Kennaugh radar back-scattering power density matrix, as summarized in detail in Boerner et al. [E19, E25]. Since then, ellipsometry and polarimetry have enjoyed steep advances. A mathematically coherent polarization matrix formalism is in the process of being introduced for which the lexicographic covariance matrix presentations [E26, E27] of signal estimation theory play an equally important role in ellipsometry as well as polarimetry [E19]. Based on Kennaugh's original pioneering work on discovering the properties of the Spinorial Polarization Fork concept [E4, E5], Huynen [E9] developed a phenomenological approach to radar polarimetry, which had a subtle impact on the steady advancement of polarimetry [E13, E14, E15] as well as ellipsometry. Haynen developed the orthogonal (group theoretic) target scattering matrix decomposition [E28, E29, E30] and extended the characteristic optimal polarization state concept of Kennaugh [E31, E4, E5], which led to the renaming of the spinorial polarization fork concept to the so called Huynen Polarization Fork in radar polarimetry [E31]. Here, we emphasize that for treating the general bistatic (asymmetric) scattering matrix case, a more general formulation of fundamental ellipsometry and polarimetry in terms of a spinorial group-theoretic approach is strictly required, which was first explored by Kennaugh but not further pursued by him due to the lack of pertinent mathematical formulations [E32, E33], and after the con-similarity matrix was fully established and utilized by E. Lueneburg, a more generalized spinorial formulation was developed by Bebbington.

In ellipsometry, the Jones and Mueller matrix decompositions rely on a product decomposition of relevant optical measurement/transformation quantities such as diattenuation, retardence, depolarization, birefringence, etc., [E34, E35, E23, E28, E29] measured in a chain matrix arrangement, or multiplicatively placing one optical decomposition device after the other. In polarimetry, the Sinclair, the Kennaugh, as well as the covariance matrix decompositions [E29] are based on a group-theoretic series expansion in terms of the principal orthogonal radar calibration targets such as the sphere or flat plate, the linear dipole and/or circular helical scatterers, the dihedral and trihedral corner reflectors, and so on - - observed in a linearly superimposed aggregate measurement arrangement [E36, E37]. This leads to various canonical target feature mappings [E38] and sorting as well as scatter-characteristic decomposition theories [E39, E27, E40]. In addition, polarization-dependent speckle and noise reduction play an important role in both ellipsometry and polarimetry, which in radar polarimetry were first pursued with rigor by J-S. Lee [E41, E42, E43, E44]. The implementation of all of these novel methods will fail unless one is given fully calibrated scattering matrix information, which applies to each element of the Jones and Sinclair matrices.

It is here noted that it has become common usage to replace ellipsometry by optical polarimetry and expand polarimetry to radar polarimetry in order to avoid confusion [E45, E18]. This is a nomenclature adopted in the remainder of this paper.

Very remarkable improvements beyond classical non-polarimetric radar target detection, recognition and discrimination, and identification were made especially with the introduction of the covariance matrix optimization procedures of Tragl [E46], Novak et al. [E47 – E51], Lüneburg [E52 – E55], Cloude [E56], and of Cloude and Pottier [E27]. Special attention must be placed on the Cloude-Pottier polarimetric entropy H, anisotropy A, feature-angle ($\overline{\alpha}$) parametric decomposition [E57] because they allow for unsupervised target feature interpretation [E57, E58]. By using the various fully polarimetric (scattering matrix) target feature syntheses [E59], polarization contrast optimization, [E60, E61] and polarimetric entropy/anisotropy classifiers, very considerable progress was

made in interpreting and analyzing POL-SAR image features [E62, E57, E63, E64, E65, E66]. This includes the reconstruction of Digital Elevation Maps (DEMs) directly from POL-SAR Covariance-Matrix Image Data Takes [E67 – E69] next to the familiar method of DEM reconstruction from IN-SAR Image data takes [E70, E71, E72]. In all of these techniques well calibrated scattering matrix data takes are becoming an essential pre-requisite, without which little can be achieved [E18, E19, E45, E73]. In most cases multi-look-compressed SAR image data take MLC- formatting suffices for completely polarized SAR image algorithm implementation [E74]. However, in the sub-aperture polarimetric studies, in Polarimetric SAR Image Data Take Calibration, and in POL-IN-SAR Imaging, the SLC (Single Look Complex) SAR Image Data Take Formatting becomes an absolute must [E19, E1]. Of course, for SLC-formatted image data in particular, various speckle-filtering methods must always be applied. Implementation of the Lee Filter – explored first by Jong-Sen Lee for speckle reduction in polarimetric SAR image reconstruction, and of the Polarimetric Lee-Wishart distribution for improving image feature characterization, have further contributed toward enhancing the interpretation and display of high quality SAR Imagery [E41 – E44, E75].

E 2.0 The Electromagnetic Vector Wave and Key Polarization Descriptors

The fundamental relations of radar polarimetry are obtained directly from Maxwell's equations [E86, E34], where for the source-free isotropic, homogeneous, free space propagation space, and assuming IEEE standard [E102] time-dependence $\exp(+j\omega t)$, the electric $\mathbf{E}$ and magnetic $\mathbf{H}$ fields satisfy with μ being the free space permeability and ε the free space permittivity:

$$\nabla \mathrm{x}\mathbf{E}(\mathbf{r}) = -j\omega\mu\mathbf{H}(\mathbf{r}), \qquad \nabla \mathrm{x}\mathbf{H}(\mathbf{r}) = j\omega\varepsilon\,\mathbf{E}(\mathbf{r}) \tag{E 2.1}$$

For the time-invariant case this results in

$$(\nabla + k^2)\mathbf{E} = 0, \qquad \mathbf{E}(\mathbf{r}) = E_0 \frac{\exp(-jkr)}{r}, \qquad \mathbf{H}(\mathbf{r}) = H_0 \frac{\exp(-jkr)}{r} \tag{E 2.2}$$

for an outgoing spherical wave with propagation constant $k = \omega\,(\varepsilon\,\mu)^{1/2}$ and $c = (\varepsilon\,\mu)^{-1/2}$ being the free space velocity of electromagnetic waves. No further details are presented here, and we refer to Stratton [E86] and Mott [E76] for full presentations.

E 2.1 Polarization Vector and Complex Polarization Ratio

With the use of the standard spherical coordinate system $(r, \theta, \phi\,;\, \hat{\mathrm{u}}_r, \hat{\mathrm{u}}_\theta, \hat{\mathrm{u}}_\phi)$ with r, θ, ϕ denoting the radial, polar, azimuthal coordinates, and $\hat{\mathrm{u}}_r, \hat{\mathrm{u}}_\theta, \hat{\mathrm{u}}_\phi$ the corresponding unit vectors, respectively; the outward travelling wave is expressed as:

$$\mathbf{E} = \hat{\mathrm{u}}_\theta\, E_\theta + \hat{\mathrm{u}}_\phi E_\phi \quad \mathbf{H} = \hat{\mathrm{u}}_\theta\, H_\theta + \hat{\mathrm{u}}_\phi\, H_\phi \;,\; \mathbf{P} = \frac{\hat{\mathrm{u}}_r}{2}\left|\mathbf{E}\times\mathbf{H}^*\right| = \frac{\hat{\mathrm{u}}_r\,|\mathrm{E}|^2}{2Z_0} \;,\; Z_0 = \left(\frac{\mu_0}{\varepsilon_0}\right)^{1/2} = 120\pi\ [\Omega]\,. \tag{E 2.3}$$

$\mathbf{P}$ denotes the Poynting power density vector and Z_0 is the intrinsic impedance of the medium (here vacuum). Far from the antenna in the far field region [E86, E76], the radial waves of (E 2.2) take on plane wave characteristics, and assuming the wave to travel in positive z-direction of a right-handed Cartesian coordinate system (x, y, z), the electric field $\mathbf{E}$, denoting the polarization vector, may be rewritten as:

$$\mathbf{E} = \hat{\mathrm{u}}_x E_x + \hat{\mathrm{u}}_y E_y = |E_x| \exp(j\phi_x)\{\hat{\mathrm{u}}_x + \hat{\mathrm{u}}_y \left|\frac{E_y}{E_x}\right| \exp(j\phi)\} \tag{E 2.4}$$

$|E_x|$ & $|E_y|$ are the amplitudes, ϕ_x & ϕ_y the phases, $\phi = \phi_y - \phi_x$ the relative phase, $|E_x / E_y| = \tan\alpha$ with ϕ_x, ϕ_y, α and ϕ defining the Deschamps parameters [E6, E103]. Using these definitions, the normalized complex polarization vector $\mathbf{p}$ and the complex polarization ratio ρ can be defined as:

$$\mathbf{p} = \frac{\mathbf{E}}{|\mathbf{E}|} = \frac{\hat{\mathrm{u}}_x E_x + \hat{\mathrm{u}}_y E_y}{|\mathbf{E}|} = \frac{E_x}{|\mathbf{E}|}\left(\hat{\mathrm{u}}_x + \rho\,\hat{\mathrm{u}}_y\right) \tag{E 2.5}$$

with $|\mathbf{E}|^2 = \mathbf{E}\cdot\mathbf{E}^* = E_x^{\,2} + E_y^{\,2}$ $|\mathbf{E}| = E$ defines the wave amplitude and ρ is given by

$$\rho = \frac{E_y}{E_x} = \left|\frac{E_y}{E_x}\right| \exp(j\phi), \qquad \phi = \phi_y - \phi_x \quad . \tag{E 2.6}$$

E 2.2 The Polarization Ellipse and its Parameters

The tip of the real time-varying vector $\mathbf{E}$, or $\mathbf{p}$, traces an ellipse for general phase difference ϕ, where we distinguish between right-handed (clockwise) and left-handed (counter-clockwise) when viewed by the observer in direction of the travelling wave [E76, E19]. This is shown in Fig. E 2.1 for the commonly used horizontal H (by replacing x) and vertical V (by replacing y) polarization states.

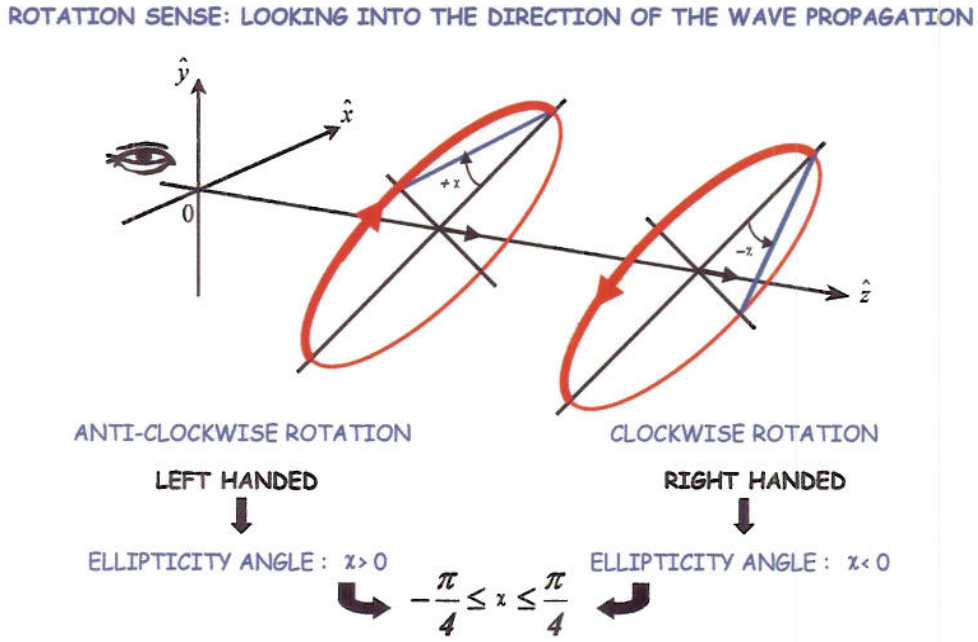

(a) Rotation Sense (Courtesy of Prof. E. Pottier)

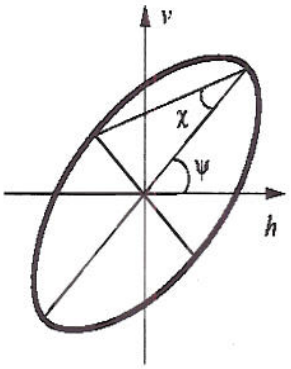

(b) Orientation ψ and Ellipticity χ Angles.

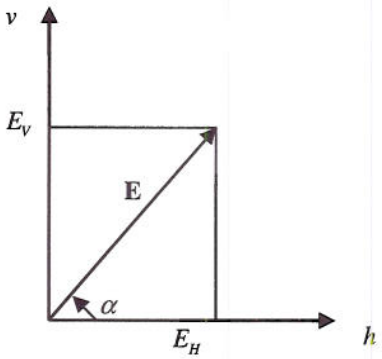

(c) Electric Field Vector.

Fig. E 2.1 Polarization Ellipse.

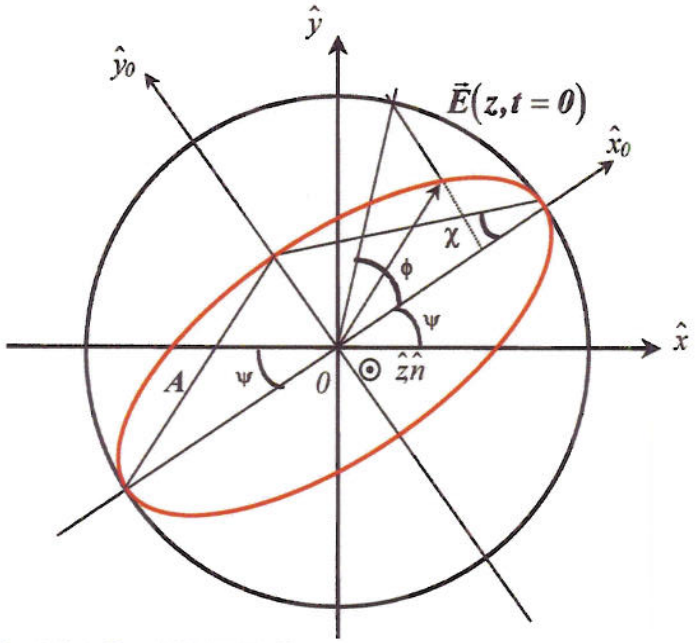

A : WAVE AMPLITUDE $\quad$ ϕ: ABSOLUTE PHASE

ψ: ORIENTATION ANGLE $-\frac{\pi}{2} \le \psi \le \frac{\pi}{2}$ $\quad$ χ : ELLIPTICITY ANGLE $0 \le \chi \le \frac{\pi}{4}$

Fig. E 2.2 Polarization Ellipse Relations (Courtesy of Prof. E. Pottier)

There exist unique relations between the alternate representations, as defined in Fig. E 2.1 and Fig. E 2.2 with the definition of the orientation ψ and ellipticity χ angles expressed respectively as

$$\alpha = |\rho| = \frac{|E_y|}{|E_x|},\ 0 \le \alpha \le \pi/2 \quad \text{and} \quad \tan 2\psi = \tan(2\alpha)\cos\phi \qquad -\pi/2 \le \psi \le +\pi/2 \tag{E 2.7}$$

$$\tan\chi = \pm \textit{minor axis/major axis}, \qquad \sin 2\chi = \sin 2\alpha \sin\phi\ , \qquad -\pi/4 \le \chi \le \pi/4\ , \tag{E 2.8}$$

where the $+$ and $-$signs are for left- and right-handed polarizations respectively.
For a pair of orthogonal polarizations $\mathbf{p_1}$ and $\mathbf{p_2} = \mathbf{p_{1_\perp}}$,

$$\mathrm{p}_1 \cdot \mathrm{p}_2^{\,*} = 0 \qquad \rho_2 = \rho_{1\perp} = -1/\rho_1^* \ , \qquad \psi_1 = \psi_2 + \frac{\pi}{2} \qquad \chi_1 = -\chi_2\ . \tag{E 2.9}$$

In addition, the following useful transformation relations exist:

$$\rho = \frac{\cos 2\chi \sin 2\psi + j \sin 2\chi}{1 + \cos 2\chi \cos 2\psi} = \tan\alpha \exp(j\phi) \quad , \tag{E 2.10}$$

where (α, ϕ) and (ψ, χ) are related by the following equations:

$$\cos 2\alpha = \cos 2\psi \cos 2\chi, \quad \tan\phi = \tan 2\chi / \sin 2\psi \tag{E 2.11}$$

and inversely

$$\psi = \frac{1}{2}\arctan\left(\frac{2\mathrm{Re}\{\rho\}}{1-\rho\rho^*}\right)+\pi \quad ...\bmod(\pi) \qquad \chi = \frac{1}{2}\arcsin\left(\frac{2\mathrm{Im}\{\rho\}}{1-\rho\rho^*}\right) \quad . \tag{E 2.12}$$

Another useful formulation of the polarization vector $\mathbf{p}$ was introduced by Huynen in terms of the parametric formulation [E9, E104], derived from group-theoretic considerations based on the Pauli SU(2) matrix set $\psi_P\{[\sigma_i]\ ,\ i=0,1,2,3\}$ as further pursued by Pottier [E105]. According to (E 2.10) and (E 2.11), for $\psi = 0$, and then rotating this ellipse by ψ:

$$\mathbf{p}(|\mathbf{E}|,\phi,\psi,\chi) = |\mathbf{E}|\exp(j\phi)\begin{bmatrix}\cos\psi & -\sin\psi\\ \sin\psi & \cos\psi\end{bmatrix}\begin{bmatrix}\cos\chi\\ -j\sin\chi\end{bmatrix}. \tag{E 2.13}$$

This will be utilized later on. $\psi_P\{[\sigma_i]\ ,\ i=0,1,2,3\}$ is defined in terms of the classical unitary Pauli matrices $[\sigma_i]$ as

$$[\sigma_0]=\begin{bmatrix}1 & 0\\ 0 & 1\end{bmatrix},\quad [\sigma_1]=\begin{bmatrix}1 & 0\\ 0 & -1\end{bmatrix},\quad [\sigma_2]=\begin{bmatrix}0 & 1\\ 1 & 0\end{bmatrix},\quad [\sigma_3]=\begin{bmatrix}0 & -j\\ j & 0\end{bmatrix}. \tag{E 2.14}$$

The $[\sigma_i]$ matrices satisfy the unitarity condition as well as commutation properties given by:

$$[\sigma_i]^{-1}=[\sigma_i]^{T^*},\quad \left|Det\{[\sigma_i]\}\right|=1,\quad [\sigma_i][\sigma_j]=-[\sigma_j][\sigma_i],\quad [\sigma_i][\sigma_i]=[\sigma_0], \tag{E 2.15}$$

satisfying the ordinary matrix product relations.

E 2.3 The Jones Vector and Changes of Polarization Bases

Instead of the basis {x y} or {H V} we can introduce an alternative presentation {m n} as a linear combination of two arbitrary orthonormal polarization states, $\mathbf{E}_m$ and $\mathbf{E}_n$, for which

$$\mathbf{E} = \hat{\mathbf{u}}_m E_m + \hat{\mathbf{u}}_n E_n . \tag{E 2.16}$$

If the standard basis vectors are in general orthonormal, i.e.

$$\hat{\mathrm{u}}_m \cdot \hat{\mathrm{u}}_n^\dagger = 0,\quad \hat{\mathrm{u}}_m \cdot \hat{\mathrm{u}}_m^\dagger = \hat{\mathrm{u}}_\mathrm{n} \cdot \hat{\mathrm{u}}_n^\dagger = 1, \tag{E 2.17}$$

with † denoting the hermitian adjoint operator [21, 52, 53], then the Jones vector $\mathbf{E}_{mn}$ may be defined as

$$\mathbf{E}_{mn}=\begin{bmatrix}E_m\\ E_n\end{bmatrix}=\begin{bmatrix}|E_m|\exp j\phi_m\\ |E_n|\exp j\phi_n\end{bmatrix}=E_m\begin{bmatrix}1\\ \rho\end{bmatrix}=\frac{|\mathbf{E}|\exp(j\phi_m)}{\sqrt{1+\rho\rho^*}}\begin{bmatrix}1\\ \rho\end{bmatrix}=|\mathbf{E}|\exp(j\phi_m)\begin{bmatrix}\cos\alpha\\ \sin\alpha\exp(j\phi)\end{bmatrix}, \tag{E 2.18}$$

with $\tan\alpha = |E_n / E_m|$ and $\phi = \phi_n - \phi_m$. This states that the Jones vector possesses, in general, four degrees of freedom. The Jones vector descriptions for characteristic polarization states are provided in Fig. E 2.3.

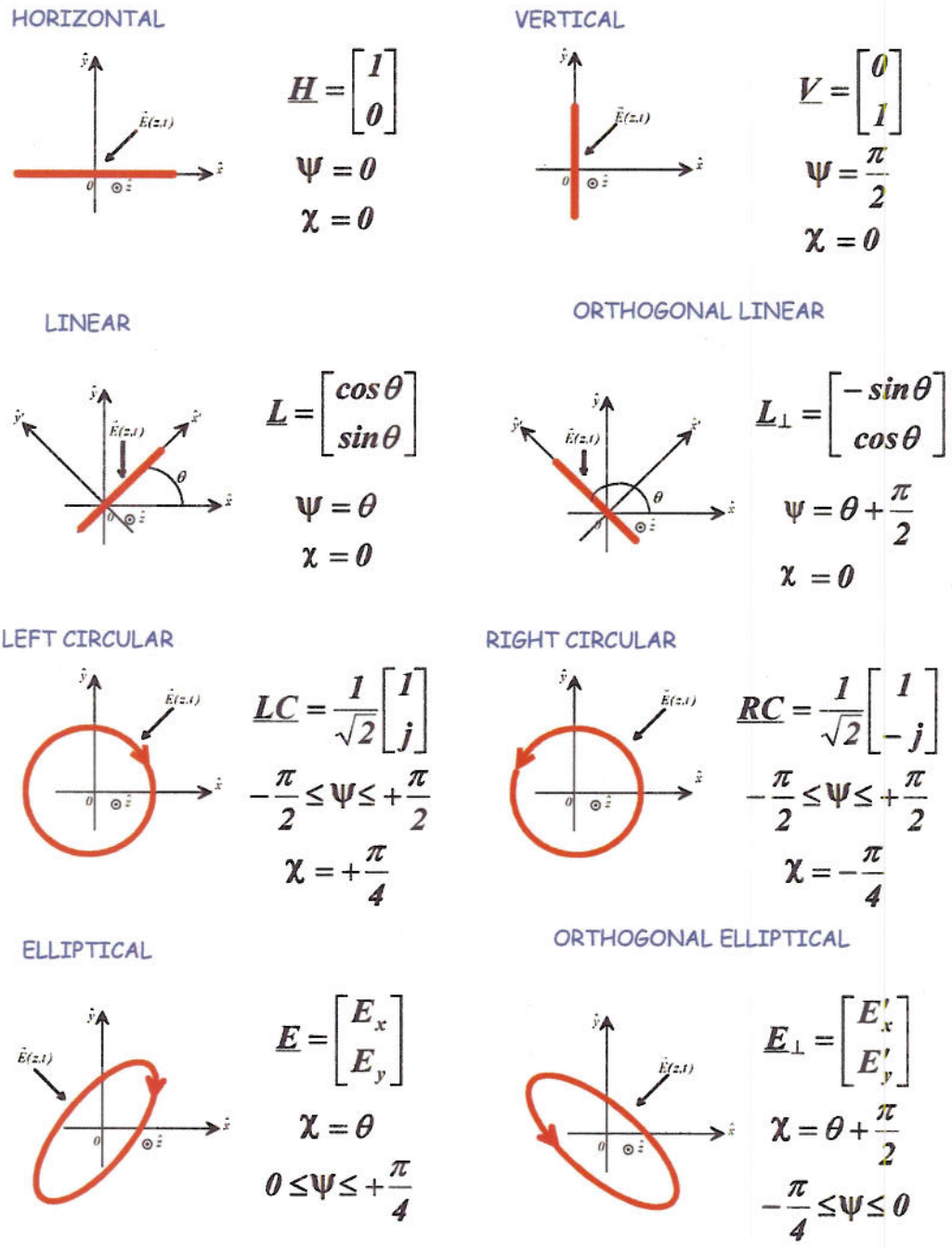

Fig. E 2.3 Jones Vector Descriptions for Characteristic Polarization States with direction of propagation out of the page (Courtesy of Prof. E. Pottier)

Since any monochromatic plane wave can be expressed as a linear combination of two orthonormal linear polarization states defining the reference polarization basis, there exist an infinite number of such bases {i j} or {A B} for which

$$\mathbf{E} = \hat{\mathbf{u}}_m E_m + \hat{\mathbf{u}}_n E_n = \hat{\mathbf{u}}_i E_i + \hat{\mathbf{u}}_j E_j = \hat{\mathbf{u}}_A E_A + \hat{\mathbf{u}}_B E_B . \qquad \text{(E 2.19)}$$

The corresponding Jones vectors are presented in two alternate, most commonly used notations:

$$\mathbf{E}_{mn} = \mathbf{E}(m,n) = \begin{bmatrix} E_m \\ E_n \end{bmatrix} \quad \mathbf{E}_{ij} = \mathbf{E}(i,j) = \begin{bmatrix} E_i \\ E_j \end{bmatrix} \quad \text{and} \quad \mathbf{E}_{AB} = \mathbf{E}(A,B) = \begin{bmatrix} E_A \\ E_B \end{bmatrix}. \tag{E 2.20}$$

The unique transformation from the $\{\hat{\mathbf{u}}_m \ \hat{\mathbf{u}}_n\}$ to the arbitrary $\{\hat{\mathbf{u}}_i \ \hat{\mathbf{u}}_j\}$ or $\{\hat{\mathbf{u}}_A \ \hat{\mathbf{u}}_B\}$ bases is sought which is a linear transformation in the two-dimensional complex space so that

$$\mathbf{E}_{ij} = [U_2]\mathbf{E}_{mn} \quad or \quad \mathbf{E}(i,j) = [U_2]\mathbf{E}(m,n) \quad \text{with} \quad [U_2]\,[U_2]^{\dagger} = [I_2] \tag{E 2.21}$$

satisfying wave energy conservation and $[I_2]$ being the 2x2 identity matrix. We may choose, as shown in [E81],

$$\hat{\mathbf{u}}_i = \frac{\exp(j\phi_i)}{\sqrt{1+\rho\rho^*}}\begin{bmatrix} 1 \\ \rho \end{bmatrix} \text{ and } \hat{\mathbf{u}}_j = \hat{\mathbf{u}}_{i_\perp} = \frac{\exp(j\phi_i)}{\sqrt{1+\rho\rho^*}}\begin{bmatrix} 1 \\ -\rho^{*^{-1}} \end{bmatrix} = \frac{\exp(j\phi_i)}{\sqrt{1+\rho\rho^*}}\begin{bmatrix} -\rho^* \\ 1 \end{bmatrix}, \tag{E 2.22}$$

with $\phi_j' = \phi_j + \phi + \pi$ so that

$$[U_2] = \frac{1}{\sqrt{1+\rho\rho^*}}\begin{bmatrix} \exp(j\phi_i) & -\rho^*\exp(j\phi_j) \\ \rho\exp(j\phi_i) & \exp(j\phi_j) \end{bmatrix}. \tag{E 2.23}$$

This yields $Det\{[U_2]\} = \exp\{j(\phi_i + \phi_j')\}$ with $\phi_i + \phi_j' = 0$.

Since $[U_2]$ is a special unitary 2x2 complex matrix with unit determinant, implying that (i) the amplitude of the wave remains independent of the change of the polarization basis, and that (ii) the phase of the (absolute) wave may be consistently defined as the polarization basis is changed, we finally obtain,

$$[U_2] = \frac{1}{\sqrt{1+\rho\rho^*}}\begin{bmatrix} 1 & -\rho^* \\ \rho & 1 \end{bmatrix}\begin{bmatrix} \exp(j\phi_i) & 0 \\ 0 & \exp(j\phi_i) \end{bmatrix}. \tag{E 2.24}$$

This possesses three degrees of freedom similar to the normalized Jones vector formulation, but in most cases the phase reference is taken as $\phi_i = 0$, which may not be the case in polarimetric interferometry [E96]. For further details on the group-theoretic representations of the proper transformation relations see the formulations derived by Pottier in [E106].

E 2.4 Complex Polarization Ratio in Different Polarization Bases

Any wave can be resolved into two orthogonal components (linearly, circularly, or elliptically polarized) in the plane transverse to the direction of propagation. For an arbitrary polarization basis {A B} with unit vectors $\hat{\mathrm{a}}$ and $\hat{\mathrm{b}}$, one may define the polarization state

$$\mathbf{E}(AB) = E_A\,\hat{\mathrm{a}} + E_B\,\hat{\mathrm{b}}, \tag{E 2.25}$$

where the two components E_A and E_B are complex numbers. The polarization ratio ρ_{AB} in an arbitrary basis {A B} is also a complex number, and it may be defined as

$$\rho_{AB} = \frac{E_B}{E_A} = \frac{|E_B|}{|E_A|}\exp\{j(\phi_B - \phi_A)\} = |\rho_{AB}|\exp\{j\phi_{AB}\}. \tag{E 2.26}$$

$|\rho_{AB}|$ is the ratio of magnitude of two orthogonal components of the field $|E_A|$ and $|E_B|$ and ϕ_{AB} is the phase difference between E_A and E_B. The complex polarization ratio ρ_{AB} depends on the polarization basis {A B} and can be used to specify the polarization of an electromagnetic wave

$$\begin{aligned}\mathbf{E}(AB) &= \begin{bmatrix} E_A \\ E_A \end{bmatrix} = |E_A|\exp\{j\phi_A\}\begin{bmatrix} 1 \\ \rho_{AB} \end{bmatrix} = |E_A|\exp\{j\phi_A\}\frac{\sqrt{1+\dfrac{E_B E_B^*}{E_A E_A^*}}}{\sqrt{1+\dfrac{E_B E_B^*}{E_A E_A^*}}}\begin{bmatrix} 1 \\ \rho_{AB} \end{bmatrix} \\ &= |\mathbf{E}|\exp\{j\phi_A\}\frac{1}{\sqrt{1+\rho_{AB}\rho_{AB}^*}}\begin{bmatrix} 1 \\ \rho_{AB} \end{bmatrix}\end{aligned} \tag{E 2.27}$$

where $|\mathbf{E}| = \sqrt{E_A E_A^* + E_B E_B^*}$ is the amplitude of the wave $\mathbf{E}(AB)$. If we choose $|\mathbf{E}| = 1$ and disregard the absolute phase ϕ_A, the above representation becomes

$$\mathbf{E}(AB) = \frac{1}{\sqrt{1+\rho_{AB}\rho_{AB}^*}}\begin{bmatrix} 1 \\ \rho_{AB} \end{bmatrix}. \tag{E 2.28}$$

This representation of the polarization state using the polarization ratio ρ_{AB} is very useful, for example, if we want to represent a left-handed circular (LHC) polarization state and a right-handed circular (RHC) polarization state in a linear basis {H V} using the polarization ratio. For a left-handed circular (LHC) polarization, $|E_H| = |E_V|$, $\phi_{HV} = \phi_V - \phi_H = \pi/2$, and according to (E 2.26), the polarization ratio ρ_{HV} is j. Using (E 2.28) with $\rho_{HV} = j$, we obtain for the left-handed circular (LHC) polarization

$$\mathbf{E}(HV) = \frac{1}{\sqrt{2}}\begin{bmatrix} 1 \\ j \end{bmatrix}. \tag{E 2.29}$$

Similarly, the polarization ratio ρ_{HV} of a right-handed circular (RHC) polarization state in a linear basis {H V} is $-j$ because the relative phase $\phi_{HV} = -\pi/2$, and its representation is

$$\mathbf{E}(HV) = \frac{1}{\sqrt{2}}\begin{bmatrix} 1 \\ -j \end{bmatrix}. \tag{E 2.30}$$

The complex polarization ratio ρ is important in radar polarimetry. However, the value of the polarization ratio ρ defined in a certain polarization basis is different from that defined in the other polarization basis even if the physical polarization state is the same.

E 2.4.1 Complex Polarization Ratio in the Linear Basis {H V}

In the linear {H V} basis with unit vectors $\hat{\mathrm{h}}$ and $\hat{\mathrm{v}}$, a polarization state may be expressed as:

$$\mathbb{E}(HV) = E_H\,\hat{\mathrm{h}} + E_V\,\hat{\mathrm{v}}\ . \tag{E 2.31}$$

The polarization ratio ρ_{HV}, according to (E 2.6), can be described as:

$$\rho_{HV} = \frac{E_V}{E_H} = \left|\frac{E_V}{E_H}\right| \exp(j\phi_{HV}) = \tan\alpha_{HV}\exp(j\phi_{HV}), \qquad \phi_{HV} = \phi_V - \phi_H\ . \tag{E 2.32}$$

The angle α_{HV} is defined in Fig. E 2.1c only in the {H V} basis and

$$\begin{aligned} |E_H| &= \sqrt{E_H^2 + E_V^2}\cos\alpha_{HV} \\ |E_V| &= \sqrt{E_H^2 + E_V^2}\sin\alpha_{HV} \end{aligned}\ . \tag{E 2.33}$$

Also, for a single, monochromatic, uniform TEM (transverse electromagnetic) traveling plane wave in the positive z direction, the real instantaneous electric field is written as:

$$\boldsymbol{\varepsilon}(z,t) = \begin{bmatrix} \varepsilon_x(z,t) \\ \varepsilon_y(z,t) \\ \varepsilon_z(z,t) \end{bmatrix} = \begin{bmatrix} |E_x|\cos(\omega t - kz + \phi_x) \\ |E_y|\cos(\omega t - kz + \phi_y) \\ 0 \end{bmatrix}\ . \tag{E 2.34}$$

In a cartesian coordinate system, the $+x$-axis is commonly chosen as the horizontal basis (H) and the $+y$-axis as the vertical basis (V). Substituting (E 2.33) into (E 2.34), we find

$$\begin{aligned} \boldsymbol{\varepsilon}(z,t) &= \begin{bmatrix} \sqrt{E_H^2 + E_V^2}\cos\alpha_{HV}\cos(\omega t - kz + \phi_H) \\ \sqrt{E_H^2 + E_V^2}\sin\alpha_{HV}\cos(\omega t - kz + \phi_V) \end{bmatrix} = \\ &= \sqrt{E_H^2 + E_V^2}\exp\left\{\begin{bmatrix} \cos\alpha_{HV} \\ \sin\alpha_{HV}\exp(j\phi) \end{bmatrix}\exp\{j(\omega t - kz + \phi_H)\}\right\}, \end{aligned} \tag{E 2.35}$$

where $\phi = \phi_V - \phi_H$ is the relative phase. The expression in the square bracket is a spinor [E32] which is independent of the time-space dependence of the traveling wave. The spinor parameters (α, ϕ) are easy to be located on the Poincaré sphere and can be used to represent the polarization state of a plane wave. In Fig. E 2.4c, the polarization state, described by the point P_E on the Poincaré sphere, can be expressed in terms of these two angles, where $2\alpha_{HV}$ is the angle subtended by the great circle drawn from the point P_E on the equator measured from H toward V; and ϕ_{HV} is the angle between the great circle and the equator.

From equations, (E 2.7) and (E 2.8) for the {H V} basis we have

$$\begin{aligned} \sin 2\chi &= \sin 2\alpha_{HV}\sin\phi_{HV} \\ \tan 2\psi &= \tan(2\alpha_{HV})\cos\phi_{HV} \end{aligned}, \tag{E 2.36}$$

which describes the ellipticity angle χ and the tilt or orientation angle ψ in terms of the variables α_{HV} and ϕ_{HV}. Also, from (E 2.11) for the {H V} basis, an inverse pair that describes the α_{HV} and ϕ_{HV} in terms of χ and ψ is given in (E 2.37):

$$\cos 2\alpha_{HV} = \cos 2\psi \cos 2\chi$$
$$\tan \phi_{HV} = \frac{\tan 2\chi}{\sin 2\psi} \qquad \text{(E 2.37)}$$

It is convenient to describe the polarization state by either of the two set of angles (α_{HV}, ϕ_{HV}) or (χ, ψ) which describe a point on the Poincaré sphere. The complex polarization ratio ρ_{HV} can be used to specify the polarization of an electromagnetic wave expressed in the {H V} basis. Some common polarization states expressed in terms of (χ, ψ), ρ, and the normalized Jones vector $\mathbf{E}$ are listed in Table E 2.1 at the end of this section.

E 2.4.2 Complex Polarization Ratio in the Circular Basis {L R}

In the circular basis {L R}, we have two unit vectors $\hat{\mathrm{L}}$ (left-handed circular) and $\hat{\mathrm{R}}$ (right- handed circular). Any polarization of a plane wave can be expressed by

$$\mathbf{E}(LR) = E_L \hat{\mathrm{L}} + E_R \hat{\mathrm{R}} \quad . \qquad \text{(E 2.38)}$$

A unit amplitude left-handed circular polarization has only the L component in the circular basis {L R}. It can be expressed by

$$\mathbf{E}(LR) = 1 * \hat{\mathrm{L}} + 0 * \hat{\mathrm{R}} = \begin{bmatrix} 1 \\ 0 \end{bmatrix}. \qquad \text{(E 2.39)}$$

The above representation of a unit (LHC) polarization in the circular basis {L R} is different from that in the linear basis {H V} of (E 2.29). Similarly, a unit amplitude right-handed circular polarization has only the R component in the circular basis {L R}

$$\mathbf{E}(LR) = 0 * \hat{\mathrm{L}} + 1 * \hat{\mathrm{R}} = \begin{bmatrix} 0 \\ 1 \end{bmatrix}, \qquad \text{(E 2.40)}$$

which is different from that in the linear {H V} basis.

The polarization ratio ρ_{LR}, according to (E 2.26) is

$$\rho_{LR} = \frac{E_R}{E_L} = \frac{|E_R|}{|E_L|} \exp\{j(\phi_R - \phi_L)\} = |\rho_{LR}| \exp\{j\phi_{LR}\} = \tan \alpha_{LR} \exp\{j\phi_{LR}\} \quad , \qquad \text{(E 2.41)}$$

where $|\rho_{LR}|$ is the ratio of magnitudes of the two orthogonal components $|E_L|$ and $|E_R|$, and ϕ_{LR} the phase difference. The angles α_{LR} and ϕ_{LR} are also easy to find on the Poincaré sphere (see Fig. E 2.6) like the angles α_{HV} and ϕ_{HV}. Some common polarization states in terms of ρ_{LR}, are listed in Table E 2.1.

E 2.4.3 Complex Polarization Ratio in the Linear Basis {45° 135°}

In the linear {45° 135°} basis with unit vectors $45\hat{}^{\circ}$ and $135\hat{}^{\circ}$, a polarization state may be expressed as

$$\mathbf{E}(45^{\circ}135^{\circ}) = E_{45^{\circ}} 45\hat{}^{\circ} + E_{135^{\circ}} 135\hat{}^{\circ} \,, \qquad \text{(E 2.42)}$$

where E_{45° and E_{135° are the 45° component and the 135° component, respectively. The polarization ratio according to (E 2.26) is

$$\rho_{45^\circ 135^\circ} = \frac{E_{135^\circ}}{E_{45^\circ}} = \frac{|E_{135^\circ}|}{|E_{45^\circ}|}\exp\{j(\phi_{135^\circ} - \phi_{45^\circ})\} = |\rho_{45^\circ 135^\circ}|\exp\{j\phi_{45^\circ 135^\circ}\} = \tan\alpha_{45^\circ 135^\circ}\exp\{j\phi_{45^\circ 135^\circ}\}, \quad \text{(E 2.43)}$$

where $|\rho_{45^\circ 135^\circ}|$ is the ratio of magnitudes of the two orthogonal components $|E_{135^\circ}|$ and $|E_{45^\circ}|$, and $\phi_{45^\circ 135^\circ}$ the phase difference. The angles $\alpha_{45^\circ 135^\circ}$ and $\phi_{45^\circ 135^\circ}$ are also easy to find on the Poincaré sphere (see Fig. E 2.6).

TABLE E 2.1
POLARIZATION STATES IN TERMS OF (χ, ψ), POLARIZATION RATIO ρ AND NORMALIZED JONES VECTOR $\mathbf{E}$

POLARIZATION	χ	ψ	{H V} basis		{45° 135°} basis		{L R} basis	
			ρ_{HV}	$\mathbf{E}$	$\rho_{45^\circ 135^\circ}$	$\mathbf{E}$	ρ_{LR}	$\mathbf{E}$
Linear Horizontal	0	0	0	$\begin{bmatrix}1\\0\end{bmatrix}$	-1	$\frac{1}{\sqrt{2}}\begin{bmatrix}1\\-1\end{bmatrix}$	1	$\frac{1}{\sqrt{2}}\begin{bmatrix}1\\1\end{bmatrix}$
Linear Vertical	0	$\frac{\pi}{2}$	∞	$\begin{bmatrix}0\\1\end{bmatrix}$	1	$\frac{1}{\sqrt{2}}\begin{bmatrix}1\\1\end{bmatrix}$	-1	$\frac{1}{\sqrt{2}}\begin{bmatrix}-j\\j\end{bmatrix}$
45° Linear	0	$\frac{\pi}{4}$	1	$\frac{1}{\sqrt{2}}\begin{bmatrix}1\\1\end{bmatrix}$	0	$\begin{bmatrix}1\\0\end{bmatrix}$	j	$\frac{1}{2}\begin{bmatrix}1 & -j\\1 & j\end{bmatrix}$
135° Linear	0	$-\frac{\pi}{4}$	-1	$\frac{1}{\sqrt{2}}\begin{bmatrix}-1\\1\end{bmatrix}$	∞	$\begin{bmatrix}0\\1\end{bmatrix}$	$-j$	$\frac{1}{2}\begin{bmatrix}-1 & -j\\-1 & j\end{bmatrix}$
Left-handed Circular	$\frac{\pi}{4}$		j	$\frac{1}{\sqrt{2}}\begin{bmatrix}1\\j\end{bmatrix}$	j	$\frac{1}{2}\begin{bmatrix}1 & j\\-1 & j\end{bmatrix}$	0	$\begin{bmatrix}1\\0\end{bmatrix}$
Right-handed Circular	$-\frac{\pi}{4}$		$-j$	$\frac{1}{\sqrt{2}}\begin{bmatrix}1\\-j\end{bmatrix}$	$-j$	$\frac{1}{2}\begin{bmatrix}1 & -j\\-1 & -j\end{bmatrix}$	∞	$\begin{bmatrix}0\\1\end{bmatrix}$

E 2.5 The Stokes Parameters

So far, we have seen completely polarized waves for which $|E_A|, |E_B|$, and ϕ_{AB} are constants or at least slowly varying functions of time. If we need to deal with partial polarization, it is convenient to use the Stokes parameters q_0, q_1, q_2 *and* q_3 introduced by Stokes in 1852 [E107] for describing partially polarized waves by observable power terms and not by amplitudes (and phases).

E 2.5.1 The Stokes vector for the completely polarized wave

For a monochromatic wave, in the linear {H V} basis, the four Stokes parameters are

$$
\begin{aligned}
q_0 &= |E_H|^2 + |E_V|^2 \\
q_1 &= |E_H|^2 - |E_V|^2 \\
q_2 &= 2|E_H||E_V|\cos\phi_{HV} \\
q_3 &= 2|E_H||E_V|\sin\phi_{HV}
\end{aligned}
\quad . \tag{E 2.44}
$$

For a completely polarized wave, there are only three independent parameters, which are related as follows:

$$
q_0^2 = q_1^2 + q_2^2 + q_3^2 \ . \tag{E 2.45}
$$

The Stokes parameters are sufficient to characterize the magnitude and the relative phase, and hence the polarization of a wave. The Stokes parameter q_0 is always equal to the total power (density) of the wave. q_1 is equal to the power in the linear horizontal or vertical polarized components, q_2 is equal to the power in the linearly polarized components at tilt angles $\psi = 45^\circ$ or 135°, and q_3 is equal to the power in the left-handed and right-handed circular polarized components. If any of the parameters q_0, q_1, q_2 or q_3 has a non-zero value, it indicates the presence of a polarized component in the plane wave. The Stokes parameters are also related to the geometric parameters A, χ, and ψ of the polarization ellipse

$$
\mathbf{q} = \begin{bmatrix} q_0 \\ q_1 \\ q_2 \\ q_3 \end{bmatrix} = \begin{bmatrix} |E_H|^2 + |E_V|^2 \\ E_H|^2 - |E_V|^2 \\ 2|E_H||E_V|\cos\phi_{HV} \\ 2|E_H||E_V|\sin\phi_{HV} \end{bmatrix} = \begin{bmatrix} A^2 \\ A^2\cos 2\psi\cos 2\chi \\ A^2\sin 2\psi\cos 2\chi \\ A^2\sin 2\chi \end{bmatrix} . \tag{E 2.46}
$$

For the normalized case, $q_0^2 = e^2 = e_H^2 + e_V^2 = 1$ and

$$
\mathbf{q} = \begin{bmatrix} q_0 \\ q_1 \\ q_2 \\ q_3 \end{bmatrix} = \frac{1}{\sqrt{|E_H|^2 + |E_V|^2}} \begin{bmatrix} |E_H|^2 + |E_V|^2 \\ E_H|^2 - |E_V|^2 \\ 2\,\mathrm{Re}\{E_H^* E_V\} \\ 2\,\mathrm{Im}\{E_H^* E_V\} \end{bmatrix} = \begin{bmatrix} e_H^2 + e_V^2 \\ e_H^2 - e_V^2 \\ 2e_H e_V\cos\phi \\ 2e_H e_V\sin\phi \end{bmatrix} = \begin{bmatrix} e^2 \\ e^2\cos 2\psi\cos 2\chi \\ e^2\sin 2\psi\cos 2\chi \\ e^2\sin 2\chi \end{bmatrix} . \tag{E 2.47}
$$

E 2.5.2 The Stokes vector for the partially polarized wave

The Stokes parameter presentation [E34] possesses two main advantages in that all of the four parameters are measured as intensities, a crucial fact in optical polarimetry, and the ability to present partially polarized waves in terms of the 2x2 complex hermitian positive semi-definite wave coherency matrix $[J]$ also called the Wolf's coherence matrix [E34]. This is defined as:

$$
[J] = \left\langle \mathbf{E}\mathbf{E}^\dagger \right\rangle = \begin{bmatrix} \langle E_H E_H^* \rangle & \langle E_H E_V^* \rangle \\ \langle E_V E_H^* \rangle & \langle E_V E_V^* \rangle \end{bmatrix} = \begin{bmatrix} J_{HH} & J_{HV} \\ J_{VH} & J_{VV} \end{bmatrix} = \begin{bmatrix} q_0 + q_1 & q_2 + jq_3 \\ q_2 - jq_3 & q_0 - q_1 \end{bmatrix} , \tag{E 2.48}
$$

where $\langle ... \rangle = \lim_{T\to\infty}\left[\frac{1}{2T}\int_{-T}^{T}\langle ... \rangle dt\right]$ indicates temporal or ensemble averaging assuming stationarity of the wave.

We can associate the Stokes vector $\mathbf{q}$ with the coherency matrix $[J]$:

$$\begin{aligned} q_0 &= |E_H|^2 + |E_V|^2 = \langle E_H E_H^* \rangle + \langle E_V E_V^* \rangle = J_{HH} + J_{VV} \\ q_1 &= |E_H|^2 - |E_V|^2 = \langle E_H E_H^* \rangle - \langle E_V E_V^* \rangle = J_{HH} - J_{VV} \\ q_2 &= 2|E_H||E_V|\cos\phi_{HV} = \langle E_H E_V^* \rangle + \langle E_V E_H^* \rangle = J_{HV} + J_{VH} \\ q_3 &= 2|E_H||E_V|\sin\phi_{HV} = j\langle E_H E_V^* \rangle - j\langle E_V E_H^* \rangle = jJ_{HV} - jJ_{VH} \end{aligned} \quad \text{(E 2.49)}$$

Since $[J]$ is a positive semidefinite matrix,

$$Det\{[J]\} \geq 0 \quad or \quad q_0^2 \geq q_1^2 + q_2^2 + q_3^2 \quad \text{(E 2.50)}$$

The diagonal elements present the intensities, the off-diagonal elements the complex cross-correlation between E_H and E_V, and the $Trace\{[J]\}$ represents the total energy of the wave. For $J_{HV} = 0$ no correlation between E_H and E_V exists, and $[J]$ is diagonal with $J_{HH} = J_{VV}$. That is, the wave is unpolarized or completely depolarized, and possesses *one degree of freedom only : amplitude.* For $Det\{[J]\} = 0$, we find that $J_{VH}J_{HV} = J_{HH}J_{VV}$, and the correlation between E_H and E_V is maximum, and the wave is completely polarized. In this case the wave *possesses three degrees of freedom: amplitude, orientation, and ellipticity of the polarization ellipse.* Between these two extreme cases lies the general case of partial polarization, where $Det\{[J]\} > 0$ indicates a certain degree of statistical dependence between E_H and E_V, which can be expressed in terms of the degree of coherency μ and the degree of polarization D_p as:

$$\mu_{HV} = |\mu_{HV}|\exp(j\beta_{HV}) = \frac{J_{HV}}{\sqrt{J_{HH}J_{VV}}} \quad \text{(E 2.51)}$$

$$D_p = \left(1 - \frac{4Det\{[J]\}}{\left(Trace\{[J]\}\right)^2}\right)^{1/2} = \frac{\left(q_1^2 + q_2^2 + q_3^2\right)^{1/2}}{q_0} \quad \text{(E 2.52)}$$

$\mu = D_p = 0$ for totally depolarized waves and $\mu = D_p = 1$ for fully polarized waves, respectively. However, under a change of polarization basis the elements of the wave coherency matrix $[J]$ depend on the choice of the polarization basis, where according to [E52, E53], $[J]$ transforms through a unitary similarity transformation as

$$\langle [J_{ij}] \rangle = [U_2]\langle [J_{mn}] \rangle [U_2]^{\dagger}. \quad \text{(E 2.53)}$$

The fact that the trace and the determinant of a hermitian matrix are invariant under unitary similarity transformations means that both the degree of polarization as well as the total wave intensity are not affected by polarimetric basis transformations. Also, note that the degree of coherence μ_{mn} does depend on the polarization basis. Table E 2.2 gives the Jones vector $\mathbf{E}$, Coherency Matrix $[J]$, and Stokes Vector $\mathbf{q}$ for special cases of purely monochromatic wave fields in specific states of polarization.

TABLE E 2.2
JONES VECTOR $\mathbf{E}$, COHERENCY MATRIX $[J]$, AND STOKES VECTOR $\mathbf{q}$ FOR SOME STATES OF POLARIZATION

POLARIZATION	{H V} BASIS		
	$\mathbf{E}$	$[J]$	$\mathbf{q}$
Linear Horizontal	$\begin{bmatrix}1\\0\end{bmatrix}$	$\begin{bmatrix}1 & 0\\0 & 0\end{bmatrix}$	$\begin{bmatrix}1\\1\\0\\0\end{bmatrix}$
Linear Vertical	$\begin{bmatrix}0\\1\end{bmatrix}$	$\begin{bmatrix}0 & 0\\0 & 1\end{bmatrix}$	$\begin{bmatrix}1\\-1\\0\\0\end{bmatrix}$
45° Linear	$\frac{1}{\sqrt{2}}\begin{bmatrix}1\\1\end{bmatrix}$	$\frac{1}{2}\begin{bmatrix}1 & 1\\1 & 1\end{bmatrix}$	$\begin{bmatrix}1\\0\\1\\0\end{bmatrix}$
135° Linear	$\frac{1}{\sqrt{2}}\begin{bmatrix}-1\\1\end{bmatrix}$	$\frac{1}{2}\begin{bmatrix}1 & -1\\-1 & 1\end{bmatrix}$	$\begin{bmatrix}1\\0\\-1\\0\end{bmatrix}$
Left-handed Circular	$\frac{1}{\sqrt{2}}\begin{bmatrix}1\\j\end{bmatrix}$	$\frac{1}{2}\begin{bmatrix}1 & -j\\j & 1\end{bmatrix}$	$\begin{bmatrix}1\\0\\0\\1\end{bmatrix}$
Right-handed Circular	$\frac{1}{\sqrt{2}}\begin{bmatrix}1\\-j\end{bmatrix}$	$\frac{1}{2}\begin{bmatrix}1 & j\\-j & 1\end{bmatrix}$	$\begin{bmatrix}1\\0\\0\\-1\end{bmatrix}$

E 2.6 The Poincaré Polarization Sphere

The Poincaré sphere, shown in Fig. E 2.4 for the representation of wave polarization using the Stokes vector and the Deschamps parameters (α, ϕ) is a useful graphical aid for the visualization of polarization effects. There is one-to-one correspondence between all possible polarization states and points on the Poincaré sphere. The linear polarizations map onto the equatorial plane (x = 0) with the zenith presenting left-handed circular and the nadir right-handed circular polarization states, according to the IEEE standard notation $\exp(+j\omega t)$ [E102]. Any set of orthogonally fully polarized polarization states are mapped into antipodal points on the Poincaré sphere [E108].

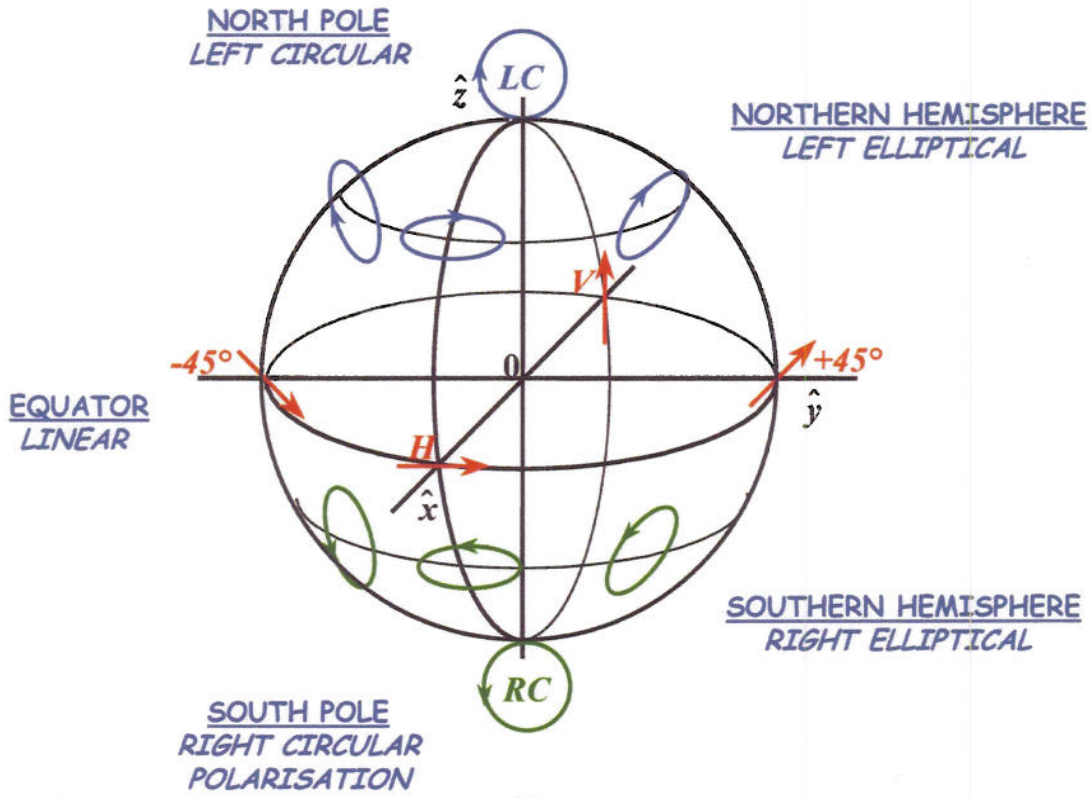

Fig. E 2.4 Poincaré Sphere Representations (Courtesy of Prof. E. Pottier)

E 2.6.1 The polarization state on the Poincaré sphere for the {H V} basis

In the Poincaré sphere representation, the polarization state is described by a point P on the sphere, where the three Cartesian coordinate components are q_1, q_2, and q_3 according to (E 2.46). So, for any state of a completely polarized wave, there corresponds one point $P(q_1, q_2, q_3)$ on the sphere of radius q_0, and vice versa. In Fig. E 2.5, we can see that the longitude and latitude of the point P are related to the geometric parameter of the polarization ellipse and they are 2ψ and 2χ respectively.

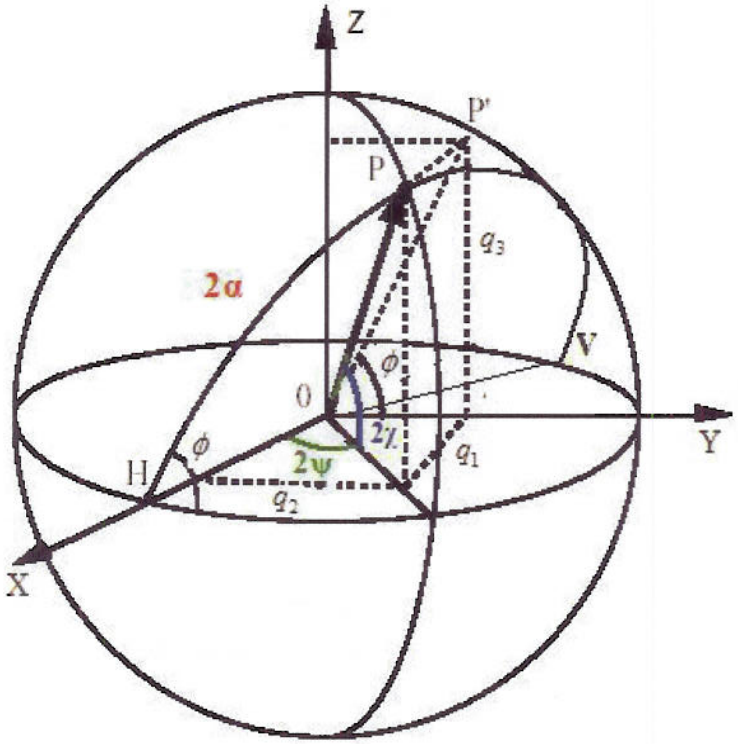

Fig. E 2.5 The Poincaré sphere and the parameters α_{HV} and ϕ_{HV}

In addition, the point P on the Poincaré sphere can also be represented by the angles α_{HV} and ϕ_{HV}. From (E 2.37) and (E 2.46) we find that

$$\frac{q_1}{q_0} = \cos 2\psi \cos 2\chi = \cos 2\alpha_{HV} \ , \tag{E 2.54}$$

where $\cos 2\alpha_{HV}$ is the direction cosine of the Stokes vector $\mathbf{q}$ with respect to the X-axis. That is, the angle $2\alpha_{HV}$ is the angle between $\mathbf{q}$ and the X-axis. The angle ϕ_{HV} is the angle between the equator and the great circle with basis diameter HV through the point P, and it is equal to the angle between the XOY plane and the XOP plane. Drawing a projecting line from point P to the YOZ plane, the intersecting point P' is on the XOP plane, so $\phi_{HV} = \angle \mathrm{YOP}'$ ($\phi_{HV} = \phi$ in Fig. E 2.5). On the YOZ plane we find that

$$\tan \phi_{HV} = \tan \angle \mathrm{YOP}' = \frac{q_3}{q_2} = \frac{\tan 2\chi}{\sin 2\psi} \ , \tag{E 2.55}$$

which satisfies equations (E 2.46) and (E 2.37).

E 2.6.2 The polarization ratio on the Poincaré sphere for different polarization bases

Also, it can be shown that a polarization state can be represented in different polarization bases. Any polarization basis consists of two unit vectors which are located at two corresponding antipodal points on the Poincaré sphere. Fig E 2.6 shows how the polarization state P on the Poincaré sphere can be represented in three polarization bases, {H V}, {45° 135°}, and {L R}. The complex polarization ratios are given by

$$\rho_{HV} = |\rho_{HV}| \exp(j\phi_{HV}) = \begin{cases} \tan\alpha_{HV} \exp(j\phi_{HV}) & 0 < \alpha_{HV} < \dfrac{\pi}{2} \\ -\tan\alpha_{HV} \exp(j\phi_{HV}) & \dfrac{\pi}{2} < \alpha_{HV} < \pi \end{cases} \quad \text{(E 2.56)}$$

$$\rho_{45°135°} = |\rho_{45°135°}| \exp(j\phi_{45°135°}) = \begin{cases} \tan\alpha_{45°135°} \exp(j\phi_{45°135°}) & 0 < \alpha_{45°135°} < \dfrac{\pi}{2} \\ -\tan\alpha_{45°135°} \exp(j\phi_{45°135°}) & \dfrac{\pi}{2} < \alpha_{45°135°} < \pi \end{cases} \quad \text{(E 2.57)}$$

$$\rho_{LR} = |\rho_{LR}| \exp(j\phi_{LR}) = \begin{cases} \tan\alpha_{LR} \exp(j\phi_{LR}) & 0 < \alpha_{LR} < \dfrac{\pi}{2} \\ -\tan\alpha_{LR} \exp(j\phi_{LR}) & \dfrac{\pi}{2} < \alpha_{LR} < \pi \end{cases} \quad \text{(E 2.58)}$$

$\tan\alpha_{HV}$, $\tan\alpha_{45°135°}$, and $\tan\alpha_{LR}$ are the ratios of the magnitudes of the corresponding orthogonal components, and ϕ_{HV}, $\phi_{45°135°}$, and ϕ_{LR} are the phase differences between the corresponding orthogonal components.

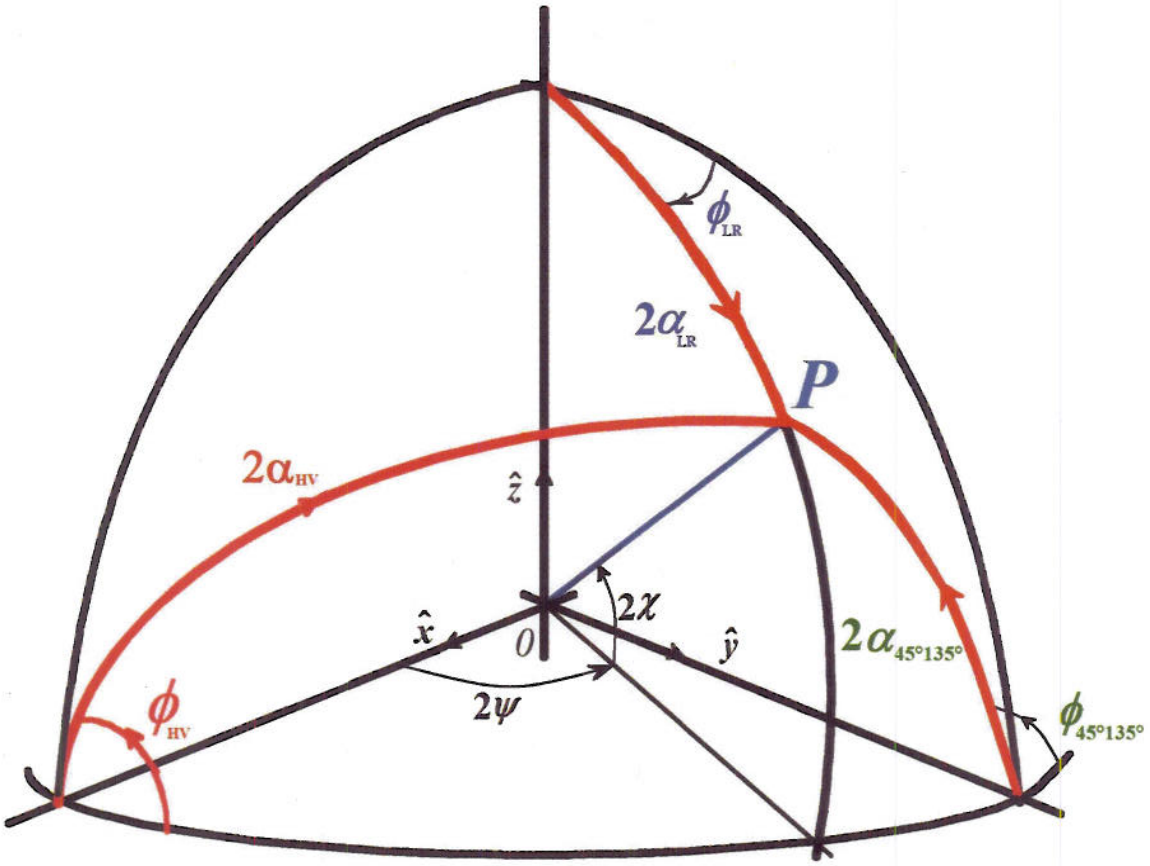

Fig E 2.6 The Polarization State P in Different Polarization Bases

E 2.6.3 **The relationship between the Stokes vector and the polarization ratio for different polarization bases**

First, consider the polarization ratio ρ_{HV} defined in the {H V} basis. Because $\cos 2\alpha_{HV}$ is the direction cosine of the Stokes vector $\mathbf{q}$ with respect to the X-axis, we find

$$\frac{q_1}{q_0} = \cos 2\alpha_{HV} = \frac{1-\tan^2 \alpha_{HV}}{1+\tan^2 \alpha_{HV}} = \frac{1-|\rho_{HV}|^2}{1+|\rho_{HV}|^2} . \tag{E 2.59}$$

The straight forward solution for $|\rho_{HV}|$ is

$$|\rho_{HV}| = \sqrt{\frac{q_0 - q_1}{q_0 + q_1}} . \tag{E 2.60}$$

From (E 2.54) we find

$$\phi_{HV} = \angle \mathrm{YOP'} = \tan^{-1}\left(\frac{q_3}{q_2}\right) . \tag{E 2.61}$$

Combining above two equations yields

$$\rho_{HV} = |\rho_{HV}| \exp(j\phi_{HV}) = \sqrt{\frac{q_0 - q_1}{q_0 + q_1}} \exp\left\{ j \tan^{-1}\left(\frac{q_3}{q_2}\right)\right\} . \tag{E 2.62}$$

For a completely polarized wave, we may obtain the Stokes vector in terms of the polarization ratio ρ_{HV} by applying

$$
\begin{aligned}
q_0 &= \sqrt{q_1^2 + q_2^2 + q_3^2} = 1 \\
q_1 &= \frac{1-|\rho_{HV}|^2}{1+|\rho_{HV}|^2} = \cos 2\alpha_{HV} \\
q_2 &= \frac{2|\rho_{HV}|\cos\phi_{HV}}{1+|\rho_{HV}|^2} = \frac{2\tan\alpha_{HV}\cos\phi_{HV}}{1+|\tan\alpha_{HV}|^2} = \sin(2\alpha_{HV})\cos\phi_{HV} \\
q_3 &= \frac{2|\rho_{HV}|\sin\phi_{HV}}{1+|\rho_{HV}|^2} = \sin(2\alpha_{HV})\sin\phi_{HV}
\end{aligned}
\qquad \text{(E 2.63)}
$$

The sign of the three components of the Stokes vector is summarized in Table E 2.3.

TABLE E 2.3

THE SIGN OF THE q_1, q_2, AND q_3 PARAMETERS IN THE {H V} BASIS

ϕ_{HV}	α_{HV}	q_1	q_2	q_3
$0 < \phi_{HV} < \frac{\pi}{2}$	$0 < 2\alpha_{HV} < \frac{\pi}{2}$	+	+	+
	$\frac{\pi}{2} < 2\alpha_{HV} < \pi$	−	+	+
	$0 < 2\alpha_{HV} < \frac{3\pi}{2}$	−	−	−
	$\frac{3\pi}{2} < 2\alpha_{HV} < 2\pi$	+	−	−
$-\frac{\pi}{2} < \phi_{HV} < 0$	$0 < 2\alpha_{HV} < \frac{\pi}{2}$	+	+	−
	$\frac{\pi}{2} < 2\alpha_{HV} < \pi$	−	+	−
	$0 < 2\alpha_{HV} < \frac{3\pi}{2}$	−	−	+
	$\frac{3\pi}{2} < 2\alpha_{HV} < 2\pi$	+	−	+

Secondly, consider the polarization ratio $\rho_{45°135°}$ defined in the {45° 135°} basis. $\cos 2\alpha_{45°135°}$ is the direction cosine of the Stokes vector $\mathbf{q}$ with respect to the Y-axis. Then

$$
\begin{aligned}
&q_0 = 1 \\
&\left|\rho_{45°135°}\right| = \sqrt{\frac{q_0 - q_2}{q_0 + q_2}} \\
&\phi_{45°135°} = \tan^{-1}\left(-\frac{q_3}{q_1}\right)
\end{aligned}
\qquad \text{(E 2.64)}
$$

The polarization ratio $\rho_{45°135°}$ can be determined by the Stokes vector $\mathbf{q}$

$$
\rho_{45°135°} = \sqrt{\frac{q_0 - q_2}{q_0 + q_2}} \exp\left\{ j \tan^{-1}\left(-\frac{q_3}{q_1}\right)\right\}. \qquad \text{(E 2.65)}
$$

Also, the Stokes vector $\mathbf{q}$ can be determined by the polarization ratio $\rho_{45°135°}$ as follows:

$$
\begin{aligned}
&q_0 = 1 \\
&q_1 = \frac{2\left|\rho_{45°135°}\right|\cos\phi_{45°135°}}{1+\left|\rho_{45°135°}\right|^2} = -\sin 2\alpha_{45°135°}\cos\phi_{45°135°} \\
&q_2 = \frac{1-\left|\rho_{45°135°}\right|^2}{1+\left|\rho_{45°135°}\right|^2} = \cos 2\alpha_{45°135°} \\
&q_3 = \frac{2\left|\rho_{45°135°}\right|\sin\phi_{45°135°}}{1+\left|\rho_{45°135°}\right|^2} = \sin 2\alpha_{45°135°}\sin\phi_{45°135°}
\end{aligned}
\qquad \text{(E 2.66)}
$$

Finally, consider the polarization ratio ρ_{LR} defined in the {L R} basis. Similarly, because $\cos 2\alpha_{LR}$ is the direction cosine of the Stokes vector $\mathbf{q}$ with respect to the Z-axis, the polarization ratio ρ_{LR} can be determined by the Stokes vector $\mathbf{q}$ as:

$$
\rho_{LR} = \sqrt{\frac{q_0 - q_3}{q_0 + q_3}} \exp\left\{ j \tan^{-1}\left(\frac{q_2}{q_1}\right)\right\}. \qquad \text{(E 2.67)}
$$

Inversely,

$$
\begin{aligned}
&q_0 = 1 \\
&q_1 = \frac{2\left|\rho_{LR}\right|\cos\phi_{LR}}{1+\left|\rho_{LR}\right|^2} = \sin 2\alpha_{LR}\cos\phi_{LR} \\
&q_2 = \frac{2\left|\rho_{LR}\right|\sin\phi_{LR}}{1+\left|\rho_{LR}\right|^2} = \sin 2\alpha_{LR}\sin\phi_{LR} \\
&q_3 = \frac{1-\left|\rho_{LR}\right|^2}{1+\left|\rho_{LR}\right|^2} = \cos 2\alpha_{LR}
\end{aligned}
\qquad \text{(E 2.68)}
$$

TABLE E 2.4
ALTERNATE EXPRESSIONS FOR NORMALIZED STOKES VECTOR PRESENTATIONS ON THE POLARIZATION SPHERE

	χ,ψ	α_{HV},ϕ_{HV}	$\alpha_{45°135°},\phi_{45°135°}$	α_{LR},ϕ_{LR}
q_0	1	1	1	1
q_1	$\cos 2\chi \cos 2\psi$	$\cos 2\alpha_{HV}$	$-\sin 2\alpha_{45°135°} \cos \phi_{45°135°}$	$\sin 2\alpha_{LR} \cos \phi_{LR}$
q_2	$\cos 2\chi \sin 2\psi$	$\sin 2\alpha_{HV} \cos \phi_{HV}$	$\cos 2\alpha_{45°135°}$	$\sin 2\alpha_{LR} \sin \phi_{LR}$
q_3	$\sin 2\chi$	$\sin 2\alpha_{HV} \sin \phi_{HV}$	$\sin 2\alpha_{45°135°} \sin \phi_{45°135°}$	$\cos 2\alpha_{LR}$

E 2.6.4 The Poincaré polarization sphere and complex polarization ratio plane

Using the Riemann transformation, Poincaré introduced the polarization sphere representation of Fig. E 2.5, which gives a relationship between the polarization ratio ρ and its corresponding spherical coordinates on the Poincaré sphere. First we need to introduce an auxiliary complex parameter $\mathrm{u}(\rho)$, which is defined by the Riemann transformation [E14] of the surface of the sphere onto the polar grid as follows:

$$\mathrm{u}(\rho) = \frac{1 - j\rho}{1 + j\rho} . \tag{E 2.69}$$

In the {H V} basis, $\rho_{HV} = \tan\alpha_{HV} \exp\{j\phi_{HV}\} = \tan\alpha_{HV}(\cos\phi_{HV} + j\sin\phi_{HV})$. Then

$$\mathrm{u} = \frac{(1 + \tan\alpha_{HV} \sin\phi_{HV}) - j\tan\alpha_{HV} \cos\phi_{HV}}{(1 - \tan\alpha_{HV} \sin\phi_{HV}) + j\tan\alpha_{HV} \cos\phi_{HV}}$$

$$|\mathrm{u}|^2 = \frac{1 + 2\tan\alpha_{HV} \sin\phi_{HV}) + \tan^2\alpha_{HV}}{1 - 2\tan\alpha_{HV} \sin\phi_{HV}) + \tan^2\alpha_{HV}}$$

$$\frac{|\mathrm{u}|^2 - 1}{|\mathrm{u}|^2 + 1} = \frac{2\tan\alpha_{HV}}{1 + \tan^2\alpha_{HV}} \sin\phi_{HV} = \sin 2\alpha_{HV} \sin\phi_{HV}$$

According to (E 2.36) and Fig. E 2.4b, the polar angle $\Theta = \pi/2 - 2\chi$ can be obtained from

$$\frac{|\mathrm{u}|^2 - 1}{|\mathrm{u}|^2 + 1} = \sin 2\chi = \sin(\pi/2 - \Theta) = \cos\Theta ,$$

so that

$$\Theta = \cos^{-1}\left(\frac{|\mathrm{u}|^2 - 1}{|\mathrm{u}|^2 + 1}\right) . \tag{E 2.70}$$

Also, according to (E 2.36) and Fig. E 2.4b, the spherical azimuthal angle $\Phi = 2\psi$ can be obtained from $-\frac{\mathrm{Im}\{\mathrm{u}\}}{\mathrm{Re}\{\mathrm{u}\}} = \frac{2\tan\alpha_{HV}\cos\phi_{HV}}{1 - \tan^2\alpha_{HV}} = \tan 2\psi = \tan\Phi$, so that the spherical azimuthal angle Φ becomes

$$\Phi = \tan^{-1}\left(\frac{\mathrm{Im}\{u\}}{\mathrm{Re}\{u\}}\right) \qquad \text{(E 2.71)}$$

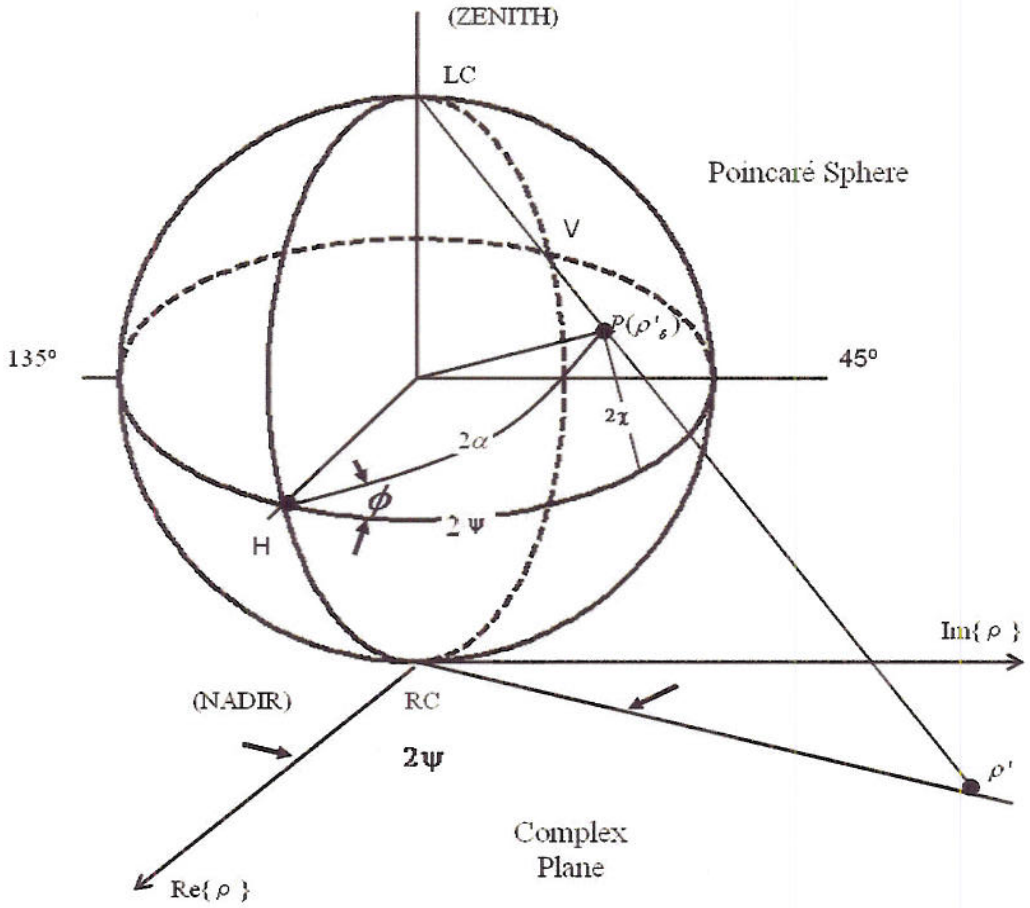

Fig. E 2.7 Poincaré Sphere and the Complex Plane

E 2.7 Wave Decomposition Theorems

The diagonalization of $\left[J_{ij}\right]$ under the unitary similarity transformation is equivalent to finding an orthonormal polarization basis in which the coherency matrix is diagonal, or

$$\begin{bmatrix} J_{mm} & J_{mn} \\ J_{nm} & J_{nn} \end{bmatrix} = \begin{bmatrix} e_{11} & e_{21} \\ e_{12} & e_{22} \end{bmatrix} \begin{bmatrix} \lambda_1 & 0 \\ 0 & \lambda_2 \end{bmatrix} \begin{bmatrix} e_{11}^* & e_{12}^* \\ e_{21}^* & e_{22}^* \end{bmatrix}. \qquad \text{(E 2.72)}$$

λ_1 and λ_2 are the real non-negative eigenvalues of $[J]$ with $\lambda_1 \geq \lambda_2 \geq 0$, and $\hat{\mathbf{e}}_1 = \left[e_{11}\ \ e_{12}\right]^T$ and $\hat{\mathbf{e}}_2 = \left[e_{21}\ \ e_{22}\right]^T$ are the complex orthogonal eigenvectors which define $[U_2]$ and a polarization basis $\left\{\hat{\mathbf{e}}_1, \hat{\mathbf{e}}_2\right\}$ in which $[J]$ is diagonal. $[J]$ is Hermitian and hence normal and every normal matrix can be unitarily diagonalized . Being positive semidefinite the eigenvalues are nonnegative.

E 2.8 The Wave Dichotomy of Partially Polarized Waves

The solution of (E 2.72) provides two equivalent interpretations of partially polarized waves [E28]. The first interpretation is separation into fully polarized $[J_1]$ and completely depolarized $[J_2]$ components

$$[J]=(\lambda_1-\lambda_2)[J_1]+\lambda_2[I_2], \tag{E 2.73}$$

where $[I_2]$ is the 2x2 identity matrix. The second interpretation is non-coherency of two orthogonal completely polarized wave states represented by the eigenvectors and weighed by their corresponding eigenvalues as

$$[J]=(\lambda_1)[J_1]+\lambda_2[J_2]=\lambda_1(\hat{\mathbf{e}}_1\cdot\hat{\mathbf{e}}_1^{\dagger})+\lambda_2(\hat{\mathbf{e}}_2\cdot\hat{\mathbf{e}}_2^{\dagger}), \tag{E 2.74}$$

where $Det\{[J_1]\}=Det\{[J_2]\}=0$. If $\lambda_1=\lambda_2$ the wave is totally depolarized (degenerate case) whereas for $\lambda_2=0$, the wave is completely polarized. Both models are unique in the sense that no other decomposition in form of a separation of two completely polarized waves or of a completely polarized with noise is possible for a given coherency matrix, which may be reformulated in terms of the degree of polarization D_p as

$$D_p=\frac{\lambda_1-\lambda_2}{\lambda_1+\lambda_2},\quad 0\ \ (\lambda_1=\lambda_2)\ \ and\ \ 1\ \ (\lambda_2=0) \tag{E 2.75}$$

for a partially unpolarized and completely polarized wave. The fact that the eigenvalues λ_1 and λ_2 are invariant under polarization basis transformation makes D_p an important basis-independent parameter.

E 2.9 Polarimetric Wave Entropy

Alternately to the degrees of wave coherency μ and polarization D_p, the polarimetric wave entropy H_ω [E28] provides another measure of the correlated wave structure of the coherency matrix $[J]$. Using the logarithmic sum of eigenvalues:

$$H_\omega=\sum_{i=1}^{2}\{-P_i\log_2 P_i\}\quad with\ \ P_i=\frac{\lambda_i}{\lambda_1+\lambda_2}, \tag{E 2.76}$$

so that $P_1+P_2=1$. The normalized wave entropy ranges from $0\le H_\omega\le 1$. For a completely polarized wave with $\lambda_2=0$, $H_\omega=0$, while a completely randomly polarized wave with $\lambda_1=\lambda_2$ possesses maximum entropy $H_\omega=1$.

E 2.10 Alternate Formulations of the Polarization Properties of Electromagnetic Vector Waves

There exist several alternate formulations of the polarization properties of electromagnetic vector waves including (i) the Four-vector Hamiltonian formulation frequently utilized by Zhivotovsky [E109] and by Czyz [E110], which may be useful in a more concise description of partially polarized waves ; (ii) the spinorial formulation used by Bebbington [E32], and in general gravitation theory [E111] ; and (iii) a pseudo-spinorial formulation by Czyz [E110]. These are most essential tools for describing the general bi-static (non-symmetric) scattering matrix cases for both the coherent (3-D Poincaré sphere and the 3-D polarization spheroid) and the partially polarized (4-D Zhivotovsky sphere and 4-D spheroid) cases [E109]. Because of the excessive additional mathematical and computational tools required not commonly accessible to engineers and applied scientists, these formulations are not presented here but deserve our fullest attention in future analyses.

E 3.0 The Electromagnetic Vector Scattering

The electromagnetic vector wave interrogation with material media is described by the Scattering Operator $[S(\mathbf{k}_s/\mathbf{k}_i)]$ with $\mathbf{k}_s, \mathbf{k}_i$ representing the wave vectors of the scattered and incident, $\mathbf{E}^s(\mathbf{r}), \mathbf{E}^i(\mathbf{r})$ respectively, where

$$\mathbf{E}^s(\mathbf{r}) = E_0^s \exp(-j\mathbf{k}_s \cdot \mathbf{r}) = \mathbf{e}_s E_0^s \exp(-j\mathbf{k}_s \cdot \mathbf{r}) \tag{E 3.1}$$

is related to

$$\mathbf{E}^i(\mathbf{r}) = E_0^i \exp(-j\mathbf{k}_i \cdot \mathbf{r}) = \mathbf{e}_i E_0^i \exp(-j\mathbf{k}_i \cdot \mathbf{r}) \tag{E 3.2}$$

$$\mathbf{E}^s(\mathbf{r}) = \frac{\exp(-j\mathbf{k}_s \cdot \mathbf{r})}{r}[S(\mathbf{k}_s/\mathbf{k}_i)]\mathbf{E}^i(\mathbf{r}) \tag{E 3.3}$$

The scattering operator $[S(\mathbf{k}_s/\mathbf{k}_i)]$ is obtained from rigorous application of vector scattering and diffraction theory, to the specific scattering scenario under investigation which is not further discussed here, but we refer to [E97] for a thought-provoking formulation of these still open problems.

E 3.1 The Scattering Scenario and the Scattering Coordinate Framework

The scattering operator $[S(\mathbf{k}_s/\mathbf{k}_i)]$ appears as the output of the scattering process for an arbitrary input $\mathbf{E}_0^i$, which must carefully be defined in terms of the scattering scenario. Its proper unique formulation is of intrinsic importance to both optical and radar polarimetry. Whereas in optical remote sensing, mainly forward scattering through translucent media is considered, in radar remote sensing back scattering from distant, opaque open and closed surfaces is of interest. In radar target backscattering we usually deal with closed surfaces whereas in SAR imaging one deals with open surfaces. These two distinct cases of optical versus radar scattering are treated separately using two different reference frames: The Forward (anti-monostatic) Scattering Alignment (FSA) versus the Back Bistatic Scattering Alignment (BSA) from which the Monostatic Arrangement is derived as shown in Fig. E 3.1. Separate details for the FSA and BSA systems are shown in Figs. E 3.2 and E 3.3.

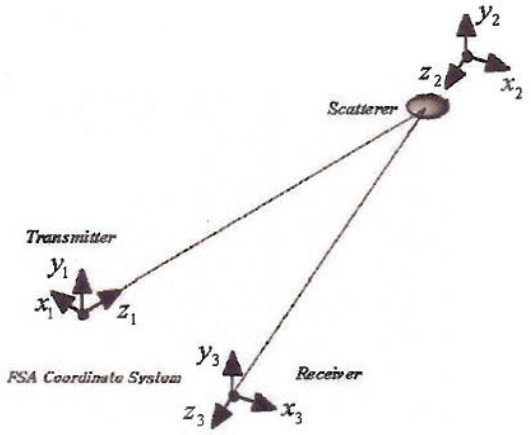

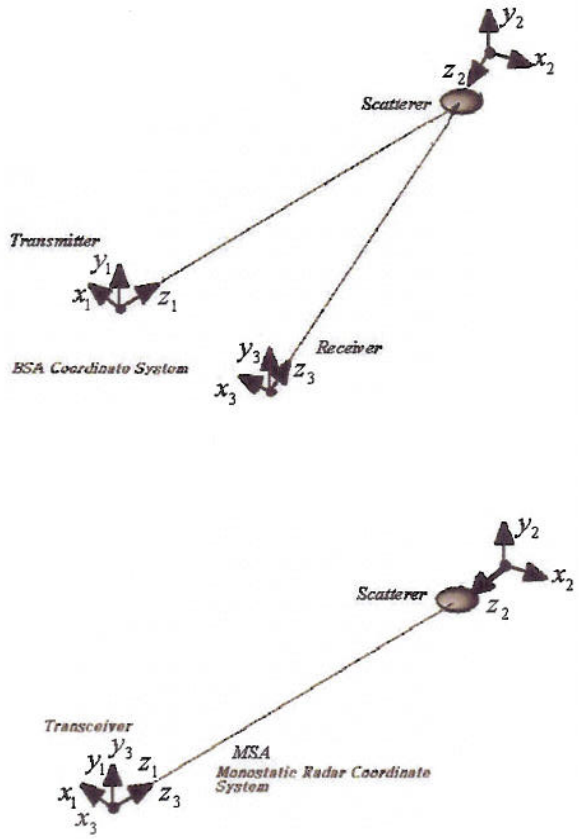

Fig. E 3.1 Comparison of the FSA, BSA, and MSA Coordinate Systems

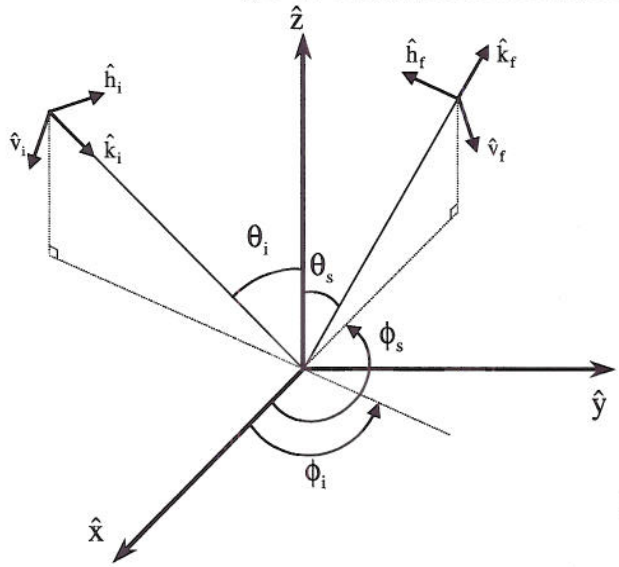

$$\hat{k}_f = \sin\theta_s \cos\phi_s \hat{x} + \sin\theta_s \sin\phi_s \hat{y} + \cos\theta_s \hat{z}$$

$$\hat{v}_f = \cos\theta_s \cos\phi_s \hat{x} + \cos\theta_s \sin\phi_s \hat{y} - \sin\theta_s \hat{z}$$

$$\hat{h}_f = -\sin\phi_s \hat{x} + \cos\phi_s \hat{y}$$

Fig. E 3.2 Detailed Forward Scattering Alignment (FSA)

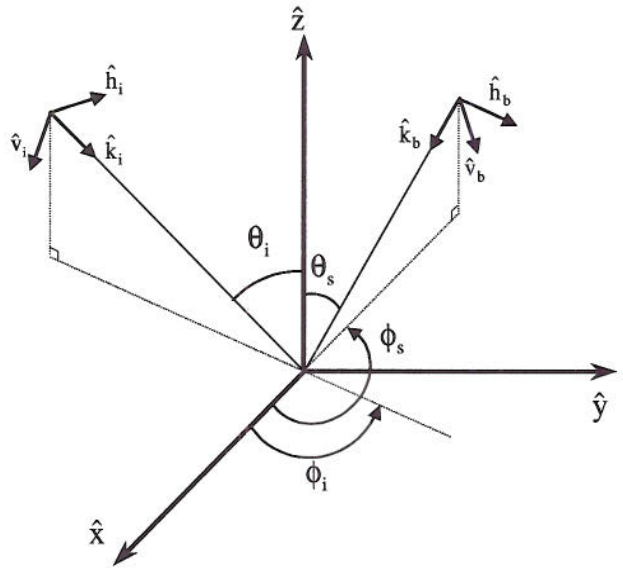

$$\hat{k}_b = -\sin\theta_s\cos\phi_s\hat{x} - \sin\theta_s\sin\phi_s\hat{y} - \cos\theta_s\hat{z}$$
$$\hat{v}_b = \cos\theta_s\cos\phi_s\hat{x} + \cos\theta_s\sin\phi_s\hat{y} - \sin\theta_s\hat{z}$$
$$\hat{h}_b = \sin\phi_s\hat{x} - \cos\phi_s\hat{y}$$

Fig. E 3.3 Detailed Back Scattering Alignment (BSA)

E 3.2 The 2x2 Jones Forward [*J*] versus 2x2 Sinclair [*S*] Back-Scattering Matrices

Since we are dealing here with radar polarimetry, interferometry, and polarimetric interferometry, the bistatic BSA reference frame is the more relevant framework and is introduced here dealing with both with the bistatic and the monostatic cases. We refer to [E52, E53], [E76] and [E19] for a full treatment of the anti-monostatic FSA reference frame. Refer to the dissertation of Papathanassiou [E97], the textbook of Mott [E76], and the meticulous derivations of Lüneburg [E52] for more detailed treatments of the subject matter, but we follow here the derivation presented in [E19]. Using the coordinates of Fig. E 3.1 with right-handed coordinate systems $x_1\ y_1\ z_1$, $x_2\ y_2\ z_2$, and $x_3\ y_3\ z_3$ denoting the transmitter, scatterer and receiver coordinates, respectively, a wave incident on the scatterer from the transmitter is given by the transverse components E_{x_1} and E_{y_1} in the right-handed coordinate system $x_1\ y_1\ z_1$ with the z_1 axis pointed at the target. The scatterer coordinate system $x_2\ y_2\ z_2$ is right-handed with z_2 pointing away from the scatterer toward a receiver. BSA Coordinate System $x_3\ y_3\ z_3$ is right-handed with z_3 pointing toward the scatterer. It would coincide with the transmitter system $x_1\ y_1\ z_1$ if the transmitter and receiver were co-located. The wave reflected by the target to the receiver may be described in either the transverse components E_{x_2} and E_{y_2} or by the reversed components E_{x_3} and E_{y_3}. Both conventions are used, leading to different matrix formulations. The incident and transmitted or reflected (scattered) fields are given by two-component vectors, therefore the relationship between them must be a 2x2 matrix. If the scattered field is expressed in $x_3\ y_3\ z_3$ coordinates (BSA), the fields are related by the Sinclair matrix $[S]$, thus

$$\begin{bmatrix} E^s_{x_3} \\ E^s_{y_3} \end{bmatrix} = \frac{1}{\sqrt{4\pi r_2}} \begin{bmatrix} S_{x_3x_1} & S_{x_3y_1} \\ S_{y_3x_1} & S_{y_3y_1} \end{bmatrix} \begin{bmatrix} E^i_{x_1} \\ E^i_{y_1} \end{bmatrix} e^{-jkr_2} \quad . \tag{E 3.4}$$

If the scattered field is in $x_2\ y_2\ z_2$ coordinates (FSA), it is given by the product of the Jones matrix $[J]$ with the incident field, thus

$$\begin{bmatrix} E^s_{x_3} \\ E^s_{y_3} \end{bmatrix} = \frac{1}{\sqrt{4\pi r_2}} \begin{bmatrix} T_{x_2x_1} & T_{x_2y_1} \\ T_{y_2x_1} & T_{y_2y_1} \end{bmatrix} \begin{bmatrix} E^i_{x_1} \\ E^i_{y_1} \end{bmatrix} e^{-jkr_2} . \qquad \text{(E 3.5)}$$

In both equations the incident fields are those at the target, the received fields are measured at the receiver, and r_2 is the distance from target to receiver. The Sinclair matrix $[S]$ is mostly used for **back-scattering**, but is readily extendible to the **bistatic scattering** case. If the name **scattering matrix** is used without qualification, it normally refers to the Sinclair matrix $[S]$. In the general bistatic scattering case, the elements of the Sinclair matrix are not related to each other, except through the physics of the scatterer. However, if the receiver and transmitter are co-located, as in the **mono-static** or back-scattering situation, and if the medium between target and transmitter is reciprocal and the Sinclair matrix $[S(AB)]$ is symmetric, (i.e. $S_{AB} = S_{BA}$). The Jones matrix is used for the forward transmission case. If the medium between target and transmitter is without Faraday rotation, the Jones matrix is usually normal. However, it should be noted that the Jones matrix is not in general normal. That is, in general the Jones matrix does not have orthogonal eigenvectors. Even the case of only one eigenvector (and a generalized eigenvector) has been considered in optics (homogeneous and inhomogeneous Jones matrices). If the coordinate systems being used are kept in mind, the numerical subscripts can be dropped.

It is clear that in the bistatic case, the matrix elements for a target depend on the orientation of the target with respect to the line of sight from transmitter to target and on its orientation with respect to the target-receiver line of sight. In the forms (E 3.4) and (E 3.5) the matrices are **absolute matrices**, and with their use the phase of the scattered wave can be related to the phase of the transmitted wave, which is strictly required in the case of polarimetric interferometry. If this phase relationship is of no interest, as in the case of mono-static polarimetry, the distinct phase term can be neglected, and one of the matrix elements can be taken as real. The resulting form of the Sinclair matrix is called the **relative scattering matrix**. In general the elements of the scattering matrix are dependent on the frequency of the illuminating wave [E19, E14, E15].

Another target matrix parameter that should be familiar to all who are interested in microwave remote sensing is the **radar cross section (RCS)**. RCS is proportional to the power received by a radar and is the area of an equivalent target that intercepts a power equal to its area multiplied by the power density of an incident wave, and re-radiates it equally in all directions to yield a receiver power equal to that produced by the real target. The radar cross section depends on the polarization of both transmitting and receiving antennas. Thus the radar cross section may be specified as HH (horizontal receiving and transmitting antennas), HV (horizontal receiving and vertical transmitting antennas), etc. When considering ground reflections, the cross section is normalized by the size of the ground patch illuminated by the wave from the radar. The cross section is not sufficient to describe the polarimetric behavior of a target. In terms of the Sinclair matrix $[S]$, and the normalized effective lengths of transmitting and receiving antennas, $\hat{\mathbf{h}}_t$ and $\hat{\mathbf{h}}_r$, respectively, the radar cross section is

$$\sigma_{rr} = \left| \hat{\mathrm{h}}_r^{\mathrm{T}} [S] \hat{\mathrm{h}}_t \right|^2 . \qquad \text{(E 3.6)}$$

A polarimetrically correct form of the **radar equation** that specifies received power in terms of antenna and target parameters is

$$W_{rr} = \frac{W_t G_t(\theta,\phi) A_{er}(\theta,\phi)}{(4\pi r_1 r_2)^2} \left| \hat{\mathrm{h}}_r^{\mathrm{T}} [\mathrm{S}] \hat{\mathrm{h}}_t \right|^2 . \qquad \text{(E 3.7)}$$

W_t is the transmitter power and subscripts t and r identify transmitter and receiver, and its properties are defined in more detail in Mott [E76] and in [E19]. The effective antenna height $\hat{\mathbf{h}}(\theta,\phi)$, is defined via the electric field $\mathbf{E}^t(r,\theta,\phi)$ radiated by an antenna in its far field, as

$$\mathbf{E}^{t}(r,\theta,\phi)=\frac{jZ_0 I}{2\lambda r}\exp(-jkr)\hat{\mathbf{h}}(\theta,\phi), \qquad \text{(E 3.8)}$$

with Z_0 the characteristic impedance, λ the wavelength, and I the antenna current.

E 3.3 Basis Transformations of the 2x2 Sinclair Scattering Matrix [S]

Redefining the incident and scattering cases in terms of the standard {H V} notation with $H = x$, $V = y$ and with proper re-normalization, we redefine (E 3.1) as

$$\mathbf{E}^{s}_{HV}=[S]_{HV}\mathbf{E}^{*}_{HV} \quad \text{or} \quad \mathbf{E}^{s}(HV)=[S(HV)]\mathbf{E}^{*}(HV)\,. \qquad \text{(E 3.9)}$$

The complex conjugation results from inversion of the coordinate system in the BSA arrangement which invites a more rigorous formulation in terms of directional Sinclair vectors including the concepts of time reversal as treated by Lüneburg [E52]. Using these Sinclair vector definitions one can show that the transformation from one orthogonal polarisation basis {H V} into another {i j} or {A B} is a unitary congruence (unitary consimilarity) transformation of the original Sinclair scattering matrix $[S]_{HV}$ into $[S]_{ij}$, where

$$[S]_{ij}=[U_2][S]_{HV}[U_2]^{T} \text{ or } [S(ij)]=[U_2]\,[S(HV)]=[U_2]^{T}\,. \qquad \text{(E 3.10)}$$

$[U_2]$ is given by (E 2.23), so that the components of the general non-symmetric scattering matrix for the bistatic case in the new polarization basis, characterized by a complex polarization ratio ρ, can be written as [E81, E25]:

$$S_{ii}=\frac{1}{1+\rho\rho^{*}}\left[S_{HH}-\rho^{*}S_{HV}-\rho^{*}S_{VH}+\rho^{*2}S_{VV}\right] \qquad \text{(E 3.11)}$$

$$S_{ij}=\frac{1}{1+\rho\rho^{*}}\left[\rho S_{HH}+S_{HV}-\rho\rho^{*}S_{VH}-\rho^{*}S_{VV}\right]$$

$$S_{ji}=\frac{1}{1+\rho\rho^{*}}\left[\rho S_{HH}-\rho\rho^{*}S_{HV}+S_{VH}-\rho^{*}S_{VV}\right]$$

$$S_{jj}=\frac{1}{1+\rho\rho^{*}}\left[\rho^{2}S_{HH}+\rho S_{HV}-\rho S_{VH}+S_{VV}\right].$$

There exist three invariants for the general bistatic case (BSA) under the change-of-basis transformation as given by (E 3.5):

$$\text{(i)}\ \kappa_4 = Span[S]=\left\{|S_{HH}|^2+|S_{HV}|^2+|S_{VH}|^2+|S_{VV}|^2\right\}=\left\{|S_{ii}|^2+|S_{ij}|^2+|S_{ji}|^2+|S_{jj}|^2\right\} \qquad \text{(E 3.12)}$$

confirms that the total power is conserved, and it is known as Kennaugh's span-invariant κ_4;

$$\text{(ii)}\ S_{HV}-S_{VH}=S_{ij}-S_{ji}\,, \text{ for monostatic case,} \qquad \text{(E 3.13)}$$

warranting symmetry of the scattering matrix in any polarization basis as long as the BSA for the strictly monostatic but not general bistatic case is implied;

$$\text{(iii)}\ Det\{[S]_{HV}\}=Det\{[S]_{ij}\} \quad \text{or} \quad Det\{[S(HV)]\}=Det\{[S(ij)]\} \qquad \text{(E 3.14)}$$

due to the fact that $Det\{[U_2]\}=1$ implies determinantal invariance.

In addition, diagonalization of the scattering matrix, also for the general bistatic case, can always be obtained but requires mixed basis representations by using the Singular Value Decomposition Theorem (SVD) [E52, E53] so that the diagonalized scattering matrix $[S_D]$ can be obtained by the left and right singular vectors, where

$$[S_D]=[Q_L][S][Q_R] \text{ with } [S_D]=\begin{bmatrix} S_{\lambda_1} & 0 \\ 0 & S_{\lambda_2} \end{bmatrix} \qquad \text{(E 3.15)}$$

and $\left|Det\{[Q_L]\}\right|=\left|Det\{[Q_R]\}\right|=1$

S_{λ_1} and S_{λ_2} denote the diagonal eigenvalues of $[S]$, and the diagonal elements S_{λ_1} and S_{λ_2} can be taken as real nonnegative and are known as the singular values of the matrix $[S]$. For the symmetric scattering matrices in the mono-static case (MSA), diagonalization is achieved according to the unitary consimilarity transform for which

$$[Q_R]=[Q_L]^T \quad , \qquad \text{(E 3.16)}$$

and above equations will simplify due to the restriction of symmetry $S_{ij}=S_{ji}$.

E 3.4 The 4x4 Mueller (Forward Scattering) [*M*] and the 4x4 Kennaugh (Back-Scattering) [*K*] Power Density Matrices

For the partially polarized cases, there exists an alternate formulation of expressing the scattered wave in terms of the incident wave via the 4x4 Mueller $[M]$ and Kennaugh $[K]$ matrices for the FSA and BSA coordinate formulations, respectively, where

$$[q^s]=[M][q^i] \; . \qquad \text{(E 3.17)}$$

For the purely coherent case, $[M]$ can formally be related to the coherent Jones Scattering Matrix $[T]$ as

$$[M]=\begin{bmatrix}1 & 1 & 1 & -1\end{bmatrix}[A]^{T-1}([T]\otimes[T]^*)[A]^{-1}=[A]([T]\otimes[T]^*)[A]^{-1} \; . \qquad \text{(E 3.18)}$$

The symbol $\otimes$ signifies the standard Kronecker tensorial matrix product relations [E112] provided in (E 6.1) and the 4x4 expansion matrix $[A]$ is given by [E76] as:

$$[A]=\begin{bmatrix} 1 & 0 & 0 & 1 \\ 1 & 0 & 0 & -1 \\ 0 & 1 & 1 & 0 \\ 0 & j & -j & 0 \end{bmatrix} \quad , \qquad \text{(E 3.19)}$$

with the elements M_{ij} of $[M]$, given in (E 6.2).

Specifically we find that if $[T]$ is normal, i.e. $[T][T]^{T^*}=[T]^{T^*}[T]$, then $[M]$ is also normal, i.e. $[M][M]^T=[M]^T[M]$.

Similarly, for the purely coherent case [E76], $[K]$ can formally be related to the coherent Sinclair matrix $[S]$ as

$$[K]=2[A]^{T-1}([S]\otimes[S]^*)[A]^{-1} \quad , \qquad \text{(E 3.20)}$$

where

$$[A]^{T-1} = \frac{1}{2}[A]^* \quad . \tag{E 3.21}$$

For a symmetric Sinclair matrix $[S]$, $[K]$ is symmetric, keeping in mind the mathematical formalism $[M] = diag[1 \quad 1 \quad 1 \quad -1][K]$ But great care must be taken in strictly distinguishing the physical meaning of $[K]$ versus $[M]$ in terms of $[S]$ versus $[T]$ respectively. Thus, if $[S]$ is symmetric, $S_{HV} = S_{VH}$, then $[K]$ is symmetric, $K_{ij} = K_{ji}$, and the correct elements for $[M]$, $[K]$ and the symmetric cases are presented in (E 6.2-E 6.6).

E 3.5 The 2x2 Graves Polarization Power Scattering Matrix [G]

Next to the Kennaugh matrix $[K]$, Kennaugh introduces another formulation for expressing the power in the scattered wave $\mathbf{E}^S$ to the incident wave $\mathbf{E}^i$ for the coherent case. This formulation is the so-called Graves polarization coherent power scattering matrix $[G]$, where

$$P^S = \frac{1}{8\pi \, Z_0 r_2^2} \mathrm{E}^{iT^*}[G]\mathrm{E}^i \quad . \tag{E 3.22}$$

In terms of the Kennaugh elements K_{ij}, defined in E 6.3, for the mono-static case

$$[G] = \langle [S]^{T^*}[S] \rangle = \begin{bmatrix} K_{11} + K_{12} & K_{13} - jK_{14} \\ K_{13} + jK_{14} & K_{11} - K_{12} \end{bmatrix} . \tag{E 3.23}$$

By using a single coordinate system for (x_1, y_1, z_1) and (x_3, y_3, z_3) for the monostatic case, as in Fig. E 3.1, and also described in detail in [E19], it can be shown that for a scatterer ensemble (e.g. precipitation) for which individual scatterers move slowly compared to a period of the illuminating wave, and quickly compared to the time-averaging of the receiver, time-averaging can be adjusted to find the decomposed power scattering matrix $\langle [G] \rangle$, as

$$\langle [G] \rangle = \langle [S(t)]^{T^*}[S(t)] \rangle = [G_H] + [G_V] = \left\{ \left\langle \begin{bmatrix} |S_{HH}|^2 & S_{HH}^* S_{HV} \\ S_{HH} S_{HV}^* & |S_{HV}|^2 \end{bmatrix} \right\rangle + \left\langle \begin{bmatrix} |S_{VH}|^2 & S_{VH}^* S_{VV} \\ S_{VH} S_{VV}^* & |S_{VV}|^2 \end{bmatrix} \right\rangle \right\} . \tag{E 3.24}$$

This shows that the time averaged Graves Power Scattering Matrix $\langle [G] \rangle$, first introduced by Kennaugh [E4, E5], can be used to divide the powers that are received by linear horizontally and vertically by polarized antennas, as discussed in more detail in [E19] and in [E113]. It should be noted that a similar decomposition also exists for the Muller/Jones matrices, commonly denoted as FSA power scattering matrix:

$$\langle [F] \rangle = \langle [T(t)]^+ [T(t)] \rangle = [F_H] + [F_V] = \left\{ \left\langle \begin{bmatrix} |T_{HH}|^2 & T_{HH}^* T_{HV} \\ T_{HH} T_{HV}^* & |T_{HV}|^2 \end{bmatrix} \right\rangle + \left\langle \begin{bmatrix} |T_{VH}|^2 & T_{VH}^* T_{VV} \\ T_{VH} T_{VV}^* & |T_{VV}|^2 \end{bmatrix} \right\rangle \right\} , \tag{E 3.25}$$

which is not further analyzed here [E113].

E 3.6 Co/Cross-Polar Backscattering Power Decomposition for the One-Antenna (Transceiver) and the Matched Two-Antenna (Quasi-Monostatic) Cases

Assuming that the scatterer is placed in free unbounded space and that no polarization state transformation occurs along the propagation path from the transmitter (T) to the scatterer incidence (S), and along that from the scatterer(s) to the receiver (R), then the value of the terminal voltage of the receiver, V_R, induced by an arbitrarily scattered wave $\mathbf{E}_R$ at the receiver, is defined by the radar brightness function V_R, and the corresponding received power P_R expression

$$V_R = \hat{\mathbf{h}}_{\mathbf{R}}^T \mathbf{E}_{\mathbf{R}} \qquad P_R = \frac{1}{2} V_R^* V_R \ . \tag{E 3.26}$$

With the definition of the Kennaugh matrix $[K]$ in terms of the Sinclair matrix $[S]$, the received power or radar brightness function may be re-expressed

$$P_{RT} = \frac{1}{2} \left| \hat{\mathbf{h}}_R \, [\mathrm{S}] \, \mathbf{E}_T \right|^2 = \frac{1}{2} \mathbf{q}_R^T \, [K] \, \mathbf{q}_T \ , \tag{E 3.27}$$

where $\mathbf{q}_R$ and $\mathbf{q}_T$ are the corresponding normalized Stokes' vectors.
For the one-antenna (transceiver) case the co-polar channel (c) and the cross-polar channel (x) powers become:

$$P_c = \frac{1}{2} \left| \hat{\mathbf{h}}_T^T \, [\mathbf{S}] \, \mathbf{E}_T \right|^2 = \frac{1}{2} \mathbf{q}_T^T \, [K_c] \, \mathbf{q}_T \tag{E 3.28}$$

$$P_x = \frac{1}{2} \left| \hat{\mathbf{h}}_{T_\perp}^T \, [\mathrm{S}] \, \mathbf{E}_T \right|^2 = \frac{1}{2} \mathbf{q}_T^T \, [K_x] \, \mathbf{q}_T \ , \tag{E 3.29}$$

with

$$[K_c] = \left([A]^{-1} \right)^T ([T] \otimes [T]^*) [A]^{-1} = [C][K] \tag{E 3.30}$$

$$[K_x] = \left([A]^{-1} \right)^T ([Y][T] \otimes [T]^*) [A]^{-1} = [C_x][K] \tag{E 3.31}$$

and

$$[C] = \begin{bmatrix} 1 & 0 & 0 & 0 \\ 0 & 1 & 0 & 0 \\ 0 & 0 & 1 & 0 \\ 0 & 0 & 0 & -1 \end{bmatrix} \quad [Y] = \begin{bmatrix} 0 & 0 & 0 & 1 \\ 0 & -1 & 0 & 0 \\ 0 & 0 & -1 & 0 \\ 1 & 0 & 0 & 0 \end{bmatrix} \quad [X] = \begin{bmatrix} 1 & 0 & 0 & 0 \\ 0 & -1 & 0 & 0 \\ 0 & 0 & -1 & 0 \\ 0 & 0 & 0 & 1 \end{bmatrix} . \tag{E 3.32}$$

For the two-antenna dual polarization case, in which one antenna serves as a transmitter and the other as the receiver, the optimal received power P_m for the matched case becomes by using the matching condition

$$\hat{\mathbf{h}}_{\mathbf{R}_m} = \mathbf{E}_s^* / \left\| \mathbf{E}_s \right\| \ , \tag{E 3.33}$$

so that

$$P_m = \mathbf{q}_T^{\ T}\,[K_m]\,\mathbf{q}_T\,,\ \text{where}\ [K_m]=[K_c]+[K_x]=[K_{11}][K],\ \text{and}\ [K_{11}]=\begin{bmatrix}1&0&0&0\\0&0&0&0\\0&0&0&0\\0&0&0&0\end{bmatrix}. \qquad \text{(E 3.34)}$$

This represents an essential relationship for determining the optimal polarization states from the optimization of the Kennaugh matrix.

E 3.7 The Scattering Feature Vectors : The Lexicographic and the Pauli Feature Vectors

Up to now we have introduced three descriptions of the scattering processes in terms of the 2x2 Jones versus Sinclair, $[T]$ versus $[S]$, the 2x2 power scattering matrices, $[F]$ versus $[G]$, and the 4x4 power density Muller versus Kennaugh matrices, $[M]$ versus $[K]$. Alternatively, the polarimetric scattering problem can be addressed in terms of a vectorial feature descriptive formulation [E114] borrowed from vector signal estimation theory. This approach replaces the 2x2 scattering matrices $[T]$ versus $[S]$, the 2x2 power scattering matrices $[F]$ versus $[G]$, and the 4x4 Muller $[M]$ versus Kennaugh $[K]$ matrices by an equivalent four-dimensional complex scattering feature vector $\mathbf{f}_4$, formally defined for the general bi-static case as

$$[S]_{HV}=\begin{bmatrix}S_{HH}&S_{HV}\\S_{VH}&S_{VV}\end{bmatrix} \Rightarrow \mathbf{f}_4 = F\{[S]\}=\frac{1}{2}Trace\{[S]\,\psi\}=[f_0 \quad f_1 \quad f_2 \quad f_3]^T\,. \qquad \text{(E 3.35)}$$

$F\{[S]\}$ is the matrix vectorization operator, $Trace\{[S]\}$ is the sum of the diagonal elements of $[S]$, and ψ is a complete set of 2x2 complex basis matrices under a hermitian inner product. For the vectorization, any complete orthonormal basis set [E97] of four 2x2 matrices that leave the (Euclidean) norm of the scattering feature vector invariant can be used, and there are two such bases favored in the polarimetric radar literature. One is the lexicographic basis $[\Psi_L]$ and the other is the Pauli spin matrix set $[\Psi_P]$. We note here that the distinction between the lexicographic and Pauli-based feature vector representation is related to Principal and Independent Component Analysis (PCA/ICA) which is an interesting topic for future research.

The Lexicographic Feature vector $\mathbf{f}_{4L}$ is obtained from the simple lexicographic expansion of $[S]$ using $[\Psi_L]$, with

$$[\Psi_L]\equiv\left\{2\begin{bmatrix}1&0\\0&0\end{bmatrix}\ 2\begin{bmatrix}0&1\\0&0\end{bmatrix}\ 2\begin{bmatrix}0&0\\1&0\end{bmatrix}\ 2\begin{bmatrix}0&0\\0&1\end{bmatrix}\right\} \qquad \text{(E 3.36)}$$

so that the corresponding feature vector becomes

$$\mathbf{f}_{4L}=[S_{HH} \quad S_{HV} \quad S_{VH} \quad S_{VV}]^T\,. \qquad \text{(E 3.37)}$$

The Pauli feature vector $\mathbf{f}_{4P}$ is obtained from the renowned complex Pauli spin matrix basis set $[\Psi_P]$ which in a properly re-normalized presentation is here defined as

$$[\Psi_P]\equiv\left\{\sqrt{2}\begin{bmatrix}1&0\\0&1\end{bmatrix}\sqrt{2}\begin{bmatrix}1&0\\0&-1\end{bmatrix}\ \sqrt{2}\begin{bmatrix}0&1\\1&0\end{bmatrix}\ \sqrt{2}\begin{bmatrix}0&-j\\j&0\end{bmatrix}\right\}, \qquad \text{(E 3.38)}$$

resulting in the polarimetric correlation phase preserving Pauli feature vector:

$$\mathbf{f}_{4P} = [f_0 \quad f_1 \quad f_2 \quad f_3]_P^T = \frac{1}{\sqrt{2}}[S_{HH} + S_{VV} \quad S_{VV} - S_{HH} \quad S_{HV} + S_{VH} \quad j(S_{HV} - S_{VH})]^T \ . \qquad \text{(E 3.39)}$$

The corresponding scattering matrix $[S]_P$ is related to $\mathbf{f}_{4P} = [f_0 \quad f_1 \quad f_2 \quad f_3]_P^T$ by

$$[S]_P = \frac{1}{\sqrt{2}}\begin{bmatrix} f_0 - f_1 & f_2 - jf_3 \\ f_2 + jf_1 & f_0 + f_1 \end{bmatrix} = [S] \ . \qquad \text{(E 3.40)}$$

E 3.8 The Unitary Transformations of the Feature Vectors

The insertion of the factor 2 in (E 3.36) versus the factor $\sqrt{2}$ in (E 3.38) arises from the total power invariance. This keeps the norm independent from the choice of the basis matrices Ψ, so that

$$\|\mathbf{f}_4\| = \mathbf{f}_4^\dagger \cdot \mathbf{f}_4 = \frac{1}{2}\text{Span}\{[S]\} = \frac{1}{2}Trace\{[S][S]^\dagger\} = \frac{1}{2}\left(|S_{HH}|^2 + |S_{HV}|^2 + |S_{VH}|^2 + |S_{VV}|^2\right) = \kappa_4 \ . \qquad \text{(E 3.41)}$$

This constraint forces the transformation from the lexicographic to the Pauli-based feature vector [E52, E53, E114], or to any other desirable one, to be unitary, where with

$$\mathbf{f}_{4P} = [D_4]\mathbf{f}_{4L} \qquad \text{and reversely} \qquad \mathbf{f}_{4L} = [D_4]^{-1}\mathbf{f}_{4P} \qquad \text{(E 3.42)}$$

we find

$$[D_4] = \frac{1}{\sqrt{2}}\begin{bmatrix} 1 & 0 & 0 & 1 \\ 1 & 0 & 0 & -1 \\ 0 & 1 & 1 & 0 \\ 0 & j & -j & 0 \end{bmatrix} \quad [D_4]^{-1} = [D_4]^\dagger = \frac{1}{\sqrt{2}}\begin{bmatrix} 1 & 1 & 0 & 0 \\ 0 & 0 & 1 & -j \\ 0 & 0 & 1 & j \\ 1 & -1 & 0 & 0 \end{bmatrix} \ . \qquad \text{(E 3.43)}$$

Furthermore, these special unitary matrices relating the feature vectors control the more general cases of transformations related to the change of polarization basis. By employing the Kronecker direct tensorial product of matrices, symbolized by $\otimes$, we obtain, the transformation for the scattering vector from the linear $\{\hat{\mathbf{u}}_H, \hat{\mathbf{u}}_V\}$ to any other elliptical polarization basis $\{\hat{\mathbf{u}}_A, \hat{\mathbf{u}}_B\}$, characterized by the complex polarization ratio by

$$\mathbf{f}_{4L}(AB) = [U_{4L}]\mathbf{f}_{4L}(HV) \quad \text{and} \quad \mathbf{f}_{4P}(AB) = [U_{4P}]\mathbf{f}_{4P}(HV) \ . \qquad \text{(E 3.44)}$$

$[U_{4L}]$ is the transformation matrix for the conventional feature vector $\mathbf{f}_{4L}$.

Here we note that in order to obtain the expression $[U_{4L}] = [U_2] \otimes [U_2]^T$, the unitary congruence (unitary consimilarity) transformation for the Sinclair scattering matrix in the reciprocal case was used. This implies however that we must distinguish between forward scattering and backscattering (and so also bistatic scattering), where for the reciprocal backscatter case the 3-dimensional target feature vectors ought to be used. These features lead to interesting questions which need more in depth analyses for which the ubiquity of the Time Reversal operation shows up again.

$$[U_{4L}] = [U_2] \otimes [U_2]^T = \frac{1}{1+\rho\rho^*} \begin{bmatrix} 1 & -\rho^* & -\rho^* & \rho^{*2} \\ \rho & 1 & -\rho\rho^* & -\rho^* \\ \rho & -\rho\rho^* & 1 & -\rho^* \\ \rho^2 & \rho & \rho & 1 \end{bmatrix} , \qquad \text{(E 3.45)}$$

and $[U_{4P}]$ is the homologous transformation matrix for the Pauli-based feature vector $\mathbf{f}_{4P}$:

$$[U_{4P}] = [D_4][U_{4L}][D_4]^\dagger \qquad \text{(E 3.46)}$$

$[U_{4L}]$ and $[U_{4P}]$ are special 4x4 unitary matrices for which with $[I_4]$ denoting the 4x4 identity matrix:

$$[U_4][U_4] = [I_4] \quad \text{and} \quad Det\{[U_4]\} = 1 \ . \qquad \text{(E 3.47)}$$

Kennaugh matrices and covariance matrices are based on completely different concepts (notwithstanding their formal relationships) and must be clearly separated which is another topic for future research.

The main advantage of using the scattering feature vector, $\mathbf{f}_{4L}$ or $\mathbf{f}_{4P}$, instead of the Sinclair scattering matrix $[S]$ and the Kennaugh matrix $[K]$, is that it enables the introduction of the covariance matrix decomposition for partial scatterers of a dynamic scattering environment. However, there does not exist a physical but only a strict mathematical relationship between the two alternate concepts for treating the partially coherent case, which is established and needs always to be kept in focus [E114]. It should be noted that besides the covariance matrices the so-called (normalized) correlation matrices are often used advantageously, especially when the eigenvalues of a covariance matrix have large variations.

E 3.9 The Polarimetric Covariance Matrix

In most radar applications, the scatterers are situated in a dynamically changing environment and are subject to spatial (different view angles as in SAR) and temporal variations (different hydro-meteoric states in RAD-MET), if when illuminated by monochromatic waves cause the back-scattered wave to be partially polarized with incoherent scattering contributions so that $\langle [S] \rangle = \langle [S(\mathbf{r},t)] \rangle$. Such scatterers, analogous to the partially polarized waves are called partial scatterers [E78, E90]. Whereas the Stokes vector, the wave coherency matrix, and the Kennaugh/Mueller matrix representations provide a first approach of dealing with partial scattering descriptions, the unitary matrix derived from the scattering feature $\mathbf{f}_4$ vector provides another approach borrowed from decision and estimation signal theory [E115] which are currently introduced in Polarimetric SAR and Polarimetric-Interferometric SAR analyses, and these need to be introduced here. However, even if the environment is dynamically changing one has to make assumption concerning stationarity (at least over timescales of interest), homogeneity and ergodicity. This can be analyzed more precisely by introducing the concept of space and time varying stochastic processes.

The 4x4 lexicographic polarimetric covariance matrix $[C_{4L}]$ and the Pauli-based covariance matrix $[C_{4P}]$ are defined using the outer product $\otimes$ of the feature vector with its conjugate transpose as:

$$[C_{4L}] = \langle \mathbf{f}_{4L} \cdot \mathbf{f}_{4L}^\dagger \rangle \quad \text{and} \quad [C_{4P}] = \langle \mathbf{f}_{4P} \cdot \mathbf{f}_{4P}^\dagger \rangle \ , \qquad \text{(E 3.48)}$$

where $\langle ... \rangle$ indicates temporal or spatial ensemble averaging, assuming homogeneity of the random medium. The lexicographic covariance matrix $[C_4]$ contains complete information in amplitude and phase variance and correlation for all complex elements of $[S]$ with

$$[C_{4L}] = \langle \mathbf{f}_{4L} \cdot \mathbf{f}_{4L}^{\dagger} \rangle = \begin{bmatrix} \langle |S_{HH}|^2 \rangle & \langle S_{HH} S_{HV}^* \rangle & \langle S_{HH} S_{VH}^* \rangle & \langle S_{HH} S_{VV}^* \rangle \\ \langle S_{HV} S_{HH}^* \rangle & \langle |S_{HV}|^2 \rangle & \langle S_{HV} S_{VH}^* \rangle & \langle S_{HV} S_{VV}^* \rangle \\ \langle S_{VH} S_{HH}^* \rangle & \langle S_{VH} S_{HV}^* \rangle & \langle |S_{VH}|^2 \rangle & \langle S_{VH} S_{VV}^* \rangle \\ \langle S_{VV} S_{HH}^* \rangle & \langle S_{VV} S_{HV}^* \rangle & \langle S_{VV} S_{VH}^* \rangle & \langle |S_{VV}|^2 \rangle \end{bmatrix} \qquad \text{(E 3.49)}$$

and

$$[C_{4P}] = \langle \mathbf{f}_{4P} \cdot \mathbf{f}_{4P}^{\dagger} \rangle = \langle [D_4] \mathbf{f}_{4L} \cdot \mathbf{f}_{4L}^{\dagger} [D_4]^{\dagger} \rangle = [D_4] \langle \mathbf{f}_{4L} \cdot \mathbf{f}_{4L}^{\dagger} \rangle [D_4]^{\dagger} = [D_4][C_{4L}][D_4]^{\dagger} \ . \qquad \text{(E 3.50)}$$

Both the Lexicographic Covariance $[C_{4L}]$ and the Pauli-based covariance $[C_{4P}]]$ matrices are hermitian positive semi-definite, which implies that these possess real non-negative eigenvalues and orthogonal eigenvectors. Incidentally, those can be mathematically related directly to the Kennaugh matrix $[K]$, which is not shown here. However, there does not exist a physical relationship between the two presentations which must always be kept in focus.

The transition of the covariance matrix from the particular linear polarization reference basis {H V} into another elliptical basis {A B}, using the change-of-basis transformations defined in (E 3.41 – E 3.45), where

$$[C_{4L}(AB)] = \langle \mathbf{f}_{4L}(AB) \cdot \mathbf{f}_{4L}^{\dagger}(AB) \rangle = [U_4] \langle \mathbf{f}_{4L}(HV) \cdot \mathbf{f}_{4L}^{\dagger}(HV) \rangle [U_4]^{\dagger} = [D_4][C_{4L}(HV)][D_4]^{\dagger} \qquad \text{(E 3.51)}$$

and

$$[C_{4P}(AB)] = \langle \mathbf{f}_{4P}(AB) \cdot \mathbf{f}_{4P}^{\dagger}(AB) \rangle = [U_4] \langle \mathbf{f}_{4P}(HV) \cdot \mathbf{f}_{4P}^{\dagger}(HV) \rangle [U_4]^{\dagger} = [D_4][C_{4P}(HV)][D_4]^{\dagger} \ . \qquad \text{(E 3.52)}$$

The lexicographic and Pauli-based covariance matrices, $[C_{4L}]$ and $[C_{4P}]$, contain, in the most general case, as defined in (E 3.49) and (E 3.50), sixteen independent parameters, namely four real power densities and six complex phase correlation parameters.

E 3.10 The Monostatic Reciprocal Back-Scattering Cases

For a reciprocal target matrix, in the mono-static (backscattering) case, the reciprocity constrains the Jones matrix to be usually normal, and the Sinclair scattering matrix to be symmetrical, i.e. $S_{HV} = S_{VH}$, which further reduces the expressions of $[G]$ and $[K]$. Furthermore, the four-dimensional scattering feature vector $\mathbf{f}_4$ reduces to a three-dimensional scattering feature vector $\mathbf{f}_3$ such that following [E97]:

$$\mathbf{f}_{3L} = [Q] \ , \ \mathbf{f}_{4L} = \begin{bmatrix} S_{HH} & \sqrt{2} S_{HV} & S_{VV} \end{bmatrix}^T \ , \ S_{HV} = S_{VH} \ . \qquad \text{(E 3.53)}$$

$[I_3]$ is the unit 3x3 matrix. Keep in mind that the transformation between lexicographic and Pauli ordering is a direct transformation of the scattering matrix (and not only of the covariance matrices)

$$[Q] = \begin{bmatrix} 1 & 0 & 0 & 0 \\ 0 & \frac{1}{\sqrt{2}} & \frac{1}{\sqrt{2}} & 0 \\ 0 & 0 & 0 & 1 \end{bmatrix} \quad \text{and} \quad [Q][Q]^T = [I_3] \ , \qquad \text{(E 3.54)}$$

and the factor $\sqrt{2}$ needs to be retained in order to keep the vector norm consistent with the span invariance κ. Similarly, the reduced Pauli feature vector $\mathbf{f}_{3P}$ becomes

$$\mathbf{f}_{3P} = [Q] \ , \mathbf{f}_{4P} = \frac{1}{\sqrt{2}}[S_{HH} + S_{VV} \quad S_{HH} - S_{VV} \quad 2S_{HV}]^{T} \ , \ S_{HV} = S_{VH} \ . \tag{E 3.55}$$

The three-dimensional scattering feature vector from the lexicographic to the Pauli-based matrix basis, and vice versa, are related as

$$\mathbf{f}_{3P} = [D_3]\mathbf{f}_{3L} \quad \text{and} \quad \mathbf{f}_{3L} = [D_3]^{-1}\mathbf{f}_{3P} \ , \tag{E 3.56}$$

with $[D_3]$ defining a special 3x3 unitary matrix:

$$[D_3] = \frac{1}{\sqrt{2}}\begin{bmatrix} 1 & 0 & 1 \\ 1 & 0 & -1 \\ 0 & \sqrt{2} & 0 \end{bmatrix} \quad \text{and} \quad [D_3]^{-1} = [D_3]^{\dagger} = \frac{1}{2}\begin{bmatrix} 1 & 1 & 0 \\ 0 & 0 & \sqrt{2} \\ 1 & -1 & 0 \end{bmatrix} \ . \tag{E 3.57}$$

The change-of-basis transformation for the reduced scattering vectors in terms of the complex polarization ratio ρ of the new basis is given by

$$\mathbf{f}_{3L}(AB) = [U_{3L}(\rho)]\mathbf{f}_{3L}(HV) \quad \text{and} \quad \mathbf{f}_{3P}(AB) = [U_{3P}(\rho)]\mathbf{f}_{3P}(HV) \ , \tag{E 3.58}$$

where

$$[U_{3L}] = \frac{1}{1+\rho\rho^{*}}\begin{bmatrix} 1 & \sqrt{2}\rho & \rho^{2} \\ -\sqrt{2}\rho^{*} & 1-\rho\rho^{*} & \sqrt{2}\rho \\ \rho^{*^2} & -\sqrt{2}\rho^{*} & 1 \end{bmatrix} \tag{E 3.59}$$

and

$$[U_{3P}] = [D_3][U_{3L}][D_3]^{\dagger} = \frac{1}{2(1+\rho\rho^{*})}\begin{bmatrix} 2+\rho^{2}+\rho^{*^2} & \rho^{*^2}-\rho^{2} & 2(\rho-\rho^{*}) \\ \rho^{2}-\rho^{*^2} & 2-(\rho^{2}+\rho^{*^2}) & 2(\rho+\rho^{*}) \\ 2(\rho-\rho^{*}) & -2(\rho+\rho^{*}) & 2(1-\rho\rho^{*}) \end{bmatrix} , \tag{E 3.60}$$

which are 3x3 special unitary matrices.

Thus, a reciprocal scatterer is completely described either by the 3x3 Polarimetric Covariance Matrix $[C_{3L}]$:

$$[C_{3L}] = \langle \mathbf{f}_{3L} \cdot \mathbf{f}_{3L}^{\dagger} \rangle = \begin{bmatrix} \langle |S_{HH}|^2 \rangle & \sqrt{2}\langle S_{HH}S_{HV}^{*} \rangle & \langle S_{HH}S_{VV}^{*} \rangle \\ \sqrt{2}\langle S_{HV}S_{HH}^{*} \rangle & 2\langle |S_{HV}|^2 \rangle & \sqrt{2}\langle S_{HV}S_{VV}^{*} \rangle \\ \langle S_{VV}S_{HH}^{*} \rangle & \sqrt{2}\langle S_{VV}S_{HV}^{*} \rangle & \langle |S_{VV}|^2 \rangle \end{bmatrix} \tag{E 3.61}$$

or by the 3x3 Polarimetric Pauli Coherency Matrix $[C_{3P}]$:

$$[C_{3P}] = \langle \mathbf{f}_{3P} \cdot \mathbf{f}_{3P}^{\dagger} \rangle = \frac{1}{2} \begin{bmatrix} \langle | S_{HH} + S_{VV} |^2 \rangle & \langle (S_{HH} + S_{VV})(S_{HH} - S_{VV})^* \rangle & 2\langle (S_{HH} + S_{VV}) S_{HV}^* \rangle \\ \langle (S_{HH} - S_{VV})(S_{HH} + S_{VV})^* \rangle & \langle | S_{HH} - S_{VV} |^2 \rangle & 2\langle (S_{HH} - S_{VV}) S_{HV}^* \rangle \\ 2\langle S_{HV} (S_{HH} + S_{VV})^* \rangle & 2\langle S_{HV} (S_{HH} - S_{VV})^* \rangle & 4\langle | S_{HV} |^2 \rangle \end{bmatrix}$$

(E 3.62)

The relation between the 3x3 Pauli coherency matrix $[C_{3P}]$ and the 3x3 covariance matrix $[C_{3L}]$ is given by

$$[C_{3L}] = \langle \mathbf{f}_{3L} \cdot \mathbf{f}_{3L}^{\dagger} \rangle = \langle [D_3] \mathbf{f}_{3P} \cdot \mathbf{f}_{3P}^{\dagger} [D_3]^{\dagger} \rangle = [D_3] \langle \mathbf{f}_{3P} \cdot \mathbf{f}_{3P}^{\dagger} \rangle [D_3]^{\dagger} = [D_3][C_{3P}][D_3]^{\dagger} \,, \qquad \text{(E 3.63)}$$

and

$$[C_{3L}(AB)] = \langle \mathbf{f}_{3L}(AB) \cdot \mathbf{f}_{3L}^{\dagger}(AB) \rangle = [U_{3L}] \langle \mathbf{f}_{3L}(HV) \cdot \mathbf{f}_{3L}^{\dagger}(HV) \rangle [U_{3L}]^{\dagger} = [U_{3L}][C_{3L}(HV)][U_{3L}]^{\dagger} \quad \text{(E 3.64)}$$

$$[C_{3P}(AB)] = \langle \mathbf{f}_{3P}(AB) \cdot \mathbf{f}_{3P}^{\dagger}(AB) \rangle = [U_{3P}] \langle \mathbf{f}_{3P}(HV) \cdot \mathbf{f}_{3P}^{\dagger}(HV) \rangle [U_{3P}]^{\dagger} = [U_{3P}][C_{3P}(HV)][U_{3P}]^{\dagger} \quad \text{(E 3.65)}$$

$$[U_{3L}(\rho)][U_{3L}(\rho)]^{+} = [I_3] \quad \text{and} \quad Det\{[U_{3L}(\rho)]\} = 1 \,, \qquad \text{(E 3.66)}$$

and

$$\| \mathbf{f}_{3L} \|^2 = \| \mathbf{f}_{3P} \|^2 = \frac{1}{2} Span\{[S]\} = \frac{1}{2} Trace\{[S][S]^{\dagger}\} = \frac{1}{2} \left\{ |S_{HH}|^2 + 2|S_{HV}|^2 + |S_{VV}|^2 \right\} = \kappa_3 \quad . \text{(E 3.67)}$$

E 3.11 Co/Cross-polar Power Density and Phase Correlation Representations

The Covariance matrix elements are directly related to polarimetric radar measurables, comprised of the co/cross-polar power densities $P_c(\rho)$, $P_x(\rho)$, $P_c^{\perp}(\rho)$, and the co/cross-polar phase correlations $R_c(\rho)$, $R_x(\rho)$, $R_x^{\perp}(\rho)$, [81], where

$$[C_{3L}(\rho)] = \begin{bmatrix} P_c(\rho) & \sqrt{2}\, R_x(\rho) & R_c(\rho) \\ \sqrt{2}\, R_x(\rho)^* & 2P_x(\rho) & \sqrt{2}\, R_x^{\perp}(\rho)^* \\ R_c(\rho)^* & \sqrt{2}\, R_x^{\perp}(\rho) & P_c^{\perp}(\rho) \end{bmatrix} . \qquad \text{(E 3.68)}$$

Once the covariance matrix has been measured in one basis, e.g., $[C_{3L}(H,V)]$ in {H V} basis, it can easily be determined analytically for any other basis by definition of (E 3.60). Plotting the mean power returns and phase correlations as function of the complex polarization ratio ρ or the geometrical polarization ellipse parameters ψ, χ, of (E 2.6 – E 2.12) yields the familiar polarimetric signature plots. In addition, the expressions for the degree of coherence $\mu(\rho)$ and polarization $D_p(\rho)$ defined in (E 2.30) and (E 2.31), respectively are given according to [E34] by

$$\mu(\rho) = \frac{|R_x(\rho)|}{\sqrt{P_c(\rho) P_x(\rho)}}, \quad D_p(\rho) = \frac{\left\{ [P_c(\rho) - P_x(\rho)]^2 + 4|R_x(\rho)|^2 \right\}^{1/2}}{(P_c(\rho) + P_x(\rho))}, \quad where \;\; 0 \le \mu(\rho) \le D_p(\rho) \le 1$$

(E 3.69)

For coherent (deterministic) scatterers $\mu = D_p = 1$, whereas for completely depolarized scatterers $\mu = D_p = 0$.

The covariance matrix possesses additional valuable properties for the reciprocal back-scattering case which can be demonstrated by transforming $[C_{3L}(H,V)]$ into its orthogonal representation for $\rho_\perp = \left(-1/\rho^*\right)$ so that

$$\left[C_{3L}\left(\rho_\perp = -1/\rho^*\right)\right] = \begin{bmatrix} P_c^\perp(\rho) & \frac{-\rho}{\rho^*}\sqrt{2}\,R_x^\perp(\rho) & \frac{\rho^2}{\rho^{*2}}R_c(\rho) \\ \frac{-\rho^*}{\rho}\sqrt{2}\,R_x^\perp(\rho)^* & 2P_x(\rho) & \frac{-\rho}{\rho^*}\sqrt{2}\,R_x(\rho)^* \\ \frac{\rho^{*2}}{\rho^2}R_c(\rho)^* & \frac{-\rho^*}{\rho}\sqrt{2}\,R_x(\rho) & P_c(\rho) \end{bmatrix} . \qquad \text{(E 3.70)}$$

This leads to the following inter-channel relations

$$P_c\left(\rho_\perp = -1/\rho^*\right) = P_c^\perp(\rho) \quad , \quad \left|R_x\left(\rho_\perp = -1/\rho^*\right)\right| = \left|R_x^\perp(\rho)\right| \qquad \text{(E 3.71)}$$

and the symmetry relations

$$P_x\left(\rho_\perp = -1/\rho^*\right) = P_x(\rho) \quad , \quad \left|R_c\left(\rho_\perp = -1/\rho^*\right)\right| = \left|R_c(\rho)\right| . \qquad \text{(E 3.72)}$$

Similar but not identical relations could be established for the Pauli-Coherency Matrix $[C_{3P}(\rho)]$, which are not presented here. There exists another polarimetric covariance matrix representation in terms of the so-called polarimetric inter-correlation parameters σ_0, ρ, δ, β, γ, and ε, where according to [E19, Chapter 5]

$$[C_{3L}] = \begin{bmatrix} 1 & \beta\sqrt{\delta} & \rho\sqrt{\gamma} \\ \beta^*\sqrt{\delta} & \delta & \varepsilon\sqrt{\gamma\delta} \\ \rho^*\sqrt{\gamma} & \varepsilon^*\sqrt{\gamma\delta} & \gamma \end{bmatrix} . \qquad \text{(E 3.73)}$$

The polarimetric inter-correlation parameters σ_0, ρ, δ, β, γ, and ε are defined as:

$$\sigma_0 = \left\langle |S_{HH}|^2 \right\rangle \qquad \rho = \frac{\left\langle S_{HH}S_{VV}^* \right\rangle}{\sigma_0\sqrt{\gamma}} = \frac{\left\langle S_{HH}S_{VV}^* \right\rangle}{\sqrt{\left\langle |S_{HH}|^2 \right\rangle \left\langle |S_{VV}|^2 \right\rangle}}$$

$$\delta = 2\frac{\left\langle |S_{HV}|^2 \right\rangle}{\sigma_0} \qquad \beta = \frac{\sqrt{2}\left\langle S_{HH}S_{HV}^* \right\rangle}{\sigma_0\sqrt{\delta}} = \frac{\left\langle S_{HH}S_{HV}^* \right\rangle}{\sqrt{\left\langle |S_{HH}|^2 \right\rangle \left\langle |S_{HV}|^2 \right\rangle}} \qquad \text{(E 3.74)}$$

$$\gamma = 2\frac{\left\langle |S_{VV}|^2 \right\rangle}{\sigma_0} \qquad \varepsilon = \frac{\sqrt{2}\left\langle S_{HV}S_{VV}^* \right\rangle}{\sigma_0\sqrt{\delta\gamma}} = \frac{\left\langle S_{HV}S_{VV}^* \right\rangle}{\sqrt{\left\langle |S_{HV}|^2 \right\rangle \left\langle |S_{VV}|^2 \right\rangle}}$$

This completes the introduction of the pertinent polarimetric matrix presentations commonly used in radar polarimetry and in polarimetric SAR interferometry. In addition, the polarimetric interference matrices need to be introduced as shown in [E19], after introducing briefly basic concepts of radar interferometry in [E70].

E 3.12 Alternate Matrix Representations

In congruence with the alternate formulations of the of the polarization properties of electromagnetic waves, there also exist the associated alternate tensorial (matrix) formulations related to the four-vector Hamiltonian and spinorial representations as pursued by Zhivotovsky [E109], and more recently by Bebbington [E32]. These formulations representing most essential tools for dealing with the general bi-static (non-symmetric) scattering cases for both the coherent (3-D Poincaré and 3-D Polarization spheroid) and partially coherent (4-D Zhivotovsky sphere and spheroid) interactions, are not further pursued here; but these more generalized treatments of radar polarimetry deserve our fullest attention.

E 4.0 Polarimetric Radar Optimization for the Coherent Case

The optimization of the scattering matrices, derived for the mono-static case is separated into two distinct classes. The first one, dealing with the optimization of $[S]$, $[G]$, and $[K]$, for the coherent case results in the formulation of *'Kennaugh's target matrix characteristic operator and tensorial polarization fork'* and the associated renamed *'Huynen Polarization Fork'* concept plus the *'co/cross-polarization power density plots'* and the 'co/cross-polarization phase correlation plots', also known as the van Zyl [79, 71] and the Agrawal plots [78, 90], respectively, in the open literature. The second one, presented in Chapter 5, deals with the optimization for the partially polarized case in terms of the *'lexicographic and the Pauli-based covariance matrices,* $[C_L]$ *and* $[C_P]$, *respectively'*, as introduced in Sections 3.7 to 3.10, resulting in the *'Cloude target decomposition theorems'* and the Cloude-Pottier [E27, E57, E58] supervised and unsupervised *'Polarimetric Entropy* H, *Anisotropy* A, *and* $\overline{\alpha}$ *- Angle Descriptors'*. In addition, the *'polarimetric contrast optimization procedure'* dealing with the separation of the desired polarimetric radar target versus the undesired radar clutter returns of which the alternate lexicographic and Pauli-based covariance matrix optimization procedures deserve special attention next to the coherent $[S]$ and partially coherent $[K]$ matrix cases.

E 4.1 Formulation of the Mono-Static Radar Optimization Procedure according to Kennaugh for the Coherent Case

Kennaugh was the first to treat the mono-static polarimetric radar optimization procedure (see Fig. E 4.1) for optimizing (E 3.9) according to the BSA formulation

$$\mathbf{E}^s(\mathbf{r}) = [S]\,\mathbf{E}^{i*}(\mathbf{r}), \tag{E 4.1}$$

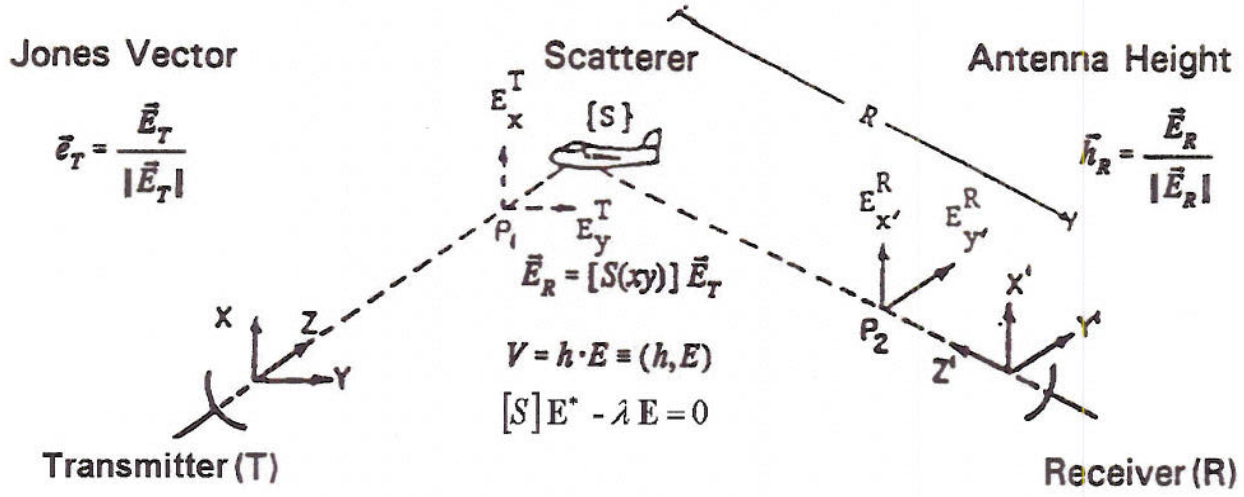

Fig. E 4.1 BSA Optimization According to Kennaugh

but with the received field $\mathbf{E}^r(\mathbf{r})$ being so aligned with the incident field $\mathbf{E}^i(\mathbf{r})$. The reversal of the scattered versus incident coordinates of the BSA system resulting in Kennaugh's psuedo-eigenvalue' [E4] problem of

Opt{[S]} such that $[S]\mathbf{E}^* - \lambda\mathbf{E} = 0$. (E 4.2)

The rigorous solution to this set of 'con-similarity eigenvalue' problems was unknown to the polarimetric radar community until the late 1980's, when Lüneburg [E54], rediscovering the mathematical tools [E116, E117], derived a rigorous but mathematically rather involved method of the associated con-similarity eigenvalue problem, not further discussed here. We refer to Lüneburg's complete treatment of the subject matter in [E52, E53]. Instead, here Chan's [E77] Three-Step Solution, as derived from Kennaugh's original work [E4], is adopted.

Three Step Procedure according to Chan [E77]

Define the polarimetric radar brightness (polarization efficiency, polarization match factor) formation according to (E 3.26) and (E 3.27) retain the factor $1/2$ (not contained in the 1983 IEEE Standard and in Mott's textbook) [E76, E102] :

$$P_R = |V_R|^2 = \frac{1}{2}\left|\mathbf{h}^{r^T}\,[\mathbf{S}]\,\mathbf{E}^i\right|^2 \quad . \tag{E 4.3}$$

In terms of the terminal voltage V_R being expressed in terms of the normalized transceiver antenna height $\mathbf{h}^r$ and the incident field $\mathbf{E}^i$, as defined in Mott [E76] and in [E19]:

$$V_R = \mathbf{h}^{r^T}\,\mathbf{E}^s = \mathbf{h}^{r^T}[S]\mathbf{E}^t \quad \textbf{with} \quad \mathbf{h}^r = \frac{\mathbf{E}^r}{\|\mathbf{E}^r\|} \, . \tag{E 4.4}$$

The total energy density of the scattered wave $\mathbf{E}^s$ may be defined by:

$$W = \mathbf{E}^{s^+}\mathbf{E}^s = \left([S]\mathbf{E}^t\right)^+\left([S]\mathbf{E}^t\right) = \mathbf{E}^{t^+}\left([S]^+[S]\right)\mathbf{E}^t = \mathbf{E}^{t^+}[G]\mathbf{E}^t \, , \tag{E 4.5}$$

where $[G] = [S]^\dagger[S]$ defines the Graves power density matrix [E7], first introduced by Kennaugh [E4, E5].

Step 1

Because the solution to the pseudo-eigenvalue problem of (E 4.2) was unknown at that time (1954 until 1984), and since $[S]$ in general could be non-symmetric and non-hermitian, Kennaugh embarked instead on determining the optimal polarization states from optimizing the power density matrix:

$$[G]\mathbf{E}^t_{\text{opt}} - \nu\,\mathbf{E}^t_{\text{opt}} = 0 \, . \tag{E 4.6}$$

Real positive eigenvalues $\nu_1 = |\lambda_1|^2$ and $\nu_2 = |\lambda_2|^2$ exist for all matrices $[S]$ since $[G]$ is Hermitian positive semidefinite. Then

$$\nu_{1,2} = \frac{1}{2}\left\{Trace\,[G] \pm \left[Trace^2\,[G] - 4Det[G]\right]^{\frac{1}{2}}\right\} \, , \tag{E 4.7}$$

where

$$\nu_1 + \nu_2 = \textbf{invariant} = Trace[G] = Span[S] = [S_{HH}]^2 + [S_{HV}]^2 + [S_{VH}]^2 + [S_{VV}]^2 = \kappa_4 \tag{E 4.8}$$

$$\nu_1 \cdot \nu_2 = \textbf{invariant} = Det[G] = (Det[S])(Det[S])^* = (S_{HH}S_{VV} - S_{HV}S_{VH})(S_{HH}S_{VV} - S_{HV}S_{VH})^* \, . \tag{E 4.9}$$

For the mono-static reciprocal symmetric $[S]$, the above equations reduce with $S_{HV} = S_{VH}$ to

$$\nu_1 + \nu_2 = \textbf{invariant} = Trace[G] = Span[S] = [S_{HH}]^2 + 2[S_{HV}]^2 + [S_{VV}]^2 = \kappa_3 \tag{E 4.10}$$

and

$$\nu_1 \cdot \nu_2 = \textbf{invariant} = Det[G] = (Det[S])(Det[S])^* = \left(S_{HH}S_{VV} - |S_{HV}|^2\right)\left(S_{HH}S_{VV} - |S_{HV}|^2\right)^* \, . \tag{E 4.11}$$

In order to establish the connection between the coneigenvalues of equation (E 4.2) and the eigenvalues of $[G]$ in (E 4.6), one may proceed to take the complex conjugate of (E 4.2) and insert back in (E 4.2). Equation (E 4.2) has orthogonal solutions if and only if $[S]$ is symmetric. The inverse step is much more difficult to prove and needs among others the symmetry of $[S]$, which provides another topic for future research.

As a result of these relations, Kennaugh defined the effective polarimetric radar cross-section ε_{K_4}, also known as **Kennaugh's Polarimetric Excess** ε_{K_4}, in [E118], where

$$\varepsilon_{K_4} = Span[S] + 2\left|Det[S]\right| . \qquad \text{(E 4.12)}$$

This comes automatically into play (also in the present formulation) when representations on the Poincare sphere are considered, and reduces to ε_{K_3} for the mono-static reciprocal case. It plays an essential role in Czyz's alternate formulation of the theory of radar polarimetry [E110], derived from a spinorial transformation concept on the generalized polarization sphere, being studied in more depth by Bebbington [E32].

Step 2

Using the resulting solutions for $\nu_{1,2}$ for the known $[G]=[S]^{+}[S]$ and $[S]$, the optimal transmit polarization states $\mathbf{E}^{t}_{\mathbf{opt}_{1,2}}$ and optimal scattered waves $\mathbf{E}^{s}_{\mathbf{opt}_{1,2}}$ can be determined as

$$\mathbf{E}^{s}_{\mathbf{opt}_{1,2}} = [S]\mathbf{E}^{t}_{\mathbf{opt}_{1,2}} . \qquad \text{(E 4.13)}$$

Step 3

The received optimal antenna height $\mathbf{h}^{r}_{\mathbf{opt}}$ is then derived from (E 4.4)

$$\text{as } \mathbf{h}^{r}_{\mathbf{opt}} = \frac{\mathbf{E}^{s^{*}}_{\mathbf{opt}}}{\left\|\mathbf{E}^{s}_{\mathbf{opt}}\right\|} = \frac{\left([S]\mathbf{E}^{t}_{\mathbf{opt}}\right)^{*}}{\left\|[S]\mathbf{E}^{t}_{\mathbf{opt}}\right\|} . \qquad \text{(E 4.14)}$$

This defines the polarization match for obtaining maximum power in terms of the polarimetric brightness function (E 4.4) introduced by Kennaugh in order to solve the polarimetric radar problem [E4].

There exist several alternate methods of determining the optimal polarization states either by implementing the generalized complex polarization ρ transformation, first pursued by Boerner et al. [E13]; the con-similarity transformation method of Lüneburg [E52, E53] , the spinorial polarization sphere transformations of Bebbington [E32], and more recently the Abelian group method of Yang [E104 – E105].

E 4.2 Huynen's Target Characteristic Operator and the Huynen Polarization Fork

Huynen [E9], utilizing Kennaugh's prior studies [E4, E5], elaborated on polarimetric radar phenomenologies extensively, and his Dissertation of 1970: Phenomenological Theory of Radar Targets [E9] re-sparked international research on Radar Polarimetry, commencing with the studies by Poelman [E10, E11], Russian studies by Kanareykin [E122], Potekhin [E123], and others [E1].

Huynen cleverly reformulated the definition of the polarization vector, as stated in [E9], so that group-theoretic Pauli-spin matrix concepts may favorably be applied, which also serve for demonstrating the orientation angle invariance which Huynen coined de-psi-ing (de-ψ-ing), using ψ for denoting the relative polarization ellipse orientation angle. Here, we prefer to divert from our notation by rewriting the parametric definition of the polarization vector

$$\mathbf{p}(|E|,\phi,\psi,\chi) = |E|\exp(j\phi)\begin{bmatrix}\cos\psi & -\sin\psi\\ \sin\psi & \cos\psi\end{bmatrix}\begin{bmatrix}\cos\chi\\ -j\sin\chi\end{bmatrix}$$

as

$$\mathbf{p}(a,\alpha,\phi,\tau) = a\exp(j\alpha)\begin{bmatrix}\cos\phi & -\sin\phi\\ \sin\phi & \cos\phi\end{bmatrix}\begin{bmatrix}\cos\tau\\ -j\sin\tau\end{bmatrix}. \qquad \text{(E 4.15)}$$

With the use of the Pauli-spin matrices $[\sigma_i]$ defined in (E 2.14), the Huynen quaternion group definitions may be re-expressed as $[I]=[\sigma_0]$, $[J]=-j[\sigma_3]$, $[K]=j[\sigma_2]$, $[L]=-j[\sigma_1]$

$$\mathbf{p}(a,\alpha,\phi,\tau) = a\exp(j\alpha)\exp(\phi[J])\exp(\tau[K])\begin{bmatrix}1\\ 0\end{bmatrix}, \qquad \text{(E 4.16)}$$

with $\exp(\phi[J]) = \cos\phi[I] + \sin\phi[J]$ and $\exp(\tau[K]) = \cos\tau[I] + \sin\tau[K]$.

In this notation the orthogonal polarization vector $\mathbf{p}_\perp$ becomes

$$\mathbf{p}_\perp(a_\perp,\alpha_\perp,\phi,\tau) = a_\perp\exp(j\alpha_\perp)\exp\{(\phi+\frac{\pi}{2})[J]\}\exp(-\tau[K])\begin{bmatrix}1\\ 0\end{bmatrix}, \qquad \text{(E 4.17)}$$

so that $\mathbf{p}\cdot\mathbf{p}^* = a^2$, $\mathbf{p}\cdot\mathbf{p}_\perp^* = 0$.

Utilizing this notation, the transformed matrix $[S'(AB)]$ becomes

$$[S'(AB)] = [U]^T[S(HV)][U] \ , \qquad \text{(E 4.18)}$$

with the orthonormal transformation matrix $[U]$ defined in (E 2.23). This may be recasted with $\mathbf{m} = \mathbf{p}_m$ the so-called maximum or null polarization as defined in [E31], into

$$[U] = [\mathbf{m}\,\mathbf{m}_\perp] \ . \qquad \text{(E 4.19)}$$

Because of the orthonormal properties of $\mathbf{m}$ and $\mathbf{m}_\perp$, which satisfy the con-similarity eigenvalue equation [E82], the off-diagonal elements of $[S'(AB)]$ vanish. This in turn can be used to solve for ρ in (E 2.23), and hence for $\mathbf{m}$ and $\mathbf{m}_\perp$, without solving the consimilarity eigenvalue problem of (E 4.6). The complex eigenvalues $\rho_{xn1,2}$ are renamed as $s_{1,2}$ and were defined by Huynen as

$$s_1 = m\exp\{2j(\upsilon+\beta)\} \qquad s_2 = m\tan^2\gamma\exp\{-2j(\upsilon-\beta)\} \ . \qquad \text{(E 4.20)}$$

Then $[S'(AB)]$ of (E 4.18) becomes

$$[S'(AB)] = [U^*(\mathbf{m},\mathbf{m}_\perp)]\begin{bmatrix}m\exp\{2j(\upsilon+\beta)\} & 0\\ 0 & m\tan^2\gamma\exp\{-2j(\upsilon-\beta)\}\end{bmatrix}[U^*(\mathbf{m},\mathbf{m}_\perp)]^T \ , \qquad \text{(E 4.21)}$$

where $m = \sigma_K, \gamma, \psi, \tau_m, \upsilon,$ *and* β are the Huynen parameters. m denotes the target matrix magnitude and may be identified to be Kennaugh's polarimetric excess σ_K defined in (E 4.12). $\mathbf{m}(\psi,\tau_m)$ may be re-normalized as

$$\mathbf{m}(\psi,\tau_m)=\begin{bmatrix}\cos\psi & -\sin\psi\\ \sin\psi & \cos\psi\end{bmatrix}\begin{bmatrix}\cos\tau_m\\ -j\sin\tau_m\end{bmatrix}=\exp(\psi[\mathbf{J}])\exp(\tau_m[\mathbf{K}])\begin{bmatrix}1\\0\end{bmatrix}. \quad \text{(E 4.22)}$$

Then

$$\begin{bmatrix}m\exp\{2j(\upsilon+\beta)\} & 0\\ 0 & m\tan^2\gamma\exp\{-2j(\upsilon-\beta)\}\end{bmatrix}=m\exp(j\beta)\begin{bmatrix}1 & 0\\ 0 & \tan^2\gamma\end{bmatrix}\exp(\upsilon[\mathbf{L}]), \quad \text{(E 4.23)}$$

where $[L]$ represents the third modified Pauli-spin matrix. This satisfies Huynen's notation

$$[L]=[J][K]=-[K][J]-\begin{bmatrix}-j & 0\\ 0 & j\end{bmatrix}, \qquad [L]^2=-[I]\ . \quad \text{(E 4.24)}$$

We then obtain Huynen's target matrix characteristic operator

$$[\mathbf{H}(m,\gamma,\beta;\phi_m,\upsilon,\tau_m)]=[U^*(\psi,\tau_m,\upsilon)]m\begin{bmatrix}1 & 0\\ 0 & \tan^2\gamma\end{bmatrix}[U^*(\psi,\tau_m,\upsilon)]^T\exp(j\beta)\ . \quad \text{(E 4.25)}$$

$$[U(\psi,\tau_m,\upsilon)]\exp(\psi[\mathbf{J}])\exp(\tau_m[\mathbf{K}])\exp(\upsilon[\mathbf{L}]) \quad \text{(E 4.26)}$$

represents the Eulerian rotations with 2ψ, $2\tau_m$, 2υ about the bi-orthogonal polarization axes $\overline{S_1S_2}$ (connecting the two cross-pol maxima), $\overline{X_1X_2}$ (connecting the two cross-pol nulls, or equivalently, co-pol maxima), and $\overline{T_1T_2}$ (connecting the two saddle optima), respectively, with more detail given in Boerner and Xi [E31]. Huynen pointed out the significance of the relative target matrix orientation angle $\Phi=\phi-\psi$, where ϕ denotes the antenna orientation angle. From the definition of $\mathbf{m}(\psi,\tau_m)$ in (E 4.22), it can be shown that it can be eliminated from the scattering matrix parameters and incorporated into the antenna polarization vectors (de-psi-ing: de-ψ-ing) , and that the Huynen parameters are orientation independent, which was more recently analyzed in depth by Pottier [E58]. The Eulerian angle are indicators of a scattering matrix's characteristic structure with υ denoting the so-called skip-angle related to multi-bounce scattering (single versus double). τ_m denotes the helicity-angle and is an indicator of target symmetry ($\tau_m=0$) or non-symmetry, and β is the absolute phase which is of particular relevance in polarimetric radar interferometry.

Huynen's Polarization Fork and its Significance to (Radar)-Polarimetry

Xi-Boerner[1] Solution of the Polarization Fork

$$[S] = [U^*(\rho)]\exp(v[L]^*)\, m \begin{bmatrix} 1 & 0 \\ 0 & \tan^2\gamma \end{bmatrix} \exp(v[L]^*)^T [U^*(\rho)]^T \exp(j\xi)$$

$$[U(\rho)]^* = \frac{1}{\sqrt{1+\rho\rho^*}} \begin{bmatrix} e^{-j\psi_1} & -\rho(\phi_m, \tau_m)\, e^{-j\psi_4} \\ \rho^*(\phi_m, \tau_m)\, e^{-j\psi_1} & e^{-j\psi_4} \end{bmatrix}$$

$$m = |\lambda_1|$$

$$\rho'_{xn1} = H = \rho'_{cm1}\,, \quad \rho'_{xn2} = V = \rho'_{cm2}$$

$$\rho'_{cn1,2} = \pm \tan(\pi/2 - \gamma)\exp[j(2\gamma + \pi/2)]$$

$$\rho'_{xm1,2} = \pm \exp[j(2\gamma + \pi/2)] \quad (LR)$$

$$\rho'_{xs1,2} = \pm \exp(j2\gamma) \qquad (45°/135°)$$

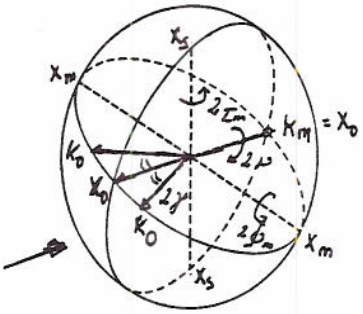

Huynen's Solution of the Polarization Fork

$$[H] = [U^*(\psi, \tau_m, v)]\, m \begin{bmatrix} 1 & 0 \\ 0 & \tan^2\gamma \end{bmatrix} [U^{*'}(\psi, \tau_m, v)] \exp(j\xi)$$

$$[U(\psi, \tau_m, v)] = e^{\psi[J]} e^{\tau_m[K]} e^{v[L]}$$

Fig. E 4.2 Huynen's Polarization Fork

E 4.3 Determination of the Polarization Density Plots by van Zyl, and the Polarization Phase Correlation Plots by Agrawal

In radar meteorology, and especially in polarimetric Doppler radar meteorology, the Kennaugh target matrix characteristic operator concept was well received and further developed in the thesis of Agrawal [E78], and especially analyzed in depth by McCormick [E127] and Antar [E128] because various hydro-meteoric parameters can directly be associated with the Huynen or alternate McCormick parameters. In radar meteorology, the Poincaré sphere visualization of the characteristic polarization states has become commonplace. In wide area SAR remote sensing, the co/cross-polarization and Stokes parameter power density plots on the unwrapped planar transformation of the polarization sphere surface are preferred, such as introduced independently in the dissertations of van Zyl [E79] and Agrawal [E78].

Because of the frequent use of the co/cross-polarization power density plots $P_c(\rho), P_{c\perp}(\rho)$ and $P_x(\rho)$, and the equally important but hitherto rarely implemented co/cross-polarization phase correlation plots $R_c(\rho), R_{c\perp}(\rho)$ and $R_x(\rho), R_{x\perp}(\rho)$, those are here introduced. Following Agrawal [E78], who first established the relation between the Scattering Matrix Characteristic Operators of Kennaugh and Huynen with the polarimetric power-density/ phase-correlation plots, we obtain for the reciprocal case $S_{AB} = S_{BA}$:

$$[C_{3L}] = \langle \mathbf{f}_{3L} \cdot \mathbf{f}_{3L}^{\dagger} \rangle = \begin{bmatrix} \langle |S_{AA}|^2 \rangle & \sqrt{2}\langle S_{AA} S_{AB}^* \rangle & \langle S_{AA} S_{BB}^* \rangle \\ \sqrt{2}\langle S_{AB} S_{AA}^* \rangle & 2\langle |S_{AB}|^2 \rangle & \sqrt{2}\langle S_{AB} S_{BB}^* \rangle \\ \langle S_{BB} S_{AA}^* \rangle & \sqrt{2}\langle S_{BB} S_{AB}^* \rangle & \langle |S_{BB}|^2 \rangle \end{bmatrix} . \qquad \text{(E 4.27)}$$

Re-expressed in terms of the co/cross-polarimetric power density expressions:

$$P_c(\rho) = \langle |S_{AA}|^2 \rangle \qquad P_{c\perp}(\rho) = \langle |S_{BB}|^2 \rangle \qquad P_x(\rho) = \langle |S_{AB}|^2 \rangle = P_{x\perp}(\rho) \qquad \text{(E 4.28)}$$

and the co/cross-polarization phase correlation expressions:

$$R_c(\rho) = \langle S_{AA} S_{BB}^* \rangle \qquad R_{c\perp}(\rho) = \langle S_{BB} S_{AA}^* \rangle \qquad R_x(\rho) = \langle S_{AA} S_{AB}^* \rangle \qquad R_{x\perp}(\rho) = \langle S_{BB} S_{AB}^* \rangle \quad , \text{(E 4.29)}$$

so that $[C_{L3}(\rho)]$ may be rewritten according to (E 3.68) – (E 3.72) as

$$[C_{3L}(\rho)] = \begin{bmatrix} P_c(\rho) & \sqrt{2}\, R_x(\rho) & R_c(\rho) \\ \sqrt{2}\, R_x(\rho)^* & 2P_x(\rho) & \sqrt{2}\, R_x^{\perp}(\rho)^* \\ R_c(\rho)^* & \sqrt{2}\, R_x^{\perp}(\rho) & P_c^{\perp}(\rho) \end{bmatrix} . \qquad \text{(E 4.30)}$$

According to (E 3.70) and (E 3.71) this satisfies the following inter-channel and symmetry relations:

$$P_c\left(\rho_{\perp} = -1/\rho^*\right) = P_c^{\perp}(\rho) \qquad \left|R_x\left(\rho_{\perp} = -1/\rho^*\right)\right| = \left|R_x^{\perp}(\rho)\right|$$

$$P_x\left(\rho_{\perp} = -1/\rho^*\right) = P_x(\rho) \qquad \left|R_c\left(\rho_{\perp} = -1/\rho^*\right)\right| = \left|R_c(\rho)\right| , \qquad \text{(E 4.31)}$$

and frequently also the degree of polarization $D_p(\rho)$ and the degree of coherency $\mu(\rho)$ in terms of the directly measurable $P_c(\rho), P_{c\perp}(\rho)$ and $P_x(\rho)$; $R_c(\rho), R_{c\perp}(\rho)$ and $R_x(\rho), R_{x\perp}(\rho)$. This requires a 'dual-orthogonal, dual-channel measurement system for coherent and partially coherent scattering ensembles is available, requiring high-resolution, high channel isolation, high side-lobe reduction, and high sensitivity polarimetric amplitude and phase correlation, where

$$\mu(\rho) = \frac{|R_x(\rho)|}{\sqrt{P_c(\rho) P_x(\rho)}}, \quad D_p(\rho) = \frac{\left\{[P_c(\rho) - P_x(\rho)]^2 + 4|R_x(\rho)|^2\right\}^{1/2}}{(P_c(\rho) + P_x(\rho))}, \quad \textit{where} \;\; 0 \le \mu(\rho) \le D_p(\rho) \le 1 . \qquad \text{(E 4.32)}$$

For coherent (deterministic) scatterers $\mu = D_p = 1$, whereas for completely depolarized scatterers $\mu = D_p = 0$.

The respective power-density profiles and phase-correlation plots are then obtained from the normalized polarimetric radar brightness functions as functions of (ϕ, τ) with $\frac{-\pi}{2} \le \phi \le \frac{\pi}{2}$, $\frac{-\pi}{4} \le \tau \le \frac{\pi}{4}$ so that

$$\begin{aligned} V_{AA}(\phi,\tau) &= \mathbf{p}^T(\phi,\tau)[S(HV)]\mathbf{p}(\phi,\tau) \\ V_{AB}(\phi,\tau) &= \mathbf{p}_{\perp}^{\dagger}(\phi,\tau)[S(HV)]\mathbf{p}(\phi,\tau) \\ V_{BA}(\phi,\tau) &= \mathbf{p}^T(\phi,\tau)[S(HV)]\mathbf{p}_{\perp}(\phi,\tau) \end{aligned} \qquad \text{(E 4.33)}$$

$$V_{BB}(\phi,\tau)=\mathbf{p}_{\perp}^{\dagger}(\phi,\tau)[S(HV)]\mathbf{p}_{\perp}(\phi,\tau)$$

where

$$P_c=|V_{AA}|^2=|S_{AA}(\phi,\tau)|^2$$

$$\begin{aligned}
P_x &= |V_{AB}|^2=|S_{AB}(\phi,\tau)|^2 \\
R_c &= |\phi_{AA}-\phi_{BB}|=|\arg V_{AA}(\phi,\tau)-\arg V_{BB}(\phi,\tau)| \\
R_x(\phi,\tau) &= |\phi_{AA}-\phi_{AB}|=|\arg V_{AA}(\phi,\tau)-\arg V_{AB}(\phi,\tau)| \\
R_{x\perp}(\phi,\tau) &= |\phi_{BB}-\phi_{BA}|=|\arg V_{BB}(\phi,\tau)-\arg V_{BA}(\phi,\tau)|
\end{aligned} \qquad \text{(E 4.34)}$$

In addition, the Maximum Stokes Vector $\mathbf{q}_{0MAX}$ and the maximum received power density P_m may be obtained from

$$P_m(\phi,\tau)=\mathbf{q}_0(\phi,\tau)=[K]\mathbf{q}(\phi,\tau)\ . \qquad \text{(E 4.35)}$$

Examples are provided in Fig. E 4.3 for one specific matrix case [E31, E82] given by

$$[S(HV)]=\begin{bmatrix} 2j & 0.5 \\ 0.5 & -j \end{bmatrix} \qquad \text{(E 4.36)}$$

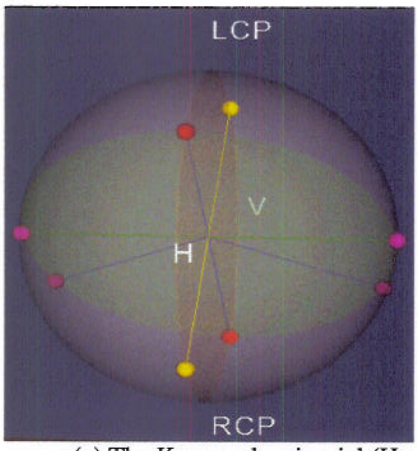

(a) The Kennaugh spinorial (Huynen)

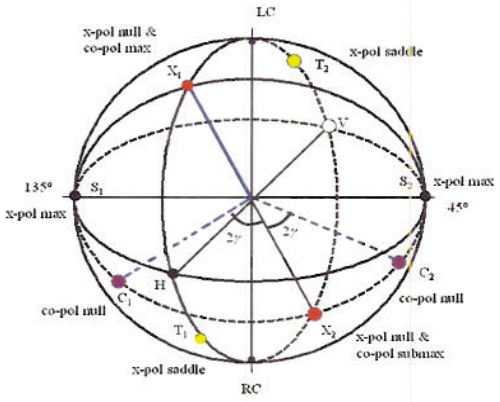

(b) Associated optimal polarization states polarization fork

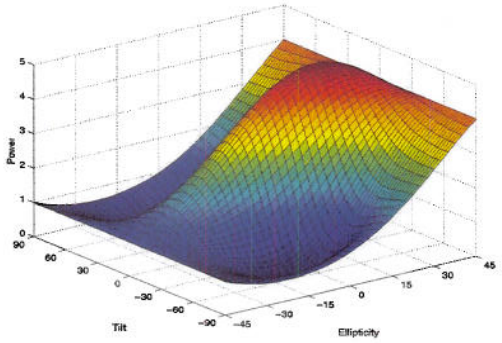

(c) Power density Co-pol

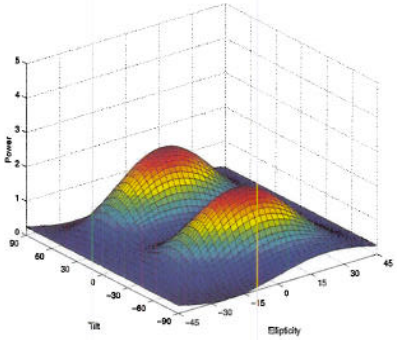

(d) Power density x-pol

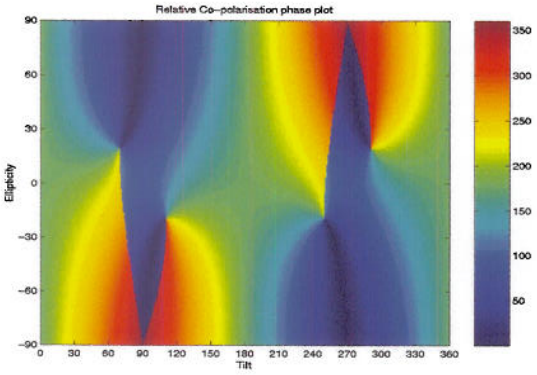

(e) Phase correlation co-pol

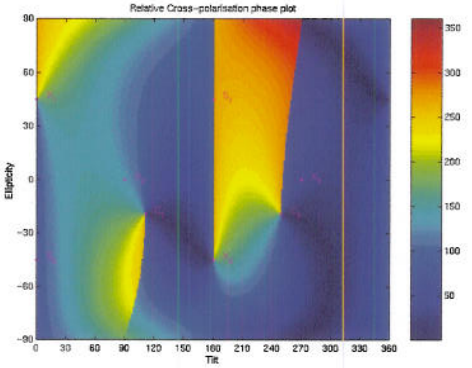

(f) Phase Correlation x-pol.

Fig. E 4.3 Power Density and Phase Correlation Plots (by courtesy of Dr. James Morris)

E 4.4 Optimal Polarization States and its Correspondence to the Density Plots for the Partially Polarized Cases

According to the wave dichotomy portrayed for partially polarized waves, there exists one case for which the coherency matrix for the partially polarized case may be separated into one fully polarized and one completely depolarized component vector according to Chandrasekhar [E34]. This principle will here be loosely applied to the case for which a completely polarized wave is incident on either a temporally incoherent (e.g., hydro-meteoric) or

spatially incoherent (e.g., rough surface viewed from different depression angles as in synthetic aperture radar imaging) scatterer. This allows us to obtain a first order approximation for dealing with partially coherent and/or partially polarized waves when the polarimetric entropy is low.

The energy density arriving at the receiver back-scattered from a distant scatterer ensemble subject to a completely polarized incident wave may be separated into four distinct categories where the Stokes vector is here redefined, with $\mathbf{q}_p$ and $\mathbf{q}_u$ denoting the completely polarized and the unpolarized components, respectively

$$\mathbf{q}=\mathbf{q_p}+\mathbf{q_u}=\begin{bmatrix} q_0 \\ q_1 \\ q_2 \\ q_3 \end{bmatrix}=\begin{bmatrix} D_p q_0 \\ q_1 \\ q_2 \\ q_3 \end{bmatrix}+\begin{bmatrix} (1-D_p)q_0 \\ 0 \\ 0 \\ 0 \end{bmatrix} . \qquad \text{(E 4.37)}$$

$\mathbf{q}$ as well as D_p were defined earlier, so that the following four categories for optimization of partially polarized waves can be defined as:

q_0 total energy density in the scattered wave before it reaches the receiver

$q_0 D_p$ completely polarized part of the intensity

$q_0(1-D_p)$ noise of the unpolarized part

(E 4.38)

$\frac{1}{2}q_0(1+D_p)$ maximum of the total receptable intensity, the sum of the matched polarized part and one half of the unpolarized part: $\{D_p q_0\}+\left\{\frac{1}{2}(1-D_p)q_0\right\}=\left\{\frac{1}{2}(1+D_p)q_0\right\}$.

Considering a time-dependent scatterer which is illuminated by a monochromatic (completely polarized wave) $\mathbf{E}^t$, for which the reflected wave $\mathbf{E}^s$ is in general non-monochromatic, and therefore partially polarized. Consequently, the Stokes vector and Kennaugh matrix formulism will be applied to the four types of energy density terms defined above in (E 4.38).

E 4.5 Optimization of the Adjustable Intensity $D_p q_0$

The energy density $D_p q_0$, contained in the completely polarized part $\mathbf{q}_p$ of $\mathbf{q}$, is called the adjustable intensity because one may adjust the polarization state of the receiver to ensure the polarization match as shown previously for the coherent case. We may rewrite the scattering process in index notation as

$$q_i^s=\sum_{j=0}^{3}K_{ij}q_j^t \qquad where \quad j=0,1,2,3 . \qquad \text{(E 4.39)}$$

The adjustable intensity $D_p q_0$ can be re-expressed as

$$D_p q_0^s=\left(\sum_{i=0}^{3}q_i^{s2}\right)^{1/2}=\left[\sum_{i=1}^{3}\left(\sum_{j=0}^{3}K_{ij}q_j^t\right)^2\right]^{1/2} , \qquad \text{(E 4.40)}$$

where the q_i^t are the elements of the Stokes vector of the transmitted wave. The partial derivative of $(D_p q_0)^2$ with respect to q_k^t can be derived as

$$\frac{\partial (D_p q_0^s)^2}{\partial q_k^t} = \sum_{i=1}^{3} \frac{\partial q_i^{s2}}{\partial q_k^t} = 2\sum_{i=1}^{3} q_i^s K_{ik} = 2\sum_{i=1}^{3}\sum_{j=0}^{3} K_{ij} K_{ik} q_j^t \quad . \tag{E 4.41}$$

For optimizing the adjustable intensity, we apply the method of Lagrangian multipliers, which yields

$$\frac{\partial (D_p q_0^s)^2}{\partial q_k^t} - \mu \frac{\partial \phi}{\partial q_k^t} = 2\sum_{i=1}^{3}\sum_{j=0}^{3} K_{ij} K_{ik} q_j^t - \mu q_k^t \quad , \tag{E 4.42}$$

where ϕ is the constraint equation

$$\phi(q_1^t, q_2^t, q_3^t) = (q_1^{t2}, q_2^{t2}, q_3^{t2})^{1/2} - 1 = 0 \quad . \tag{E 4.43}$$

Equation (E 4.42) subject to (E 4.43) constitutes a set of inhomogeneous linear equations in $q_1^t(\mu)$, $q_2^t(\mu)$ *and* $q_3^t(\mu)$, with solutions as three functions of μ. Substituting $q_i^t(\mu; i = 1, 2, 3)$ into the constrained condition (E 4.43) leads to a sixth-order polynomial Galois equation of μ. For each μ value, q_1^t, q_2^t, q_3^t, *and* $D_p q_0^s$ are calculated according to (E 4.39) to (E 4.41). The largest (or smallest) intensity is the optimal intensity and the corresponding $\mathbf{q}^t$ is the optimal polarization state of the transmitted wave.

E 4.6 Minimizing the Noise-Like Energy Density Term: $q_0^s(1 - D_p)$

An unpolarized wave can always be represented by an incoherent sum of any two orthogonal completely polarized waves of equal intensity [E14, E15],which leads to 50% efficiency for the reception of the unpolarized wave. In order to receive as much 'polarized energy' as possible, the noise-like energy needs to be minimized. The total energy density of the unpolarized part of the scattered wave is given by:

$$(1 - D_p) q_0^s = q_0^s - D_p q_0^s = \sum_{j=0}^{3} K_{0j} q_j^t - \sqrt{\sum_{i=1}^{3} \left(\sum_{j=0}^{3} K_{ij} q_j^t \right)^2} \quad . \tag{E 4.44}$$

Hitherto, no simple method was found for finding the analytic closed form solution for the minimum. Instead, numerical solutions have been developed and are in use.

E 4.7 Maximizing the Receivable Intensity in the Scattered Wave: $\frac{1}{2} q_0 (1 + D_p)$

The total receivable energy density consists of two component parts: 100% reception efficiency for the completely polarized part of the scattered wave and 50% reception efficiency for the unpolarized part. The resulting expression for the total receivable intensity:

$$\frac{1}{2}(1 + D_p) q_0^s = D_p q_0^s + \frac{1}{2}(1 - D_p) q_0^s = \frac{1}{2}\sum_{j=0}^{3} K_{0j} q_j^t + \frac{1}{2}\sqrt{\left(\sum_{i=1}^{3}\sum_{j=0}^{3} K_{ij} q_j^t \right)^2} \tag{E 4.45}$$

can only be solved using numerical analysis and computation. The resulting maximally received Stokes vector is plotted in Fig. E 4.4 (where q was replaced by p), and we observe that for the fully polarized case no depolarization

pedestal exists. It appears as soon as $p < 1$. For $p = 0$ it reaches its maximum of 0.5 for which the polarization diversity profile has deteriorated into the flat equal power density profile, stating that the polarization diversity becomes meaningless.

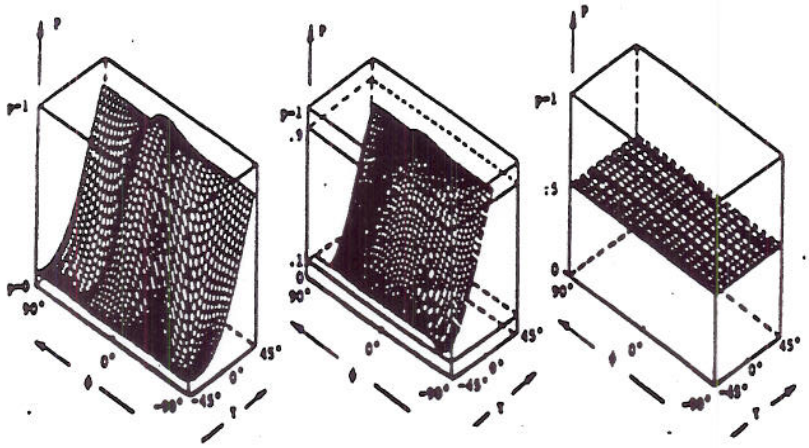

p=1	p = .8	p = 0
coherent	distributed partially	total polarization
point scatterer	coherent scatterer	noise

Fig. E 4.4 Optimal Polarization States for the Partially Polarized Case

In conclusion, we refer to Boerner et al. [E31, E82], where an optimization procedure for (E 4.37 – E 4.40) in terms of $[K]$ for a completely polarized incident wave is presented together with numerical examples. It should be noticed here that Yang more recently provided another more elegant method in [E119 – E121] for analyzing the statistical optimization procedure of the Kennaugh matrix.

E 5.0 Polarimetric Target Decomposition According to Cloude & Pottier

Another essential feature provided by polarimetric scattering matrix data, when express in terms of its Lexicographic and Pauli-based Covariance Matrices $[C_{3L}(\rho)]$ and $[C_{3P}(\rho)]$, is the possibility to decompose the scattering process of random scattering mechanisms into the sum of independent scattering contributions associated with certain pre-specified elementary scattering mechanisms. A comprehensive review of several matrix decomposition approaches, developed in radar polarimetry, was given by Cloude and Pottier [E27], dating back to Kennaugh's extensive investigations of 1949 to 1959 [E5] based on group-theoretic concepts of quantum mechanics, which were cleverly mined by Huynen [E9]. In his thought provoking dissertation monograph [E9], Huynen followed Chandrasekhar and introduced the single (point-target) versus random (noise-target) scatterer decomposition of the Kennaugh Matrix $[K]=[K_T]+[K_N]$ therewith proposing one part of a polarimetric scattering dichotomy. As was demonstrated previously this approach may apply for vanishing entropy $(H \leq \approx 0.3)$, but its performance deteriorates with increasing H.

Specifically, Pottier [E126] shows that any and all of the current decomposition methods of the Sinclair, Graves, and degenerate-coherent Kennaugh matrices, $[S]$, $[G]$, and $[K]$, including the Huynen [E9], the Barnes-Holm [E131], the Krogager [E30], the Cameron [E124, E125], and any other such decompositions [E27], are not unique and cannot be applied to the general incoherent and/or partially fluctuating scatterer ensemble scenario. However, notwithstanding these shortcomings, these matrix decomposition approaches, and especially when expressed in a combination of the unitary orthonormal Pauli matrix set $\psi_P\{[\sigma_i], i=0,1,2,3\}$ of (E 2.14), are most useful for scatterer feature sorting in case sufficient *a priori* knowledge of the appearance of specific scatterers within the scattering scenario is available. These matrix decomposition approaches are also useful when the depolarized component is low with the polarimetric entropy approaching $H \rightarrow 0$.

The next question then arises on whether the implementations of, for example, the Lexicographic Covariance Matrix $[C_L]$ are superior to that of the Pauli-based Covariance matrix $[C_P]$, or vice versa. For the partially coherent, general non-reciprocal bi-static scattering scenario, the covariance matrices $[C_{4L}]$ and $[C_{4P}]$ are of full rank, i.e. rank 4. For the reciprocal mono-static case $[C_{3L}]$ and $[C_{3P}]$ are of rank 3. For the coherent (deterministic) case both incoherent and/or coherent cases possess rank 1, without the need for ensemble averaging, and Kennaugh's characteristic optimal polarization scattering operator concept strictly applies. Both the Lexicographic and the Pauli-based Covariance matrices are by definition hermitian positive semi-definite matrices which imply that they possess real non-negative eigenvalues and orthogonal eigenvectors, as was shown for the Lexicographic Covariance matrix. Since the transformations of the covariance matrices, are of the unitary similarity class, both matrices possess identical eigenvalues but different eigenvectors. However, the lexicographic feature vector $\mathbf{f}_L$ is directly and more explicitly related to the polarimetric complex radar cross-sections $S_{AA}, S_{AB}, S_{BA}, S_{BB}$ of the (non-symmetric) Sinclair matrix $[S]$. It thus displays the relative functional behaviour of any one S_{ij} versus the complete feature vector set $S_{AA}, S_{AB}, S_{BA}, S_{BB}$ and its Frobenius norm of $\kappa = Span\{[S(AB)]\}$ is invariant. The Pauli feature vector $\mathbf{f}_P$ allows for decomposition in terms of the complete Pauli spin matrix set $\psi_P\{[\sigma_i], i=0,1,2,3\}$ of (E 2.14), which relates to the matrix transformations and preserves the correct phase correlation between the complex polarimetric radar cross-section S_{ij} in terms of $\{(S_{AA} \pm S_{BB}),\ (S_{AB}+S_{BB}),\ j(S_{AB}-S_{BB})\}$ of $[S(AB)]$. Thus, in consideration of these latter rather crucial polarimetric correlation phase and rotational transformation preserving capabilities, in a certain sense the implementations of the Pauli-based Covariance Matrix $[C_{4P}]$ may have to be considered preferable above all of the other presentations. However, direct and unique mathematical transformation relations strictly exist among all of the various polarimetric matrices $[S]$, $[G]$, $[K]$ with $[C_L]$ and/or $[C_P]$. Therefore, the optimization and pertinent invariant decomposition of the Pauli-based Covariance Matrix $[C_P]$ are introduced below, following the recent exposition of Pottier [E126] most closely by considering the reciprocal mono-static case of the symmetric $[C_{3P}]$ only.

In the following two figures, Figure E 5.1a and E 5.1b a comparison is made of presenting lexicographic versus Pauli-based image presentations, clearly showing that very valuable additional information is recovered by the Pauli-based feature vector as compared to the lexicographic feature vector presentations.

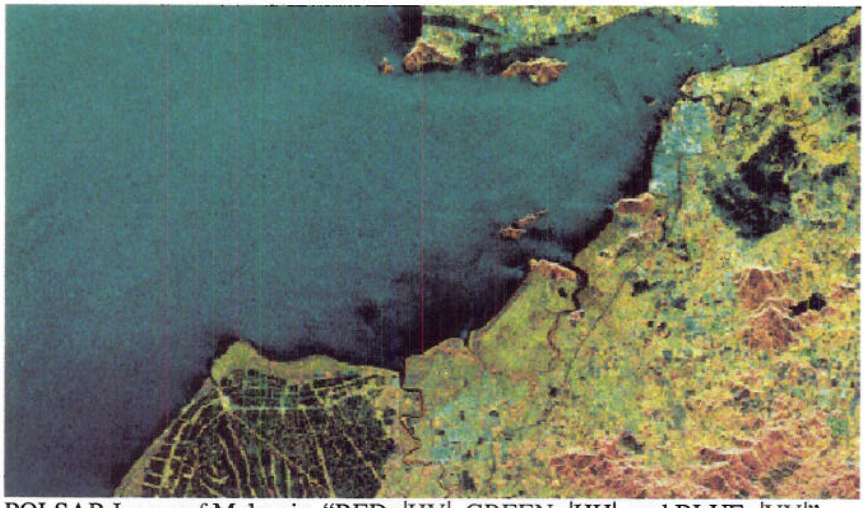

(a) POLSAR Image of Malaysia, "RED=|HV|, GREEN=|HH|, and BLUE=|VV|"

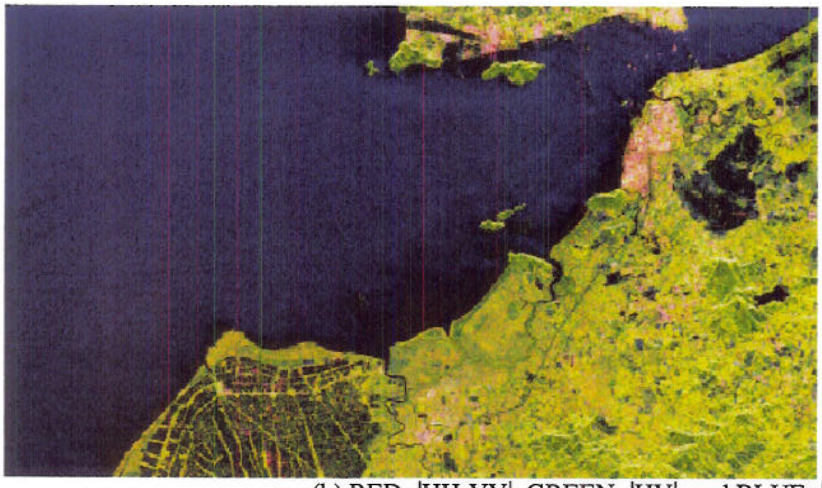

(b) RED=|HH-VV|, GREEN=|HV|, and BLUE=|HH+VV|"

Fig. E 5.1 SIR-C L-Band POLSAR image of Malaysia. The phase differences between HH and VV were used to enhance the effect of scattering mechanisms imbedded in POLSAR data.

E 5.1 Eigenvector-based Decomposition of the Pauli-based Covariance Matrix for the Reciprocal Monostatic Scattering Scenario $[C_{3P}]$

In order to accommodate polarimetric synthetic aperture radar (POL-SAR) image analysis, nowadays access to POL-SAR image data takes is given either to the complex coherent Sinclair scattering matrix $[S]$ in terms of single-look-complex (SLC) formatted image data takes or to ensemble-averaged Kennaugh matrix $[K]$ in terms of multi-look compressed (MLC) formatted image data takes. Whereas the SLC-formatted image data takes preserve absolute scatter phase, the MLC-formatted image data takes do not. In any of the polarimetric SAR image analyses, the MLC formatted data, which can be converted to the relative phase $[S]_{RP}$ Matrix image data set uniquely, are sufficient. This is, however, not the case for polarimetric SAR interferometry for which the absolute polarimetric scattering phase $\{\exp(j\phi)\}$ plays a major and decisive role.

The ensemble averaging process leads to the concept of the distributed target which has its own structure, different from the stationary or pure-point target as expressed in the definitions of $[S]$ and $[G]$, which was explored in great detail by Ostrovityanov [E132], Pothekin and Tatarinov [E133] as well as Kaselev [E133b].

The instantaneous (single-look: pixel) target returns from a spatially extended scatterer, comprised of many diverse distributed point targets, can be characterized by its complex Sinclair matrix $[S]$ which relates to the spatial voltage or by its 3x3 coherency matrices $[C_{3L}]$ or $[C_{3P}]$, which then relates to spatial power when applied to POL-SAR imaging. In the case of spatial ensemble averaging, i.e., recovering '$\langle [C_{3P}] \rangle$', this process may be defined as

$$\langle [C_{3P}] \rangle = \frac{1}{N} \sum_{i=1}^{N} \mathbf{f}_{3P_i} \mathbf{f}_{3P_i}^{*T} = \frac{1}{N} \sum_{i=1}^{N} [C_{3P_i}] \quad . \tag{E 5.1}$$

For the reciprocal monostatic case this possesses 3x3 = 9 independent parameters (3 real diagonal and 3 complex off-diagonal elements), whereas a point scatterer expressed in terms of $[S]$ is given by not more than 5 parameters as per definition of the Kennaugh characteristic.

Therefore, for the general incoherent case of high entropy, the averaged target characteristic operator cannot be represented by an equivalent effective mean point scatterer plus its point scatterer variance, since it possesses four additional degrees of freedom. Derivations introduced in previous sections must be assessed most critically, especially when the entropy H is no longer small.

In order to determine the eigenvalues and corresponding eigenvectors of $[C_{3P}(AB)]$ from the measured data set $[C_{3P}(HV)]$,

$$[C_{3P}(AB)] = [U_{3P}][C_{3P}(HV)][U_{3P}]^{-1} \tag{E 5.2}$$

where $[U_{3P}]$, instead of (E 3.65) [E80], is here redefined as

$$[U_{3P}] = [\hat{\mathbf{u}}_{3P_1} \quad \hat{\mathbf{u}}_{3P_2} \quad \hat{\mathbf{u}}_{3P_3}] \, . \tag{E 5.3}$$

The $\hat{\mathbf{u}}_{3P_i}$ represent the three orthonormal eigenvectors, with λ_i denoting the corresponding real eigenvalues, so that

$$\langle [C_{3P}] \rangle = \sum_{i=1}^{3} \{\lambda_i \langle [C_{3P_i}] \rangle\} = \sum_{i=1}^{3} \lambda_i \hat{\mathbf{u}}_{3P_i} \cdot \hat{\mathbf{u}}_{3P_i}^{*T} \quad . \tag{E 5.4}$$

If only one eigenvalue is non-zero ($\lambda_1 = \lambda_2 = 0, \lambda_3 \neq 0$), then the statistical weight reduces to that of a point-scattering Sinclair matrix $[S]$, and the Kennaugh target characteristic operator theory applies firmly. At the other extreme, if all eigenvalues are non-zero and identical $(\lambda_1 = \lambda_2 = \lambda_3 \neq 0)$, then $\langle [C_{3P}] \rangle$ represents a completely de-correlated, non-polarized random scattering structure. However, such a structure rarely exists, and in between the two extremes, the case of distributed, partially polarized scatterers prevails. In order to define the statistical disorder of each distinct scatter type within the ensemble, the polarimetric entropy H, according to von Neumann [E136], provides an efficient and suitable basis-invariant parameter. It is a peculiarity of a complex covariance matrix $[C]$ that the orthonormal eigenvectors of $[C]$ are determined only up to a phase term. This can be seen very easily. For instance, in (E 5.4) one may substitute $\hat{\boldsymbol{u}}_{3P_i} \cdot \hat{\boldsymbol{u}}_{3P}^{*T} = (e^{j\phi} \hat{\boldsymbol{u}}_{3P_i}) \cdot (e^{j\phi} \hat{\boldsymbol{u}}_{3P_i})^{*T}$.

E 5.2 The Polarimetric Entropy for the Mono-Static Reciprocal Case: H_3

Following Cloude and Pottier [E57], and especially Pottier [E58], the polarimetric entropy H_3 may then be defined, according to von Nuemann [E136], in terms of the logarithmic sum of eigenvalues of $\langle[C_{3P}]\rangle$ as

$$H_3 = -\sum_{i=1}^{3} P_i \log_3(P_i), \qquad P_i = \lambda_i \left(\sum_{j=1}^{3} \lambda_j \right)^{-1}. \tag{E 5.5}$$

P_i are the corresponding probabilities recovered from the eigenvalues λ_i as further discussed in [E55].

If the polarimetric entropy H_3 is low $(H_3 \leq 0.3)$, then the system may be considered weakly depolarizing and the dominant scattering mechanism in terms of a specifically identifiable equivalent point scatterer may be recovered. The eigenvector corresponding to the largest eigenvalue is chosen, and the other eigenvector components may be neglected. In this case the polarization power density plots for the partially polarized case apply. However, if the entropy is high, then the scatterer ensemble is depolarizing and no longer does there exist a single equivalent point scatterer, and a mixture of possible point scatterer types must be considered from the full eigenvalue spectrum. As the polarimetric entropy H_3 further increases, the number of distinguishable classes identifiable from polarimetric observations is reduced. In the limit, when $H_3 = 1$, $\mu = D_p = 0$, and polarization diversity becomes meaningless.

E 5.3 Polarimetric Span Invariant κ_3, and the Scattering Anisotropy A_3 for the Mono-Static Reciprocal Case

The eigenvalues λ_i, $i = 1,\ 2,\ 3$ possess additional properties, where the total sum, the span invariant κ_3, represents the total achievable power scattered by the scatter ensemble. $\kappa_3 = \sum_{i=1}^{3} \lambda_i = \text{invariant}$, is independent of the antenna polarization state and collected for the reciprocal back-scatterer case by an orthogonally polarized antenna pair, which corresponds to the Frobenius norm (span) of the scattering matrix as defined by (E 3.67), and is known as Kennaugh's span invariant κ_3

$$\kappa_3 = \|\mathbf{f}_{3P}\| = \frac{1}{2} span\{[S]\} = \frac{1}{2} Trace\{[S][S]^{\dagger}\} = \sum_{i=1}^{3} \lambda_i = \frac{1}{2}\left(|S_{HH}|^2 + 2|S_{HV}|^2 + |S_{VV}|^2\right). \tag{E 5.6}$$

On the other hand, the polarimetric entropy H is a useful scalar descriptor of the randomness of the scattering process. The third invariant parameter, originally introduced by van Zyl [E134], and denoted as polarimetric anisotropy A_3 by Cloude and Pottier [E57], is defined by taking into account that the eigenvalues have been ordered as $0 \leq \lambda_1 \leq \lambda_2 \leq \lambda_3$:

$$A_3 = \frac{\lambda_2 - \lambda_3}{\lambda_2 + \lambda_3}. \tag{E 5.7}$$

The relation to van Zyl's formulation requires further interpretation.

When $A_3 = 0$, then $\lambda_2 = \lambda_3$, in which case if $\lambda_2 = \lambda_3 = 0$, and the 'coherent' deterministic case results for which $\kappa_3 = \lambda_1$. For $\lambda_1 = \lambda_2 = \lambda_3$, the entropy attains its largest value, $H_3 = 1$, which corresponds to the

completely depolarized case. It should be noted here that in nature completely polarized target and/or and completely unpolarized scatterer ensembles may only exist rarely.

E 5.4 The Cloude and Pottier Probabilistic Random Media Scattering Model

Considering Bragg scattering for a Bragg scattering surface, Cloude and Pottier introduced a revised parameterization of the eigenvector $\hat{\mathbf{u}}_{3P_i}$ of $[C_{3p}]$; where

$$\hat{\mathbf{u}}_{3P} = [\cos\alpha \quad \sin\alpha\cos\beta\exp(j\delta) \quad \sin\alpha\sin\beta\exp(j\gamma)]^T . \tag{E 5.8}$$

With a revised parameterization of the Pauli Coherency Matrix $[C_{3p}]$ one obtains

$$\langle[C_{3P}]\rangle = [U_{3P}]\begin{bmatrix}\lambda_1 & 0 & 0\\ 0 & \lambda_2 & 0\\ 0 & 0 & \lambda_3\end{bmatrix}[U_{3P}]^{*T} . \tag{E 5.9}$$

It is a peculiarity of a complex covariance matrix $[C]$ that the orthonormal eigenvectors of $[C]$ are determined only up to a phase term, which follows from substituting into (E 5.4) the expression $\hat{\boldsymbol{u}}_{3P_i}\cdot\hat{\boldsymbol{u}}_{3P}^{*T} = (e^{j\phi}\hat{\boldsymbol{u}}_{3P_i})\cdot(e^{j\phi}\hat{\boldsymbol{u}}_{3P_i})^{*T}$. In particular the first element of any one or all eigenvectors may be chosen as real, where

$$[U_{3P}] = \exp(j\phi)\begin{bmatrix}\cos\alpha_1 & \cos\alpha_2\exp(j\phi_2) & \cos\alpha_3\exp(j\phi_3)\\ \sin\alpha_1\cos\beta_1\exp(j\delta_1) & \sin\alpha_2\cos\beta_2\exp(j\delta_2) & \sin\alpha_3\cos\beta_3\exp(j\delta_3)\\ \sin\alpha_1\sin\beta_1\exp(j\gamma_1) & \sin\alpha_2\sin\beta_2\exp(j\gamma_2) & \sin\alpha_3\sin\beta_3\exp(j\gamma_3)\end{bmatrix}. \tag{E 5.10}$$

The 3x3 unitary matrix $[U_{3p}]$ is parameterized in terms of column vectors of different $\alpha_i, \beta_i, \phi_i, \delta_i$, and γ_i, $i = 1,2,3$ and ϕ denoting physically an absolute phase to enable a probabilistic interpretation of the scattering process. In a first approach, Cloude and Pottier [E57] introduced a 3-symbol Bernoulli process whereby the scattering process was modelled in terms of three distinct Sinclair matrices $[S_i]$, one each to correspond to a column of $[U_{3p}]$ which occur within probabilities P_i so that $\sum_{i=1}^{3} P_1 = 1$. Cloude and Pottier [E57] then introduced a mean parameter of random sequences associated with the Bernoulli process so that the dominant scattering matrices from the 3x3 Pauli Coherency matrix $[C_{3p}]$ may be defined as a mean target vector $\hat{\mathbf{u}}_{3P_m}$:

$$\hat{\mathbf{u}}_{3m} = [\cos\overline{\alpha} \quad \sin\overline{\alpha}\cos\overline{\beta}\exp(j\overline{\delta}) \quad \sin\overline{\alpha}\sin\overline{\beta}\exp(j\overline{\gamma})]^T . \tag{E 5.11}$$

The mean $\overline{\alpha}$ may then also be defined as

$$\overline{\alpha} = \sum_{i=1}^{3} P_i\alpha_i = P_1\alpha_1 + P_2\alpha_2 + P_3\alpha_3 , \tag{E 5.12}$$

with P_i and the α_i needing to be determined.

However, this method is strictly model-dependent, and, similar to the $[S]$ matrix decomposition into the Pauli matrix set $\psi_P\{[\sigma_i], i=0,1,2,3\}$, is not unique. But it invites further studies for the development of other model dependent decompositions of the eigen-vectors $\hat{\mathbf{u}}_{3P_i}$. The direct relation of the respective set of $[S]$ and $[C_{3p}]$ model-dependent Pauli spin matrix decompositions is sought and may shed more light into the polarimetric scatter dichotomy which establishes an essential part of polarimetric radar theory.

E 5.5 Huynen's Roll Invariance

The rotation about the radar line of sight can be expressed in terms of the unitary similarity transformation with $[U_{3p}(\theta)]$ denoting the rotation transformation matrix. According to [E57] unitary congruence (consimilarity) and ordinary similarity agree for (real) rotations: $[U_{3P}(\theta)]^{-1} = [U_{3P}(\theta)]^T = [U_{3P}(-\theta)]$.

$$\langle[C_{3P}(\theta)]\rangle = [U_{3P}(\theta)]\langle[C_{3P}(AB)]\rangle[U_{3P}(\theta)]^{-1} \qquad \text{(E 5.13)}$$

and

$$[U_{3p}(\theta)] = \begin{bmatrix} 1 & 0 & 0 \\ 0 & \cos 2\theta & \sin 2\theta \\ 0 & -\sin 2\theta & \cos 2\theta \end{bmatrix}, \qquad \text{(E 5.14)}$$

so that

$$\langle[C_{3P}(\theta)]\rangle = [U_{3P}(\theta)][U_{3P}]\langle[C_{3P}(HV)]\rangle[U_{3P}]^{*T}[U_{3P}(\theta)]^{-1} = [U'_{3P}]\langle[C_{3P}(HV)]\rangle[U'_{3P}]^{*T}. \qquad \text{(E 5.15)}$$

$$[U'_{3P}] = [U_{3P}(\theta)][U_{3P}] = \exp(j\phi)\begin{bmatrix} \cos\alpha_1 & \cos\alpha_2 \exp(j\phi'_2) & \cos\alpha_3 \exp(j\phi'_3) \\ \sin\alpha_1 \cos\beta'_1 \exp(j\delta'_1) & \sin\alpha_2 \cos\beta'_2 \exp(j\delta'_2) & \sin\alpha_3 \cos\beta'_3 \exp(j\delta'_3) \\ \sin\alpha_1 \sin\beta'_1 \exp(j\gamma'_1) & \sin\alpha_2 \sin\beta'_2 \exp(j\gamma'_2) & \sin\alpha_3 \sin\beta'_3 \exp(j\gamma'_3) \end{bmatrix}$$
$$= [\bar{v}_1 \quad \bar{v}_2 \quad \bar{v}_3], \qquad \text{(E 5.16)}$$

where the $\bar{v}_i$ are the new orthonormal eigenvectors. Completing the parameterization of the 3x3 unitary matrix $[U_{3p}]$, one observes that the three parameters $(\alpha_1, \alpha_2, \alpha_3)$ remain invariant similar to the three eigenvalues $(\lambda_1, \lambda_2, \lambda_3)$. Therefore, the following important result of roll-invariance is obtained: $\underline{\kappa_3}$

$$\{\textit{span } \kappa, \textit{ entropy } H, \textit{ anisotropy } A, \textit{ mean roll-angle } \bar{\alpha}\} = \textit{Roll-Invariant} \qquad \text{(E 5.17)}$$

Thus, among the mean parameters $\bar{\alpha}, \bar{\beta}, \bar{\gamma}, \bar{\delta}$, the dominant scattering mechanism is the point scatterer associated with the eigenvector for the largest eigenvalue, which can be extracted from $[C_{3p}(HV)]$. It is apparent from above analysis that the main parameter for identifying the dominant scattering mechanisms is the mean $\bar{\alpha}$, according to the Karhunen-Loeve expansion [E53]. However, this entire concept is not unique but strongly model-based [E27] just the same as with the Huynen, Barnes-Holm, Krogager, Cameron, or any other $[S]$ matrix decomposition implementing the Pauli matrix set $\psi_P\{[\sigma_i], i=0,1,2,3\}$.

The mean roll-angle $\overline{\alpha}$ possesses some rather useful polarimetric scattering characteristics, especially applicable to rough surface scattering, where for:

(i) scattering in the geometrical optics limit: $\overline{\alpha} = 0^\circ$.

(ii) scattering in the physical optics limit to Bragg surface scattering: $0^\circ \le \overline{\alpha} \le 45^\circ$.

(iii) Bragg surface scattering (encompassing dipole scattering or single scattering by a cloud of anisotropic particles): $\overline{\alpha} = 45^\circ$. (E 5.18)

(iv) double bounce scattering between two dielectric surfaces: $45^\circ \le \overline{\alpha} \le 90^\circ$.

(v) dihedral scatter from metallic surfaces: $\overline{\alpha} = 90^\circ$.

Thus, the mean $\overline{\alpha}$ parameter estimate can be related in the first order to the underlying physical scattering mechanisms, associating polarimetric observables to physical properties of an extended scattering medium (surface). The meaning and uniqueness of the mean angle parameters $\overline{\alpha}, \overline{\beta}, \overline{\gamma}, \overline{\delta}$, still requires extensive future analysis.

E 5.6 The Cloude-Pottier $\overline{\alpha}$, H, A Feature Vector $\mathbf{f}_{3P_{CP}}(\overline{\alpha}, H, A)$

Cloude and Pottier [E57], and Pottier and Cloude [E27], introduced another most useful feature vector $\mathbf{f}_{3P_{CP}}(\overline{\alpha}, H, A)$, derived from the roll-invariance, where with $\kappa = span\{[S]\} = \text{invariant}$,

$$\mathbf{f}_{3P_{CP}} = [\overline{\alpha} \quad HA \quad (1-H)A \quad H(1-A) \quad (1-H)(1-A)]^T . \tag{E 5.19}$$

The total power κ is assumed scattered by a natural environment and collected by an orthogonally polarized antenna pair, and is an incoherent combination of the different types of scattering mechanisms, where the different types of scattering processes correspond to the

(i) $(1 - H)(1 - A)$ combination for a single dominant scattering process $(H \approx 0,\ A \approx 0)$ with $\lambda_1 \neq 0,\ \lambda_2 \approx \lambda_3 \approx 0$,

(ii) $H\ (1 - A)$ combination for random scattering $(H \approx 1,\ A \approx 0)$ with $\lambda_1 \approx \lambda_2 \approx \lambda_3 \approx 0$, (E 5.20)

(iii) HA combination for two scattering mechanism of identical probability $(H \approx 1,\ A \approx 1)$ with $\lambda_3 \approx 0$,

(iv) $(1 - H)\,A$ combination for two scattering mechanisms with one dominant process y $(0 \le H \le 0.5)$ and a second with medium probability $(A \approx 1)$ and with $\lambda_3 \approx 0$.

The information contained in this feature vector $\mathbf{f}_{3P_{CP}}(\overline{\alpha}, H, A)$, corresponds to the type of scattering process which occurs within the pixel to be classified (combination of entropy H and anisotropy A) and to the corresponding interactive physical scattering mechanism ($\overline{\alpha}$ parameter). However, it is to be noted that this approach is not unique, but strongly model-based.

E 5.7 Application of the Cloude-Pottier $[C_{3P}(\rho)]$ Decomposition for the Interpretation of Vector Scattering Mechanisms in terms of the $\overline{\alpha}$ - H Plots including Lee's Polarimetric Speckle Reduction and Polarimetric Wishart Distribution Methods

Utilizing the Pauli Coherency matrix invariants (κ, H, A) and the roll-invariant parameters $(\overline{\alpha}, \kappa, H, A)$, Cloude and Pottier introduced a scheme for parameterizing scattering processes, and an unsupervised quantitative analysis of fully polarimetric POL-SAR image data takes. This method relies on the eigenvalue analysis of the Pauli coherency matrix $\langle [C_{3p}(HV)] \rangle$, and it employs a three-level Bernoulli statistical model, as presented in Section E 3.10, to generate estimates of the average scattering matrix parameters from the given POL-SAR image data takes provided either in SLC or MLC format. The two essential parameters are the polarimetric scattering entropy H and -the mean roll angle $\overline{\alpha}$, with the anisotropy parameter A playing a secondary but not inessential role, whereas the parameters β, γ, δ seem to be all-too model-dependent and have been discarded in the formulation of the unsupervised POL-SAR image feature characterization algorithm, as discussed in detail in Cloude and Pottier [E57, E27].

E 5.8 The Unsupervised POL-SAR Image Feature Characterization Scheme: The $\overline{\alpha}$ - H Plane

By determining H, $\overline{\alpha}$ and A from $\langle [C_{3p}(HV)] \rangle$ Cloude and Pottier established the feasible region of the $\overline{\alpha}$ - H plane which lies between two bounding curves CP_I and CP_{II} on the maximal and the minimal observable $\overline{\alpha}$ - values as function of entropy H, displayed in Fig. E 5.2. These curves have been determined from H - $\overline{\alpha}$ variations for Pauli coherency matrix $\langle [C_{3p}(HV)] \rangle$ with degenerate minor eigenvalues with amplitude $m(0 \le m \le 1)$:

$$
\begin{aligned}
\left[C_{3P}(0 \le m \le 1)\right]_I &= \begin{bmatrix} 1 & 0 & 0 \\ 0 & m & 0 \\ 0 & 0 & m \end{bmatrix} \\
\left[C_{3P}(0 \le m \le 0.5)\right]_{II_s} &= \begin{bmatrix} 1 & 0 & 0 \\ 0 & 1 & 0 \\ 0 & 0 & 2m \end{bmatrix} \\
\left[C_{3P}(0.5 \le m \le 1)\right]_{II_l} &= \begin{bmatrix} 2m-1 & 0 & 0 \\ 0 & 1 & 0 \\ 0 & 0 & 1 \end{bmatrix}
\end{aligned}
\quad . \qquad \text{(E 5.21)}
$$

By evaluating the entropy $H(m)$ for the two generic curves, the upper $\left|C_{3p}(0 \le m \le 1)\right|_I$, and the lower $\left|C_{3p}(0 \le m \le 1)\right|_{II} = \left|C_{3p}(0 \le m \le 0.5)\right|_{II_s} + \left|C_{3p}(0.5 \le m \le 1)\right|_{II_l}$, result as shown in Fig. E 5.2.

All experimental results hitherto collected lie inside this feasible region of $\overline{\alpha}$ - H plane, and so classification must take place inside the limited zone of the $\overline{\alpha}$ - H space.

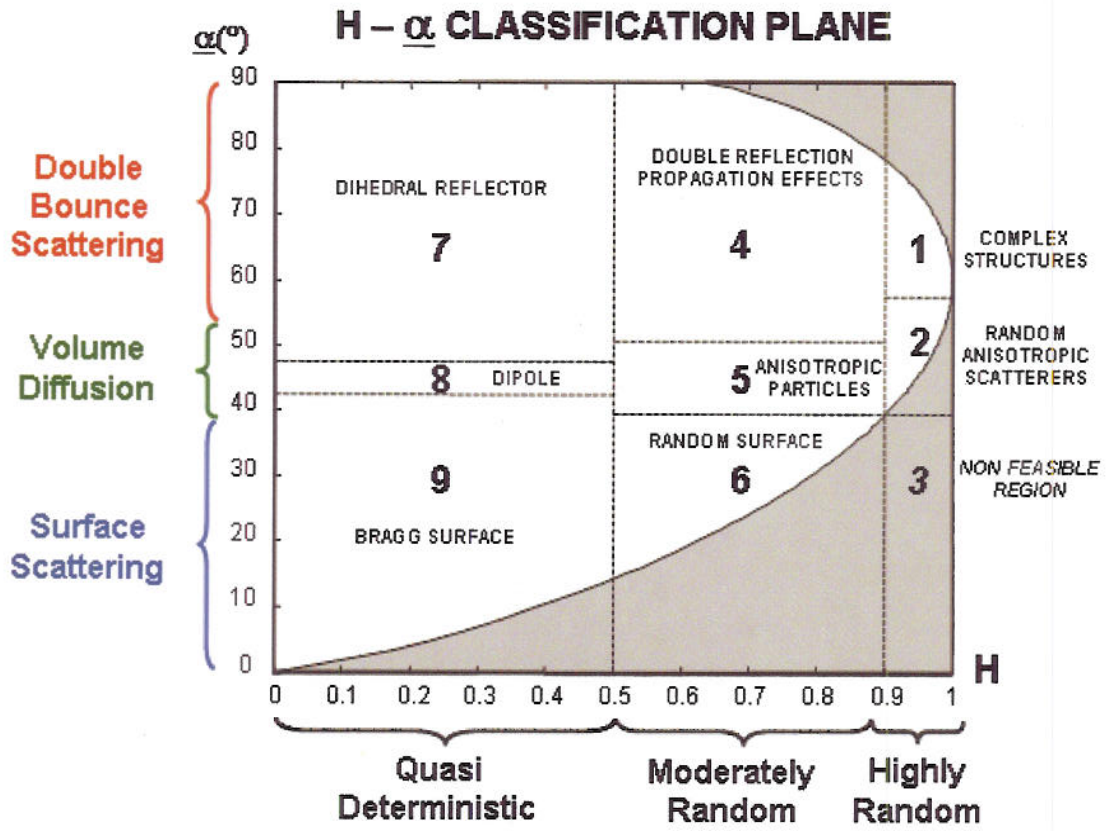

Fig. E 5.2 $H/\overline{\alpha}$ Classification

E 5.9 The Hierarchical Sub-Zoning of the Feasible $\overline{\alpha}$ - H Space

A first-order classification is achieved by sub-zoning the $\overline{\alpha}$ - H space in order to separate the POL-SAR image data into scattering mechanisms on a pixel-by-pixel basis, and attempting to relate those to physical scattering mechanisms. The separating boundaries between the sub-zones were chosen generically, i.e., based on the general scattering mechanisms, and are not dependent on a particular POL-SAR image data take set, so that an unsupervised classification procedure is achieved. In Figure E 5.1, nine zones are specified, related to specific scattering characteristics that can be measured via $\langle[C_{3p}(HV)]\rangle$, where according to [E57]:

- **Zone 9: Low Entropy Surface Scatter**
  In this zone occur low entropy scattering processes with alpha values less than 42.5°. These include GO and PO surface scattering, Bragg surface scattering and specular scattering phenomena which do not involve 180 degree phase inversions between HH and VV. Physical surfaces such as water an L and P-Bands, sea-ice at L-Band, as well as very smooth land surfaces, all fall into this category.

- **Zone 8: Low Entropy Dipole Scattering**
  In this zone occur strongly correlated mechanism which have a large imbalance between HH and VV in amplitude. An isolated dipole scatterer would appear here, as would scattering from vegetation with strongly correlated orientation of anisotropic scattering elements. The mean angle of orientation would then be given by the β parameter in $\vec{\mathbf{f}}_{3P}$. The width of this zone is determined by the ability of the Radar to measure the HH/VV ratio i.e., on the quality of the calibration.

- **Zone 7: Low Entropy Multiple Scattering Events**
  This zone corresponds to low entropy double or 'even' bounce scattering events, such as provided by isolated dielectric and metallic dihedral scatterers. These are characterized by $\overline{\alpha} > 47.5^{\circ}$. The lower bound chosen for

this zone is dictated by the expected dielectric constant of the dihedrals and by the measurement accuracy of the Radar. For $e_r > 2$, for example, and using a Bragg surface model for each surface, it follows that $\overline{\alpha} > 50^\circ$. The upper entropy boundary for these first three zones is chosen on the basis of tolerance to perturbations of first order scattering theories (which generally yield zero entropy for all scattering processes. By estimating the level of entropy change due to second and higher order events, tolerance can be built into the classifier so that the important first order process can still be correctly identified. Note also that system measurement noise will act to increase the entropy and so the system noise floor should also be used to set the boundary. $H = 0.2$ is chosen as a typical value accounting for these two effects.

- **Zone 6: Medium Entropy Surface Scatter**
  This zone reflects the increase in entropy due to changes in surface roughness and due to canopy propagation effects. In surface scattering theory the entropy of low frequency theories like Bragg scatter is zero. Likewise, the entropy of high frequency theories like Geometrical Optics is also zero. However, in between these two extremes, there is an increase in entropy due to the physics of secondary wave propagation and scattering mechanisms. Thus as the roughness/correlation length of a surface changes, its entropy will increase. Further, a surface cover comprising oblate spheroidal scatterers (leafs or discs for example) will generate an entropy between 0.6 and 0.7. In Fig. E 5.2 we set a bound of $H = 0.9$ as an upper limit for these changes.

- **Zone 5: Medium Entropy Vegetation Scattering**
  Here again we have moderate entropy but with a dominant dipole type scattering mechanism. The increased entropy is due to a central statistical distribution of orientation angle. Such a zone would include scattering from vegetated surfaces with anisotropic scatterers and moderate correlation of scatterer orientations.

- **Zone 4: Medium Entropy Multiple Scattering**
  This zone accounts for dihedral scattering with moderate entropy. This occurs for example in forestry applications, where double bounce mechanisms occur at P and L bands following propagation through a canopy. The effect of the canopy is to increase the entropy of the scattering process. A second important process in this category is urban areas, where dense packing of localized scattering centres can generate moderate entropy with low order multiple scattering dominant. The boundary between zones 4, 5, 6, and 1, 2, 3, is set as 0.9. This is chosen on the basis of the upper limit for surface, volume, and dihedral scattering before random distributions apply.

- **Zone 3: High Entropy Surface Scatter**
  This class is not part of the feasible region in H - $\overline{\alpha}$ space i.e., we cannot distinguish surface scattering with entropy $H > 0.9$. This is a direct consequence of our increasing ability to classify scattering types with increasing entropy. It is included to reinforce the idea that increasing entropy really does limit our ability to use polarimetric behavior to classify targets. Radar Polarimetry will then, in our view, be most successfully applied to low entropy problems.

- **Zone 2: High Entropy Vegetation Scattering**
  High entropy volume scattering arise when $\overline{\alpha} = 45^\circ$ and $H = 0.95$. This can arise for single scattering from a cloud of anisotropic needle like particles or from multiple scattering from a cloud of low loss symmetric particles. In both cases however, the entropy lies above 0.9, where the feasible region of H - $\overline{\alpha}$ space is rapidly shrinking. Scattering from forest canopies lies in this region, as does the scattering from some types of vegetated surfaces with random highly anisotropic scattering elements. The extreme behavior in this class is random noise i.e., no polarization dependence, a point which lies to the extreme right of Fig. E 5.2.

- **Zone 1: High Entropy Multiple Scattering**
  From $\left[C_{3p}(0 \le m \le 1)\right]_{II} = \left[C_{3p}(0 \le m \le 0.5)\right]_{II_s} + \left[C_{3p}(0.5 \le m \le 1)\right]_{II_l}$, we see that in the $H > 0.9$ region we can still distinguish double bounce mechanisms in a high entropy environment. Again such mechanisms can be observed in forestry applications or in scattering from vegetation which has a well developed branch and crown structure.

There is of course some degree of arbitrariness over where to locate the boundaries within Figure E 5.2, based for example on the knowledge of the POL-SAR systems parameters, radar calibration, measurements noise floor,

variance of parameters estimates, etc. Cloude and Pottier [E57] offered this segmentation of the H-$\overline{\alpha}$ space merely to illustrate the classification strategy and to emphasize the geometrical segmentation of physical scattering processes. It is this key feature which makes this an unsupervised, measurement-data-independent approach to the scatter feature classification problem. Nonetheless, these boundaries, although rather simply chosen, do offer sensible segmentation of experimental SAR data for well-known test sites. This again lends support to the idea that the scheme is closely linked with physical scattering mechanisms.

E 6.0 Matrix Representations

E 6.1 The Standard Kronecker Tensorial Matrix Product

Consider a matrix $[A]=\left[a_{ij}\right]$ of order (*mxn*) and a matrix $[B]=\left[b_{ij}\right]$ of order (*rxs*). The Kronecker product of the two matrices, denoted $[A]\otimes[B]$ is defined as the partitioned matrix

$$[A]\otimes[B]=\begin{bmatrix} a_{11}[B] & a_{12}[B] & \cdots & a_{1n}[B] \\ a_{21}[B] & a_{22}[B] & \cdots & a_{2n}[B] \\ \vdots & \vdots & & \vdots \\ a_{m1}[B] & a_{m2}[B] & \cdots & a_{mn}[B] \end{bmatrix} \qquad \text{(E 6.1)}$$

$[A]\otimes[B]$ is of order (*mrxns*). It has *mn* blocks; the $(i,j)th$ block is the matrix $a_{ij}[B]$ of order (*rxs*).

E 6.2 The Mueller Matrix

For the purely coherent case, the Mueller matrix $[M]$ can formally be related to the coherent Jones scattering matrix $[T]$ as

$$[M]=[1 \quad 1 \quad 1 \quad -1][A]^{T-1}([T]\otimes[T]^{*})[A]^{-1}=[A]([T]\otimes[T]^{*})[A]^{-1} \qquad \text{(E 6.2)}$$

with the 4x4 expansion matrix $[A]$ given by:

$$[A]=\begin{bmatrix} 1 & 0 & 0 & 1 \\ 1 & 0 & 0 & -1 \\ 0 & 1 & 1 & 0 \\ 0 & j & -j & 0 \end{bmatrix}$$ so that the elements M_{ij} of $[M]$ are:

$$
\begin{aligned}
M_{11} &= \tfrac{1}{2}\left(|T_{xx}|^2 + |T_{xy}|^2 + |T_{yx}|^2 + |T_{yy}|^2 \right) \\
M_{12} &= \tfrac{1}{2}\left(|T_{xx}|^2 - |T_{xy}|^2 + |T_{yx}|^2 - |T_{yy}|^2 \right) \\
M_{13} &= \mathrm{Re}\left(T_{xx}T_{xy}^* + T_{yx}T_{yy}^* \right) \\
M_{14} &= \mathrm{Im}\left(T_{xx}T_{xy}^* + T_{yx}T_{yy}^* \right) \\
M_{21} &= \tfrac{1}{2}\left(|T_{xx}|^2 + |T_{xy}|^2 - |T_{yx}|^2 - |T_{yy}|^2 \right) \\
M_{22} &= \tfrac{1}{2}\left(|T_{xx}|^2 - |T_{xy}|^2 - |T_{yx}|^2 + |T_{yy}|^2 \right) \\
M_{23} &= \mathrm{Re}\left(T_{xx}T_{xy}^* - T_{yx}T_{yy}^* \right) \\
M_{24} &= \mathrm{Im}\left(T_{xx}T_{xy}^* - T_{yx}T_{yy}^* \right) \\
M_{31} &= \mathrm{Re}\left(T_{xx}T_{yx}^* + T_{xy}T_{yy}^* \right) \\
M_{32} &= \mathrm{Re}\left(T_{xx}T_{yx}^* - T_{xy}T_{yy}^* \right) \\
M_{33} &= \mathrm{Re}\left(T_{xx}T_{yy}^* + T_{xy}T_{yx}^* \right) \\
M_{34} &= \mathrm{Im}\left(T_{xx}T_{yy}^* - T_{xy}T_{yx}^* \right) \\
M_{41} &= \mathrm{Im}\left(T_{xx}^*T_{yx} + T_{xy}^*T_{yy} \right) \\
M_{42} &= \mathrm{Im}\left(T_{xx}^*T_{yx} - T_{xy}^*T_{yy} \right) \\
M_{43} &= \mathrm{Im}\left(T_{xx}^*T_{yy} + T_{xy}^*T_{yx} \right) \\
M_{44} &= \mathrm{Re}\left(T_{xx}T_{yy}^* - T_{xy}T_{yx}^* \right)
\end{aligned}
\qquad \text{(E 6.3)}
$$

If $[T]$ is normal, i.e. $[T][T]^{T^*} = [T]^{T^*}[T]$, then $[M]$ is also normal, i.e. $[M][M]^T = [M]^T[M]$

E 6.3 The Kennaugh Matrix

Similarly, for the purely coherent case, $[K]$ can formally be related to the *coherent Sinclair matrix* $[S]$ with

$$[A]^{T-1} = \frac{1}{2}[A]^* \text{ as}$$

$$[K] = 2[A]^{T-1}([S] \otimes [S]^*)[A]^{-1} \qquad \text{(E 6.4)}$$

$$
\begin{aligned}
K_{11} &= \tfrac{1}{2}\left(|S_{xx}|^2 + |S_{xy}|^2 + |S_{yx}|^2 + |S_{yy}|^2 \right) \\
K_{12} &= \tfrac{1}{2}\left(|S_{xx}|^2 - |S_{xy}|^2 + |S_{yx}|^2 - |S_{yy}|^2 \right) \\
K_{13} &= \mathrm{Re}\left(S_{xx} S_{xy}^* + S_{yx} S_{yy}^* \right) \\
K_{14} &= \mathrm{Im}\left(S_{xx} S_{xy}^* + S_{yx} S_{yy}^* \right) \\
K_{21} &= \tfrac{1}{2}\left(|S_{xx}|^2 + |S_{xy}|^2 - |S_{yx}|^2 - |S_{yy}|^2 \right) \\
K_{22} &= \tfrac{1}{2}\left(|S_{xx}|^2 - |S_{xy}|^2 - |S_{yx}|^2 + |S_{yy}|^2 \right) \\
K_{23} &= \mathrm{Re}\left(S_{xx} S_{xy}^* - S_{yx} S_{yy}^* \right) \\
K_{24} &= \mathrm{Im}\left(S_{xx} S_{xy}^* - S_{yx} S_{yy}^* \right) \\
K_{31} &= \mathrm{Re}\left(S_{xx} S_{yx}^* + S_{xy} S_{yy}^* \right) \\
K_{32} &= \mathrm{Re}\left(S_{xx} S_{yx}^* - S_{xy} S_{yy}^* \right) \\
K_{33} &= \mathrm{Re}\left(S_{xx} S_{yy}^* + S_{xy}^* S_{yx} \right) \\
K_{34} &= \mathrm{Im}\left(S_{xx} S_{yy}^* + S_{xy}^* S_{yx} \right) \\
K_{41} &= \mathrm{Im}\left(S_{xx} S_{yx}^* + S_{xy} S_{yy}^* \right) \\
K_{42} &= \mathrm{Im}\left(S_{xx} S_{yx}^* - S_{xy} S_{yy}^* \right) \\
K_{43} &= \mathrm{Im}\left(S_{xx} S_{yy}^* - S_{yx} S_{xy}^* \right) \\
K_{44} &= -\mathrm{Re}\left(S_{xx} S_{yy}^* - S_{xy} S_{yx}^* \right)
\end{aligned}
\qquad \text{(E 6.5)}
$$

If $[S]$ is symmetric, $S_{xy} = S_{yx}$, then $[K]$ is symmetric, $K_{ij} = K_{ji}$, so that for the symmetric case

$$K_{11} = \tfrac{1}{2}\left(\left| S_{xx} \right|^2 + 2\left| S_{xy} \right|^2 + \left| S_{yy} \right|^2 \right) = \tfrac{1}{2} Span[S]$$

$$K_{12} = 0$$

$$K_{13} = 0$$

$$K_{14} = 0$$

$$K_{21} = 0$$

$$K_{22} = \tfrac{1}{2}\left(\left| S_{xx} \right|^2 - 2\left| S_{xy} \right|^2 + \left| S_{yy} \right|^2 \right)$$

$$K_{23} = \mathrm{Re}\left(S_{xx} S_{xy}^* - S_{yx} S_{yy}^* \right)$$

$$K_{24} = 0$$

$$K_{31} = 0$$

$$K_{32} = 0$$

$$K_{33} = \left| S_{xy} \right|^2 + \mathrm{Re}\left(S_{xx} S_{yy}^* \right)$$

$$K_{34} = 0$$

$$K_{41} = 0$$

$$K_{42} = 0$$

$$K_{43} = 0$$

$$K_{44} = \left| S_{xy} \right|^2 - \mathrm{Re}\left(S_{xx} S_{yy}^* \right)$$

(E 6.6)

with

$$K_{11} = \sum_{i=2}^{4} K_{ii} = \frac{1}{2} \sum_{i=1}^{4} K_{ii} = \frac{1}{2} \sum_{i=1}^{2} \lambda_i([S]^*[S]) = Span[S]$$

E 7.0 Summary

This appendix, which is based on the M. Sc. Thesis of Jorge J. Morisaki, attempted to develop a cohesive presentation on the fundamentals of radar polarimetry using exclusively the standard vector formulation developed by Sinclair [E2, E3], Kennaugh [E4, E5], Boerner [E13, E14, E15], and Mott [E76]. The selected material includes basic formulations of the polarization vector, and places major emphasis on the complex polarization ratio formulations first explored by Boerner et al. as summarized in [E14, E15] and its relation to the Poincaré polarization sphere mapping [E77, E78]. The complete set of the basic polarimetric scattering matrices for the optical FSA (Forward Scattering Alignment), the bistatic radar BSA (Backscattering Alignment), and the monostatic MSA (Monostatic Scattering Alignment) scattering scenarios were introduced together with the pertinent polarization vector and matrix transformations, separately for optical versus radar polarimetry.

Thereupon, the polarimetric radar optimization approach of Kennaugh was introduced together with the three-stage procedure [E4, E14] for identifying the three pairs of bi-orthogonal canonical optimal polarization states. These states define the spinorial polarization fork together with its polarimetric power density and polarimetric phase correlation plots, using the resulting Huynen polarization fork together with the van Zyl polarimetric power density and Agrawal polarimetric phase correlation signatures, respectively. The polarimetric properties of isolated point scatterers were presented and reviewed.

The properties of slightly incoherent scatterers of polarization factor $\rho \geq 0.7$ were presented by extending the coherent polarimetric approach of Kennaugh et al, proving its invalidity for the general partially coherent case. This then led to the introduction of the lexicographic and Pauli-based covariance matrices for dealing with the general partially polarized distributed scatterer case. For this purpose, the Cloude-Pottier polarimetric entropy H, angle $\overline{\alpha}$, and anisotropy A descriptors were introduced and interpreted for some specific canonical examples. Finally the polarimetric speckle reduction filter of Lee with implementation of the Wishart distribution functions was briefly summarized, which completed the first attempt of developing a cohesive presentation of the fundamental polarimetric radar theory.

E 8.0 References

E1. Boerner, W-M., "Recent advances in extra-wide-band polarimetry, interferometry and polarimetric interferometry in synthetic aperture remote sensing, and its applications," *IEE Proc.-Radar Sonar Navigation, Special Issue of the EUSAR-02,* vol. 150, no. 3, June 2003, pp. 113-125

E2. Sinclair, G., "Modification of the Radar Target Equation for Arbitrary Targets and Arbitrary Polarization", Report 302-19, Antenna Laboratory, The Ohio State University Research Foundation, 1948.

E3. Sinclair, G., "The Transmission and Reception of Elliptically Polarized Waves", *Proceedings of the IRE*, vol. 38, no. 2, pp. 148-151, 1950.

E4. Kennaugh, E. M., "Polarization Properties of Radar Reflections", Master's thesis, Ohio State University, Columbus, March 1952.

E5. Kennaugh, E.M., "Effects of the Type of Polarization on Echo Characteristics", Reports 381-1 to 394-24, Antenna Laboratory, The Ohio State University Research Foundation, 1949-1954.

E6. Deschamps, G.A., "Geometrical Representation of the Polarization of a Plane Electromagnetic Wave", *Proceedings of the IRE*, vol.39, no.5, pp. 540-544, 1951.

E7. Graves, C.D., "Radar Polarization Power Scattering Matrix", *Proceedings of the IRE*, vol. 44, no. 5, pp. 248-252, 1956.

E8. Copeland, J.R., "Radar Target Classification by Polarization Properties", *Proceedings of the IRE*, vol. 48, no. 7, pp. 1290-1296, 1960.

E9. Huynen, J.R., "Phenomenological Theory of Radar Targets", Ph.D. thesis, University of Technology, Delft, The Netherlands, December 1970.

E10. Poelman, A.J. and J.R.F. Guy, 1985, "Polarization information utilization in primary radar"; in Boerner, W-M. et al. (eds), 1985, *"Inverse Methods in Electromagnetic Imaging"*, Proceedings of the NATO-Advanced Research Workshop, (18-24 Sept. 1983, Bad Windsheim, FR Germany), Parts 1&2, NATO-ASI C-143, (1,500 pages), D. Reidel Publ. Co., Part 1, pp. 521-572.

E11. Poelman, A.J. and K.J. Hilgers, 1988, "Effectiveness of multi-notch logic-product polarization filters for countering rain clutter", in *Proceedings of the NATO Advanced Research Workshop on Direct and Inverse Methods in Radar Polarimetry*, W.-M. Boerner et al (eds), Bad Windsheim, Germany, September 18-24, 1988; Kluwer Academic Publishers, Dordrecht 1992; NATO ASI Series C-350, Part 2, pp. 1309-1334.

E12. Root, L.W., ed., 1982, *Proceedings of the First Workshop on Polarimetric Radar Technology*, GACIAC, Chicago, IL: 295 p. See also Proceedings of the second and third workshops, 1983 and 1989 respectively, with the same publisher.

E13. Boerner, W-M, and M.B. El-Arini, "Polarization Dependence in Electromagnetic Inverse Problem", *IEEE Transactions on Antennas and Propagation*, vol.29, no. 2, pp. 262-271, 1981.

E14. Boerner, W-M, (ed.), *Direct and Inverse Methods in Radar Polarimetry*, NATO ASI Series C, Math. and Phys. Science, Kluwer Academic Publishers, Netherlands, 1985.

E15. Boerner, W-M, (ed.), *Inverse Methods in Electromagnetic Imaging*, NATO ASI Series C, Math. and Phys. Science, Kluwer Academic Publishers, Netherlands, 1992.

E16. Boerner, W-M., "Use of Polarization in Electromagnetic Inverse Scattering", Radio Science, Vol. 16(6) (Special Issue: 1980 Munich Symposium on EM Waves), pp. 1037-1045, Nov./Dec. (1981b).

E17. Boerner, W-M, "Polarimetry in Remote Sensing and Imaging of Terrestrial and Planetary Environments", Proceedings of Third International Workshop on Radar Polarimetry (JIPR-3, 95), IRESTE, Univ.-Nantes, France, pp. 1-38, 1995b.

E18. Boerner, W-M., 'Recent Advances in Polarimetric Interferometric SAR Theory & Technology and its Application' ESA-CEOS-MRS'99, SAR Cal-Val-Workshop, CNES, Toulouse, FR, 1999 Oct. 25-29

E19. Boerner, W-M, H. Mott, E. Lüneburg, C. Livingston, B. Brisco, R. J. Brown and J. S. Paterson with contributions by S.R. Cloude, E. Krogager, J. S. Lee, D. L. Schuler, J. J. van Zyl, D. Randall P. Budkewitsch and E. Pottier, "Polarimetry in Radar Remote Sensing: Basic and Applied Concepts", Chapter 5 in F.M. Henderson, and A.J. Lewis, (eds.), Principles and Applications of Imaging Radar, Vol. 2 of Manual of Remote Sesning, (ed. R.A. Reyerson), 3rd Ed., John Willey & Sons, New York, 1998.

E20. Boerner, W-M, S.R. Cloude, and A. Moreira, 2002, "User collision in sharing of electromagnetic spectrum: Frequency allocation, RF interference reduction and RF security threat mitigation in radio propagation and passive and active remote sensing", *URSI-F Open Symp.*, Sess. 3AP-1, 2002 Feb. 14, Garmisch-Partenkirchen, Germany.

E21. Azzam, R. M. A. and N. M. Bashara, 1977, *Ellipsometry and Polarized Light*, North Holland, Amsterdam: 539 p.

E22. Beckmann, P., 1968. *The Depolarization of Electromagnetic Waves*, The Golem Press, Boulder, CO: 214 p.

E23. Chipman, R. A., and J. W. Morris, eds., "Polarimetry: Radar, Infrared, Visible, Ultraviolet, X-Ray", Proc. SPIE-1317, 1990 (also see SPIE Proc. 891, 1166, 1746, 1988, 1989, and 3121).

E24. Jones, R., 1941, "A new calculus for the treatment of optical systems, I. Description and discussion", J. Opt. Soc. Am., 31 (July 1941), pp. 488-493; "II. Proof of the three general equivalence theorems, ibid. pp. 493-499; III. The Stokes theory of optical activity", ibid. pp. 500-503; ibid. 32 (1941), pp. 486-493 , ibid. 37 (1947), pp. 107-110 (See also Swindell, W., 1975, *Polarized Light*, Halsted Press/John Wiley & Sons, Stroudsburg, PA: pp. 186-240).

E25. Boerner, W-M, C. L. Liu, and Zhang, "Comparison of Optimization Processing for 2x2 Sinclair, 2x2 Graves, 3x3 Covariance, and 4x4 Mueller (Symmetric) Matrices in Coherent Radar Polarimetry and its Application to Target Versus Background Discrimination in Microwave Remote Sensing", EARSeL Advances in Remote Sensing, Vol. 2(1), pp. 55-82, 1993.

E26. Cloude S.R., "Polarimetry in Wave Scattering Applications", Chapter 1.6.2 in SCATTERING, Eds R Pike, P Sabatier, Academic Press, to be published December 1999

E27. Cloude, S.R. and E. Pottier, "A review of target decomposition theorems in radar polarimetry", IEEE Trans. GRS, vol. 34(2), pp. 498-518, Mar. 1996.

E28. Cloude, S. R., 1992, Uniqueness of Target Decomposition Theorems in Radar Polarimetry. *Direct and Inverse Methods in Radar Polarimetry*, Part 1, Boerner, W-M, ed. Kluwer Academic Publishers, Dordrecht, The Netherlands: 267-296.

E29. Cloude, S.R., Polarimetry: The Characterization of Polarimetric Effects in EM Scattering, Ph.D. thesis, University of Birmingham, Faculty of Engineering, Birmingham, England/UK, Oct. 1986.

E30. Krogager, E., Decomposition of the Sinclair Matrix into Fundamental Components with Application to High Resolution Radar Target Imaging, *Direct and Inverse Methods in Radar Polarimetry*, Part 2, Boerner, W-M., ed. Kluwer Academic Publishers, Dordrecht, The Netherlands: 1459-1478, 1992.

E31. Boerner, W-M. and A-Q. Xi, 1990, The Characteristic Radar Target Polarization State Theory for the Coherent Monostatic and Reciprocal Case Using the Generalized Polarization Transformation Ratio Formulation, *AEU*, 44 (6): X1-X8.

E32. Bebbington, D.H.O, "The Expression of Reciprocity in Polarimetric Algebras", Progress in Electromagnetics Research Symposium (PIERS'98), *Procs. Fourth Int'l. Workshop on Radar Polarimetry (JIPR-98)*, pp. 9-18, IRESTE, Nantes, July 1998.

E33. Czyz, Z.H., "Basic Theory of Radar Polarimetry - An Engineering Approach", Prace PIT, No.119, 1997, Warsaw, Poland, pp.15-24.

E34. Born, M. and E. Wolf, *Principles of Optics*, 3rd ed. Pergamon Press, New York: 808 p., 1965.

E35. Goldstein, D. H. and R. A. Chipman, "Optical Polarization: Measurement, Analysis, and Remote Sensing", Proc. SPIE-3121, 1997 (see Proc. SPIE 891, 1166, 1317, 1746, 1988, 1989: OPT-POL).

E36. Krogager, E. and W-M. Boerner, On the importance of utilizing complete polarimetric information in radar imaging and classification, AGARD Symposium: Remote Sensing - A Valuable Source of Information, Toulouse, France, 1996 April 22-25, *AGARD Proc.*, (528 pp.), pp. 17.1 - 17.12.

E37. Krogager, E., Aspects of Polarimetric Radar Imaging, Ph.D. thesis, Technical University of Denmark (TUD), Electromagnetics Institute, Lyngby, DK, March 1993.

E38. Krogager, E., Comparison of Various POL-RAD and POL-SAR Image Feature Sorting and Classification Algorithms, Journées Internationales de la Polarimétrie Radar, Proc. JIPR'98, pp. 77-86, Nantes, France, 13-17 July, 1998.

E39. Krogager, E., and Z.H. Czyz, "Properties of the Sphere, Di-plane and Helix Decomposition" Proc. of 3rd International Workshop on Radar Polarimetry, IRESTE, University of Nantes, France, pp. 106-114, April 1995.

E40. Krogager, E., W.-M. Boerner, S.N. Madsen; "Feature-Motivated Sinclair Matrix (sphere/di-plane/helix) Decomposition and Its Application to Target Sorting For Land Feature Classification," SPIE-3120, 144-154, 1997..

E41. Lee, J. S, M R Grunes, T L Ainsworth, L J Du, D L Schuler, S R Cloude, "Unsupervised Classification using Polarimetric Decomposition and the Complex Wishart Distribution", IEEE Transactions Geoscience and Remote Sensing, Vol 37/1, No. 5, p 2249-2259, September 1999

E42. Lee, J.S. and M.R. Grunes, Polarimetric SAR Speckle Filtering and Terrain Classification-An Overview 26p., Book Ch. in XX, World Sci. Publ., Singapore, 1999

E43. Lee, J.S., "Speckle suppression and analysis for synthetic aperture radar images", *SPIE Optical Engineering*, Vol. 25 No. 5, pp. 636-643, May 1986.

E44. Lee, J-S., M.R. Grunes and R. Kwok, Classification of multi-look polarimetric SAR imaging based on complex Wishart distributions, *Int'l Journal of Remote Sensing*, Vol. 15(11), pp. 2299-2311, 1994.

E45. Boerner W-M., *'Report on POL & POL-IN Session'*, ESA-CEOS-MRS'99, SAR Cal-Val-Workshop., CNES Toulouse, FR, 1999 Oct. 29.

E46. Tragl, K. "Polarimetric Radar Back-scattering from Reciprocal Random Targets", IEEE Trans. GRS-28(5), pp. 856 - 864, Sept. 1990 (see Dr. -Ing. Thesis, 1989).

E47. Novak L.M., S. D. Halversen, G. J. Owirka, M. Hiett, "Effects of Polarization and Resolution on SAR ATR," IEEE Trans. AES, Vol. 33(1), pp. 102-116, Jan. 1997.

E48. Novak, L.M., and C.M. Netishen, "Polarimetric Synthetic Aperture Radar Imaging", *Int'l Journal of Imaging Systems and Technology*, John Wiley & Sons, New York, NY, vol. 4, pp. 306-318, 1992.

E49. Novak, L.M., and M.C. Burl, "Optimal Speckle Reduction in Polarimetric SAR Imagery" *IEEE Trans. AES*, vol. 26, no.2, pp. 293-305, 1990.

E50. Novak, L.M., and M.C. Burl, and W.W. Irving, "Optimal Polarimetric Processing for Enhanced Target Detection", *IEEE Trans. AES*, vol. 29, no.1, pp. 234-244, 1993.

E51. Novak, L.M., and S.R. Hesse, "Optimal Polarizations for Radar Detection and Recognition of Targets in Clutter", *Proceedings, 1993 IEEE National Radar Conference*, Lynnfield, MA, April 20-22, 1993, pp. 79-83.

E52. Lüneburg, E., Radar polarimetry: A revision of basic concepts, in "Direct and Inverse Electromagnetic Scattering", H. Serbest and S. Cloude, eds., Pittman Research Notes in Mathematics Series 361, Addison Wesley Longman, Harlow, U.K., 1996, pp. 257 – 275.

E53. Lüneburg, E., "Principles of Radar Polarimetry", Proceedings of the IEICE Trans. on the Electronic Theory, Vol. E78-C, no. 10, pp. 1339-1345, 1995 (see also: Lüneburg, E., Polarimetric target matrix decompositions and the 'Karhunen-Loeve expansion', *IGARSS'99, Hamburg, Germany*, June 28-July 2, 1999).

E54. Lüneburg, E., Comments on "The Specular Null Polarization Theory" IEEE Trans. Geoscience and Remote Sensing, Vol. 35, 1997, pp. 1070 – 1071.

E55. Lüneburg, E., V. Ziegler, A. Schroth, and K. Tragl, "Polarimetric Covariance Matrix Analysis of Random Radar Targets", pp.27.1 - 27.12, in Proc. NATO-AGARD-EPP Symposium on Target and Clutter Scattering and Their Effects on Military Radar Performance, Ottawa.Canada,1991 May 6 – 10 (also see: Lüneburg, E., M. Chandra, and W.-M. Boerner, Random target approximations, *Proc. PIERS Progress in Electromagnetics Research Symposium, Noordwijk, The Netherlands, July 11-15, 1994, CD Kluwer Publishers*, 1366-1369).

E56. Cloude, S.R., Potential New Applications of Polarimetric Radar / SAR Interferometry, Proc. On Advances in Radar methods - with a view towards the Twenty First Century, EC-JRC/SAI (ISPRA) Hotel Dino, Baveno, Italy, 1998 July 20-22, (Proc. to be published in Fall 98)

E57. Cloude S.R. and E. Pottier, "An Entropy-Based Classification Scheme for Land Applications of Polarimetric SAR", IEEE Trans GRS-35(1), 68-78, 1997

E58. Kostinski, A.B., B.D. James, and W-M. Boerner, 1988, Polarimetric Matched Filter for Coherent Imaging, *Canadian Journal of Physics*, 66: 871-877.

E59. Krogager, E., S.R. Cloude, J.-S. Lee, T.L. Ainsworth, and W.-M. Boerner, Interpretation of high resolution polarimetric SAR data, Journées Internationales de la Polarimétrie Radar, Proc. JIPR'98, pp. 165-170, Nantes, France, 13-17 July, 1998.

E60. Kozlov, A. I., "Radar Contrast between Two Objects", *Radioelektronika*, 22 (7): 63-67, 1979.

E61. Mott, H. and W-M. Boerner, editors, "Radar Polarimetry, SPIE's Annual Mtg., Polarimetry Conference Series", 1992 July 23 - 24, San Diego Convention Center, SPIE Conf. Proc. Vol. 1748, 1992

E62. Boerner, W-M., B. Y. Foo, and H. J. Eom, 1987, Interpretation of the Polarimetric Co-Polarization Phase Term (φ_{HH} - φ_{VV}) in High Resolution SAR Imaging Using the JPL CV-990 Polarimetric L-Band SAR Data, Special IGARSS Issue of *IEEE Transactions on Geoscience and Remote Sensing*, 25 (1): 77-82.

E63. Freeman, A. and S.T. Durden, "A Three-Component Scattering Model for Polarimetric SAR Data", IEEE Trans. GRS, Vol. 36(3), pp. 963-973, 1998.

E64. Lee, J.S., M.R. Grunes and W.M. Boerner, "Polarimetric Property Preserving in SAR Speckle Filtering," Proceedings of SPIE, Vol. 3120, 236-242, San Diego, 1997.

E65. van Zyl, J. J. "Application of Cloude's Target Decomposition Theorem to Polarimetric Imaging Radar Data", SPIE Proceedings (H. Mott, W-M Boerner eds.), Vol. 1748, San Diego, CA, 23-24 July 1992.

E66. van Zyl, J. J., "An Overview of the Analysis of Multi-frequency Polarimetric SAR Data", Proceedings of the US-AU PACRIM Significant Results Workshop, MHPCC, Kihei, Maui, HI, 1999 August 24 - 26 (10 pages).

E67. Schuler, D.L., J.S. Lee, G. De Grandi, "Measurement of Topography using Polarimetric SAR Images," *IEEE Trans. on Geoscience and Remote Sensing*, vol. 34, no.5, pp. 1266-1277, 1996.

E68. Schuler, D.L, J.S. Lee, and T.L. Ainsworth, "Topographic mapping using polarimetric SAR data", *International Journal of Remote Sensing*, vol. 19(1), pp 141-160, 1988.

E69. Schuler, D.L., J.S. Lee, T.L. Ainsworth, and M.R. Grunes, "Terrain topography measurement using multi-pass polarimetric synthetic aperture radar data," *Radio Science*, vol. 35, no.3, pp. 813-832, May-June 2000.

E70. Bamler, R. and P. Hartl, "Synthetic Aperture Radar Interferometry", State of the Art Review, Inverse Problems, Vol. 14, pp. R1-R54, IOC Publications, Bristol, UK, 1998.

E71. Zebker, H.A. and J.J. van Zyl, Imaging Radar Polarimetry: A Review, *Proceedings of the IEEE*, Vol. 79, pp. 1,583-1,606, 1991.

E72. Madsen, S.N and H.A. Zebker, "Imaging Radar Interferometry," Chapter 6 (pp. 359-380) in *Manual of Remote Sensing*, Vol. 2, Principles and Applications of Imaging Radar, F. M. Henderson and A. J. Lewis, Eds., American Society for Photogrammetry and Remote Sensing, Wiley, New York, 940 p, 1998

E73. Boerner, W-M., et al., (Guest Eds.), IEEE Transactions on the Antennas & Propagation Society, Vol. 29(2), Special Issue, Inverse Methods in Electromagnetics, (417 pages) 1980-81(1981a).

E74. Dubois, P.C. and L. Norikane, 1987, "Data Volume Reduction for Imaging Radar Polarimetry", *Proceedings of IGARSS'87*, pp. 691-696, 1987.

E75. Lee, J.S., K.P. Papathanassiou, T. L. Ainsworth, M.R. Grunes and A. Reigber, "A New Technique for Noise Filtering of SAR Interferometric Phase Images", IEEE Trans. GRS Vol. 36 , No.5 pp. 1456-1465.

E76. Mott, H., Antenna*s for Radar and Communications, A Polarimetric Approach*, John Wiley & Sons, New York, 1992, 521 p.

E77. Chan, C-Y., *Studies on the Power Scattering Matrix of Radar Targets*, M.S. thesis, University of Illinois, Chicago, Illinois, 1981.

E78. Agrawal, A. P., "A Polarimetric Rain Back-scattering Model Developed for Coherent Polarization Diversity Radar Applications", Ph.D. thesis, University of Illinois, Chicago, IL, December 1986.

E79. van Zyl, J. J. "On the Importance of Polarization in Radar Scattering Problems", Ph.D. thesis, California Institute of Technology, Pasadena, CA, December 1985.

E80. Papathanassiou, K. P., "Polarimetric SAR Interferometry", Ph.D. thesis, Tech. Univ. Graz, 1999.

E81. Boerner, W-M., W-L. Yan, A-Q. Xi and Y. Yamaguchi, "On the Principles of Radar Polarimetry (Invited Review): The Target Characteristic Polarization State theory of Kennaugh, Huynen's Polarization Fork Concept, and Its Extension to the Partially Polarized Case", IEEE Proc., Special Issue on Electromagnetic Theory, Vol. 79(10), pp. 1538-1550, Oct. 1991.

E82. Xi, A-Q and W-M. Boerner, "Determination of the Characteristic Polarization States of the target scattering matrix [S(AB)] for the coherent Monostatic and Reciprocal Propagation Space Using the Polarization Transformation Ratio Formulation", JOSA-A/2, 9(3), pp. 437-455, 1992.

E83. van Zyl, J.J. and H. A. Zebker, 1990, Imaging Radar Polarimetry, *Polarimetric Remote Sensing, PIER 3*, Kong, J. A., ed. Elsevier, New York: 277-326.

E84. van Zyl, J. J., H. Zebker, and C. Elachi, "Imaging Radar Polarization Signatures: Theory and Application", Radio Science, vol. 22, no. 4, pp. 529-543, 1987.

E85. Pellat-Finet, P., "An introduction to a vectorial calculus for polarization optics", *Optik*, vol. 84 (5), pp. 169 – 175, 1990: Pellat-Finet, P., 1991, "Geometrical approach to polarization optics I: geometrical structure of polarized light", *Optik*, vol. 87, pp. 68-77.

E86. Stratton, J.A., *Electromagnetic Theory*, McGraw-Hill, New York, 1941

E87. Ulaby, F. T. and C. Elachi, Editors, Radar Polarimetry for Geo-science Applications, Artech House, Inc., Norwood, MA, 1990, 364p.

E88. Lee, J.S., W-M Boerner, T. Ainsworth, D. Schuler, I. Hajnsek, and E. Lüneburg, "A Review of Polarimetric SAR Algorithms and its Applications", *Chinese Journal of Remote Sensing*, Chong-Li, Taiwan, in print, 2003.

E89. Kostinski, A.B. and W.-M. Boerner, "On the polarimetric contrast optimization", *IEEE Trans. Antennas Propagt.*, vol. AP-35(8), pp. 988-991, 1987.

E90. Agrawal, A. B. and W.-M. Boerner, "Redevelopment of Kennaugh's target characteristic polarization state theory using the polarization transformation ratio formalism for the coherent case", *IEEE Trans. Geosci. Remote Sensing*, AP-27(1), pp. 2-14, 1989.

E91. Cameron, W.L., "Simulated polarimetric signatures of primitive geometrical shapes", *IEEE Trans. Geoscience Rem. Sens.*, 34, 3 793-803, 1996.

E92. Pottier, E., *Contribution à la Polarimétrie Radar: de l'approche fondamentale aux applications*, Habilitation a Diriger des Recherches; Dr. Ing. habil., Ecole Doctorale Sciences pour l'Ingenieur de Nantes, Université de Nantes, l'IRESTE, La Chantrerie, Rue Pauc, BP 60601, F-44306 NANTES CED-3, 98-11-12, 1998 ; ibid., *"Radar Polarimetry : Towards a future Standardization"*, Annales des Télécommunications, vol 54 (1-2), pp 137-141, Janvier 1999.

E93. Ferro-Famil, L.E., E. Pottier and J.S. Lee, "Unsupervised Classification of Multifrequency and Fully Polarimetric SAR Images Based on H/A/Alpha-Wishart Classifier," *IEEE Trans. GRS*, vol. 39(11), pp. 2332-2342, 2001.

E94. Raney, R. K., "Processing Synthetic Aperture Radar Data", *Int'l JRS*, Vol. 3(3), pp. 243-257, 1982.

E95. Cloude, S.R. and K. P. Papathanassiou, "Polarimetric optimization in radar interferometry", *Electronic Letters*, vol. 33(13), pp. 1176-1178, 1997.

E96. Cloude, S.R. and K. P. Papathanassiou, Coherence optimization in polarimetric SAR interferometry, IGARSS'97Proc., Singapore, 1997 Aug. 03-09,Vol. IV, pp. 1932-1934, 1997.

E97. Papathanassiou, K.P. and S.R. Cloude, "Single-baseline polarimetric SAR interferometry", *IEEE Trans. GRS*. 39 (6), pp. 2352-2363, 2001.

E98. Papathanassiou, K.P. and J.R. Moreira, "Interferometric analysis of multi-frequency and multi-polarization SAR data", *Proc. IGARSS '96*, Lincoln, NE, Vol. III, pp. 1227-1229, 1996.

E99. Reigber, A., *"Polarimetric SAR Tomography"*, Dissertation, University of Stuttgart, 2001 October 15 (ISSN 1434-8454, ISRN DLR-FB-2002-02), 2001.

E100. Reigber A., A. Moreira, "First Demonstration of SAR Tomography using Polarimetric Airborne SAR Data". *IEEE Trans. GRS*, vol. 38 (5-1), pp 2142 -2152, 2000.

E101. Reigber, A., A. Moreira and K.P. Papathanassiou, "First demonstration of airborne SAR tomography using multi-baseline data". *Proc. IGARSS-99* (06-28_07-02), A03_10:50, Hamburg, Germany, 1999.

E102. IEEE 1983 *Standard Test Procedures for Antennas*, ANSI/IEEE-Std. 149-1979, IEEE-Publishing, ISBN 0-471-08032-2 (also see: Number 145-1983: Definitions of Terms for Antennas, *IEEE Transactions on Antennas and Propagation*, AP-31(6), November 1983, pp. II – 26).

E103. Deschamps, G. A. and P. E. Mast, 1973, Poincaré Sphere Representation of Partially Polarized Fields, *IEEE Transactions on Antennas and Propagation*, 21 (4): 474-478.

E104. Eaves, J. L. and E. K. Reedy, eds., 1987, *Principles of Modern Radar*, Van Nostrand Reinhold Company, New York: 712 p.

E105. Cloude, S.R., E. Pottier, W-M Boerner, "Unsupervised Image Classification using the Entropy/Alpha/Anisotropy Method in Radar Polarimetry", *NASA-JPL, AIRSAR-02 Workshop*, Double Tree Hotel, Pasadena, CA, 2002 March 04-06.

E106. Pottier, E., *"La Polarimétrie Radar Appliquée à la Télédétection"* Ecole Supérieure des Télécommunications de Tunis, Tunis, Tunisie, 1999 December 17.

E107. Stokes, G.G., "On the composition and resolution of streams of polarized light from different sources", *Trans. Cambridge Philos. Soc.*, vol. 9, pp. 399-416, 1852 (also see: Stokes, G. G., 1901, Stokes's Mathematical and Physical Papers, Univ. Press, Cambridge).

E108. Poincaré, H., *Théorie Mathématique de la Lumière*, Georges Carre, Paris, 310 p, 1892.

E109. Zhivotovsky, L. A., Optimum Polarization of Radar Signals, *Radio Engineering and Electronic Physics*: 630-632, 1973, ibid. "The Polarization Sphere Modification to Four Dimensions for the Representation of Partially Polarized Electromagnetic Waves", Radiotechnica i Electronica, vol. 30, no. 8, pp. 1497-1504, 1985.

E110. Czyz, Z.H., Czyz, Z.H., "Advances in the Theory of Radar Polarimetry," Prace PIT, No.117, Vol. XLVI, 1996, Warsaw, Poland, pp.21-28.

E111. Misner, C.W., K.S. Thorne and A Wheeler, 1997, *Gravitation*, W.H. Freeman & Co., New York (twentieth printing: 1997)

E112. Graham, A., *Kronecker Products and Matrix Calculus: with Applications*, New York: Ellis Horwood Ltd (John Wiley & Sons), 130 p, 1981.

E113. Yan, W-L., et al, and W-M. Boerner, "Optimal polarization state determination of the Stokes reflection matrices [M] for the coherent case, and of the Mueller matrix [M] for the partially polarized case", *JEWA*, vol. 5(10), pp. 1123-1150, 1991.

E114. Ziegler, V., E. Lüneburg, and A. Schroth, Mean Backscattering Properties of Random Radar Targets: A Polarimetric Covariance Matrix Concept, *Proceedings of IGARSS'92*, May 26-29, Houston Texas, pp. 266-268, 1992.

E115. Priestley, M. B., *Spectral Analysis and Time Series, Volumes 1 & 2, Univariate and Multivariate Series, Prediction and Control*, Academic Press, New York, 1981.

E116. Takagi, T., On an algebraic problem related to an analytical theorem of Caratheodory and Fejer and on an allied theorem of Landau, Japanese J. Math., 1, pp. 83-93, 1927

E117. Horn, R. A. and Ch. R. Johnson, Topics in Matrix Analysis, Cambridge University Press, New York, 1991; ibid: Matrix Analysis, Cambridge University Press, New York, 1985

E118. Kennaugh, E.M., "Polarization dependence of radar cross sections - A geometrical interpretation", *IEEE Trans. Antennas Propag.*, (Special Issue on Inverse Methods in Electromagnetic Scattering, W.-M. Boerner, A; K. Jordan, I. W. Kay, Gust Editors), vol. AP-29(3), pp. 412-414, 1981.

E119. Yang, J., Y. Yamaguchi, H. Yamada, M. Sengoku, S. M. Lin, "Stable Decomposition of Mueller Matrix", IEICE Trans. Comm., vol. E81-B(6), pp. 1261-1268, June 1998
E120. Yang, J., Yoshio Yamaguchi, Hiroyoshi Yamada, "Co-null of targets and co-null Abelian group," Electronics Letters, vol.35, no.12, pp.1017-1019, June 1999.
E121. Yang, J., Yoshio Yamaguchi, Hiroyoshi Yamada, Masakazu Sengoku, Shi -Ming Lin, Optimal problem for contrast enhancement in polarimetric radar remote sensing, J-IEICE Trans. Commun., vol.E82-B, no.1, pp.174-183, Jan. 1999
E122. Bogorodsky, V.V., D.B. Kanareykin, and A.I. Kozlov, "Polarization of the Scattered Radio Radiation of the Earth's Covers", Leningrad: Gidrometeorizdat, 1981 (in Russian).
E123. Kanareykin, D.B., N.F. Pavlov, U.A. Potekhin, "The Polarization of Radar Signals", Moscow: Sovyetskoye Radio, Chap. 1-10 (in Russian), 1986, (English translation of Chapters 10-12: "Radar Polarization Effects", CCM Inf. Corp., G. Collier and McMillan, 900 Third Ave., New York, NY 10023).
E124. Cameron, W.L. and L.K. Leung, "Feature-motivated scattering matrix decomposition", *Proc. IEEE Radar Conf.*, Arlington, VA, May 7-10, 1990, pp. 549-557, 1990.
E125. Barnes, R.M., "Roll Invariant Decompositions for the Polarization Covariance Matrix", Internal Report, Lincoln Laboratory, MIT, Lex., MA 02173-0073.
E126. Pottier, E., Contribution de la Polarimétrie dans la Discrimination de Cibles Radar, Application à l'Imagérie Electromagnétique haute Resolution, Ph.D. thesis, IRESTE, Nantes, France, December 1990.
E127. McCormick, G. C., "The Theory of Polarization Diversity Systems (in Radar Meteorology): The partially polarized case", *IEEE Trans. Ant. & Prop.*, vol. AP-44(4), pp. 425-433, 1996. (McCormick, G. C. and A. Hendry, 1985, "Optimum polarizations for partially polarized backscatter", *IEEE Trans. Antennas Propagation*, AP-33(1), pp. 33-39).
E128. Antar, Y.M.M., "Polarimetric Radar Applications to Meteorology", in W-M Boerner et al. (eds.) *Direct and Inverse Methods in Radar Polarimetry*, Part 2, pp. 1683-1695, Kluwer Academic Publishers, Dordrecht, NL, 1992.
E129. Kostinski, A.B, and W-M. Boerner, "On foundations of radar polarimetry", *IEEE Trans. Antennas Propagation*, vol. AP-34, pp. 1395-1404, 1986; H. Mieras, "Comments on 'Foundations of radar polarimetry'", ibid, pp. 1470-1471; "Authors's reply to 'Comments' by H. Mieras", ibid. pp. 1471-1473.
E130. Yamaguchi, Y., Y. Takayanagi, W-M. Boerner, H. J. Eom and M. Sengoku, "Polarimetric Enhancement in Radar Channel Imagery", IEICE Trans. Communications, vol. E78-B, no. 1, pp. 45-51, Jan 1996
E131. Holm, W.A., R.M.. Barnes, "On radar polarization mixed target state decomposition techniques", *Proceedings of the 1988 National Radar Conference*, pp. 248-254, April 1988.
E132. Ostrobityanov, R.V., and F.A. Basalov, "Statistical Theory of Distributed Targets", Dedham, MA: Artech House, 364 pages, 1985.
E133. Potekhin, V.A. and V.N. Tatarinov, "The Theory of Coherence of Electromagnetic Fields", Moscow, M. Sov. Radio, 1978.
E134. Touzi R., A. Lopes, J. Bruniquel , and P. Vachon, "Unbiased estimation of the coherence for SAR Imagery", IEEE Trans. Geoscience Remote Sensing, Vol. 37, No. 1, Jan. 1999
E135. Rignot, E., R. Chellapa, and P. Dubois, Unsupervised segmentation of polarimetric SAR data using the covariance matrix, IEEE Trans. Geoscience and Remote Sensing, 30(4) 697-705, 1992.
E136. Von Neumann, J., "Distribution of the ratio of the mean-square successive difference to the variance". *Ann. Math. Statist.*, 12, 367-395.
E137. Goodman, N. R., Statistical analysis based on a certain multi-variate complex Gaussian distribution (an introduction), *Annals of Mathematics and Statistics*, 34 (1963) 152-177

Appendix F: A Fisher's Information Criterion for Space-Time Transmit Signal Selection

Introduction

A key characteristic of any radar sensor is the form of its transmit signal. The ambiguity function of its transmit waveform specifies the ability of the sensor to resolve targets as a function of delay and Doppler. The ideal transmit signal would produce an ambiguity function with zero value for all non-zero delay and Doppler (i.e., a "thumbtack"), indicating that the responses from dissimilar targets are perfectly uncorrelated. However, a fundamental property of the delay-Doppler ambiguity function is that the energy of the function is an invariant. Through proper signal design, the energy in an ambiguity function can be moved to specific regions in the delay-Doppler plane, but it cannot be eliminated. Thus, the ideal ambiguity function cannot be formed— there is no ideal radar signal. Accordingly, a long-standing radar engineering problem is transmit waveform design—an effort to design a signal with a desired, but realizable, ambiguity function. Examples of these efforts include Costas, Barker and Frank Codes.

The delay-Doppler ambiguity function is most relevant for traditional single-aperture, monostatic radar designs. However, advances in microwave monolithic technology, coupled with the constant improvement in data processing capabilities, have enabled the development of multi-static radar systems. These sensors are formed with spatial arrays of antenna elements, each implemented with its own coherent receiver and/or transmitter. These antennas in this array may be arranged contiguously, or dispersed widely over a large volume to form a sparse radar array. These systems thus sample scattered fields as a function of both space and time, and thus can resolve targets in terms of delay, Doppler, and two dimensions of spatial frequency.

In addition to receiving scattered information across space and time, these transmit signal for these systems are also a function of space
and time. Although the space-time transmit signal can be described as a separable function of space and time (with the spatial function describing the array weighting function), we can likewise transmit a more general (non-separable) space-time signal. In other words, each transmit element can send independent, dissimilar signals in time. A two-dimensional ambiguity function can likewise be defined for these space-time sensors, again defining the resolving capabilities of the radar. However, an important characteristic of this space-time
ambiguity function is that its energy is not an invariant. Thus, for a given system design, there are optimum space-time transmit codes, in the sense that energy in the ambiguity function can be minimized.

The design of space-time codes and waveforms has become an important research topic in wireless communication systems, and is beginning to generate interest in the radar community as well. To see how these waveforms can be useful, and how optimal codes can be designed, we present a linear model of the radar problem, where described the measured space-time values are described in terms of the illuminated targets and the transmitted space-time waveform. We begin by defining a general position vector specifying a point in three dimensions of space and one of time space-time:

$$\bar{x} = [x, y, z, t] = [\bar{r}; t]$$

Four position vectors are denoted, to describe fields over each of 3 domains: the transmitted fields ($\bar{x}_t$), the scattered fields (x_s), and the received fields ($\bar{x}_r$). The received space-time field is expressed as in terms of a three-dimensional vector $\vec{r}$, which is required to define the polarization of this received signal across space and time.

$$\vec{r}(\bar{x}_r) = \int \bar{H}(\bar{x}_r; \bar{x}_s) \cdot \vec{y}(x_s) \cdot \int \ddot{G}(\bar{x}_s; \bar{x}_t) \cdot \vec{s}(\bar{x}_t) \, d\bar{x}_t \, d\bar{x}_s$$

The field $\vec{s}(\bar{x}_t)$ describes the transmit source over time and space.

The matrix functions $\ddot{G}(\bar{x}_i; \bar{x}_t)$ and $\ddot{H}(\bar{x}_r; \bar{x}_s)$ are essentially dyadic Green's functions that describe the propagation from the radar to the illuminated scatterers and back, while the dyadic $\ddot{y}(\bar{x}_s)$ describes the polarimetric scattering response of all illuminated targets, both distributed and point. We can approximate the space-time transmit source by representing it in terms of a finite set of N vector space-time basis functions:

$$\vec{s}(\bar{x}_t) \approx \sum_{n=1}^{N} s_n \hat{\varphi}_n(\bar{x}_t)$$

We can likewise approximate the scattering function $\ddot{y}(\bar{x}_s)$ as in terms of Mbasis functions $\ddot{\psi}_m(\bar{x}_s)$:

$$\ddot{y}(\bar{x}_s) \approx \sum_{m=1}^{M} y_m \ddot{\psi}_m(\bar{x}_s)$$

Combining the three previous equations, we find:

$$\vec{r}(\bar{x}_r) = \sum_m y_m \sum_n s_n \int \ddot{H}(\bar{x}_r; \bar{x}_s) \cdot \ddot{\psi}_m(\bar{x}_s) \cdot \int \ddot{G}(\bar{x}_s; \bar{x}_t) \cdot \vec{\varphi}_n(\bar{x}_t) \, d\bar{x}_t \, d\bar{x}_s$$

Finally, we can expand vector field $\vec{r}(\bar{x}_r)$ using a set of L vector basis functions $\vec{\varphi}_l(\bar{x}_r)$

$$\vec{r}(\bar{x}_r) \approx \sum_{l=1}^{L} r_l \vec{\varphi}_l(\bar{x}_r)$$

If these vector basis functions are orthogonal, the scalar values r_l can be found as:

$$r_l = \int \vec{r}(\bar{x}_r) \cdot \vec{\varphi}_l(\bar{x}_r) \, d\bar{x}_r.$$

Therefore,

$$r_l = \sum_m y_m \sum_n s_n \int \varphi_l(\bar{x}_r) \cdot \int \vec{H}(\bar{x}_r;\bar{x}_s) \cdot \psi_m(x_s) \cdot \int \vec{G}(x_s;x_t) \cdot \vec{\varphi}_n(\bar{x}_t)\, d\bar{x}_t\, d\bar{x}_s\, d\bar{x}_r$$

Evaluating the integrals, we can simplify this expression to:

$$r_l = \sum_m y_m \sum_n s_n a_{lmn}$$

where a_{lmn} is a complex scalar value:

$$a_{lmn} = \int \vec{\varphi}_l(\bar{x}_r) \cdot \int \vec{H}(\bar{x}_r;\bar{x}_s) \cdot \vec{\psi}_m(\bar{x}_s) \cdot \int \vec{G}(\bar{x}_s;\bar{x}_t) \cdot \vec{\varphi}_n(\bar{x}_t)\, d\bar{x}_t\, d\bar{x}_s\, dx_r$$

We now specify the sets of scalar values r_l, y_m, and s_n as column vectors:

$$Y = [Y_1, Y_2, Y_3, Y_4, \ldots, Y_M]^T$$

$$s = [s_1, s_2, s_3, s_4, \ldots, s_N]^T$$

$$r = [r_1, r_2, r_3, r_4, \ldots, r_L]^T$$

The set of scalar values a_{lmn} can be organized into a "data cube" in each of the three dimensions of *l*, *m*, and *n*. This data cube can be described as a set of *MN* column vectors with dimension *L*:

$$a_{mn} = [a_{1mn}, a_{2mn}, a_{3mn}, \cdots, a_{Lmn}]^T$$

The data cube can alternatively be described as a set of M, LxN matrices:

$$A_m = [a_{m1}; a_{m2}; a_{m3}; \ldots; a_{mN}]$$

or as set of N, LxM matrices:

$$B_n = [a_{1n}; a_{2n}; a_{3n}; \cdots; a_{Mn}]$$

Using these definitions, we can write the measurement vector **r** as:

$$\begin{aligned} r &= \sum_n s_n B_n y \\ &= \sum_n s_n v_n \\ &= Ys \end{aligned}$$

where we have defined vector $\mathbf{v}_n$ as:

$$\mathbf{v}_n = \mathbf{B}_n \gamma$$

and matrix Υ as:

$$\Upsilon = [v_1; v_2; v_3; \ldots v_N]$$

It is apparent that matrix Υ relates the transmit signal vector **s** to the measurement vector **r**. The matrix Υ is therefore a linear operator that describes the linear system that the transmit signal passes through as it moves from transmitter to receiver. As such, it includes the description of the scatterers it encounters (i.e., γ). The vector $\mathbf{v}_n$ can be viewed as the normalized response at the receiver due to transmit symbol s_n. In other words, $\mathbf{r} = \mathbf{v}_n$ if the transmit signal consist of only the single symbol $s_n = 1$. Therefore, the measurement vector **r** can be viewed as a weighted superposition of the response due to each transmit symbol.

However, we can alternatively write the measurement vector as:

$$\begin{aligned} r &= \sum_m y_m A_m s \\ &= \sum_m y_m \rho_m \\ &= \mathrm{P}\gamma \end{aligned}$$

where we have defined vector $\boldsymbol{\rho}_m$ as:

$$\rho_m = A_m s$$

and matrix **P** as:

$$\mathrm{P} = [\rho_1; \rho_2; \rho_3; \ldots; \rho_M]$$

In this case, it is apparent that the matrix **P** relates the scattering parameters γ to the measurements **r.** In this case, we can view the "signal" as γ , which passes through a linear system described by matrix **P**. This system is of course dependent on the transmitter signal, and thus matrix **P** is a function of vector **s**. Each vector $\boldsymbol{\rho}_m$ can be viewed as the normalized response of scatterer y_m. In other words, $r = \rho_m$ if only the only scatter illuminated is $y_m = 1$. Therefore, the measurement vector **r** can be viewed as a weighted superposition of the response from each illuminated target.

Note that:

$$P = \sum_{n=1}^{N} s_n \mathbf{B}_n = \sum_{m=1}^{M} A_m s 1'_m$$

and that:

$$Y = \sum_{m=0}^{M} y_m A_m = \sum_{n=1}^{N} B_n y 1'_n$$

where 1_n is a vector whose elements are all zero valued, with the exception of element n, whose value is one. For example :

$$1_3 = [0, 0, 1, 0, \ldots]^T$$

The usefulness of these representations is dependent on the desired engineering task. For example, the most prevalent radar problem is estimating the parameters of the illuminated targets. For this task, the representation $\mathbf{r} = \mathbf{P\gamma}$ is the obvious choice. Adding a random noise vector to the equation, or measurement is modeled as:

$$\mathbf{r} = \mathbf{P\gamma} + \mathbf{n}$$

For linear estimation, we seek a $M \times L$ weight matrix $\mathbf{W}$ in order to provide our scattering estimate $\hat{y}$:

$$\hat{\mathbf{y}} = \mathbf{Wr} .$$

The Minimum Mean Squared Error (MMSE) estimator, which incorporates the covariance matrices $K_y = E\{yy'\}$ and $K_n = E\{nn'\}$ (where $\{\}$ E is the expected value operator):

$$\begin{aligned} W_{mmse} &= K_y P' [P K_y P' + K_n]^{-1} \\ &= [K_y^{-1} + P' K_n^{-1} P]^{-1} P' K_n^{-1} \end{aligned}$$

The mean squared error of this estimator has the covariance matrix:

$$\begin{aligned} K_\varepsilon &= E\{(y - \hat{y})(y - \hat{y})'\} \\ &= K_y - K_y P' (P K_y P' + K_n)^{-1} P K_y \\ &= K_y - W_{mmse} P K_y \\ &= (I - W_{mmse} P) K_y \end{aligned}$$

or alternatively:

$$\begin{aligned} K_\varepsilon &= \mathrm{E}\{(y - \hat{y})(y - \hat{y})'\} \\ &= [K_y^{-1} + P' K_n^{-1} P]^{-1} \\ &= W_{mmse} K_n P [P' P]^{-1} \text{ ??} \end{aligned}$$

More generally, we find that the mmse estimator is:

$$W_{mmse} = K_{yr} K_r^{-1}$$

and

$$K_\varepsilon = K_y - K_{yr} K_r^{-1} K_{ry}$$

where:

$$\begin{aligned} K_r &= E\{rr'\} \\ &= E\{(Py+n)(Py+n)'\} \\ &= E\{Pyy'P' + Pyn' + ny'P' + n'n\} \\ &= PE\{yy'\}P' + PE\{yn'\} + E\{ny'\}P' + E\{n'n\} \\ &= P K_y P' + K_n \end{aligned}$$

$$\begin{aligned} K_{yr} &= E\{yr'\} \\ &= E\{y(Py+n)'\} \\ &= E\{yy'P' + yn'\} \\ &= E\{yy'\}P' + E\{yn'\} \\ &= K_y P' \end{aligned}$$

$$\begin{aligned} K_{ry} &= E\{ry'\} \\ &= E\{yr'\}' \\ &= (K_p P')' \\ &= P K'_y \end{aligned}$$

More specifically, we find that:

$$\begin{aligned} K_r &= E\{rr'\} \\ &= E\left\{\left(\sum_m Y_m A_m s + n\right)\left(\sum_n Y_n A_n s + n\right)'\right\} \\ &= \sum_{m=1}^{M}\sum_{n=1}^{M} A_m s 1'_m K_y 1_n s' A'_n + K_n \\ &= \sum_{m=1}^{M}\sum_{n=1}^{M} K_y^{mn} A_m s s' A'_n + K_n \end{aligned}$$

or:

$$
\begin{aligned}
K_r &= E\{rr'\} \\
&= E\left\{\left(\sum_m s_m B_m y + n\right)\left(\sum_n s_n B_n y + n\right)'\right\} \\
&= \sum_m \sum_n s_m s_n^* \mathbf{B}_{ms} K_y B'_n + K_n
\end{aligned}
$$

Likewise:

$$
\begin{aligned}
K_{yr} &= E\{yr'\} \\
&= E\left\{y\left(\sum_m y_m A_m s + n\right)'\right\} \\
&= K_y \sum_{m=1}^{M} 1_m s' A'_m \\
&= \sum_{m=1}^{M} k_m s' A'_m
\end{aligned}
$$

where k_{yn} is the n-th column of matrix K_y:

$$
k_{yn} = [K_{y1n}, K_{y2n}, \cdots K_{y1M}]
$$

Or alternatively:

$$
\begin{aligned}
K_{yr} &= E\{yr'\} \\
&= E\left\{y\left(\sum_n s_n B_n y + n\right)'\right\} \\
&= \sum_n s_n{}^* K_y B'_n \\
&= K_y \sum_n s_n{}^* B'_n
\end{aligned}
$$

Therefore, the error covariance matrix can be specified as:

$$
\begin{aligned}
K_\varepsilon &= K_y - K_{yr} K_r^{-1} K_{ry} \\
&= K_y - \sum_n k_{\wedge n} A'_n s' \left(\sum_m \sum_n K_{ymn} A_m s s' A'_n + K_n\right)^{-1} \sum_n s A_n k'_{\wedge n}
\end{aligned}
$$

Or as,

$$K_\varepsilon = K_y - K_{yr} K_r^{-1} K_{ry}$$
$$= K_y - \sum_n s_n K_y B_n \left(\sum_m \sum_n s_m s_n^* B_m K_y B'_n + K_n \right)^{-1} \sum_n B'_n K'_y s_n^*$$

Likewise, using the form of error covariance:

$$K_\varepsilon = [K_y^{-1} + P' K_n^{-1} P]^{-1}$$

Inserting:

$$\mathrm{P} = \sum_{m=1}^{M} A_m s 1'_m$$

we find:

$$K_\varepsilon = \left[K_y^{-1} + \sum_n 1_n s' A'_n K_n^{-1} \sum_m A_m s 1'_m \right]_n^{-1}$$
$$= \left[K_y^{-1} + \sum_n \sum_m 1_n s' A'_n K_n^{-1} A_m s 1'_m \right]_n^{-1}$$
$$= \left[K_y^{-1} + \sum_n \sum_m \left(s' A'_n K_n^{-1} A_m s \right) 1_n 1'_m \right]_n^{-1}$$

Likewise:

$$P = \sum_n s_n B_n$$

$$P' = \sum_n s_n^* B'_n$$

Therefore:

$$K_\varepsilon = \left[K_y^{-1} + P' K_n^{-1} P \right]^{-1}$$
$$= \left[K_y^{-1} + \sum_n s_n^* B'_n K_n^{-1} \sum_n s_n B_n \right]^{-1}$$
$$= \left[K_y^{-1} + \sum_m \sum_n s_n^* s_m B'_n K_n^{-1} B_m \right]^{-1}$$

$$K_\varepsilon = K_y - K_{yr} K_r^{-1} K_{ry}$$
$$= K_y - \sum_n k_{\wedge n} A'_n s' \left(\sum_m \sum_n K_{ymn} A_m s s' A'_n + K_n \right)^{-1} \sum_n s A_n k'_{\wedge n}$$

Fisher's Information

Using a information theoretic interpretation, we can view the covariance matrix K_y as the initial entropy (i.e., uncertainty) of vector **y**. Since the elements of this random vector are jointly Gaussian, it can be shown that the Fisher's Information (J_y) about **y** is simply the inverse of this entropy:

$$J_y = K_y^{-1}$$

Moreover, the Fisher's information contained in the observation vector **r** is determined to be:

$$J_r = P' K_n^{-1} P$$

Thus, the total Fisher's Information—the sum of the initial information and the information revealed by observation **r**—is:

$$J_T = J_R + J_y$$
$$= P' K_n^{-1} P + K_y^{-1}$$

Note that the inverse of the total information matrix is equal to the error covariance matrix of the mmse estimator:

$$J_T^{-1} = [P' K_n^{-1} P + K_y^{-1}]^{-1} = K_\varepsilon$$

From an information theoretic viewpoint, K_ε expresses the entropy (uncertainty) of vector **y**, once the observation **r** is revealed. We can likewise define **mutual information** as the reduction in uncertainty by observing measurement **r:**

$$\Delta K = K_y - K_\varepsilon$$
$$= K_y - \left(K_y - K_y P' (P K_y P' + K_n)^{-1} P K_y \right)$$
$$= K_y P (P K_y P' + K_n)^{-1} P K_y$$

Or, in terms of transmit vector **s:**

$$
\begin{aligned}
\Delta K &= K_y P'(P K_y P' + K_n)^{-1} P K_y \\
&= \sum_n k_{\wedge n} A'_n s' \left(\sum_m \sum_n K_{ymn} A_m s s' A'_n + K_n \right)^{-1} \sum_n s A_n k'_{\wedge n} \\
&= \sum_n s_n K_y B_n \left(\sum_m \sum_n s_m s_n^* B_m K_y B'_n + K_n \right)^{-1} \sum_n B'_n K'_y s_n^*
\end{aligned}
$$

This mutual information can be used to **adaptively** determine the space-time transmit signal **s.** Selecting the signal **s** that maximizes the determinant of this matrix will the additional information collected by the sensor to be maximized, with respect to the current information expressed by K_y^{-1}.

Appendix G: Space-Time Radar Transmission, Target, and Measurement Model

Abstract

This appendix contains mathematics describing an arbitrary space-time transmit signal, target set, and space-time receive measurements. The receive measurements are related to the target and transmit signal description via far-field propagation operators. The result allows for an accurate set of complex receiver samples that accurately reflect the measurements (e.g., A/D samples) of an arbitrary space-time radar when illuminating an arbitrary and diverse target set.

A. Transmit Signal

First, we describe the **transmit** signal as consisting of a set of complex valued samples existing in a multi-dimensional space. More specifically, this multi-dimensional space consists of two subspaces, the temporal (e.g., time-frequency) subspace, and the spatial (e.g., 3 physical dimensions) subspace. Each sample in the multi-dimensional subspace is then expressed as the sum of two vector components. One component is an element selected from a set of vectors lying completely in the temporal subspace, while the second vector component is an element selected from a set of vectors lying completely in the spatial subspace. We thus use the following definitions:

Z_t = integer value expressing the dimension of the temporal subspace. For example, if our transmit signal is defined in terms of both time and frequency, this value would be 2.

Z_s = integer value expressing the dimension of the spatial subspace. For example, if our transmit signal is defined in terms of three spatial dimensions, this value would be 3.

$Z = Z_s + Z_t$ integer value expressing the dimension of the total transmit signal space. For example, if our transmit signal is defined in terms of time, frequency, and three spatial dimensions this value would be 5 (=2+3).

J = integer expressing the number of samples in the spatial subspace. For example, if our radar had 18 transmit antenna elements, this value would be 18. The location of each sample in a three dimensional space (Z_s=3) would thus be represented by a three dimensional vector .

K= integer expressing the number of samples in the temporal subspace. For example, if our radar had 1000 transmit time-frequency samples, this value would be 1000. We can often interpret this value K as the time-bandwidth product of the transmit temporal signal, although it can be less.

N = JK= integer number representing the total number of transmit samples. Note that for every spatial sample there will be K temporal samples, or equivalently, for every temporal sample there will be J spatial samples. As a result, the total number of transmit samples N equals the product of J and K.

$\bar{z}_j^s$ = real-valued position vector of the j-th transmit sample in the (z_s -dimensional) spatial transmit signal subspace (e.g., $\bar{z}_j^s = [x_j, y_j, z_j]^T$). Note the collection of J vector essentially describes the spatial transmit antenna array configuration.

$\bar{z}_k^t$ = real-valued position vector of the k-th transmit sample in the (Z_t-dimensional) temporal transmit signal subspace (e.g., $\bar{z}_k^t = [t_k, \omega_k]^T$).

$\bar{z}_{jk}$ = real-valued position vector (of dimension Z) of the jk-th transmit sample (one of N samples) in the total transmit signal space. Note that this vector is:

$$\bar{z}_{jk} = [(\bar{z}_j^s)^T, (\bar{z}_k^t)^T]^T .$$

For example, we might find:

$$\bar{z}_{jk} = [x_j, y_j, z_j, t_k, \omega_k]^T .$$

$s(\bar{z}_{jk}) = \dot{s}_{jk}$ = the complex value of transmit sample jk. Note that there is **no** such complex value as s_j or s_k, such that $s_j s_k = s_{jk}$. Note also that we can organize these values in a number of ways.

$\bar{s}_k^s = [s_{1k}, s_{2k}, s_{3k} \cdots s_{Jk}]^T$ = vector (dimension J) of complex values of for every position vector $\bar{z}_{jk}$ associated with a specific temporal position vector $\bar{z}_k^t$. Note that there are K such vectors, one for each temporal position vector $\bar{z}_k^t$.

$\bar{s}_j^t = [s_{j1}, s_{j2}, s_{j3} \cdots s_{jK}]^T$ = vector (dimension K) of complex values of for every position vector $\bar{z}_{jk}$ associated with a specific spatial position vector $\bar{z}_j^s$. Note that there are J such vectors, one for each spatial position vector $\bar{z}_j^s$.

Likewise, we can arrange all elements s_{jk} into a single complex vector **s**, with N=JK elements:

$$\bar{s} = [(\bar{s}_1^s)^T, (\bar{s}_2^s)^T, (\bar{s}_3^s)^T, \ldots, (\bar{s}_K^s)^T]^T .$$

Thus, the complex vector element s_n is related to the element s_{jk} by the mapping j, k →n:

$$n = (kJ + j) - J ,$$

where:

$$1 \le j \le J \quad \text{and} \quad 1 \le k \le K ,$$

so that $1 \le n \le N = JK$.

Likewise, a position vector $\overline{z}_{jk}$ is related to $\overline{z}_n$ by this same mapping.

In other words:

$$s_n = s_{jk} \text{ and } \overline{z}_n = \overline{z}_{jk} \text{ where } n = (kJ + j) - J .$$

Thus, the transmitter is completely characterized by the complex signal vector **s, and** the set of N position vectors $\overline{z}_n$.

B. Target

Now, we describe the scattering targets as:

N_t = integer number of targets.

$\overline{y}_y$ = real-valued location of target t in target position space (e.g., position, radial velocity).

y = integer dimension of target position space (i.e, the dimension of vector $\overline{y}_t$)

$\gamma(\overline{y}_t) \stackrel{\bullet}{=} \gamma_t$ = complex scattering value of target t.

$\gamma = [\gamma_1, \gamma_2, \gamma_3 \ldots \gamma_T]^T$ = vector (dimension N_t) of complex transmit values, for each transmit sample t).

Thus, the **entire** target is characterized with complex vector γ, **and** the set of N_t position vectors $\overline{y}_t$.

C. Receiver Measurements

Finally, we describe the **receiver** measurements as consisting of a set of complex valued samples existing in a multi-dimensional space. More specifically, this multi-dimensional space consists of two subspaces, the temporal (e.g., time-frequency) subspace, and the spatial (e.g., 3 physical dimensions) subspace. Each sample in the multi-dimensional subspace then, is expressed as the sum of two vector components. One component is an element selected from a set of vectors lying completely in the temporal subspace, while the second vector component is an element selected

from a set of vectors lying completely in the spatial subspace. We thus use the following definitions

χ_t = integer value expressing the dimension of the temporal subspace. For example, if our received signal is defined in terms of both time and frequency, this value would be 2.

χ_s = integer value expressing the dimension of the spatial subspace. For example, if our received signal is defined in terms of three spatial dimensions, this value would be 3.

$x = \chi_s + \chi_t$ integer value expressing the dimension of the total receiver measurement space. For example, if our received signal is defined in terms of time, frequency, and three spatial dimensions this value would be 5 (=2+3).

I= integer expressing the number of samples in the spatial subspace. For example, if our radar had 18 receive antenna elements, this value would be 18. The location of each sample in a three dimensional space ($\chi_s = 3$) would thus be represented by a three dimensional vector.

K ′= integer expressing the number of samples in the temporal subspace. For example, if our radar had 1000 time-frequency receive samples, this value would be 1000. We can often interpret this value K ′ as the time-bandwidth product of the received temporal signal, although it can be less.

M = IK ′ = integer number representing the total number of receiver samples. Note that for every spatial sample there will be K ′ temporal samples, or equivalently, for every temporal sample there will be I spatial samples. As a result, the total number of transmit samples M equals the product of I and K ′. This value K ' will typically **equal** or be just **slightly more** than the transmit value K.

$\overline{x}_i^s$ = real-valued position vector of the i-th receive sample in the (χ_s -dimensional) spatial receiver measurement subspace (e.g., $\overline{x}_i^s = [x_i, y_i, z_i]^T$). Note the collection of I vectors essentially describes the spatial receive antenna array configuration.

$\overline{x}_{k'}^t$ = real-valued position vector of the k′-th receive sample in the (χ_t -dimensional) temporal receive sample subspace (e.g., $\overline{x}_{k'}^t = [t_{k'}, \omega_{k'}]^T$).

$\overline{x}_{ik'}$ = real-valued position vector (of dimension X) of the ik′-th receive sample (one of M samples) in the total receive sample space. Note that this vector is:

$$\overline{x}_{ik'} = [(\overline{x}_i^s)^T, (\overline{x}_{k'}^t)^T]^T .$$

For example, we might find:

$$\overline{x}_{ik'} = [x_i, y_i, z_i, t_{k'}, \omega_{k'}]^T .$$

$r(\overline{x}_{ik'}) = \dot{r}_{ik'}$ = the complex value of receive sample ik′. Note that there is **no** such complex value as r_i or $r_{k'}$, such that $r_i r_{k'} = r_{ik'}$. Note also that we can organize these samples in a number of ways.

$r^s_{k'} = [r_{1k'}, r_{2k'}, r_{3k'}, \ldots, r_{IK'}]^T$ = vector (dimension I) of complex samples of for every position vector $\overline{x}_{ik'}$ associated with a specific temporal position vector $\overline{x}^t_{k'}$. Note that there are K' such vectors, one for each temporal position vector $\overline{x}^t_{k'}$.

$r^t_i = [r_{i1}, r_{i2}, r_{i3}, \ldots, r_{jK'}]^T$ = vector (dimension K′) of complex samples of for every position vector $\overline{x}_{ik'}$ associated with a specific spatial position vector $\overline{x}^s_i$. Note that there are I such vectors, one for each spatial position vector $\overline{x}^s_i$.

R= a complex I by K′ matrix with all complex receiver sample values:

$$R = \begin{bmatrix} r_{11} & r_{12} & \cdots & r_{1K'} \\ r_{21} & r_{22} & \cdots & r_{2K'} \\ \vdots & \vdots & \ddots & \vdots \\ r_{J1} & r_{J2} & \cdots & r_{JK'} \end{bmatrix} .$$

Note that this matrix can be written in terms of vectors $r^s_{k'}$:

$$R = [r^s_1, r^s_2, r^s_3, \cdots r^s_{K'}],$$

or in terms of vectors r^t_i:

$$R = [r^t_1, r^t_2, r^t_3, \cdots r^t_I]^T .$$

Likewise, we can arrange all elements $r_{jk'}$ into a single complex vector **r,** with M =IK' elements:

$$r = \left[(r^s_1)^T, (r^s_2)^T, (r^s_3)^T, \ldots, (r^s_{K'})^T\right]^T .$$

Thus, the complex vector element r_m is related to the element $r_{ik'}$ by the mapping i, k′ → m:

$$m = (k'I + i) - I ,$$

where:

$$1 \le i \le I \text{ and } 1 \le k' \le K',$$

so that $1 \le m \le M = IK'$.

Likewise, a position vector $\overline{x}_{ik'}$ is related to $\overline{x}_m$ by this same mapping.

In other words:

$$r_m = r_{ik'} \text{ and } \overline{x}_m = \overline{x}_{ik'} \text{ where } m = (k'I + i) - I .$$

Thus, the receive measurement is completely characterized by the complex signal vector **r**, **and** the set of M position vectors $\overline{x}_m$.

D. Model Equations

The received signal vector **r** can be related to vectors **s** and γ. To accomplish this, the following parameters must be specified:

$\overline{\overline{K}}_\theta$ = a Y by Z, real-valued **frequency matrix**, relating the transmit signal space to the target position space. We can partition $\overline{\overline{K}}_\theta$ into two components, $\overline{\overline{K}}^s_\theta$ and $\overline{\overline{K}}^t_\theta$, where:

$$\overline{\overline{K}}_\theta = [\overline{\overline{K}}^s_\theta, \overline{\overline{K}}^t_\theta].$$

$\overline{\overline{K}}_\varphi$ = a Y by X, real-valued **frequency matrix**, relating the receive signal space to the target position space. We can partition $\overline{\overline{K}}_\varphi$ into two components, $\overline{\overline{K}}^s_\varphi$ and $\overline{\overline{K}}^t_\varphi$, where:

$$\overline{\overline{K}}_\varphi = [\overline{\overline{K}}^s_\varphi, \overline{\overline{K}}^t_\varphi] .$$

$g^t_h(k', k : t)$ = a complex function that weights and relates, for a given target t, the transmit temporal samples and receive temporal samples to each other.

$g^s_{hI}(i, t)$ = a complex function that weights the receive spatial samples for a given target t.

$g^s_{hJ}(j, t)$ = a complex function that weights the transmit spatial samples for a given target t.

$n = [n_1, n_2, n_3, \ldots, n_M]^T$ = an M dimension complex vector describing measurement noise, where n_m is a zero-mean, complex random variable with variance σ_n^2.

The vectors **s**, γ , and **n** are related to **r** as:

$$\mathbf{r} = \sum_t \gamma_t H_t \mathbf{s} + \mathbf{n} ,$$

or by defining an M-dimensional normalized measurement vector ρ_t for each target t:

$$\rho_t = H_t \mathbf{s} .$$

We thus find that the measurement vector **r** is simply a weighted superposition of normalized vectors:

$$\mathbf{r} = \sum_t \gamma_t \rho_t + \mathbf{n}.$$

Likewise, we can define an M by N_t matrix:

$$\mathbf{P} = [\rho_1, \rho_2, \rho_3, \ldots, \rho_{Nt}],$$

and therefore express the measurement vector **r** as:

$$\mathbf{r} = \mathbf{P}\gamma + \mathbf{n}.$$

Now, at the heart of this relationship is matrix H_t, which is an M by N matrix with elements of the form:

$$H_t^{mn} = g_h(m,n:t) e^{-j \bar{\bar{x}}_m^{sT} \bar{\bar{K}}_\varphi^{sT} \bar{y}_t} e^{-j \bar{y}_t^T \bar{\bar{K}}_\theta^s \bar{z}_n^s} e^{-j \bar{y}_t^T \left(\bar{\bar{K}}_\varphi^t + \bar{\bar{K}}_\theta^t \right) \bar{z}_n^t}.$$

Thus, to complete the model, we must provide an explicit form for function $g_h(m,n:t)$, as well as matrices $\bar{\bar{K}}_\theta$ and $\bar{\bar{K}}_\varphi$.

Using the mappings i, k′ →m and j, k →n, we can equivalently describe $g_h(m,n:t)$ as:

$$g_h(k',i;k,j:t),$$

so that:

$$H_t^{mn} = g_h(m,n:t)e^{-j\bar{x}_m^{sT}\bar{\bar{K}}_\varphi^{sT}\bar{y}_t}e^{-j\bar{y}_t^T\bar{\bar{K}}_\theta^s\bar{z}_n^s}e^{-j\bar{y}_t^T\left(\bar{\bar{K}}_\varphi^t+\bar{\bar{K}}_\theta^t\right)\bar{z}_n^t}$$
$$= g_h(k',i;k,j:t)e^{-j\bar{x}_m^{sT}\bar{\bar{K}}_\varphi^{sT}\bar{y}_t}e^{-j\bar{y}_t^T\bar{\bar{K}}_\theta^s\bar{z}_n^s}e^{-j\bar{y}_t^T\left(\bar{\bar{K}}_\varphi^t+\bar{\bar{K}}_\theta^t\right)\bar{z}_n^t} .$$

Now, we can separate this expression into two pieces—a temporal (time-frequency) and a spatial piece. We can assume that the function g_h is separable into spatial and temporal components, i.e.:

$$g_h(k',i;k,j:t) = g_h^s(i,j:t)\,g_h^t(k',k:t).$$

As a result, the elements of matrix H_t can be written as:

$$H_t^{mn} = g_h(k',i;k,j:t)e^{-j\bar{x}_m^{sT}\bar{\bar{K}}_\varphi^{sT}\bar{y}_t}e^{-j\bar{y}_t^T\bar{\bar{K}}_\theta^s\bar{z}_n^s}e^{-j\bar{y}_t^T\left(\bar{\bar{K}}_\varphi^t+\bar{\bar{K}}_\theta^t\right)\bar{z}_n^t}$$
$$= g_h^s(i,j:t)\,g_h^t(k',k:t)e^{-j\bar{x}_i^{sT}\bar{\bar{K}}_\varphi^{sT}\bar{y}_t}e^{-j\bar{y}_t^T\bar{\bar{K}}_\theta^s\bar{z}_j^s}e^{-j\bar{y}_t^T\left(\bar{\bar{K}}_\varphi^t+\bar{\bar{K}}_\theta^t\right)\bar{z}_k^t}$$
$$= g_h^s(i,j:t)e^{-j\bar{x}_i^{sT}\bar{\bar{K}}_\varphi^{sT}\bar{y}_t}e^{-j\bar{y}_t^T\bar{\bar{K}}_\theta^s\bar{z}_j^s}\,g_h^t(k',k:t)e^{-j\bar{y}_t^T\left(\bar{\bar{K}}_\varphi^t+\bar{\bar{K}}_\theta^t\right)\bar{z}_k^t} ,$$

where again

$$n = (kJ+j)-J \text{ and } m = (k'I+i)-I .$$

This mapping allows us to write the matrix H_t in terms of temporal matrix H_t^t and a spatial matrix H_t^s:

$$H_t = H_t^t \otimes H_t^s,$$

where H_t^t is a K′ x K matrix with elements of the form:

$$H_{k'k}^t = g_h^t(k',k:t)e^{-jy_t^T\left(\bar{\bar{K}}_\varphi^t+\bar{\bar{K}}_\theta^t\right)\bar{z}_k^t},$$

and where H_t^s is an I x J matrix with elements of the form:

$$H_{ij}^s = g_h^s(i,j:t)e^{-j\bar{x}_t^{sT}\bar{\bar{K}}_\varphi^{sT}\bar{y}_t}e^{-j\bar{y}_t^T\bar{\bar{K}}_\theta^s\bar{z}_j^s}.$$

We will further assume that the function $g_h^s(i,j:t)$ is separable such that:

$$g_h^s(i,j:t) = g_{hI}^s(i,t)\,g_{hJ}^s(j,t) ,$$

and thus

$$\begin{aligned} H_{ij}^{s} &= g_{h}^{s}(i,j:t)e^{-j\overline{x}_{t}^{sT}\overline{\overline{K}}_{\varphi}^{sT}\overline{y}_{t}}e^{-j\overline{y}_{t}^{T}\overline{\overline{K}}_{\theta}^{s}\overline{z}_{j}^{s}} \\ &= g_{hI}^{s}(i:t)e^{-j\overline{x}_{i}^{sT}\overline{\overline{K}}_{\varphi}^{sT}\overline{y}_{t}}g_{hJ}^{s}(j:t)e^{-j\overline{y}_{t}^{T}\overline{\overline{K}}_{\theta}^{s}\overline{z}_{j}^{s}} \quad . \end{aligned}$$

We can now write the matrix H_{t}^{s} as simply:

$$H_{t}^{s} = \Phi_{t}\Theta_{t}^{T},$$

where Θ_{t} is a J-dimensional complex vector:

$$\Theta_{tk} = \left[g_{hJ}^{s}(1:t)e^{-j\overline{y}_{t}^{T}\overline{\overline{K}}_{\theta}^{s}\overline{z}_{1}^{s}}, g_{hJ}^{s}(2:t)e^{-j\overline{y}_{t}^{T}\overline{\overline{K}}_{\theta}^{s}\overline{z}_{2}^{s}}, \ldots, g_{hJ}^{s}(J:t)e^{-j\overline{y}_{t}^{T}\overline{\overline{K}}_{\theta}^{s}\overline{z}_{J}^{s}} \right]^{T},$$

and Φ_{t} is an I-dimensional complex vector:

$$\Phi_{tk} = \left[g_{hI}^{s}(1:t)e^{-j\overline{x}_{1}^{sT}\overline{\overline{K}}_{\phi}^{sT}\overline{y}_{t}}, g_{hI}^{s}(2:t)e^{-j\overline{x}_{2}^{sT}\overline{\overline{K}}_{\phi}^{sT}\overline{y}_{t}}, \ldots, g_{hI}^{s}(I:t)e^{-j\overline{x}_{I}^{sT}\overline{\overline{K}}_{\phi}^{sT}\overline{y}_{t}} \right]^{T}.$$

Thus, the matrix H_{t} can be expressed as:

$$\begin{aligned} H_{t} &= H_{t}^{t} \otimes H_{t}^{s} \\ &= H_{t}^{t} \otimes (\Phi_{t}\Theta_{t}^{T}) \quad . \end{aligned}$$

If we use the temporal signal model, where:

$$\begin{aligned} \mathbf{s} &= \mathbf{FS} \\ \mathbf{s} &= (\psi \otimes I_{J})\mathbf{S} \quad , \end{aligned}$$

we find that

$$\begin{aligned} \rho_{t} &= H_{t}\mathbf{s} \\ &= H_{t}\mathbf{FS} \\ &= H_{t}(\psi \otimes I_{J})\mathbf{S} \\ &= H_{t}'\mathbf{S} \quad , \end{aligned}$$

where we have defined:

$$H'_t = H_t(\psi \otimes I_J).$$

However, using the result:

$$H_t = H_t^t \otimes (\Phi_t \Theta_t^T),$$

we get:

$$H'_t = \left[H_t^t \otimes (\Phi_t \Theta_t^T)\right](\psi \otimes I_J).$$

However, using a math identity for the Kronecker product, we can rewrite this expression in a more compact form:

$$\begin{aligned} H'_t &= \left[H_t^t \otimes (\Phi_t \Theta_t^T)\right](\psi \otimes I_J) \\ &= (H_t^t \psi) \otimes \left[(\Phi_t \Theta_t^T) I_J\right] \\ &= (H_t^t \psi) \otimes (\Phi_t \Theta_t^T). \end{aligned}$$

Thus, we come to the conclusion:

$$\begin{aligned} \rho_t &= H'_t \mathbf{S} \\ H'_t &= (H_t^t \psi) \otimes (\Phi_t \Theta_t^T). \end{aligned}$$

E. Default Values

To simplify further the model derivation, we shall describe some standard values to use as default within the model.

First, we will assume that the transmit temporal position vectors $\vec{z}_k = [t_k, \omega_K]^T$ will point to locations on a $Z_t = 2$ dimensional grid. This grid will have U samples in the time dimension and V samples in the frequency direction.

The samples in the time dimension will have spacing of T_o, while samples in the frequency dimension will have spacing of $\pi / T_o = \omega_o / 2$. That is,

$$\vec{z}_k = \left[uT_o, \frac{v\omega_o}{2}\right]^T,$$

where:

$$-\left(\frac{U-1}{2}\right) \le u \le \frac{U-1}{2} \quad \text{and} \quad -\left(\frac{V-1}{2}\right) \le v \le \frac{V-1}{2},$$

and the value of k for each u, v pair is found from the mapping u, v →k:

$$k = (uV + v) + \left(\frac{UV+1}{2}\right),$$

so that $1 \leq k \leq K = UV$.

Likewise, we will assume that the receive temporal position vectors $\vec{x}_{k'}^{t} = [t_{k'}, \omega_{k'}]^T$ will point to locations on a $X_t = 2$ dimensional grid. This grid will have U' samples in the time dimension and V' samples in the frequency direction.

The samples in the time dimension will have spacing of T_o, while samples in the frequency dimension will have spacing of $2\pi/T_o = \omega_o$. That is,

$$\vec{x}_{k'}^{t} = [u'T_o, v'\omega_o]^T,$$

where:

$$-\left(\frac{U'-1}{2}\right) \leq u' \leq \frac{U'-1}{2} \quad and \quad -\left(\frac{V'-1}{2}\right) \leq v' \leq \frac{V'-1}{2},$$

and the value of k' for each u', v' pair is found from the mapping u', v', →k' :

$$k' = (u'V' + v') + \left(\frac{U'V'+1}{2}\right),$$

so that $1 \leq k' \leq K' = U'V'$.

For the default case, we assume that the values U, V, and K are related to U',V ',K ' as:

$$U' = U + 2,$$

and

$$V' = \frac{V-1}{2} \quad or \quad V' = \frac{V+1}{2} \text{ (use odd integer value)}$$

so that:

$$U'V' = (U+2)\left(\frac{V-1}{2}\right) \quad or \quad U'V' = (U+2)\left(\frac{V+1}{2}\right).$$

We will assume for the default case that the target position vectors have the form:

$$\vec{y}_t = [x_t, y_t, z_t, v_t]^T,$$

where x_t, y_t, and z_t define the target position in a three-dimensional Cartesian space, and v_t specifies the radial target velocity (with respect to ground velocity).

We will assume that the $x_t - y_t$ plane will define the ground surface, so that z_t specifies target height. It will be assumed that the targets are arranged on the surface in a (N_x by N_y) two dimensional grid. The spacing in the x_t direction will be denoted as Δ x , while the spacing in the y_t is denoted as Δ y . Thus, we can denote the target position vectors as:

$$\overline{y}_t = [n_x \Delta x, n_y \Delta y, z_t, v_t]^T,$$

where:

$$-\left(\frac{N_x - 1}{2}\right) \le n_x \le \frac{N_x - 1}{2} \quad and \quad -\left(\frac{N_y - 1}{2}\right) \le n_y \le \frac{N_y - 1}{2},$$

and N_x and N_y are odd integer values.

The value of t' for each n_x, n_y pair is found from the mapping $n_x, n_y \rightarrow$ t:

$$t = (n_x N_y + n_y) + \left(\frac{N_x N_y + 1}{2}\right),$$

such that $1 \le t \le N_x N_y$.

Note that $N_t \ge N_x N_y$, since we **might** have more than one target at each grid point. (e.g., a stationary surface object and an airborne moving object).

Note also then that the target located at the **center** of the target grid, where $n_x = 0$ and $n_y = 0$, has the value:

$$t_{center} = \frac{N_x N_y + 1}{2}.$$

With the above assumptions, we can rewrite $g_h^t(k', k:t)$ as

$$g_h^t = (k', k, :t) = g_h^t(u', v'; u, v: n_x, n_y).$$

We will assume as the default a function of the following form:

$$g_h^t(u',v';u,v:n_x,n_y) =$$

$$\begin{cases} \dfrac{1}{V}\dfrac{\sin\left(\frac{\pi}{2}(2v'-v)\right)}{\sin\left(\frac{\pi}{V}(2v'-v)\right)}\left[\delta(u'-u)+e^{+jv\pi}\delta(u'-u-1)\right] & for\ n_y>0 \\ \dfrac{1}{V}\dfrac{\sin\left(\frac{\pi}{2}(2v'-v)\right)}{\sin\left(\frac{\pi}{V}(2v'-v)\right)}\delta(u'-u) & for\ n_y=0 \\ \dfrac{1}{V}\dfrac{\sin\left(\frac{\pi}{2}(2v'-v)\right)}{\sin\left(\frac{\pi}{V}(2v'-v)\right)}\left[\delta(u'-u)+e^{-jv\pi}\delta(u'-u+1)\right] & for\ n_y<0 \end{cases}$$

where δ (i) is a delta function defined as:

$$\delta(i)=\begin{cases}1 & if \quad i=0\\ 0 & if \quad i\neq 0\end{cases}.$$

Note that:

1. The value of $g_h^t(u',v';u,v:n_x,n_y)$ is non-zero only if u′ = u −1,

u′ = u, or u′ = u +1. In other words, $g_h^t(u',v';u,v:n_x,n_y)=0$ **if** $|u'-u|>1$.

2. The function:

$$\frac{1}{V}\frac{\sin\left(\frac{\pi}{2}(2v'-v)\right)}{\sin\left(\frac{\pi}{V}(2v'-v)\right)}$$

is indeterminate when 2v ′ = v. As a result, this function should programmed as:

$$\frac{\frac{1}{V}\dfrac{\sin\left(\frac{\pi}{2}(2v'-v)\right)}{\sin\left(\frac{\pi}{V}(2v'-v)\right)}}{} = \begin{cases} \dfrac{1}{2} & \text{if } 2v' = v \\ \dfrac{1}{V}\dfrac{\sin(2v'-v)}{\sin\left(\frac{\pi}{V}(2v'-v)\right)} & \text{if } 2v' \neq v \end{cases}$$

We will likewise assume for the default case that:

$$g^{s}_{hI}(i,t) = g^{s}_{hJ}(j,t) = 1.0.$$

Now, we make some default assumptions about the radar **geometry**:

1. The radar is flying with a velocity $v\,\hat{x}$
2. The center of the radar (both transmitter and receiver) is at an altitude h.
3. The center of the target area is located at x =0, $y = y_o$ (in other words, we assume as a default a standard sidelooking case).

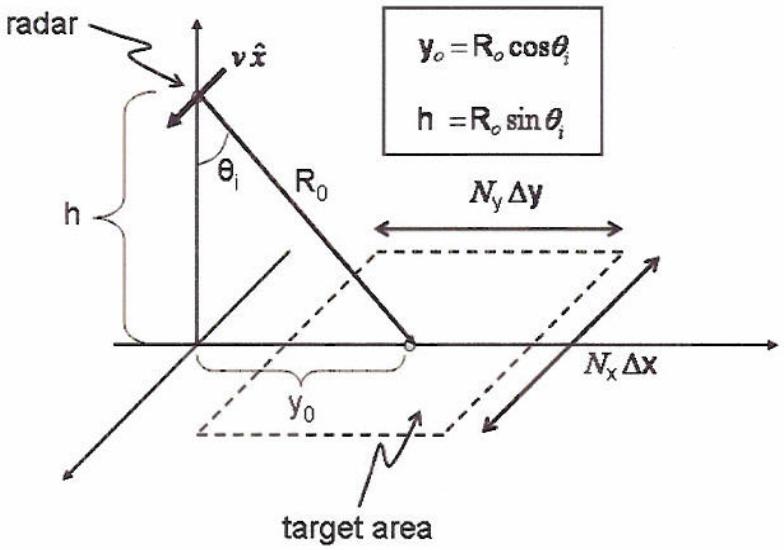

Now, we can use this geometry to define default values for matrices K_θ and K_φ. Again, define the vectors:

$$\overline{x}_{ik'} = [x_i, y_i, z_i, t_{k'}, \omega_{k'}]^T$$
$$\overline{y}_t = [x_t, y_t, z_t, v_t]^T$$
$$\overline{z}_{jk} = [x_j, y_j, t_k, \omega_k]^T \quad .$$

We can use as a default:

$$K_\theta = \frac{\omega_c}{c}\begin{bmatrix} \frac{-1}{R_o} & 0 & 0 & \frac{-v}{R_o} & 0 \\ 0 & \frac{-h^2}{R_o^3} & \frac{-h y_o}{R_o^3} & 0 & \frac{y_o}{\omega_c R_o} \\ 0 & \frac{-h y_o}{R_o^3} & \frac{-y_o^2}{R_o^3} & 0 & \frac{-h}{\omega_c R_o} \\ 0 & 0 & 0 & 0 & -1 \end{bmatrix}.$$

Here we have defined target velocity v_t as its radial velocity, with a **positive** value indicating the target is moving **toward** the radar. The value c is the velocity of propagation (i.e., the speed of light). Likewise, we find that:

$$K_\varphi = \frac{\omega_c}{c}\begin{bmatrix} \frac{-1}{R_o} & 0 & 0 & \frac{-v}{R_o} & 0 \\ 0 & \frac{-h^2}{R_o^3} & \frac{-hy_o}{R_o^3} & 0 & \frac{y_o}{\omega_c R_0} \\ 0 & \frac{-hy_o}{R_o^3} & \frac{-y_o^2}{R_o^3} & 0 & \frac{-h}{\omega_c R_o} \\ 0 & 0 & 0 & 0 & -1 \end{bmatrix}.$$

Therefore we can equivalently state this as:

$$K_\theta^s = \frac{\omega_c}{c}\begin{bmatrix} \frac{-1}{R_o} & 0 & 0 \\ 0 & \frac{-h^2}{R_o^3} & \frac{-hy_o}{R_o^3} \\ 0 & \frac{-hy_o}{R_o^3} & \frac{-y_o^2}{R_o^3} \\ 0 & 0 & 0 \end{bmatrix},$$

$$K_{\theta}^{t}=\frac{\omega_c}{c}\begin{bmatrix}\frac{-v}{R_o} & 0\\ 0 & \frac{y_o}{\omega_c R_o}\\ 0 & \frac{-h}{\omega_c R_o}\\ 0 & -1\end{bmatrix},$$

$$K_{\varphi}^{s}=\frac{\omega_c}{c}\begin{bmatrix}\frac{-1}{R_o} & 0 & 0\\ 0 & \frac{-h^2}{R_o^3} & \frac{-hy_o}{R_o^3}\\ 0 & \frac{-hy_o}{R_o^3} & \frac{-y_o^2}{R_o^3}\\ 0 & 0 & 0\end{bmatrix},$$

and

$$K_{\varphi}^{t}=\frac{\omega_c}{c}\begin{bmatrix}\frac{-v}{R_o} & 0\\ 0 & \frac{y_o}{\omega_c R_o}\\ 0 & \frac{-h}{\omega_c R_o}\\ 0 & -1\end{bmatrix}.$$

Finally, we will set the target spacing Δ x and Δ y to be equal to the **resolution** of the radar:

$$\Delta y=\frac{cR_o}{2B\,y_o}$$

and

$$\Delta x=\frac{cR_o}{2T\,v\,f_c}=\frac{cR_o}{2UT_o v\,f_c}.$$

In **summary,** our default case can be completely specified with the following values:

1. T_o, B, ω_c, c
2. v, R_o, y_o
3. U, V, I, J
4. $N_x, N_y,$

as well as the following **sets** of data:

5. z_t for all targets t.
6. v_t for all targets t.
7. $\overline{x}_i^s$ for all receiver elements i.
8. $\overline{z}_j^s$ for all transmitter elements j.

Appendix H: Transmit Signal Model

Abstract

This appendix presents the mathematics describing a radar transmit signal with time width T, bandwidth B, and repetition frequency f_o. The transmit signal is described a weighted superposition of a set of wide time width, wide bandwidth orthonormal basis functions. A widowed Fourier transform is used to describe the transmit signal in terms of (slow) time and (fast) frequency. This result is then sampled across time and frequency, such that the signal can be described as a set of BT complex values.

1. Model Inputs

The following values and functions are required as inputs to this temporal signal model.

f_c = real-valued carrier frequency (Hz).

B = real-valued transmit signal bandwidth (Hz)

f_o = real-valued signal repetition frequency (Hz)

U = an odd integer number of "pulses" sent by the transmit signal.

Q = an odd integer number indicating the number of "fast-time" basis functions.

P = an odd integer number indicating the number of "slow-time" basis functions.

$g_s(t)$ = a "mother function" used to generate a set of slow-time basis functions.

$G_f(\omega)$ = the Fourier transform a of a "mother function" used to generate a set of fast-time basis functions.

$\{\tau_q\}$ = A set of Q time delay values used to generate the fast-time basis functions.

$\{\omega_p\}$ = A set of P frequency values used to generate the slow-time basis functions

2. Secondary Model Parameters

The main input values of Section 1 can be used to determine these secondary model parameters.

$\frac{1}{f_o} = T_o$ = signal repetition interval (sec.)

$UT_o = T$ = transmit signal time width (sec.)

$\omega_o = 2\pi f_o$ = angular signal repetition frequency (radians/sec.)

3. Transmit Signal Construction

A real-valued transmit signal $v_s(t)$ will be described as:

$$v_s(t) = \mathrm{Re}\left\{S(t)e^{-j\omega_c t}\right\},$$

where ω_c is a real valued carrier frequency ($\omega_c = 2\pi f_c$), and S(t) is a complex function constructed as a weighted superposition of complex basis functions $\psi_{pq}(t)$:

$$\psi_{pq}(t) = s_p(t)\sum_u f_q(t - uT_o)e^{j\omega_c uT_o}.$$

Therefore:

$$\begin{aligned} S(t) &= \sum_p \sum_q S_{pq}\psi_{pq}(t) \\ &= \sum_p \sum_q S_{pq}s_p(t)\sum_u f_q(t - uT_o)e^{j\omega_c uT_o} \end{aligned}.$$

The functions $s_p(t)$ form a set of P "slow time" functions, each with a narrow bandwidth and time width T. Each function $s_p(t)$ is denoted by integer p, where:

$$-\left(\frac{P-1}{2}\right) \le p \le \frac{P-1}{2}.$$

The functions $f_q(t)$ form a set of Q "fast time" functions, each with a narrow time width and a wide bandwidth B (i.e., a "pulse" function). Each function $f_q(t)$ is denoted by integer q, where:

$$-\left(\frac{Q-1}{2}\right) \le q \le \frac{Q-1}{2}.$$

Likewise, the function:

$$\sum_u f_q(t - uT_o)e^{j\omega_c uT_o}$$

simply describes a "train" of U identical pulses $f_q(t)$, each occurring at a periodic interval of T_o. Note that for each different pulse function $f_q(t)$ there is a different pulse train $\sum_u f_q(t - uT_o)e^{j\omega_c uT_o}$ (i.e., there is a set of Q pulse trains).

Each pulse in the train is denoted by integer value u, where:

$$-\left(\frac{U-1}{2}\right) \le u \le \frac{U-1}{2}.$$

4. The Properties of Signal Basis Functions

The fast-time functions $f_q(t)$ are each simply a slightly delayed version of a "mother function" $g_f(t)$:

$$f_q(t) = g_f(t-\tau_q)e^{j\omega_c\tau_q} \quad \text{where} \quad \tau_q << T_o \ .$$

The mother function $g_f(t)$ has the following properties:

1. It is an even function:

$$g_f(t) = g_f(-t)$$

2. It has a very narrow time width:

$$\int_{-\infty}^{\infty} t^2 \left|g_f(t)\right|^2 dt << T_o^2$$

3. It has bandwidth B. That is, if:

$$G_f(\omega) = \int_{-\infty}^{\infty} g_f(t)e^{-j\omega t}dt$$

then:

$$\int_{-\infty}^{\infty} \omega^2 \left|G_f(\omega)\right|^2 d\omega \approx (2\pi B)^2$$

4. It has unit energy:

$$\int_{-\infty}^{\infty} \left|g_f(t)\right|^2 dt = 1.0$$

The set of P functions $s_p(t)$ are best described in terms of their Fourier transforms:

$$S_p(\omega) = \int_{-\infty}^{\infty} s_p(t)e^{-j\omega t}dt \ .$$

More specifically, the Fourier transform of each signal is related as:

$$S_p(\omega) = G_s(\omega - \omega_p) \quad \text{where} \quad \omega_p << \omega_o \ .$$

The function $G_s(\omega)$ has the following properties:

1. It is **even**:

$$G_s(\omega) = G_s(-\omega)$$

2. It has a very **narrow bandwidth**:

$$\int_{-\infty}^{\infty} \omega^2 |G_s(\omega)|^2 d\omega < \omega_o^2$$

3. It has **time width** T. That is, if:

$$g_s(t) = \frac{1}{2\pi} \int_{-\infty}^{\infty} G_s(\omega) e^{j\omega t} d\omega \ ,$$

then:

$$|g_s(t)| > 0 \quad \text{for all time} \quad -\frac{T}{2} < t < \frac{T}{2}$$

and

$$|g_s(t)| = 0 \ \text{ for all time } t < -\frac{T}{2} \ \text{ and } \ t > \frac{T}{2} \ .$$

4. It has unit energy:

$$\frac{1}{2\pi} \int_{-\infty}^{\infty} |G_s(\omega)|^2 d\omega = 1.0 \ .$$

5. The Windowed Fourier Transform of S(t)

Now returning to our signal description, we can use the fact that:

$$s_p(T) = \frac{1}{2\pi} \int_{-\infty}^{\infty} S_p(\omega) e^{j\omega t} d\omega \ ,$$

where

$$S_p(\omega) = G_s(\omega - \omega_p) \ ,$$

to write the transmit signal as:

$$
\begin{aligned}
S(t) &= \sum_p \sum_q S_{pq} \frac{1}{2\pi} \int S_p(\omega) e^{j\omega t} d\omega \sum_u f_q(t - uT_o) e^{j\omega_c uT_o} \\
&= \sum_p \sum_q S_{pq} \frac{1}{2\pi} \int G_s(\omega - \omega_p) e^{j\omega t} d\omega \sum_u f_q(t - uT_o) e^{j\omega_c uT_o} \\
&= \sum_p \sum_q S_{pq} e^{j\omega_p t} \sum_u f_q(t - uT_o) e^{j\omega_c uT_o} \frac{1}{2\pi} \int G_s(\omega) e^{j\omega t} d\omega \quad .
\end{aligned}
$$

Noting that:

$$
g_s(t) = \frac{1}{2\pi} \int G_s(\omega) e^{j\omega t} d\omega \quad ,
$$

we can write the transmit signal as simply:

$$
S(t) = \sum_p \sum_q S_{pq} e^{j\omega_p t} g_s(t) \sum_u f_q(t - uT_o) e^{j\omega_c uT_o} \quad .
$$

We now will take a **windowed Fourier transform** of the transmit signal, defined as:

$$
\begin{aligned}
s(uT_o, \omega) &= \int_{-\infty}^{\infty} S(t) w_{fu}^*(t) e^{-j\omega t} dt \\
&= \int_{-\infty}^{\infty} \left(\sum_p \sum_q S_{pq} e^{j\omega_p t} g_s(t) \sum_{u'} f_q(t - u'T_o) e^{j\omega_c uT_o} \right) w_{fu}^*(t) e^{-j\omega t} dt \quad ,
\end{aligned}
$$

where $w_{fu}(t)$ is a **window function.** Specifically, this window function has the form:

$$
w_{fu}(t) = w_f(t - uT_o) e^{+j\omega_c uT_o} \quad .
$$

In other words, every function $w_{fu}(t)$ is simply the function $w_f(t)$ delayed by some integer multiple of T_o.

The window function $w_f(t)$ has the following properties:

1. It is real valued even function.

2. It has a time width T_o. That is,

$$
w_f(t) = 0 \quad \text{for} \quad t < \frac{-T_o}{2} \text{ and } t > \frac{T_o}{2}
$$

$$
w_f(t) > 0 \quad \text{for} \quad \frac{-T_o}{2} < t < \frac{T_o}{2} \quad .
$$

3. It has a bandwidth of approximately $B_o = 1/T_o$.

4. It has unit value at t=0:

$$w_f(t=0) = 1.0 \quad .$$

As a result, a window function $w_f(t-uT_o)e^{+j\omega_c uT_o}$ effectively selects one of the pulse functions $f_q(t-uT_o)e^{j\omega_c uT_o}$ from the "train" of pulses $\sum_u f_q(t-uT_o)e^{j\omega_c uT_o}$:

$$\begin{aligned}\sum_{u'} f_q(t-u'T_o)e^{j\omega_c u'T_o} w^*_{fu}(t) &= \sum_{u'} f_q(t-u'T_o)e^{j\omega_c u'T_o} w_f(t-uT_o)e^{-j\omega_c uT_o} \\ &= f_q(t-uT_o)e^{j\omega_c uT_o} w_f(t-uT_o)e^{-j\omega_c uT_o} \\ &= f_q(t-uT_o)w_f(t-uT_o) \quad .\end{aligned}$$

The windowed Fourier transform is thus reduced to:

$$\begin{aligned}s(uT_o,\omega) &= \int_{-\infty}^{\infty} \sum_p \sum_q S_{pq} e^{j\omega_p t} g_s(t) f_q(t-uT_o) w_f(t-uT_o) e^{-j\omega t} dt \\ &= \sum_p \sum_q S_{pq} \int_{-\infty}^{\infty} e^{j\omega_p t} g_s(t) f_q(t-uT_o) w_f(t-uT_o) e^{-j\omega t} dt \quad .\end{aligned}$$

Consider now the resulting integral:

$$\int_{-\infty}^{\infty} e^{j\omega_p t} g_s(t) f_q(t-uT_o) w_f(t-uT_o) e^{-j\omega t} dt \quad .$$

Recall that the function $f_q(t-uT_o)$ has very narrow time width ($<<T_o$), so that the integrand will be approximately zero for all time t, with exception of a small region around time $t = uT_o$ (i.e., the region where $f_q(t-uT_o)$ is non-zero). Thus, the effective region of integration of this integral is very small, confined to a small region around $t = uT_o$. The integration across all other time t will approximately result in zero.

Recall also that functions $g_s(t)$ and $w_f(t)$ both have a long time width ($\geq T_o$) and a very small bandwidth ($\leq$B), so that that the values of $g_s(t)$ and $w_f(t-uT_o)$ will remain approximately constant across the small effective integration region. That is, $g_s(t) \approx g_s(uT_o)$ and $w_f(t-uT_o) \approx w_f(0) = 1.0$

Likewise, recall that $\omega_p << \omega_o$, so that the function exp $[j\omega_p t]$ will also remain approximately constant across the small effective region of integration. That is,
exp $[j\omega_p t] \approx \exp[ju\omega_p T_o]$.

As a result, the integral is simplified to:

$$\int_{-\infty}^{\infty} e^{j\omega_p t} g_s(t) f_q(t-uT_o) w_f(t-uT_o) e^{-j\omega t} dt$$

$$\approx e^{ju\omega_p T_o} g_s(uT_O)\, w_f(0) \int_{-\infty}^{\infty} f_q(t-uT_o) e^{-j\omega t} dt$$

$$= e^{ju\omega_p T_o} g_s(uT_o) \int_{-\infty}^{\infty} f_q(t-uT_o) e^{-j\omega t} dt$$

$$= e^{ju\omega_p T_o} g_s(uT_o) e^{-ju\omega T_o} \int_{-\infty}^{\infty} f_q(t) e^{-j\omega t} dt \quad .$$

Inserting this into the expression for the windowed Fourier Transform we get:

$$s(uT_o,\omega) = \sum_p \sum_q S_{pq} e^{ju\omega_p T_o} g_s(uT_o) e^{-ju\omega T_o} \int_{-\infty}^{\infty} f_q(t) e^{-j\omega t} dt$$

$$= \sum_p \sum_q S_{pq} e^{ju\omega_p T_o} g_s(uT_o) e^{-j\omega u T_o} \int_{-\infty}^{\infty} f_q(t) e^{-j\omega t} dt \quad .$$

Recalling that:

$$f_q(t) = g_f(t-\tau_q) e^{j\omega_c \tau_q}$$

we get:

$$s(uT_o,\omega) = \sum_p \sum_q S_{pq} e^{ju\omega_p T_o} g_s(uT_o) e^{-j\omega u T_o} \int_{-\infty}^{\infty} g_f(t-\tau_q) e^{j\omega_c \tau_q} e^{-j\omega t} dt$$

$$= \sum_p \sum_q S_{pq} e^{ju\omega_p T_o} g_s(uT_o) e^{-j\omega u T_o} e^{-j(\omega-\omega_c)\tau_q} \int_{-\infty}^{\infty} g_f(t) e^{-j\omega t} dt \quad .$$

Now recognizing:

$$G_f(\omega) = \int_{-\infty}^{\infty} g_f(t) e^{-j\omega t} dt \quad ,$$

we state that:

$$s(uT_o,\omega)=\sum_p\sum_q S_{pq}e^{ju\omega_pT_o}g_s(uT_o)e^{-j\omega uT_o}e^{-j(\omega-\omega_c)\tau_c}G_f(\omega)$$
$$=\sum_p g_s(uT_o)e^{ju\omega_pT_o}\sum_q S_{pq}G_f(\omega)e^{-j\omega uT_o}e^{-j(\omega-\omega_c)\tau_c}\quad .$$

6. The Sampled Windowed Fourier Transform of S(t)

We will now sample the resulting frequency spectrum $s(uT_o,\omega)$. Recall that the time extent of the signal, after windowing with $w_{fu}(t)=w_f(t-uT_o)$, is $(uT_o-T_o/2)<t<(uT_o+T_o/2)$. Thus, the Nyquist criteria is satisfied only if the sample spacing $\Delta\omega$ is:

$$\Delta\omega<\frac{2\pi}{2uT_o}\le\frac{\pi}{UT_o}=\frac{\pi}{T}$$

This sample spacing can thus be exceedingly small, and result in as many as 2BT frequency samples!

However, we note that the time-bandwidth product of the windowed signal is only BT_o, and thus we should be able to sample at a much larger spacing. To do this, we need to "shift" the windowed signal back uT_o seconds, such that it lies in the domain:

$$-T_o/2<t<T_o/2$$

meaning we can sample at a more reasonable:

$$\Delta\omega\le\frac{2\pi}{T_o}=\omega_o\quad .$$

To accomplish this shifting, we simply multiply the frequency spectrum by:

$$e^{j\omega uT_o}\quad .$$

We can now adequately sample the spectrum at sample spacings of $\Delta\omega\le\omega_o$, and we choose to "oversample" with:

$$\Delta\omega=\omega_o/2\quad .$$

In other words, we will sample at $\omega=v(\omega_o/2)$, where v is some integer value.

We can now define the complex sample value s_{uv}:

$$
\begin{aligned}
s_{uv} &= e^{j\omega uT_o}\, s(uT_o,\omega)\Big|_{\omega=v(\omega_o/2)} \\
&= e^{j\omega uT_o}\sum_p g_s(uT_o)e^{ju\omega_p T_o}\sum_q S_{pq}G_f(\omega)e^{-j\omega uT_o}e^{-j(\omega-\omega_c)\tau_q}\Big|_{\omega=v(\omega_o/2)} \\
&= \sum_p g_s(uT_o)e^{ju\omega_p T_o}\sum_q S_{pq}G_f(\omega)e^{-j(\omega-\omega_c)\tau_c}\Big|_{\omega=v(\omega_o/2)} \\
&= \sum_p g_s(uT_o)e^{ju\omega_p T_o}\sum_q S_{pq}G_f\left(\frac{v\omega_o}{2}\right)e^{-j\left(\frac{v\omega_o}{2}-\omega_c\right)\tau_c} \quad .
\end{aligned}
$$

The integer value v extends from:

$$
-\left(\frac{V-1}{2}\right)\le v\le\frac{V-1}{2} \quad ,
$$

where V is an **odd integer** approximately equal to:

$$
V\approx\frac{2\pi B}{\omega_o/2}=2BT_o+1 \quad .
$$

Note then that there are UV number of samples $s(uT_o, v\omega_o/2)$, but the integer value UV is equal to:

$$
UV=\left(\frac{T}{T_o}\right)(2BT_o+1)\approx 2BT \quad .
$$

In other words, the number of spectrum samples is equal to twice the time-bandwidth product of this temporal transmit signal.

We now define:

$$
\psi_{uv}^{pq}=g_s(uT_o)e^{ju\omega_p T_o}G_f(v\omega_o/2)e^{-j\left(\frac{v\omega_o}{2}-\omega_c\right)\tau_c} \quad ,
$$

so that the sample values can be more compactly written as:

$$
S_{uv}=\sum_p\sum_q\psi_{uv}^{pq}S_{pq} \quad .
$$

7. Reindexing the Data Samples

Note that there are PQ number of unique values S_{pq} (i.e., PQ number of basis functions) and UV number of unique spectrum samples. Let's then denote each value with a unique integer index. For the values S_{pq}, we will use the integer variable r, determined by a unique mapping from values p and q:

$$
\text{p, q} \rightarrow \text{r} \quad .
$$

An example of this mapping is:

$$r = (pQ + q) + \left(\frac{PQ+1}{2}\right) .$$

Note since:

$$-\left(\frac{P-1}{2}\right) \le p \le \frac{P-1}{2} \quad \text{and} \quad -\left(\frac{Q-1}{2}\right) \le q \le \frac{Q-1}{2} ,$$

the value r extends from:

$$1 \le r \le PQ .$$

Making the definition:

$$R = PQ ,$$

We can simply state that:

$$1 \le r \le R .$$

To index the sample values S_{uv}, we will use the integer variable k, determined by a unique mapping from values p and q:

$$u, v \rightarrow k .$$

An example of this mapping is:

$$k = (uV + v) + \left(\frac{UV+1}{2}\right) .$$

Note since:

$$-\left(\frac{U-1}{2}\right) \le u \le \frac{U-1}{2} \quad \text{and} \quad -\left(\frac{V-1}{2}\right) \le v \le \frac{V-1}{2} ,$$

the value k extends from:

$$1 \le k \le UV .$$

Making the definition:

$$K = UV ,$$

We can simply state that:

$$1 \le k \le K .$$

We can now reindex each of our model values using these mappings:

$$S_{pq} \rightarrow S_r \qquad S_{uv} \rightarrow S_k \qquad \psi_{uv}^{pw} \rightarrow \psi_{kr}$$

Thus, we can simply state our model as:

$$s_k = \sum_r \psi_{kr} S_r \ .$$

8. A Vector/Matrix Signal Model

We can form our set of R samples S_r into a vector:

$$\mathbf{S}^t = [S_1, S_2, S_3, \cdots, S_R]^T \ ,$$

and likewise form our set of K samples s_k into a vector:

$$\mathbf{s}^t = [s_1, s_s, s_3, \cdots, s_k]^T \ .$$

Now, forming the KR values ψ_{kr} into a matrix:

$$\boldsymbol{\psi} = \begin{bmatrix} \psi_{11} & \psi_{12} & \cdots & \psi_{1R} \\ \psi_{21} & \psi_{22} & \cdots & \psi_{1R} \\ \vdots & \vdots & \ddots & \vdots \\ \psi_{K1} & \psi_{K2} & \cdots & \psi_{KR} \end{bmatrix} \ .$$

Our model has simply reduced to:

$$\mathbf{s}^t = \boldsymbol{\psi} \mathbf{S}^t \ .$$

9. Extension to Space-Time Transmit Signals

Note that this model is used to determine a single temporal (time-frequency) vector $\mathbf{s}^t$. If there are more than one spatial transmit elements (i.e., there are J transmit elements), then there will be a different temporal vector for each spatial transmit element j. Thus, to denote the specific temporal vector for spatial element j, we can use the notation:

$$\mathbf{s}_j^t = [s_{j1}, s_{j2}, s_{j3}, \cdots, s_{jK}]^T$$
$$\mathbf{S}_j^t = [S_{j1}, S_{j2}, S_{j3}, \cdots, S_{jR}]^T \ .$$

Therefore:

$$\mathbf{s}_j^t = \boldsymbol{\psi} \mathbf{S}_j^t \ .$$

Note that the matrix $\boldsymbol{\psi}$ is independent of spatial element j.

Recall that the vectors $\mathbf{s}_j^t$ can be combined to form a single space-time transmit vector (of dimension JK=N) in the following fashion:

$$\mathbf{s} = \left[(\mathbf{s}_1^t)^T, (\mathbf{s}_2^t)^T, (\mathbf{s}_3^t)^T, \cdots, (\mathbf{s}_J^t)^T\right]^T .$$

Likewise, we can organize the vectors $\mathbf{s}_j^t$ into a single space-time transmit vector of dimension JR=W:

$$\mathbf{s} = \left[(\mathbf{S}_1^t)^T, (\mathbf{S}_2^t)^T, (\mathbf{S}_3^t)^T, \cdots, (\mathbf{S}_J^t)^T\right]^T .$$

However, we can also organize the space-time samples S_{jk} into a set of K vectors:

$$\mathbf{s}_k^s = \left[S_{1k}, S_{2k}, S_{3k}, \cdots S_{Jk}\right]^T ,$$

and then organize these vectors into an alternative single space-time vector of dimension N:

$$\mathbf{s} = \left[(\mathbf{s}_1^s)^T, (\mathbf{s}_2^s)^T, (\mathbf{s}_3^s)^T, \cdots, (\mathbf{s}_K^s)^T\right]^T .$$

Likewise, we can also organize the space-time samples S_{jr} into a set of R vectors:

$$\mathbf{S}_r^s = \left[S_{r1}, S_{2r}, S_{3r}, \cdots, S_{Jr}\right]^T ,$$

and then organize these vectors into an alternative single space-time vector of dimension W:

$$\mathbf{S} = \left[(\mathbf{S}_1^s)^T, (\mathbf{S}_2^s)^T, (\mathbf{S}_3^s)^T, \cdots, (\mathbf{S}_R^s)^T\right]^T .$$

We will now relate the vector of the form:

$$\mathbf{s} = \left[(\mathbf{s}_1^s)^T, (\mathbf{s}_2^s)^T, (\mathbf{s}_3^s)^T, \cdots, (\mathbf{s}_K^s)^T\right]^T$$

to the vector of the form:

$$\mathbf{s} = \left[(\mathbf{s}_1^s)^T, (\mathbf{s}_2^s)^T, (\mathbf{s}_3^s)^T, \cdots, (\mathbf{s}_K^s)^T\right]^T .$$

From the equation:

$$\mathbf{s}_j^t = \Psi \mathbf{S}_j^t ,$$

we can conclude:

$$s_{jk} = \sum_r \psi_{kr} S_{jr} \ .$$

This can be equivalently written as:

$$\begin{aligned} \mathbf{s}_k^s &= \sum_r \psi_{kr} \mathbf{S}_r^s \\ &= \sum_r \psi_{kr} I_J \mathbf{S}_r^s \\ &= \sum_r \mathbf{D}_{kr}^{\psi} \mathbf{S}_r^s \ . \end{aligned}$$

The matrix I_J is a J by J identity matrix, so that $\mathbf{D}_{kr}^{\psi}$ is a J by J diagonal matrix of the form:

$$\mathbf{D}_{kr}^{\psi} = \psi_{kr} I_J = \begin{bmatrix} \psi_{kr} & 0 & 0 & \cdots & 0 \\ 0 & \psi_{kr} & 0 & \cdots & 0 \\ 0 & 0 & \psi_{kr} & \cdots & 0 \\ \vdots & \vdots & \vdots & \ddots & 0 \\ 0 & 0 & 0 & 0 & \psi_{kr} \end{bmatrix} \ .$$

Thus, we can more concisely write:

$$\mathbf{s}_k^s = \mathbf{F}_k \mathbf{S} \ ,$$

where:

$$\mathbf{S} = \left[(\mathbf{S}_1^s)^T, (\mathbf{S}_2^s)^T, (\mathbf{S}_3^s)^T, \cdots, (\mathbf{S}_R^s)^T \right]^T$$

and $\mathbf{F}_k$ is a J by W matrix of the form:

$$\mathbf{F}_k = \left[\mathbf{D}_{k1}^{\psi} \ \mathbf{D}_{k2}^{\psi} \ \mathbf{D}_{k3}^{\psi} \cdots \mathbf{D}_{kR}^{\psi} \right] \ .$$

Thus can write our final form:

$$\mathbf{s} = \mathbf{F} \mathbf{S} \ ,$$

where

$$\mathbf{s} = \left[(s_1^s)^T, (s_2^s)^T, (s_3^s)^T, \cdots, (s_R^s)^T \right]^T$$

and **F** is an N by W matrix of the form:

$$\mathbf{F} = \begin{bmatrix} \mathbf{F}_1 \\ \mathbf{F}_2 \\ \vdots \\ \mathbf{F}_K \end{bmatrix} = \begin{bmatrix} \mathbf{D}^{\psi}_{11} & \mathbf{D}^{\psi}_{12} & \cdots & \mathbf{D}^{\psi}_{1R} \\ \mathbf{D}^{\psi}_{21} & \mathbf{D}^{\psi}_{11} & \cdots & \mathbf{D}^{\psi}_{2R} \\ \vdots & \vdots & \ddots & \vdots \\ \mathbf{D}^{\psi}_{K1} & \mathbf{D}^{\psi}_{K2} & \cdots & \mathbf{D}^{\psi}_{KR} \end{bmatrix} .$$

Finally, the matrix **F** can be more concisely and directly written in terms of ψ using the Kronecker product $\otimes$:

$$\mathbf{F} = \psi \otimes \mathbf{I}_J \ .$$

In other words, n is determined from the mapping j, k $\rightarrow$n:

$$n = (k\,J + j) - J \ ,$$

where:

$$1 \le j \le J \quad \text{and} \quad 1 \le k \le K$$

so that $1 \le n \le N = JK$.

10. Application of Signal Model to Target Model

The normalized receiver response ρ_t for target t can be related to transmit signal vector **s** using matrix $\mathbf{H}_t$, such that:

$$\rho_t = \mathbf{H}_t \mathbf{s} \ .$$

If vector **s** is of the form:

$$\mathbf{s} = \left[(\mathbf{s}_1^s)^T, (\mathbf{s}_2^s)^T, (\mathbf{s}_3^s)^T, \cdots, (\mathbf{s}_K^s)^T \right]^T$$

so that:

$$\mathbf{s} = \mathbf{F}\,\mathbf{S} \ ,$$

where:

$$\mathbf{S} = \left[(\mathbf{S}_1^s)^T, (\mathbf{S}_2^s)^T, (\mathbf{S}_3^s)^T, \cdots, (\mathbf{S}_R^s)^T \right]^T \ .$$

Then we can write:

$$\begin{aligned}\rho_t &= H_t s \\ &= H_t(FS) \\ &= (H_t F)S \\ &= H'_t S \quad ,\end{aligned}$$

where we have defined the M by W matrix H'_t as:

$$H'_t = H_t F \quad .$$

11. Sample Position Vector

Each sample s_k corresponds to a frequency $\omega = v\omega_o / 2$ and time $t = uT_o$. These two values express a point on a time-frequency plane, which we can denote using position vector:

$$\begin{aligned}\bar{z}_k &= [t_k, \omega_k]^T \\ &= [uT_o, v\omega_o / 2]^T \quad ,\end{aligned}$$

where u and v are related to k by the same mapping u, v $\rightarrow$k discussed in Section 7.

12. Default Model Values

We can define a set of default model values, which simplifies the model and its implementation.

We can assume that $g_f(t)$ has the form:

$$g_f(t) = \sqrt{B}\frac{\sin(\pi B t)}{\pi B t}$$

which satisfies all of the properties described in Section 4. Expressing this in terms of its Fourier transform, we find:

$$G_f(\omega) = \begin{cases} \dfrac{1}{\sqrt{B}} & \text{if} \quad -\pi B < \omega < \pi B \\ 0 & \text{if} \quad \omega < -\pi B \quad \text{or} \quad \omega > \pi B \end{cases} .$$

Likewise, we can assume that $G_s(\omega)$ has the form:

$$G_s(\omega) = \sqrt{T}\frac{\sin\left(\frac{\omega T}{2}\right)}{\left(\frac{\omega T}{2}\right)} \quad .$$

Taking the inverse Fourier transform:

$$g_s(t) = \begin{cases} 1/\sqrt{T} & if \quad -\frac{T}{2} < t < \frac{T}{2} \\ 0 & if \quad t < -\frac{T}{2} \quad or \quad t > \frac{T}{2} \end{cases} \quad .$$

This function likewise satisfies all properties stated in Section 4.

We likewise can assume that the value of τ_q is:

$$\tau_k = \frac{q}{B}$$

and that the value of ω_p is:

$$\omega_p = 2\pi\left(\frac{p}{T}\right) \quad .$$

Inserting these default values into the expression:

$$\psi_{uv}^{pq} = g_s(uT_o)e^{ju\omega_p T_o} G_f(v\omega_o/2)e^{-j\left(\frac{v\omega_o}{2}-\omega_c\right)\tau_q}$$

we get:

$$\begin{aligned} \psi_{uv}^{pq} &= g_s(uT_o)e^{ju\omega_p T_o} G_f(v\omega_o/2)e^{-j\left(\frac{v\omega_o}{2}-\omega_c\right)\tau_q} \\ &= \left(\frac{1}{\sqrt{T}}\right)e^{ju\left(2\pi\frac{p}{T}\right)T_o}\left(\frac{1}{\sqrt{B}}\right)e^{-j\left(\frac{v\omega_o}{2}-\omega_c\right)\left(\frac{q}{B}\right)} \\ &= \frac{1}{\sqrt{BT}}e^{j2\pi up\left(\frac{T_o}{T}\right)}e^{-jvq\left(\frac{\omega_o}{2B}\right)}e^{+jq\left(\frac{\omega_c}{B}\right)} \\ &= \frac{\sqrt{2}e^{jq\left(\frac{\omega_c}{B}\right)}}{\sqrt{UV}}e^{j\frac{2\pi up}{U}}e^{-j\frac{2\pi vq}{v}}e^{+jq\left(\frac{\omega_c}{B}\right)} \quad . \end{aligned}$$

We now make one more simplifying assumption. We assume that:

The bandwidth B is an **odd integer multiple** of $f_o/2 \quad (B >> f_o)$.

If this assumption is true, then:

$$\begin{aligned} e^{jq\left(\frac{\omega_c}{B}\right)} &= e^{j2\pi\left(\frac{qf_c}{B}\right)} \\ &= e^{j2\pi} \\ &= 1.0 \quad . \end{aligned}$$

Therefore, the default value for ψ_{kr}, when applying **all of the assumptions of this section**, is:

$$\psi_{kr} = \frac{\sqrt{2}}{\sqrt{UV}} e^{j\frac{2\pi up}{U}} e^{-j\frac{2\pi vq}{V}} \quad ,$$

where p, q $\rightarrow$r and u ,v $\rightarrow$k .

Appendix I: Determination of Numeric Model Parameters

Abstract

This appendix describes a rationale for selecting the numeric values required for the radar transmission, target, and measurement model. Several constraints are placed upon these values, which leads to a set of several dependent parameter equations. Default values are then provided for the remaining independent values.

First, we select the fundamental independent physical parameters:

$$c, h, \theta_i, v, f_c$$

from which we can determine:

$$R_o = \frac{h}{\cos\theta_i}$$

$$y_o = h\tan\theta_i$$

as well as the frequency matrices **K.**

We likewise must select N_x and N_y, the number of targets (resolution cells) in each direction, as well as a parameter denoted as β, which will be defined later.

Recall the radar resolution was determined to be:

$$\Delta y = \frac{cR_o}{2By_o} = \frac{c}{2B\sin\theta_i}$$

and

$$\Delta x = \frac{cR_o}{2Tvf_c} = \frac{cR_o}{2UT_ovf_c} \quad .$$

Now we place our first constraint on the simulation values, which is that the resolution of the radar in each direction be equal (i.e., the resolution cells are square):

$$\Delta y = \Delta x$$

$$\frac{cR_o}{2By_o} = \frac{cR_o}{2Tvf_c}$$

$$By_o = Tvf_c \quad .$$

By rearranging this result, we find a constraint on the ratio of the signal bandwidth B and time width T:

$$\frac{B}{T} = \frac{vf_c}{y_o} \quad .$$

Thus, complete specification of the signal time width and bandwidth requires a second equation. This equation is generated by the definition of value β :

$$\beta = \frac{N_x N_y}{BT} \quad ,$$

or

$$BT = \frac{N_x N_y}{\beta} \quad .$$

The value β is thus simply the ratio of the signal time-bandwidth product to the number of resolution cells. For a single aperture radar (i.e., monostatic), this value must be less than or equal to one ($\beta \leq 1$) for unambiguous imaging. However, for multi-aperture (i.e., multi-static) radar, the value of β can be greater than one, given a sufficient number of receive apertures.

Combing these two equations, we get the following expressions for B and T:

$$B = \sqrt{BT\left(\frac{B}{T}\right)}$$

$$= \sqrt{\frac{N_x N_y}{\beta}\frac{vf_c}{y_o}}$$

$$T = \sqrt{BT\left(\frac{T}{B}\right)}$$

$$= \sqrt{\frac{N_x N_y}{\beta}\frac{y_o}{vf_c}} \quad .$$

We must now determine the values of U, V and T_o, where:

$$T = UT_o$$

$$B = \frac{V}{2T_o}$$

$$BT = \frac{UV}{2} \quad .$$

Therefore, we find that:

$$\frac{UV}{2} = BT = \frac{N_x N_y}{\beta}$$

meaning

$$UV = \frac{2N_x N_y}{\beta} \quad .$$

We will now separate this expression into two (non-unique) product terms:

$$U = \frac{N_x}{\sqrt{\beta}}$$

and

$$V = \frac{2N_y}{\sqrt{\beta}} \quad .$$

Although this separation appears to be arbitrary, we keep in mind that N_x along-track resolution cells can be unambiguously resolved with U independent time samples only if $U \geq N_x$. Likewise, N_y cross-track resolution cells can be unambiguously resolved with V/2 independent frequency samples only if $V/2 \geq N_y$.

Of course, if $\beta > 1$, then at least one (and likely both) of these two conditions will be violated. However, the two equations above will ensure that each these two conditions ($U \geq N_x$ and $V/2 \geq N_y$) will be satisfied if $\beta < 1$.

Using these results, we can determine T_o:

$$T_o = \frac{T}{U} \quad ,$$

or equivalently,

$$T_o = \frac{V}{2B}$$

Finally, a necessary condition for unambiguously resolving all ($N_x N_y$) resolution cells is that the number of independent measurement samples be greater than the number of resolution cells. Since the number of independent measurement samples is approximately equal to IBT, where I is the number of spatial receive elements (i.e., receive antennas), we find that unambiguous imaging can result only when:

$$IBT > N_x N_y \quad ,$$

or

$$I > \beta = \frac{N_x N_y}{BT} \quad .$$

In other words, the number of spatial receive elements I must exceed β.

Finally, we note that throughout this document we have assumed that resolution is determined by the temporal values of signal bandwidth and time width. The implication is that that the physical extent of spatial arrays is too small to resolve resolution cells.

To enforce this condition, we first determine the resolution of the spatial elements. Assuming that the spatial extent of the array in the along-track direction is L_x, we find that the approximate width of the main beam when projected on the ground (ΔX_s), is:

$$\Delta X_s = \frac{cR_o}{f_c L_x} \quad .$$

Now we define a value η, which specifies the ratio of the spatial resolution to the temporal resolution:

$$\eta = \frac{\Delta X_s}{\Delta X} \quad .$$

Combining these two equations we arrive at the expression:

$$L_x = \frac{cR_o}{f_c \eta \Delta x} \quad ,$$

where η is now a new independent input parameter.

Summarizing, we find that given the independent values:

$$c, h, \theta_i, v, f_c, N_x, N_y, \beta, \eta \ ,$$

we can determine the values:

$$B, T, T_o, U, V, L_x, K_\varphi, K_\theta, I$$

Default Values

As assumed default values, we can use the following inputs, which are consistent with a spaceborne radar in low-Earth orbit:

$c = 3 \times 10^8$ m/s
h = 183 km
v = 7.8 km/s
$f_c = 10$ GHz
$\theta_1 = 45°$.

Therefore:

$y_o = 183$ km
$R_o = 258.8$ km .

For the image size (number of resolution cells), we can assume that:

$$N_x = N_y = 2^i - 1 \ ,$$

where i is simply some integer value. In other words, we assume the image is square, with an "almost" binary size (the subtraction of 1 ensures the values are odd). Examples of these would be $N_x = \{3,7,15,31,63,127,255,511, \cdots\}$. The selected value i depends on the goal of the simulation — Make i as large as possible while still meeting the desired goal (small i for fast results, large i for impressive results).

Additionally, assume $\beta = 4.2$ and $I = 7$ (i.e., $I > \beta$), and also assume $\eta = 5$. Use the value $\sigma = L_x/2$ for a random (Gaussian) distribution of antenna elements.

Finally, initially assume that J=1, then increase it to J=2, and finally J=I once everything is working.